Effect of ammonia co-feeding on oxygenates over K-Mo_2C in the Fischer-Tropsch synthesis

by

Wijnand Marquart

BSc Chemical Engineering

Hogeschool Utrecht, University of Applied Sciences, The Netherlands

Thesis is submitted to the University of Cape Town in partial fulfillment of the requirements for the degree Masters of Science in Chemical Engineering

Catalysis Institute
Faculty of Engineering & the Built Environment
Department of Chemical Engineering

Cape Town

February 2018

Declaration

I know the meaning of plagiarism and declare that all the work in the document, save for that which is properly acknowledged, is my own. This thesis/dissertation has been submitted to the Turnitin module (or equivalent similarity and originality checking software) and I confirm that my supervisor has seen my report and any concerns revealed by such have been resolved with my supervisor.

Signed by candidate

January 2018

Synopsis

The Fischer-Tropsch (FT) process, producing long chained waxes and transportation fuels, is competing with fuels derived from crude oils and its profitability is therefore dependent on the global oil price. However, increasing the value of synthesized products could render the profitability of the FTS independent of fluctuations in the oil price (which are mostly due to global political trends). One way to achieve this, is to target fine chemicals instead of fuels. At the Catalysis Institute, this has been investigated by adding ammonia to the feed gas stream and obtaining highly valuable amines, amides and nitriles. It has been shown that the so-called nitrogen containing compounds are formed instead of the Fischer-Tropsch typical albeit minor products alcohols, aldehydes and carboxylic acids, i.e. oxygenates. Increasing the oxygenate selectivity was investigated in numerous studies as no commercial FT based process exists which produces oxygenates at a significant yield.

Typically, transition metals such as Fe, Co, Rh and Ni are active for the FT synthesis. Based on reaction conditions employed, commercial Fe and Co based catalysts have been shown to produce between 6 and 12 C% oxygenates. Rh has been shown to have a high oxygenate selectivity, but the associated high raw material cost becomes prohibitive for use as a commercial FT catalyst. Catalysts other than the traditionally known FT active transition metals have shown promising results in terms of oxygenate selectivity. Transition metal carbides such as Mo_2C, have been investigated under Fischer-Tropsch conditions. While the bare catalyst produces mainly methane and other hydrocarbons, upon promotion with potassium the selectivity shows a significant shift towards oxygenates.

This project investigates the use of potassium promoted molybdenum carbide as a catalyst for high oxygenate selectivity in the Fischer-Tropsch synthesis. β-Mo_2C was synthesized and subsequently promoted with different levels of potassium and its Fischer-Tropsch synthesis performance was evaluated in a stainless steel fixed bed reactor. The influence of catalyst synthesis protocols, reactor pressure and temperature, feed gas space velocity, and K/Mo wt.% promotion on catalyst activity and selectivity were studied. At a stable CO conversion (±10%) and its related oxygenate selectivity (±35 C%) ammonia was co-fed to the catalyst to study the conversion of oxygenates to nitrogen containing compounds.

In summary, an unpromoted β-Mo_2C catalyst reached CO conversions to ±40% at the conditions applied. Initial promotion of the catalyst with potassium showed a significant drop in catalyst activity, however, an increase in potassium content did not further decrease catalyst activity. The selectivity towards oxygenates was greatly enhanced from 10 C% up to 42 C% (CO_2-free) at similar reaction conditions. Simultaneously, the oxygenate distribution shifted towards higher alcohols. The initial methanol content in the total oxygenate slate was around 60 C%, decreasing to about 20 C% upon potassium promotion. During co-feeding of ammonia, N-containing compounds were observed in the form of nitriles (±9 C%, CO_2-free) and small traces of amides

(±0.1 C%, CO_2-free). Acetonitrile was the most dominating formed N-containing compound (≥58 C%). Upon the co-feeding of ammonia, the oxygenate selectivity decreased by roughly 10 C% points (CO_2-free) but did not reach zero. Catalyst activity was slightly affected but recovered with time on stream. A slowly building up blockage appeared after 1-3 hours TOS simultaneously with a decreasing CO_2 selectivity, suggesting the reaction with NH_3 forming ammonium carbonate. This could however not be confirmed.

The benefits of producing N-containing compounds using a potassium promoted β-Mo_2C needs to be further investigated, trying to avoid the blockage by suppressing the WGS-activity of the catalyst. It is promising that the activity is hardly affected and that in the short period of time on stream N-containing compounds were observed.

Acknowledgements

This study started in February 2016 and was completed by January 2018 at the Catalysis Institute in the Department of Chemical Engineering at the University of Cape Town, South Africa.

At first, I would like to extend my gratitude to my supervisors, Assoc. Prof. Nico Fischer and Prof. Michael Claeys, for giving me the opportunity to do this project. For their patience, guidance and advice throughout the project. A special thanks to Assoc. Prof. Nico Fischer for the time he made available to assist me every time I knocked on his office door, ready for discussions. I look forward to embarking on my next journey under his supervision, i.e. doing my PhD.

I would like to thank everyone in the Catalysis Institute and especially my research group for their support, advise, assistance and demonstrations in and outside the laboratories, whenever it was required.

To DST-NRF Centre of Excellence in Catalysis c*change for their financial support throughout this work.

A big thank you to my friends (and of course my brother) in Cape Town, whom treated me like family while being so far apart from my family in the Netherlands. They were always there to assist, support and make my time in Cape Town very much enjoyable outside University life.

Finally, my last but most definitely not the least, a huge thank you to my parents for allowing me to continue my studies in Cape Town, South Africa. There are no words that can describe the appreciation I have for them, for always showing the love and support I needed to be about ±13000 kilometers away from them.

Table of Contents

List of Figures

List of Tables

Nomenclature

$(NH_4)6Mo_7O_{24}\cdot 4H_2O$	Ammonium molybdate
[x]	Concentration of compound x
ΔG	Gibbs free energy
ΔH	Heat of reaction
CH_3OH	Methanol
^{13}C	Carbon-13
^{13}CO	13c-carbon monoxide
Θ	Diffraction angle
A	Area in chromatogram
Å	Angström
AC	Activated carbon
Al_2O_3	Alumina
Alc.	Alcohols
Ar	Argon
ASF	Anderson-Schulz-Flory
C	Carbon
C%	Carbon percentage
CeO_2	Cerium(iv)oxide
CFB	Circulating fluidized bed
CH*	Carbyne
CH_2	Carbene
CH_4	Methane
C_n	Carbon chain with ‘n’ chain length
CN	Carbon number
CNT	Carbon nanotube
Co	Cobalt
CO	Carbon monoxide
CO_2	Carbon dioxide
C_{obs}	Observed carbon number
Cr_2O_3	Chromium(iii)oxide
Cs	Cesium
Cu	Copper
d	Desorption
DFT	Density functional theory
e.g.	Exempli gratia (for example)
EPA	Environmental protection agency
eq.	Equation
eV	Electron volt
fcc	Face centered cubic

Fe	Iron
FFB	Fluidize fixed bed
FID	Flame ionization detector
FT	Fischer-Tropsch
FTS	Fischer-Tropsch synthesis
g	Growth
g_{cat}	Gram of catalyst
GC-TCD	Gas chromatography with thermal conductivity detector
GHSV	Gas hour space velocity
GTL	Gas to liquid
H	Hydrogen atom
h	Hour
H_2	Hydrogen
H_2O	Water
H_2S	Hydrogen sulfide
H_3BO_3	Boric acid
HAS	Higher alcohol synthesis
HC	Hydrocarbon
HCl	Hydrochloric acid
hcp	Hexagonal close packed
HF	Hydrogen fluoride
HNO_3	Nitric acid
HTFT	High temperature Fischer-Tropsch
i.d. / ID	Inner diameter
i.e.	Id est (that is)
ICP-OES	Inductively coupled plasma optical emission spectrometry
IFP	Institut Français du Pétrole
IS	Internal standard
K	Potassium
K_2CO_3	Potassium carbonate
KI	Kovats indices
kV	Kilo volt
LiCl	Lithium chloride
LTFT	Low temperature Fischer-Tropsch
m^2	Square meter
mA	Milliampere
MeOH	Methanol
MgO	Magnesium oxide
min	Minute
mL	Milliliter
mmole(s)	Millimole(s)

Mo	Metallic molybdenum
Mo_2C / Mo_xC	Molybdenum carbide
Mo_2N	Molybdenum nitride
Mo_4O_{11}	Molybdenum oxide
MoO_2	Molybdenum dioxide
MoO_3	Molybdenum trioxide
MoS_2	Molybdenum sulfide
ms	Milliseconds
MTBE	Methyl tert-butyl ether
MW	Megawatt
$\dot{n}$	Molar flow rate
N	Nitrogen atom
N_2	Nitrogen
n-alcohols	Linear alcohols
NCH_4	Methyl amide
NH_2	Amide
NH_3	Ammonia
NH_4OH	Ammonium hydroxide
Ni	Nickel
nm	Nanometer
o.d.	Outer diameter
O_2	Oxygen
OH	Hydroxide
ON	Octane number
P	Pressure
pp	Partial pressure
ppm	Parts per million
rf_z	Response factor of compound z
Rh	Rhodium
ROH	Alcohols
SiO_2	Silica
Sp	Surface species
SV	Space velocity
T	Temperature
TEM	Transmission electron microscopy
ThO_2	Thoria
TiO_2	Titania
TOF	Time of flight
TOS	Time one stream
TPH	Temperature programmed hydrogenation

TPRe	Temperature programmed reaction
T_{ramp}	Temperature ramp rate
$T_{reaction}$	Reaction temperature
UHV	Ultra-high vacuum
vol.%	Volume percentage
WGS	Water-gas-shift
wt.%	Weight percentage
XCO	Co conversion
XPS	X-ray photoelectron spectroscopy
XRD	X-ray diffraction
ZnO	Zinc oxide
ZrO_2	Zirconium dioxide
α	Chain growth probability
α-MoC_1-x	Fcc molybdenum carbide
β-Mo_2C	Hcp molybdenum carbide
λ	Wavelength
µV	Microvolt

1 Introduction

The Fischer-Tropsch synthesis (FTS) can be described as the formation of hydrocarbons (paraffins and olefins) as well as oxygenates (alcohols, aldehydes, ketones and carboxylic acids) and water through a catalytic surface polymerization reaction of synthesis gas (syngas). Syngas is typically a mixture of carbon monoxide and hydrogen derived from a carbonaceous feedstock such as coal, biomass or natural gas via reforming or gasification processes. Commercially, the focus of the FTS is the production of transportation fuels such as gasoline or diesel, wax and to a smaller extent chemicals [1].

A commercial FT-plant includes three main process steps. The first step is the preparation of the synthesis gas from coal, biomass or natural gas (methane). This is completed using an air separation unit, an expensive technology which accounts for approximately 70% of the total plant operating costs [1-3]. The produced syngas is converted into products such as paraffins, olefins, water and, to a certain extent, oxygenates via a highly exothermic surface polymerization reaction by means of a transition metal catalyst. The FTS is thus a network of reactions leading to a non-selective product distribution [3-5]. Most of the Group VIII metals are active for the Fischer-Tropsch synthesis, however, commonly used catalysts in commercial FT-plants are iron and cobalt as they are highly active (cobalt) or least expensive (iron) [1, 6, 7]. In the last step, the products undergo separation and distribution for usage or further processing towards fuels, waxes and other chemicals.

Besides the focus on the production of transportation fuels, of which the profitability is mostly dependent on fluctuations of the global crude oil price, the product spectrum derived from the FTS process can also be altered to focus on more valuable chemicals [7]. Typical, albeit minor products, such as oxygenates can further be processed to produce a range of high value products. By doing this, the profitability of the FTS process is therefore less dependent on global crude oil price fluctuations. An example of this type of upgrading of the product spectrum, and which has attracted some interest, is the conversion of oxygenates to amines, amides and nitriles. These nitrogen-containing compounds have been shown to form upon the addition of NH_3 to the feed gas and are highly valuable fine chemicals which can be used in a range of industries such as the production of agricultural products, medicine and solvents [8-14].

Co-feeding of ammonia has previously been investigated at the Catalysis Institute of the University of Cape Town, South Africa [9, 14-16]. These studies showed that when utilizing potassium promoted iron catalysts with a high selectivity towards long chained oxygenates, N-containing compounds were produced at the expense of the initially formed oxygenates [5]. It was proposed that oxygenates reabsorbed to the catalytic surface, or precursors of the oxygenates, react with the co-fed NH_3 gas. In addition, Fischer *et al.* (2016) [9] showed the formation of acetonitrile using an iron-rhodium alloy catalyst. Once again, the simultaneous formation of N-containing compounds with a concomitant decrease in oxygenates was observed. de Vries (2017)

[15] studied the effect of co-feeding ammonia in the FTS on iron catalysts and observed the formation of amides and amines at the expense of the formation of oxygenates. DFT calculations suggested that the activation energy for CO dissociation is lowered upon co-feeding of NH_3 due to the proximity of NH_2 and CO. NH_2 is seen as the inserted species during chain growth of the carbon chains forming amines, as it appears that certain NH_2 and CO 'islands' on the surface of the catalyst are formed.

The above observations are supported by other research groups. For example, Henkel (2012) [10] studied the effect of NH_3 co-feeding when utilizing un-promoted and potassium promoted iron catalysts. They found that with the unpromoted sample, which had a low selectivity towards oxygenates, no N-containing compounds were formed. However, the promoted catalysts with a high oxygenate selectivity at normal FT-conditions, showed a decrease in oxygenate selectivity in conjunction with an observed formation of amines, amides and nitriles upon commencement of NH_3 co-feeding.

Transition metal carbides, such as molybdenum carbide (Mo_2C), have shown promising results towards the formation of higher oxygenates upon promotion with an alkali metal such as potassium [17-21]. Besides their propensity for the formation of higher alcohols, Mo_2C has been shown to be resistant to sulphur poisoning (which is a typical catalyst poison, especially in synthesis gas derived from coal).

This study therefore focuses on the synthesis of a β-Mo_2C catalyst that exhibits a high selectivity towards oxygenates under adapted Fischer-Tropsch conditions. The catalyst was subsequently exposed to ammonia gas co-fed along with synthesis gas, to study the effect on catalyst activity and product selectivity. The formation of any nitrogen-containing compounds at the expense of oxygenates was monitored. The scope of this study encompasses the synthesis of β-Mo_2C catalysts which are reported to form long chain oxygenates at high selectivities [18-22]. The catalysts were promoted with different levels of potassium to potentially further enhance oxygenate selectivity. Catalyst testing was conducted in a stainless-steel U-tube reactor where process conditions were optimized for high oxygenate selectivity. At a stable CO conversion and oxygenate selectivity, ammonia-gas was co-fed to the catalyst to study the conversion of oxygenates to nitrogen-containing compounds.

2 Literature review

2.1 The Fischer-Tropsch synthesis

The Fischer-Tropsch synthesis is a catalytic surface polymerization reaction producing paraffins, olefins and water as its major products from syngas (combination of CO and H_2). Minor side products are as alcohols, aldehydes, ketones and acids. The process was first described by Franz Fischer and Hans Tropsch in 1926 [7, 23-31] at the Kaiser Wilhelm Institute for Coal Research in Germany, after the pioneering work from Sabatier and Senderens describing the catalytic formation of methane from carbon monoxide and hydrogen [32, 33].

The first step of the Fischer-Tropsch process is the production of syngas from a carbonaceous feedstock such as coal, natural gas or biomass. A crucial necessity of these feedstocks is that they contain carbon bound to hydrogen which can be reformed to synthesis gas. In case no hydrogen is present in the feedstock, hydrogen could be extracted from water via electrolysis or thermal water splitting, however energy would be required to split the molecule [6].

Depending on the feedstock, production of syngas can be achieved via one of the two major methods i.e. gasification or reforming. Gasification is the reaction of organic matter or fossil fuels (such as coal) with a controlled amount of oxygen at high temperatures (±1200 °C), without combustion taking place, into CO, CO_2 and H_2 mixtures. The final H_2/CO ratio obtained from the gasification of coal is about 1.8 [1].

The reforming process includes several technologies, such as steam reforming (eq. 2.1) and dry reforming (eq. 2.2). Steam reforming of natural gas, which has become abundant through the discovery and utilization of shale gas globally in addition to conventional natural gas reserves which consist mostly out of CH_4, is the most common reforming method to produce hydrogen and carbon monoxide [34, 35]. Steam reforming is operated in several different types of reactors: adiabatic pre-reformers, tubular or primary steam reformers and numerous types of heat exchange reformers [6]. These reactors combust part of the feedstock to generate heat for the endothermic reaction. To avoid dilution with nitrogen, the combustion is conducted with a pure oxygen stream and not with air. Air separation is however an expensive technology and therefore it is currently the most expensive part of a FT plant, accounting for about 60-70% of the total investment costs [1, 2]. A common side reaction of steam reforming is the water-gas-shift (WGS) reaction, producing CO_2, which is undesired (eq. 2.3). Therefore, the dry-reforming process has gained interest in recent years, as it replaces steam as a reactant with CO_2, reducing greenhouse gas emissions. However, a lack of catalyst stability has so far prevented the technology from industrialization.

Another possible way to produce syngas is the use of adiabatic oxidative reforming (eq. 2.4), which includes homogenous reactions, heterogenous reactions and a combination of the two. In adiabatic oxidative reforming, the heat is provided from within the reaction by combustion of part

of the reactants. The type of feed into the reaction characterizes the process used. If the feed is coming directly from a desulphurization unit or a pre-reformer, the reaction is performed homogenously without a reforming catalyst and can therefore be called gasification or non-catalytic partial oxidation. In case of using a heterogenous catalyst, the reaction is called catalytic partial oxidation. A combination of the two, where the reaction starts homogenously followed by a heterogenous catalytic reaction, it is called autothermal reforming [35].

$$CH_4 + H_2O \leftrightarrow CO + 3H_2 \quad \Delta H^\circ = +\ 206\ \text{kJ/mol} \qquad (2.1)$$

$$CH_4 + CO_2 \leftrightarrow 2CO + 2H_2 \quad \Delta H^\circ = +\ 247.1\ \text{kJ/mol} \qquad (2.2)$$

$$CO + H_2O \leftrightarrow CO_2 + H_2 \quad \Delta H^\circ = -\ 41.2\ \text{kJ/mol} \qquad (2.3)$$

$$CH_4 + \frac{1}{2}O_2 \leftrightarrow CO + 2H_2 \quad \Delta H^\circ = -\ 35.9\ \text{kJ/mol} \qquad (2.4)$$

A further consideration in the production of syngas, is the removal of impurities that could poison the Fischer-Tropsch catalyst. Should the feedstock contain high concentrations of impurities (heteroatoms beyond C and H) these must be removed at a great expense. As an example, sulphur (S) compounds are well known catalyst poisons having a negative impact on their activity, selectivity and lifetime. Although S impurities could be present in very low concentrations, which makes it hard to detect, it would still be sufficient to harm catalyst performance. Acceptable amounts of S compounds differ per catalyst and reaction (conditions), but in purified synthesis gas the concentration requirements have been reported to be below 1 mole ppm [34, 36-38].

The prepared and cleaned synthesis gas stream is led over a transition metal catalyst and reacts in a highly exothermic surface polymerization type reaction to mainly straight chained paraffins and olefins (branched species are also formed at lower concentrations) as well as water. Side products, in their quantity depending on reaction conditions and catalyst material chosen, include alcohols, aldehydes, ketones, carboxylic acids as well as aromatics.

Hydrocarbon formation during the FT synthesis process involves multiple steps with several intermediates. These steps can be summarized as followed [7]:

1. CO adsorbs on the surface of the catalyst
2. 2 H_2 molecules adsorb dissociatively on the surface of the catalyst
3. Adsorbed CO reacts with the H_2 (at a certain moment in the reaction it splits, depending on the proposed mechanism, which is described in detail in section 2.1.1)
4. 2 H* and O form water and desorb.
5. C on the surface is hydrogenated
6. Hydrogenated species on the surface form new C-C bonds

The major products are n-paraffins (eq. 2.5) and α-olefins (eq. 2.6). Minor products are oxygenates (eq. 2.7) and branched hydrocarbons [6].

$$nCO + (2n+1)H_2 \rightarrow C_nH_{(2n+2)} + nH_2O \qquad \Delta H^\circ = -346.6 \text{ kJ/mol (for n = 2)} \quad (2.5)$$

$$nCO + 2nH_2 \rightarrow C_nH_{2n} + nH_2O \qquad \Delta H^\circ = -210.2 \text{ kJ/mol (for n = 2)} \quad (2.6)$$

$$nCO + 2nH_2 \rightarrow C_nH_{2n+1}OH + (n-1)H_2O \qquad \Delta H^\circ = -255.6 \text{ kJ/mol (for n = 2)} \quad (2.7)$$

In addition to the reactions of H_2 and CO, carbon monoxide can also be converted with the product water in the WGS to CO_2 and H_2 (eq. 2.3) [6]. Catalysts which support the WGS reaction under FTS conditions therefore influence the synthesis gas composition reducing the CO content in favour of H_2.

Another possible side reaction is the Boudouard reaction (eq. 2.8). Two CO molecules react and form CO_2 and carbon depositions on the surface of the catalyst (which could potentially cover active sites and/or block transport pores thus contributing to catalyst deactivation, see section 2.1.4).

$$2CO \leftrightarrow C + CO_2 \qquad \Delta H^\circ = -172.5 \text{ kJ/mol} \quad (2.8)$$

Like the WGS reaction, this reaction increases the CO consumption and consequently increases the H_2:CO ratio. A higher hydrogen content in the reactant gas also affects the availability of H* and carbonaceous species on the catalyst's surface, in turn supporting the hydrogenation activity. This leads to a decrease in chain growth, producing shorter hydrocarbon chains [39], and an overall more paraffinic product.

Iron-based catalysts are known for their high WGS-activity which influences the H_2:CO ratio in the synthesis gas as hydrogen is produced and CO consumed. This makes iron based catalysts suitable for hydrogen lean synthesis gas mixtures as are obtained from the gasification of coal [1]. However, at higher reaction temperatures, the water-gas-shift reaction could approach equilibrium (Figure 2-1). In this case, CO_2 can act as a reactant, depending on the prevailing gas composition, favouring the reverse water-gas-shift reaction. Cobalt-based catalysts' WGS-activity is usually much lower producing only small amounts of CO_2 [6].

Besides iron and cobalt; nickel and ruthenium are also typical Fischer-Tropsch catalysts [7]. Ruthenium is the most active of all four and is suitable for low reaction temperatures (150 °C). Due to its high cost, it is however unfeasible for application in the industrial environment [3]. Nickel is also highly active, however, at high pressures and low temperatures, nickel forms volatile nickel carbonyl [40]. At higher temperatures, mostly methane is formed. Nickel is known to be a catalyst for commercial methanation plants [7].

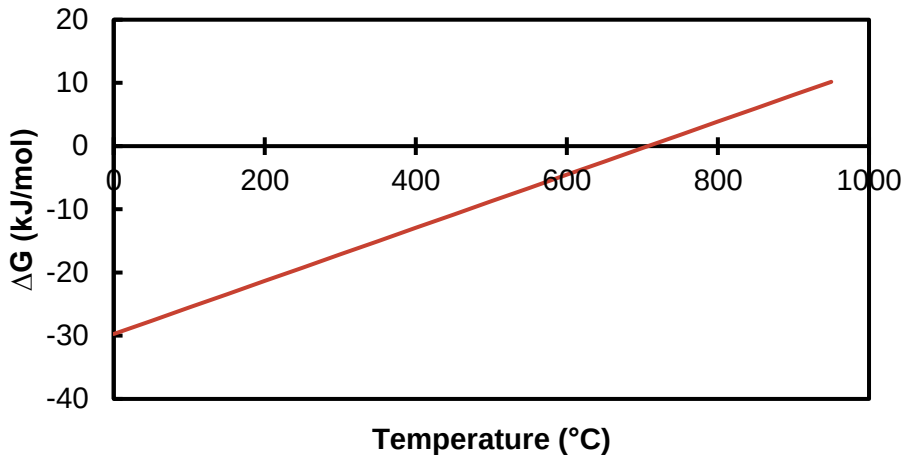

Figure 2-1: Gibbs free energy of the water-gas-shift reaction. Thermodynamic data is taken from [41].

Two different FT-operation modes are commonly used commercially. Low temperature Fischer-Tropsch synthesis (LTFT) at about 200-240 °C and high temperature Fischer-Tropsch synthesis (HTFT) at about 300-350 °C. It was shown that FT reactions are highly exothermic and at large scale plants it is a necessity to remove the heat from the catalyst, to avoid overheating. Flowing high linear space velocities through long narrow tubes achieving turbulent flow, or operating fluidized bed reactors, is required to gain high rates of heat exchange. In general, the fixed fluidized bed reactor (FFB) and the circulating fluidized bed reactor (CFB) are used for the HTFT, where the use of a tubular fixed bed reactor or slurry bed reactor is suitable for LTFT. The choice of operating system depends on the required products. LTFT is generally used to produce long chain hydrocarbons, such as wax. This process is suitable for iron and cobalt catalysts. HTFT produces mainly short chain hydrocarbons and olefins. Only iron is suitable at these conditions as the hydrogenation activity of Co based catalysts dominates over chain growth at higher temperatures [6].

The first large scale Fischer-Tropsch plant was launched in Oberhausen, Germany, in 1936. A capacity of 660 000 tons of primary product was reached in Germany just two years later. The initial cobalt based catalyst ($Co/ThO_2/MgO$/kieselguhr, 100/5/8/200) and syngas produced from coal were used in fixed bed reactors [6, 42]. In 1955 Sasol built the first Fischer-Tropsch plant in South Africa, based on the technology proposed by ARGE (Arbeitsgemeinschaft Ruhrchemie und Lurgi) using a fixed bed reactor, and Kellog, using a circulating catalyst bed. The discovery of huge oil reserves in the Middle East did not favour the profitability of the large plants, however, the process survived due to the production of high priced FT waxes. In 1980 and 1982 SASOL launched a second and third plant, respectively, due to a sharp increase in crude oil prices during the oil crisis in the 1970s. During the oil embargo against South Africa in 1987, coal was their only source to produce liquid fuels. Operating with fluidized bed reactors, the main products of the two plants were ethylene, gasoline and diesel fuel.

Other operating industrial plants were established in [1, 3, 43]:

- Mossgas GTL, PetroSA, South Africa (1992); syngas from off-shore natural gas; using circulating fluidized bed FT reactors; producing mainly gasoline and diesel fuel.
- Bintulu GTL, Shell, Malaysia (1993); syngas produced by non-catalytic partial oxidation of CH_4; using cobalt based fixed bed reactor; producing high quality diesel fuel and waxes.
- Oryx GTL, SASOL, Qatar (2007); liquid petroleum products from natural gas using iron based low temperature slurry bed reactors.
- Pearl GTL, Shell, Qatar (2011), the world's largest gas-to-liquid (GTL) plant; producing 120,000 barrels per day of natural gas liquids and ethane using a cobalt based catalyst.
- Escravos GTL, CNL, Nigeria (2014); a GTL plant using natural gas as carbon source. Production is focused on premium environmentally friendly fuel, diesel and GTL naphtha products.

The profitably of the FT plants is highly dependent on the global price of crude oil, which has significantly fluctuated since 1970 (Figure 2-2). The second and third Sasol plants came on-line on the exact same period when the price of crude oil was above US$ 30,00 per barrel. The plants launched from 1985 were on stream while the oil prices were falling [1]. Over the last two decades the crude oil price continued its fluctuations significantly. Between 2000 and 2008 the annual average crude oil price rose from US$ 27.39 to US$ 91.48, with a high of almost US$ 150 (inflation adjusted) in June 2008. This was mainly due to the emerging economies in China and India, increasing its demand and a lack of production in the Middle East. The steep drop right after happened because of a deep global recession. Recovery from the economic recession helped the oil price to increase again back to an annual average between US$ 71-91. This lasted until 2014, when again a steep drop was observed. Several reasons were found for this sudden drop. The same countries that were the cause of the increase between 2000 and 2008, showed a significant drop in the population growth rate, with a lower demand in oil. With China being the world's largest population, the lower demand in oil has a significant effect on its price. Other countries showing the same trend were Russia, India and Brazil. The United States and Canada started producing their own oil from several resources such as oil sand, which lead to a significant drop in the oil import. At the same time, Saudi Arabia did not cut its conventional and cheaper oil production, supporting the rapid decrease in oil price and tried in this way to make the oil productions in Canada and the U.S. less economical.

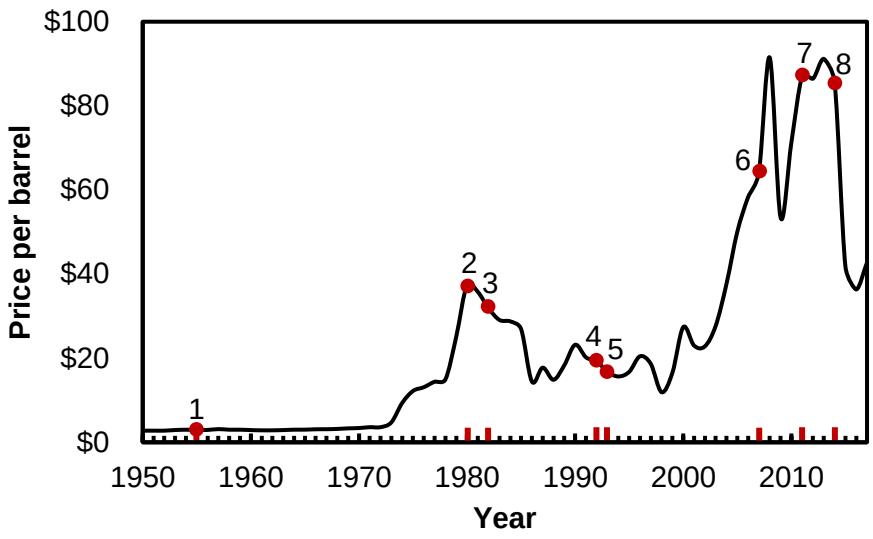

Figure 2-2: Annual average crude oil prices (nominal prices) with launching of commercial FT-plants: 1) Sasol 1; 2) Sasol 2; 3) Sasol 3; 4) Mossgas; 5) Bintulu GTL; 6) Oryx GTL; 7) Pearl GTL; 8) Escarvos GTL. Figure is adapted from McMahon (2017) [44].

2.1.1 Fischer-Tropsch reaction mechanisms

The reaction pathway in the Fischer-Tropsch synthesis is a complicated and intricate network of different surface reactions, performed on different catalyst surfaces (e.g. the bulk of the catalyst ranges from interstitial metals to pure metals, with a variety of possible metal oxides as support material), together with a wide range of process conditions (such as temperature, pressure and reactor system). Therefore, several aspects of the FTS mechanism are not fully understood and it is unlikely that only one mechanism is present/dominating the FTS [45]. Extensive research in the field has however lead to several proposed pathways. All proposed mechanisms have in common that they follow a surface polymerization type process, which includes the following steps:

1. Adsorption of reactants on the surface of the catalyst
2. Formation of a monomer and a chain starting species (e.g. initiation)
3. Chain formation and its growth (e.g. propagation)
4. Chain termination followed by product desorption

Four of the most common mechanisms proposed for the primary reactions taking place in the Fischer-Tropsch synthesis will be discussed in the following; the alkyl, alkenyl, enol and CO-insertion mechanism [5]. The word primary already indicates that also secondary reactions occur in the FTS. Some of the products produced during the primary reactions (e.g. α-olefins, paraffins and oxygenates) can re-adsorb onto the surface of the catalyst and undergo several reactions (hydrogenation, isomerisation, re-insertion, hydrogenolysis and hydroformylation) forming

secondary FTS products, such as internal olefins and additional paraffins. These secondary reactions can have a significant influence on the product spectrum [46].

The ***alkyl mechanism***, originally proposed by Fischer and Tropsch [26] (Figure 2-3) involves the dissociative adsorption of CO on the catalyst surface forming separate adsorbed surface C and O species. Hydrogenation forms H_2O and CH to be followed by CH_2 (monomer) and CH_3 (chain initiator), as surface species. DFT studies have shown that the formation of water is difficult and slow, notably the step from OH + H → H_2O (1.6 eV barrier on a cobalt catalyst) [47, 48]. Chain growth occurs via the reaction between the surface monomer and the chain initiator (now indicated as 'R', as the process of chain initiation and further growth is identical). Products are formed by either addition or abstraction of hydrogen on the α or β carbon, producing n-paraffins and α-olefins respectively. The formation of n-alcohols cannot be explained by this mechanism but the addition of surface hydroxyl species into the alkyl chain has been suggested to occur for the formation of n-alcohols [49].

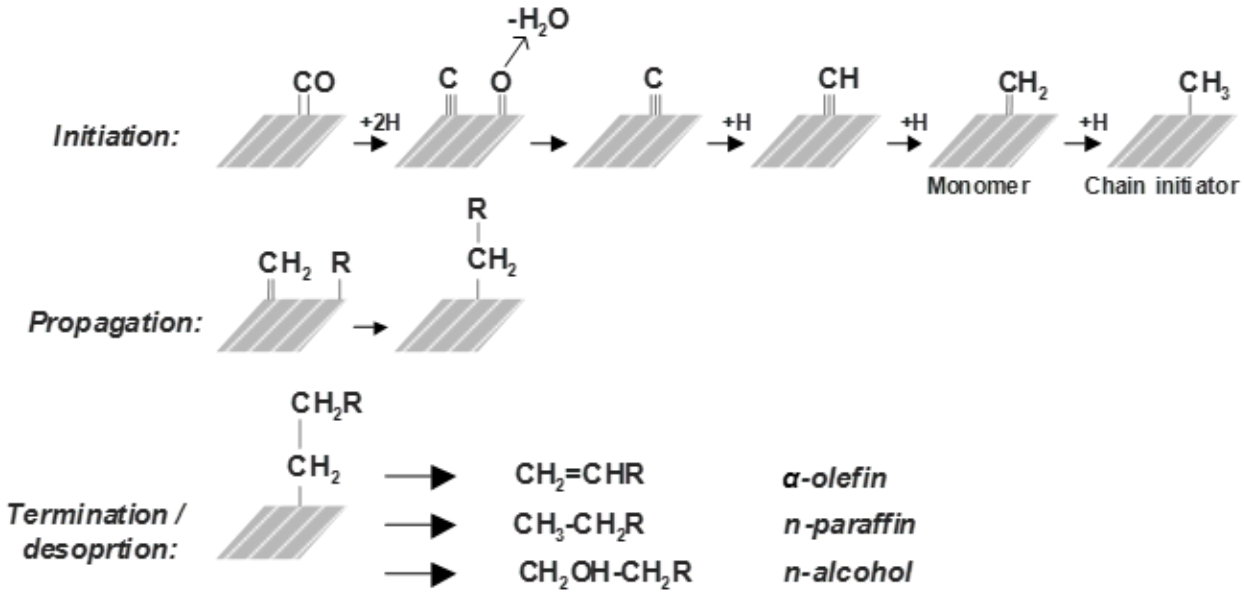

Figure 2-3: The proposed alkyl mechanism. Figure is adapted from van Steen and Claeys (2004) [5].

Branched hydrocarbons (Figure 2-4) cannot be explained by the main reaction mechanism of the alkyl mechanism. A surface reaction of alkylidene and methyl species has been proposed for their formation [50, 51]. Another possibility is that the primarily formed α-olefins re-adsorb on the catalyst surface via the β carbon and undergo secondary reactions forming branched hydrocarbons [52].

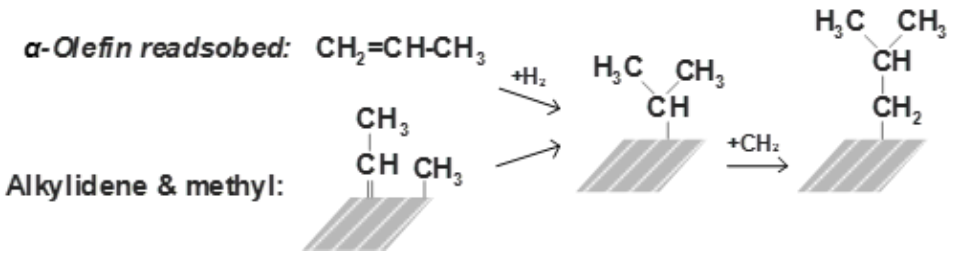

Figure 2-4: Proposed mechanisms for the formation of branched hydrocarbons. Figure is adapted from van Steen and Claeys (2004) [5].

The initial steps of the ***alkenyl mechanism*** (Figure 2-5), proposed by Maitlis *et al.* (1996) [53] are identical to the alkyl mechanism. However, a vinyl group is recognized as the chain initiator, formed by the combination of a CH with the monomer CH_2 surface species. The propagation step is completed by a reaction of the vinyl species with an additional monomer, forming surface allyl species. Subsequently, double bond isomerization of the allyl and vinyl surface species produces alkenyl species. Hydrogenation of the alkenyl species forms the α-olefin products [54].

The formation of n-paraffins as primary product cannot be explained by this mechanism. In order to form these products, it would need a second parallel or consecutive reaction mechanism [55].

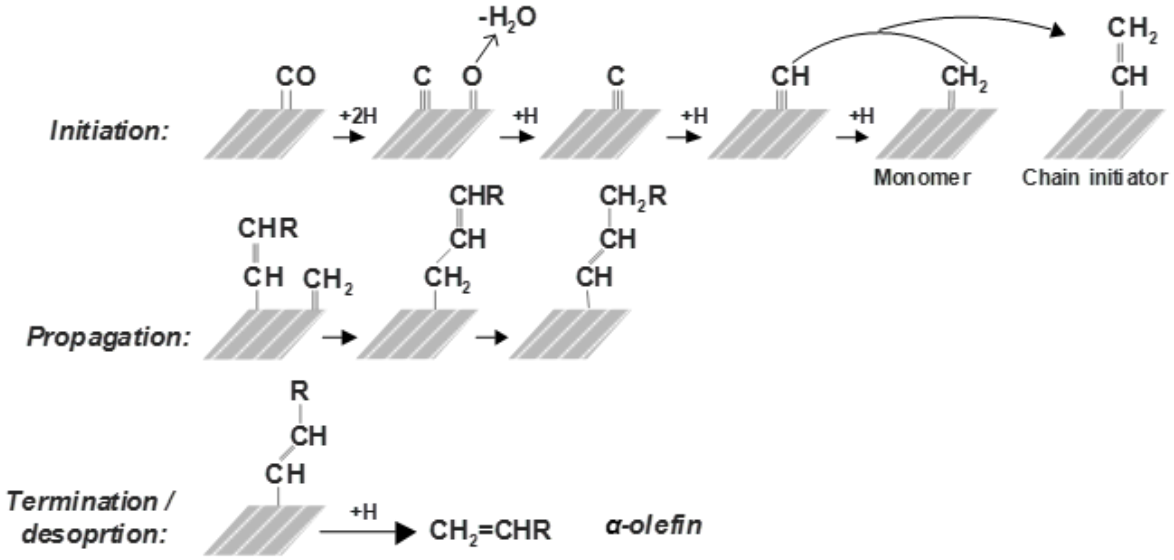

Figure 2-5: The proposed alkenyl mechanism. Figure is adapted from van Steen and Claeys (2004) [5].

The formation of oxygenates can be rationalized by the ***enol mechanism*** (Figure 2-6). CO chemisorbed on the catalyst surface is hydrogenated to enol species. Combination of two enol species forms water and an intermediate CH_2ROH. The intermediate can be the start of the formation of branched hydrocarbons. However, n-paraffins as a primary product cannot be rationalized with this mechanism. Termination of the chain yields oxygenates and α-olefins. N-paraffins can be formed in a secondary reaction step through the hydrogenation of re-adsorbed olefins [56].

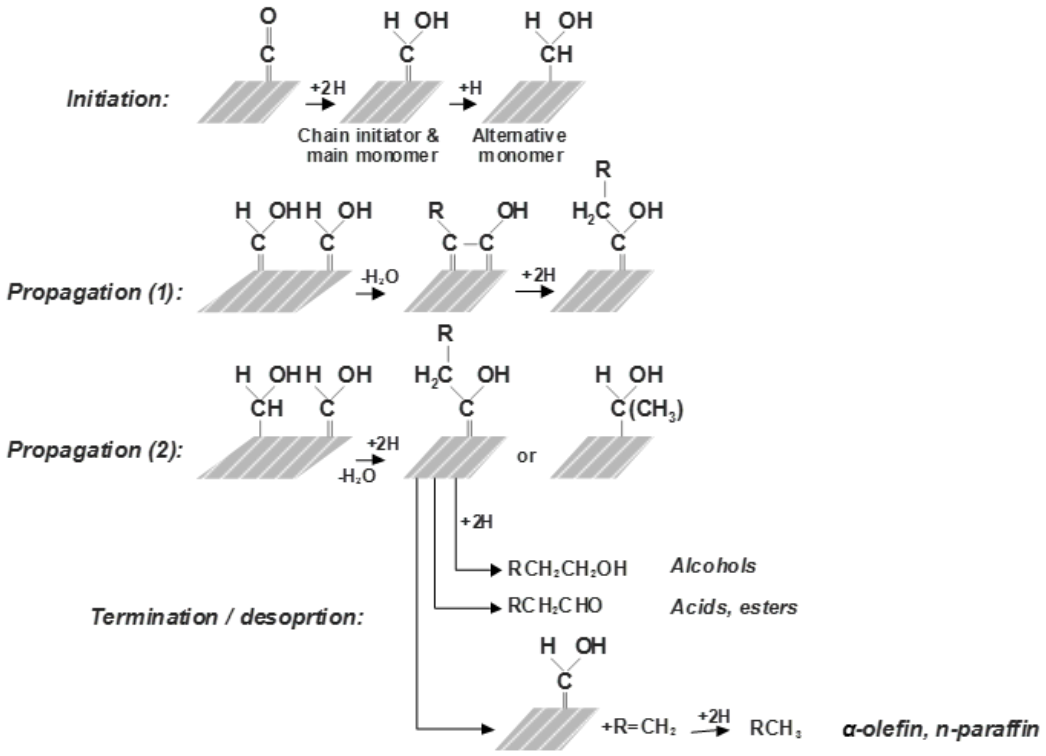

Figure 2-6: Proposed enol mechanism. Figure is adapted from van Steen and Claeys (2004) [5].

A well-known route to form oxygenates is the ***CO-insertion mechanism****,* originally proposed by Sternberg and Wender (1959) [57] and Roginski (1965) [58] but fully refined by Pichler and Schulz (1970) [59]. After hydrogenation of the chemisorbed CO on the catalyst surface, it forms a surface methyl species (chain initiator). The chain grows by CO-insertion followed by hydrogenation and water formation. Different desorption pathways form n-paraffins, α-olefins and oxygenates (Figure 2-7). Hindermann *et al.* (1993) [60] mentioned that up to now real evidence supporting the CO insertion mechanism comes from studies on homogeneous rhodium catalysts [61, 62].

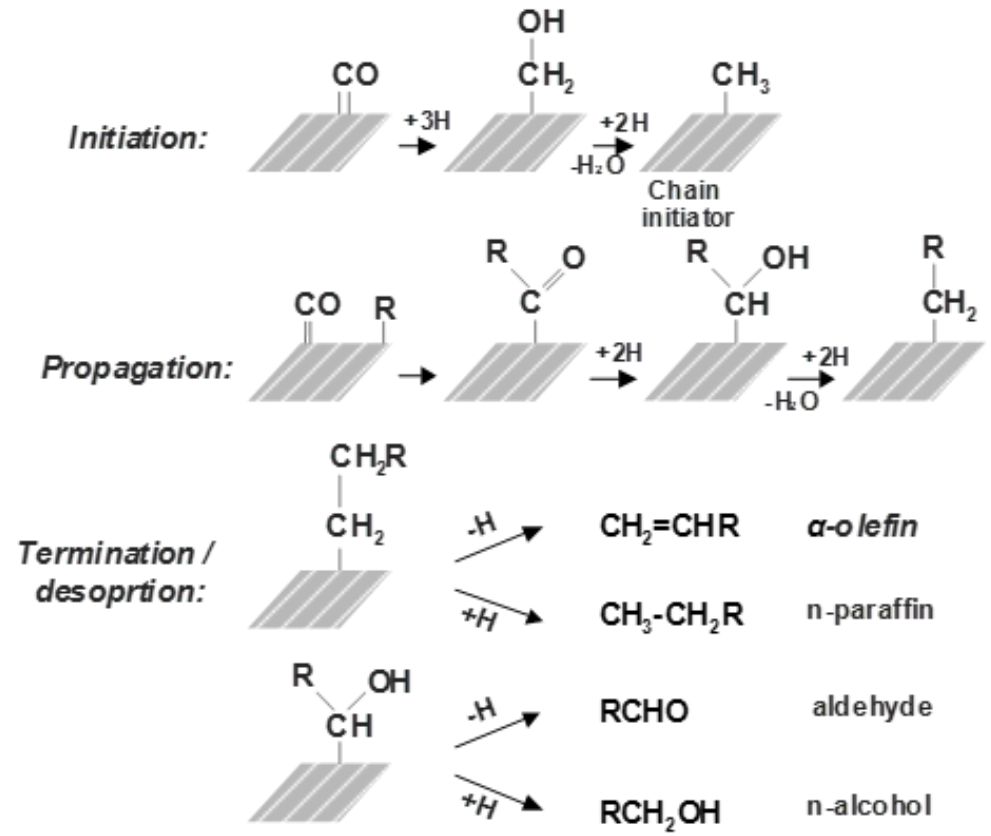

Figure 2-7: Proposed CO-insertion mechanism. Figure is adapted from van Steen and Claeys (2004) [5].

2.1.2 Current views on the FT-mechanisms

The four proposed mechanisms introduced in the previous section are a good indication of what can happen during the Fischer-Tropsch synthesis, however, they are not fully accepted in the research community. Some recent studies elaborating on potential mechanisms were published by Weststrate *et al.* (2016) [63], [64, 65] and Ledesma *et al.* (2014) [66].

Weststrate *et al.* (2016) [64] studied the chain growth mechanism on a Co catalyst. In the alkyl mechanism described earlier, the new chain is initiated by the surface reaction of the chain initiator (*CH_3-species) with the monomer (*CH_2-species), forming a *CH_2CH_3 surface species. In an earlier publication Weststrate *et al.* (2014) [65] proposed the alkylidene mechanism, basically showing that CH is the most stable C_1H_x species on many metal surfaces, including Co(0001). The chain is subsequently initiated by CH + CH → CH=CH, again the most stable C_2H_x species on Co(0001). The initiating step is continued with a hydrogenation to ethylidyne. Further chain growth is likely to happen by the insertion of CH into the C_2H_3 species, forming propyne, which is again the most stable C_3H_x species on Co(0001). Another hydrogenation step converts the propyne into propylidene, and so it can continue growth (Figure 2-8). Termination is via hydrogenation, in one or multiple steps. Either the alkylidyne or the alkyne is thus hydrogenated to alkanes or alkenes [63-65].

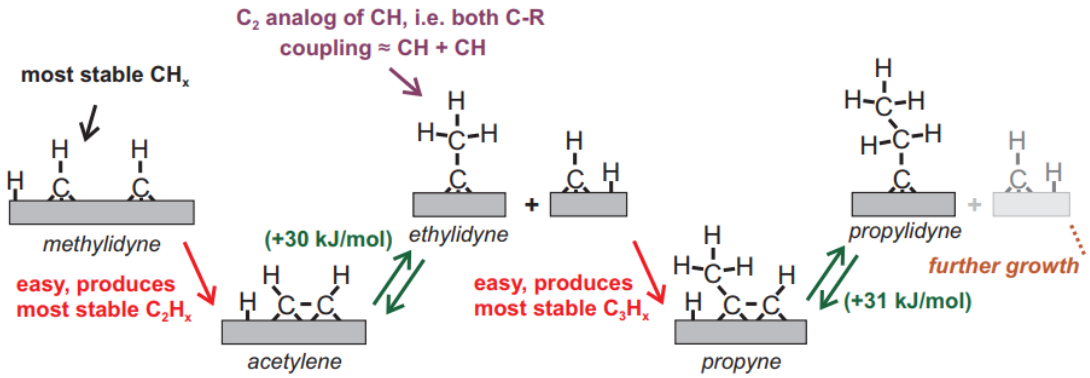

Figure 2-8: Proposed alkylidene mechanism, figure adapted from Weststrate et al. (2014) [65].

Ledesma *et al.* (2014) [66] presented a review article on the use of Steady-State Isotopic Transient Kinetic Analysis (SSITKA), which is found to be a very powerful technique to study heterogenous catalyzed reactions, close to the molecular level. The technique was developed by Happel, Bennett and Biloen [67-69]. One of the main findings regarding the FTS was reported by van Dijk *et al.* (2001) [70] who proposed a mechanism where C_x and CH_x species are the active C_1 species, being the chain initiator. Chain growth proceeds by forming reactive C_2 species such as C_2H_x, which could be extended to C_3 species. Yang *et al.* (2013) [71] published DFT calculations together with the SSITKA method, determining the equilibrium constants of CO and H_2 adsorption under methanation conditions over a catalyst containing 20 wt.% Co supported on carbon nanotubes. It was observed that the CO activation proceeds by hydrogen-assisted CO dissociation, leading to two different carbon intermediates, CH_2O^* and CH_x^*, with two reaction pathways for the formation of methane (Figure 2-9).

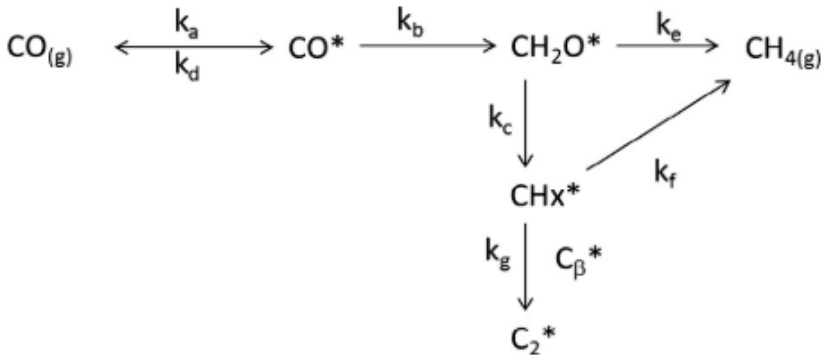

Figure 2-9: Proposed methane formation mechanism. Figure is adapted from Yang et al. (2013) [71].

2.1.3 Fischer-Tropsch products

The main Fischer-Tropsch products are n-paraffins and α-olefins, with side products such as oxygenates and branched compounds. The product distribution depends on several parameters such as reactor type, pressure, temperature, time on stream, syngas composition and the actual

catalyst used. Independent of the conditions applied, the Fischer-Tropsch product spectrum always follows a certain pattern. This is due to the stepwise formation of products (as explained in section 2.1.1) which can be desorbed after each growth step. A common term used for the explanation of this process is the chain growth probability (α), which can be expressed as the rate of chain growth (r_g) related to the rate of product desorption (r_d):

$$\alpha = \frac{r_g}{r_g + r_d} \quad (2.9)$$

If assumed that the formation of products follows an ideal polymerization reaction (Figure 2-10), which can be expressed mathematically with the Anderson-Schulz-Flory (ASF) distribution:

$$\log\frac{W_{N_c}}{N_c} = N_c \cdot \log\alpha + \log\frac{1-\alpha}{\alpha} \quad (2.10)$$

Where W_{N_c} is the weight fraction of a product with a certain carbon number (N_c).

The ASF-distribution specifies that the Fischer-Tropsch synthesis is an unselective process, where the molar content of the products decreases exponentially with an increase in carbon number. The selectivity towards methane is always the highest but is also the only product that can be formed with a 100% selectivity, at certain operating conditions resulting in a chain growth probability of zero.

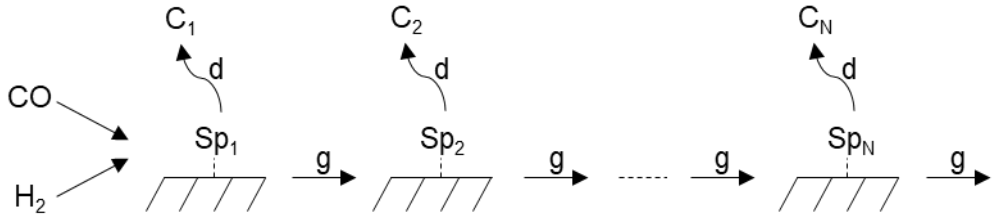

Figure 2-10: Ideal product formation (C_N) describing the chain growth mechanism forming one product class from its surface species (Sp) (N: carbon number, g: growth, d: desorption). Figure is adapted from van Steen and Claeys (2004) [5].

However, as discussed earlier, the reaction mechanisms above showed a wide variety of products (Figure 2-7), which involve secondary reactions by re-adsorption of previously formed products (α-olefins and oxygenates). All these different products have different desorption behaviors which means that they also have potentially different chain growth probabilities. If we combine all the above in a schematic as in Figure 2-10, the chain growth of the different products can be explained (Figure 2-11). Experimentally known deviations to the ideal ASF-distribution are higher methane and lower ethane concentrations and a different α-value at higher carbon numbers [5].

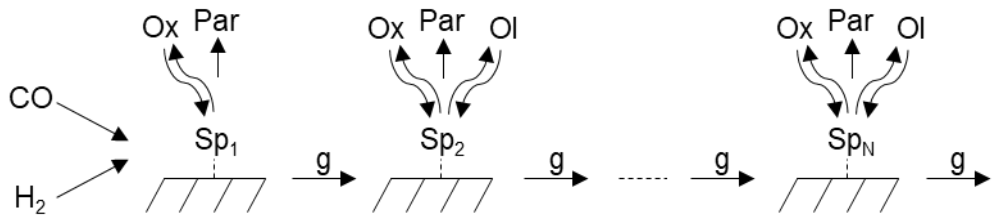

Figure 2-11: Description of the product formation and distribution of the oxygenates (Ox), paraffins (Par) and olefins (Ol) on one class of surface species (Sp), with N = carbon number and g = growth. Figure is adapted from van Steen and Claeys (2004) [5].

Reaction conditions directly affect the chain growth probability and product composition. An increase in temperature increases the desorption rate yielding more short chain hydrocarbons. Increasing the H_2 to CO ratio in the feed gas enhances hydrogenation also leading to more short chain hydrocarbons. Besides that, it also increases secondary product hydrogenation leading to a higher total amount of paraffins at the expense of the olefins and oxygenates. Higher temperature enhances chain branching and carbon deposition, with the latter being further supported at low H_2 to CO ratios. An increase in space velocity would also decrease chain growth probability due to the shortened residence time. A summary of these effects is given in Table 2-1.

Table 2-1: Influence of operating conditions on the product distribution within the FTS. With '+' = increase with increasing parameter, '-' = decrease with increasing parameter and '~' = no clear effect. Table is adapted from Claeys (1997) [72].

	Temperature	Pressure	H_2:CO	Residence time
CH_4 selectivity	+	-	+	+
Chain growth	-	+	-	~
Chain branching	+	-	~	~
Olefin selectivity	~	~	-	-
Oxygenate selectivity	-	+	-	-
Carbon deposition	+	~	-	~

2.1.4 Catalyst deactivation

A major issue in the use of heterogenous catalysts is the loss of activity with time on stream, e.g. the limited lifetime of a catalyst. Depending on the type of catalyst and process, the lifetime of a catalyst has shown to vary between seconds and years [73, 74]. Several deactivation mechanisms have been identified. In Table 2-2 a short description is given of the main catalyst deactivation mechanisms. These changes to the surface of the catalyst are usually followed by a decrease in activity or alterations to the product selectivity. The previous described reaction mechanisms (Chapter 2.1.1) are disrupted or completely prevented from occurring.

Table 2-2: Catalyst deactivation mechanisms. Table is adapted from Bartholomew (2001) [73].

Mechanism	Type	Brief description
Poisoning	Chemical	Strong chemisorption of species on the catalyst surface, therefore blocking catalytic active sites
Fouling	Mechanical	Physical deposition of species from fluid phase onto the surface of the catalyst and pores
Thermal degradation	Thermal	Thermally induced loss of catalytic surface area, support area and active phase-support reactions
Vapor formation	Chemical	Reaction of gas with catalyst phase to produce volatile compounds
Vapor-solid and solid-solid reactions	Chemical	Reaction of fluid, support or promoter with catalytic phase to produce inactive phase
Attrition/crushing	Mechanical	Loss of catalytic material due to abrasion; loss of internal surface area due to mechanical-induced crushing of the catalyst particle

Poisoning is a classic example within the catalytic synthesis gas conversion, which needs to be purified from poisonous compounds that strongly chemisorb on the active sites of the catalyst and then have an electronic or spatial influence on the adsorption capacity of other species [75]. Poisons can be classified as selective or non-selective. Non-selective poisons can chemisorb on all sites available, thus the loss of activity is in a linear relationship to the amount of poison chemisorbed. Selective poisons selectively chemisorb on certain sites of the catalytic surface, potentially resulting in complex relationships between the loss of activity/selectivity and the amount of poison chemisorbed [76]. Another classification possible within poisonous compounds is between reversible and irreversible poisons. If the poisonous compound is not too strongly adsorbed on the surface, it can usually be regenerated by simply removing the poison from the feed. For example, iron based catalysts used for ammonia synthesis adsorb oxygen containing compounds, such as water and CO. These species block the active sites for N-adsorption which limits the catalytic activity. Removal of the oxygen containing compounds and a subsequent reduction treatment with hydrogen, removes these species from the iron surface. An example of irreversible poisoning is the generally rapid and strong adsorption of sulfur compounds on CO hydrogenation catalysts [73, 76].

Carbon deposition or ***coking*** is a form of the deactivation mechanism fouling. As it was described in the Boudouard reaction (eq. 2.8), which is one of the possible side reactions in the FTS, carbon can be deposited on the surface of the catalyst, blocking active sites and pore mouths. Catalysts known for carbon deposition are iron, cobalt and nickel. The type of carbon deposited on the catalytic surface is very dependent on the temperature in which the carbon deposition takes place. A variety of carbon types have been found on the surface, such as surface carbide, amorphous

carbon and graphitic carbon. Nickel is a catalyst that can in addition suffer from carbon deposition by decomposing CO [75, 77].

Thermal degradation/sintering is a form of deactivation that is induced by temperature. High catalytic surface areas are generally facilitated by small crystallite sizes, well dispersed particles over a support material by the formation of porous compounds or a combination thereof. High temperature can affect these characteristics by, for example, sintering of catalyst particles, leading to bigger particles and thus smaller specific surface areas. The growth of the metal particles can include crystallite migration or atomic migration. The support material could also collapse/sinter, which leads to loss of support area and thus less dispersed particles on the support [78].

Loss of active material can be observed if the catalytic material can form **volatile phases**, such as metal carbonyls, oxides, sulfides and halides under reaction conditions. Nickel and iron carbonyls are formed at relatively low temperatures but require high pressures. Halides are quickly formed in the presence of halogens at low temperatures. The probability for the formation of volatile oxides is very dependent on the catalyst material, between room temperature (ruthenium) and above 500 °C (platinum). Formation of sulfides has been observed using MoS_2 as catalyst, which requires co-feeding of H_2S for the higher alcohol synthesis (HAS) [75, 79, 80].

Vapor-solid interactions (chemical degradation), are commonly reported for the FTS on iron catalysts and more recently also for Co. Water is a major product in the FTS. High amounts of CO_2 can be formed at WGS-active catalysts, specifically during HTFT. The active phase of the iron catalyst, the carbide phase (Fe_5C_2), has shown to oxidize to the non-catalytic active phase, Fe_2O_3, in the presence of water vapor and/or CO_2 at high CO conversion, during the FTS [81].

Attrition is the mechanical breakage/crushing of catalyst particles, which is more likely in a reactor concept where the catalyst is in constant movement, such as fluidized or circulating bed reactors. The crushed particles can exit the reactor, carried away by the feed gas, which leads to a loss in catalytic activity. Expansion of the catalyst bed by, for example, excessive formation of carbon, can press the catalyst pallets against the reactor walls, which can lead to attrition [73].

2.1.5 Catalyst synthesis

There are multiple ways of preparing heterogenous catalysts, however, the most common types of catalysts used in the industry are; un-supported, supported and coated catalysts. Un-supported means that the catalysts consist only of the active phase(s). This concept is generally applied for the cheaper materials, such as iron. The more expensive materials are commonly applied on an inert support material, which maximizes the catalytic surface area, therefore a lower amount of material can be used. Examples are cobalt, ruthenium and rhodium. The coated catalyst can be imagined as a shape giving inert material on the inside with a very thin layer of catalytically active material around it.

The two main methods of preparing catalysts on an industrial scale are the precipitation and the impregnation technique [82, 83].

Precipitation of a heterogenous catalyst is done in the presence of a precipitating agent. The solid is formed from a homogenous solution after addition of the agent. The resulting ‘precipitate’ is treated and formed into the catalytically active material. Co-precipitation, a variation of the precipitation technique, makes it possible to form a bi-metallic catalyst or form the support and the active phase in one step. The obtained precipitates are usually amorphous hydroxides or carbonates and need to be washed to remove excess precipitation agent. Followed by a drying and heating step, the hydroxide/carbonates decompose to the metal oxides. This method can be used to prepare very small particles with high surface areas, however, it is very difficult to control the crystallite sizes [82].

During impregnation, a solution of the active material precursor is contacted with a solid support material, depositing the active material in the porous structure of the support, generally followed by a drying process and then calcination at elevated temperatures, to stabilize the material onto the support. This method is also a commonly used method for the introduction of promoters. Incipient wetness impregnation describes the synthesis when the volume of the metal solution is equal or lower to that of the pore volume of the support. Wet impregnation is done by using an excess amount of the metal solution. After a certain time the excess solvent is removed by a drying step [83].

2.2 Increasing Fischer-Tropsch product value

The commercial Fischer-Tropsch synthesis is focused on the production of waxes and transportation fuels and hence, its profitability is highly dependent on the global oil price, as it is continuously competing with fuels derived from crude oil [1]. It is therefore of interest to investigate catalysts that display a higher selectivity towards the more valuable products of the FTS, such as long chained (C_{2+} carbon number) alcohols, aldehydes and carboxylic acids. These oxygenated compounds are well reported by-products of the Fischer-Tropsch synthesis [60].

2.2.1 Higher alcohol synthesis

Producing long chained oxygenates (e.g. higher alcohol synthesis) at high selectivity, has been of interest for many years for several different reasons. In the past two decades, a lot of research has been focused on producing cleaner gasoline. Gasoline engines require a certain octane number (ON), which is defined as the volumetric percentage of iso-octane in the gasoline. To put it in perspective, pure iso-octane has an ON of 100 and *n*-heptane an ON of 0. A high octane number in the gasoline (usually ON of 93-97) prevents its engine from ‘’knocking’’ (premature burning of the fuel in the combustion chamber causing a small explosion in the engine before the piston has achieved full compression). Initially, the increase of the octane number was achieved by adding lead containing compounds such as tetraethyl lead to the gasoline [84]. However, the environmental protection agency (EPA) called for reducing lead concentrations in gasoline as lead is a pollutant and poison. Nowadays, the octane number in gasoline can be increased by the addition of aromatic hydrocarbons or oxygenates. The use of aromatics produces more particulates, smog, as well as an increase of released benzene to the atmosphere, which is known as a carcinogenic compound [85]. Methyl tert-butyl ether (MTBE) is also known to increase the ON however, the addition of MTBE has shown to contaminate water resources [86]. Oxygenates added to the gasoline help to combust the fuel to a higher degree due to the additional presence of oxygen. Therefore, it increases the efficiency of the combustion process and reduces the emission of pollutants into the air. Pure ethanol has an octane ratio of over 100, thus for example, 84 octane gasoline can be blended with 10 percent ethanol to reach the minimum requirement ON of 87 (based on US-values) for retail gasoline [86, 87].

The commercial Fischer-Tropsch plants produce a low amount of oxygenates relative to the produced hydrocarbons. For example, the iron-based HTFT Sasol plant’s typical selectivity towards oxygenates is around 6% on a carbon basis [5, 88].

2.2.2 Catalysts used for higher alcohol synthesis

An increase in selectivity towards higher alcohols has previously been investigated by using a wide variety of catalysts, such as noble metals, modified methanol catalysts [89, 90], modified Fischer-Tropsch catalyst and alkali-doped molybdenum catalysts. Earlier it was mentioned that only iron and cobalt are used for commercial Fischer-Tropsch plants due to the high costs of other

FT-active catalysts, such as the noble metals rhodium and ruthenium. However, targeting the formation of higher alcohols, leading to an increase in product value, can offset the investment into more expensive metals. In that case the noble metals are usually supported on certain oxides, such as SiO_2, Al_2O_3, CeO_2, ZrO_2 and MgO. Rhodium has shown to be a promising catalyst for high oxygenate selectivity. The most well-known examples are described in the patents by Union Carbide and the Sagami Chemical Company [91, 92]. Bhasin *et al.* (1978) [93] studied the conversion of syngas over silica supported rhodium and rhodium-iron catalysts varying the iron content in 2.5% rhodium on silica. It was observed that an increase in the H_2/CO ratio had a negative influence on the formation of higher alcohols. The addition of iron to the rhodium catalyst decreased methane formation while methanol and ethanol formation increased, becoming the major products. However, very little oxygenates larger than ethanol were formed. Hanaoka *et al.* (2000) [94] tested CO hydrogenation over modified and unmodified silica supported rhodium catalysts. They investigated the influence of particle size and the addition of alkali metal chlorides on the formation of oxygenates under high pressures. Increase in particle size showed an increase in CO conversion and a significant alteration in the product selectivity was observed. At crystallite sizes below 2 nm, methanol was the main product. As the crystallite size increased (up to 5.5 nm) the methanol selectivity dropped significantly. The optimum particle size for the formation of C_{2+} oxygenates (higher alcohols) was identified between 2.5 and 5.0 nm. Alkali addition in the form of LiCl had a positive effect on the formation of C_{2+} oxygenates.

The Institut Français du Pétrole (IFP) patented the production of a mixture of methanol and higher alcohols using copper-cobalt-alloy catalysts [95]. The functionality behind the alloy is based on the different roles the two metals have. Cobalt is generally observed to dissociate CO to eventually form hydrocarbons, following the classical ASF-distribution. This indicates that cobalt can form C-C bonds followed by chain growth of the hydrocarbon chains. Copper is known as a methanol synthesis catalyst, which can be explained by its characteristic non-dissociative activation of CO and inactivity for C-C bond formation. An alloy of the two metals can combine these properties, with cobalt forming the hydrocarbon group and copper adding the alcohol functionality. It has been proposed that the formation of dual sites of the two metals enables the catalyst to form carbon chains followed by CO-insertion [96]. These IFP-catalysts have shown high selectivity towards higher alcohols, with a very low amount of methanol produced. However, the catalysts have been shown to have low activity due to the suppression of hydrocarbon formation and to be unstable in the long term [97].

Matsuzaki *et al.* (1991) [98] has also shown that the addition of alkali metals to cobalt catalysts on a silica support enhances the formation of C_{2+} oxygenates. CO hydrogenation was performed using a fixed bed reactor with a H_2:CO ratio of 2 and a temperature range of 300-380 °C at 21 bar total pressure. They observed a significant drop in CO conversion, however simultaneously an increase in oxygenates upon addition of different alkali cations. The C_2/C_{3+} oxygenate ratio decreased and an increase in the olefin/paraffin ratio was observed. Ethanol and paraffins are

believed to be formed from acetaldehyde and olefins, respectively, and therefore it is suggested that the promotion of the catalyst with alkali metals reduces the catalyst's ability of hydrogenation.

As the previously mentioned investigations still use the more expensive metals, rhodium and cobalt, Gupta *et al.* (2011) [99] reviewed a less-expensive material suitable for higher alcohol synthesis and investigated the use of copper-based catalysts. Alkali metals were added to enhance the formation towards higher alcohols. Promising results have been observed at a temperature range of 280-310 °C at pressures between 40-100 bar. H_2/CO ratios below 2 favour the formation of higher alcohols, but reduced activities were observed. The effect of an optimum promotion of alkali compounds such as potassium seemed to be the most significant.

The use of an alkali doped molybdenum-based catalyst for the formation of higher alcohols is patented by Dow Chemical [100]. In general, molybdenum sulfide requires the co-feeding of H_2S for stability and the formation of higher alcohols. This leads to the formation of sulphur-containing compounds in the product stream. Molybdenum carbide has been investigated numerous times and was found to be highly active in CO hydrogenation and resistant to sulphur poisoning, therefore it has gained much interest for the formation of higher alcohols as well. Unpromoted molybdenum carbide has been shown to produce mainly hydrocarbons, however upon the promotion with alkali metals, it has been shown to significantly shift the selectivity towards oxygenates [19, 101-103]. A more detailed description of the use of molybdenum-based catalyst can be found in Chapter 2.4.

2.2.3 Influence of process parameters on higher alcohol synthesis

The choice of catalyst is not the only parameter that influences the formation of higher alcohols during the Fischer-Tropsch synthesis. Process conditions have been shown to have a significant influence on the formation of higher alcohols as well. The H_2:CO ratio, temperature of reaction, pressure in the reactor and space velocity of the feed gases over the catalyst have been investigated.

2.2.3.1 Influence of H_2:CO ratio

The ratio of hydrogen to carbon monoxide is an important parameter in the Fischer-Tropsch synthesis. A range of 0.5-5:1 has been reported in literature [1, 3, 5, 7, 8, 104]. If the water-gas-shift reaction is a favourable reaction at the conditions applied, it produces a high amount of H_2 which influences the initial H_2:CO ratio. In general, an increase the hydrogen content increases hydrogenation, thus the activity of the catalyst and lowers the coke formation (a form of deactivation). A larger amount of hydrogen in the reactant gas would increase the formation of short chain hydrocarbons and methanol. A low H_2:CO ratio will favour the CO insertion mechanism and thus increase chain growth probability and the formation of higher alcohols [99, 105]. Higher hydrogen content in the syngas could support hydrogen assisted CO dissociation, which can be followed by the alkyl or alkenyl mechanism, increasing the formation of hydrocarbons [106].

2.2.3.2 *Influence of temperature*

Higher temperatures increase the possibility of sintering of the catalyst, which lowers the active surface area resulting in a decrease in catalyst activity. Temperature has also a significant influence on the selectivity towards oxygenates and the product distribution in general. Increasing temperature has been shown in several studies to increase the formation of higher alcohols. For example Subramanian *et al.* (2010) [107] used unpromoted and promoted Rh/(V and/or La)/SiO_2, testing all catalysts at 230 °C and 270 °C. It was found that an increase in temperature increased the selectivity towards ethanol and higher alcohols at the expense of the formation of methanol. However, increasing temperature also increases the formation of hydrocarbons and CO_2, which could lead to an overall drop of total oxygenates [22, 99, 107, 108]. Thermodynamically, the formation of higher alcohols (eq. 2.11) is favoured (the more negative the value, the more spontaneous the reaction) over the formation of methanol with increasing temperature (Figure 2-12). Methanol reaches an equilibrium constant of 1 at around 140 °C, whereas the longer oxygenates reach an equilibrium constant of 1 at temperatures used for the Fischer-Tropsch reactions (>280 °C). Kinetically it is much more complicated, therefore still very much unknown, to explain the formation of higher alcohols (C_{2+}) and other oxygenates such as aldehydes, carboxylic acids or ketones [105].

$$nCO + 2nH_2 = C_nH_{2n+1}OH + (n-1)H_2O \qquad (2.11)$$

$$\Delta G^0 = -158.35 + 65.6 + (0.229n - 0.01)\,T\ (kJ \cdot mol^{-1})$$

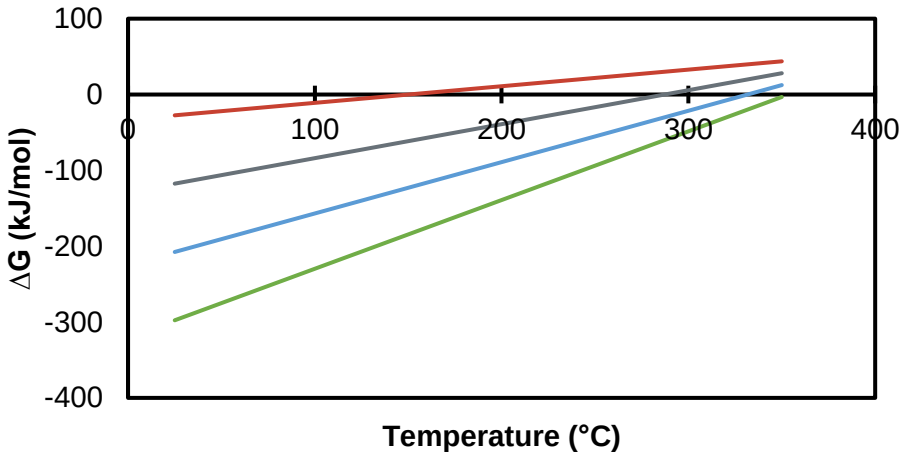

Figure 2-12: ΔG energy of the formation of C_1 (red), C_2 (grey), C_3 (blue) and C_4 (green) alcohols from CO and H_2 (eq. 2.11). Thermodynamic data is taken from [41].

The above presented thermodynamic results are in line with the results reported by Boz *et al.* (1994) [104]. A commercial methanol synthesis catalyst modified with alkali promotion, K_2CO_3, was used to increase the selectivity towards higher alcohols. The study investigated the effect of temperature on the selectivity and oxygenate distribution of a 0.5 wt.% $K_2O/CuO/ZnO/Al_2O_3$ catalyst at three different temperatures. The formation of methanol and aldehydes were favoured

at low temperatures, where the selectivities towards higher alcohols and hydrocarbons increased upon an increase in temperature (Figure 2-13). The steady state activity at the three temperatures was recorded as 31.6% (275 °C), 30.0% (295 °C) and 17.9%, at 305 °C. The loss of activity was accounted for by the sintering of the Cu, evidenced by a decrease of the surface Cu/Zn ratio by 65% (analyzed using XPS), thus a loss of active surface area. Therefore, it is interesting to see that the decrease in activity affects the formation of all alcohols, except iso-butanol (Figure 2-14).

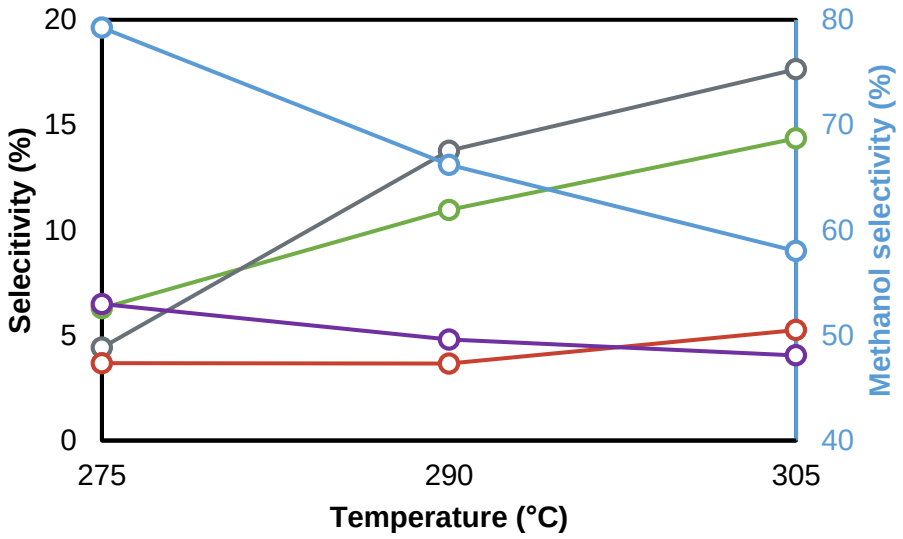

Figure 2-13: Effect of temperature on the selectivity towards methane (red), higher hydrocarbons (grey), methanol (blue), higher alcohols (green) and aldehydes (purple). Figure is adapted from Boz et al. (1994) [104].

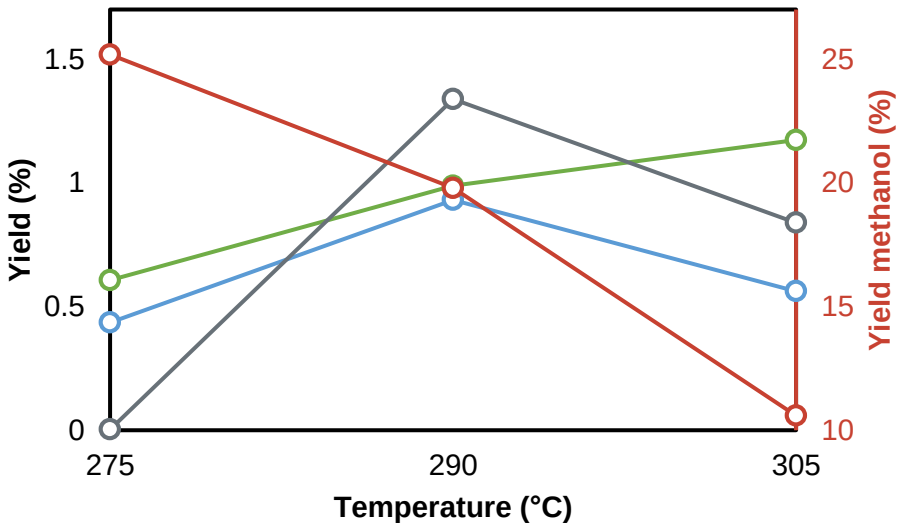

Figure 2-14: Effect of temperature on alcohol distribution; methanol (red), ethanol (grey), n-propanol (blue) and i-butanol (green). Figure is adapted from Boz et al. (1994) [104].

Fang *et al.* (2009) [109] described the use of a nickel promoted molybdenum sulfide catalyst for mixed alcohol synthesis. The temperature used was 300 °C and 340 °C with a pressure of 95 bar, syngas ratio of 1 and GHSV of 8500 h^{-1}. With the increase in temperature, an increase in CO conversion was observed (Figure 2-15). The selectivity towards alcohols decreased with an increase in temperature, however, the distribution of the alcohols changed in favour of the higher alcohols (Figure 2-16).

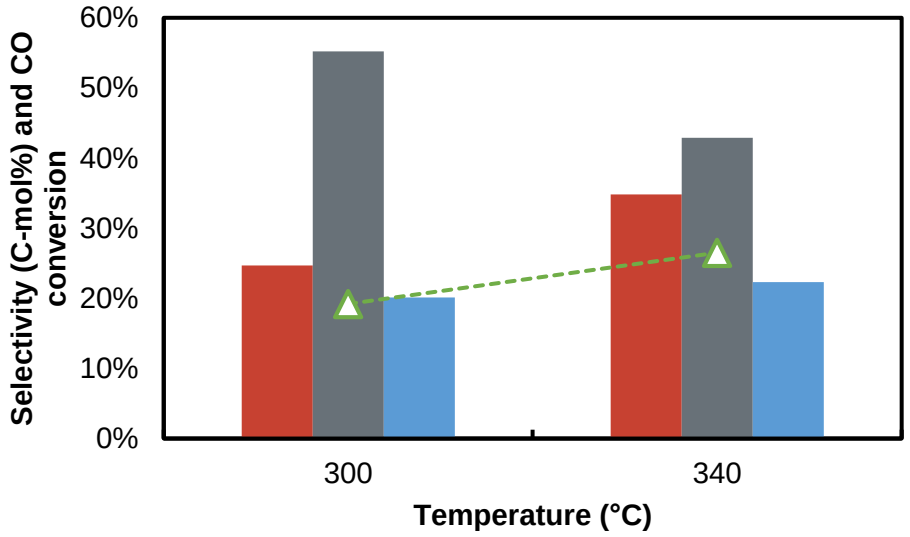

Figure 2-15: Product selectivity during the use of Ni/MoS_2-based catalyst for mixed alcohol synthesis; hydrocarbons (red), alcohols (grey), CO_2 (blue) and CO conversion (green). P = 95 bar, H_2/CO = 1.0 and GHSV = 8500 h^{-1}. Figure is adapted from the results presented by Fang et al. (2009) [109].

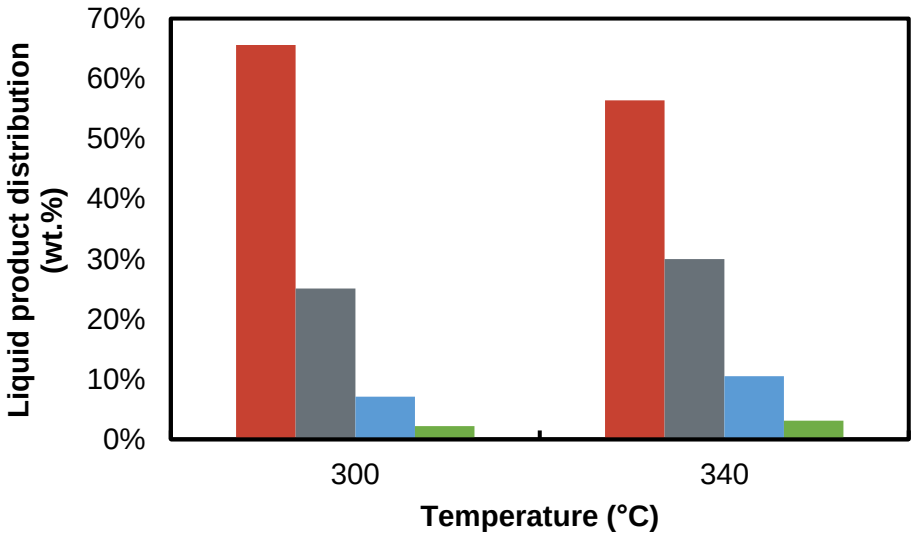

.

Figure 2-16: Alcohol distribution during the use of Ni/MoS_2-based catalyst for mixed alcohol synthesis; methanol (red), ethanol (grey), propanol (blue) and butanol (green). P = 95 bar, H2/CO = 1.0 and GHSV = 8500 h^{-1}. Figure is adapted from the results presented by Fang, et al. [66].

2.2.3.3 *Influence of pressure*

Following Le Chatelier's principle, increasing pressure moves the position of the equilibrium to the side of the reaction with the least number of molecules. Therefore, increasing pressure favours the overall formation of products. The oxygenates to hydrocarbons ratio increases slightly with an increase in pressure, as hydrocarbon formation increases to a lesser extent than oxygenates. Besides the increase in formation of hydrocarbons and oxygenates, the amount of water also increases, which leads to an increase of the water-gas-shift reaction [22].

Herman (2000) [110] observed the formation of alcohols with a two-stage catalyst system using a $Cs/Cu/ZnO/Cr_2O_3$ catalyst for the formation of methanol and a $Cs/ZnO/Cr_2O_3$ catalyst for the formation of higher alcohols. As shown in Figure 2-17, increasing pressure has greatly enhanced the formation of methanol. Simultaneously, the synthesis towards higher alcohols was also increased, but to a much lesser degree. Hydrocarbon formation rates showed the least change.

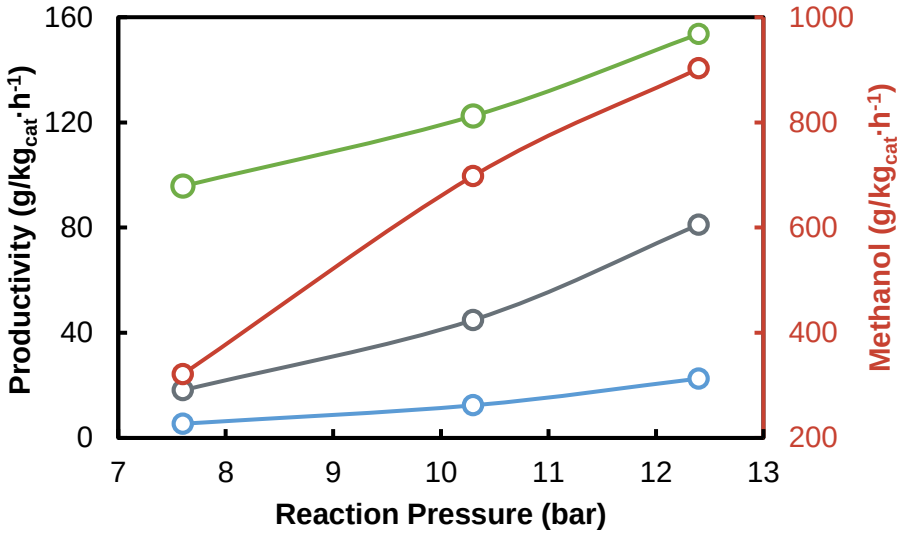

Figure 2-17: Effect of reaction pressure on the space time yields of the products methanol (red), ethanol (grey), propanol (blue) and iso-propanol (green) over a $Cs/Cu/ZnO/Cr_3O_3||Cs/ZnO/Cr_2O_3$ double bed reactor. Process conditions applied: H_2:CO = 1, GHSV = 1837 L/kg$_{cat}$/h, T = 325 °C (top bed) and 425 °C (bottom bed). Note the secondary Y-axis for the methanol productivity. Figure is adapted from Herman (2000) [110].

2.2.3.4 *Influence of space velocity*

A lower space velocity, i.e. higher contact times of the reactants with the catalyst surface, is usually favourable for the formation of higher alcohols as they are formed at a slower rate than methanol. Decreasing space velocity also enhances CO conversion [22].

Boz *et al.* (1994) [104] studied the effect of contact time on the activity and selectivity of a 0.5 wt.% $K_2O/CuO/ZnO/Al_2O_3$ catalyst. Conditions applied were 40 bar total pressure, 290 °C reactor temperature and a feed gas composition of 0.5 H_2:CO. The space velocity was varied between

1000 and 6000 h^{-1}. They observed, with an increase in contact time, an increase in conversion, methane, higher alcohols and CO_2 selectivity. Methanol selectivity decreased and the selectivity towards aldehydes passed through a maximum.

Xu and Iglesia (1999) [111] used a 2.9 wt.% Cs-Cu/ZnO/Al_2O_3 catalyst studying the formation of ethanol by co-feeding methanol ($^{12}CH_3OH$) with the feed gas (^{13}CO and H_2) in relation to the bed residence time, calculated from the gas flow rate at reaction temperature and pressure and the total catalyst bed volume. The CO conversion of the experiments was below 1% under the process conditions applied (265 °C, 20 bar and H_2:^{13}CO = 1). They observed a linear increase in ethanol formation below 1.5s residence time. Upon a further increase of bed residence time to 3s, the ethanol formation rate increases but at a slower rate, due to possible secondary reactions happening with intermediate species. Propanol formation has a consistent linear increase with residence time. Methanol synthesis has not reached equilibrium at these conditions and thus methanol formation increases slowly with residence time.

The formation of ethanol was monitored by the distribution of ^{13}C in the product (Figure 2-19). The ^{13}C content in ethanol increased with increasing residence time. By extrapolation of the data to zero, it was shown that the ethanol still contains 14% ^{13}C. It was suggested that the ethanol is mainly formed by two $^{12}CH_3OH$ molecules. The ^{13}C content in methanol increases in parallel to the ^{13}C content in ethanol, with a very similar rate. This would suggest that the formation of ethanol is subsequent to that of methanol or that they have the same C_1-monomers. However, the second option is not supported by the earlier statement describing the formation of ethanol at zero residence time.

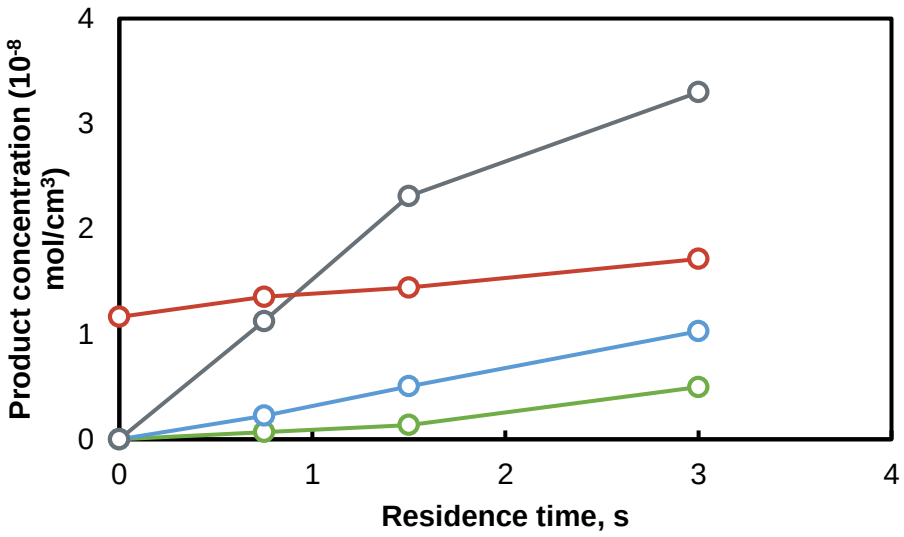

Figure 2-18: Effect of residence time on product concentration for 2.9 wt.% Cs-Cu/ZnO/Al_2O_3; methanol[a] (red), ethanol (grey), 1-propanol (blue) and iso-butanol (green) with process conditions T = 265 °C, P = 20 bar and 13CO/H_2/12CH_3OH = 100/100/1.3. [a] Methanol concentration x 0.04. Figure is adapted from Xu and Iglesia (1999) [111].

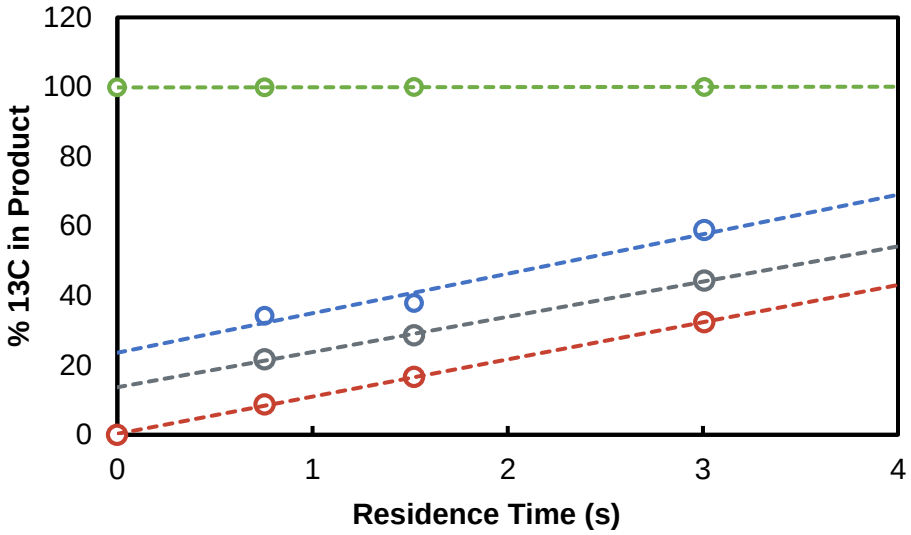

Figure 2-19: Effect of residence bed time on the distribution if ^{13}C in the products; methanol (red), ethanol (grey), 1-propanol (blue) and CO (green) over a 2.9 wt.% Cs-Cu/ZnO/Al_2O_3. Process conditions: T = 265 °C, P = 20 bar, $^{13}CO/H_2/^{12}CH_3OH$ = 100/100/1.3). Figure is adapted from Xu and Iglesia (1999) [111].

2.3 Further upgrading of the products by co-feeding NH_3

Another way in which the dependence of FTS's profitability on global oil prices can be mitigated is by modifying the process to increase the value of the product spectrum further. It was observed, and published in the form of patents [8, 112-114], that co-feeding ammonia to synthesis gas could yield highly valuable nitrogen-containing compounds such as amines, amides and nitriles [9, 14, 15]. It is hypothesized that these nitrogen-containing compounds are formed at the expense of oxygenates. [8, 10, 11, 13, 14, 115, 116]. In the following chapter, it is discussed how these nitrogen-containing compounds are proposed to be formed, their applications and some recent studies about the co-feeding of ammonia to the Fischer-Tropsch process.

2.3.1 Amines

Amines are carbon chains with one (primary), two (secondary) or three (tertiary) carbon-nitrogen single bonds. Nitrogen has three bonds available to either a carbon atom or a hydrogen atom. The easiest examples are ammonia (NH_3), methyl amine, dimethyl amine and trimethyl amine (Figure 2-20).

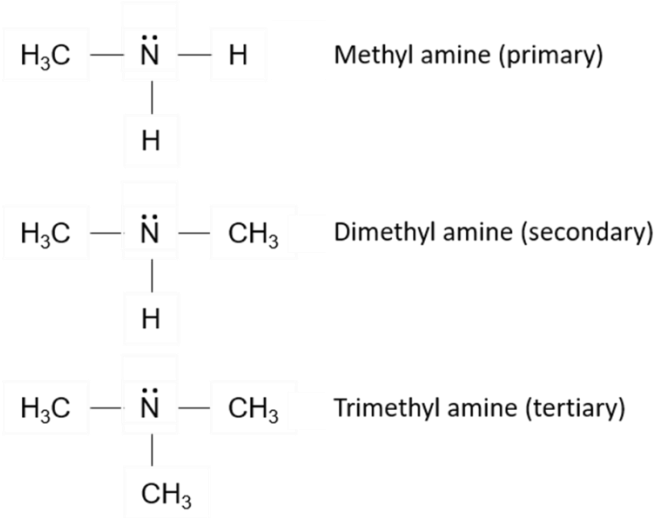

Figure 2-20: Illustration of primary, secondary and tertiary methyl-amines.

Amines are important base chemicals in the production of pharmaceuticals, agrochemicals, polymers, dyestuff, pigments, emulsifiers and plasticizing agents. The terminal primary amines are the most valuable compounds. However, they have a very high reactivity and are thus difficult to form selectively [117]. Currently the commercial production of amines is mainly based on the heterogenous reaction of alcohols with ammonia in an amination reaction (eq. 2.12). Like the FTS, it requires high temperatures and pressures and undergoes many side reactions forming alkenes and alkanes. A catalytic reaction, forming selectively primary amines, directly from alcohols and ammonia is desired both on an economic and environmental basis [15, 117].

$$C_nH_{2n+1}OH + NH_3 \rightarrow C_nH_{2n+1}NH_2 + nH_2O \quad \Delta H^\circ = -250.4 \text{ kJ/mol (for n = 2)} \quad (2.12)$$

Other possible methods for the formation of amines are the synthesis of linear amines from internal olefins [118] or by hydrogenation of amides (up to 85% selectivity) [119]. One of the disadvantages of the current methods of producing amines is that they are mainly conducted by using homogenous catalysts, where in the FTS heterogenous catalysts are used, which is favoured due to the ease of product separation [10].

2.3.2 Amides

Amides can be formed by the condensation reaction of amines and carboxylic acids (Figure 2-21), a minor product class within the oxygenates of the Fischer-Tropsch reaction. An acid has a functional group (-COOH), where the (-OH) is replaced by a ($-NH_2$) group, forming the ($-CONH_2$) functional group, with water as a side product. Amides can be used for or appear in products such as black pepper, in the form of *Piper nigrum* L, which can also be used as a treatment for stomach diseases [120]. Acrylamide has been found in coffee [121] and anandamide in chocolate [122]. Other applications for the use of amides is the production of polymers and antibiotics. The simplest forms of amides are methanamide (C_1), ethanamide (C_2) and propanamide (C_3) [123].

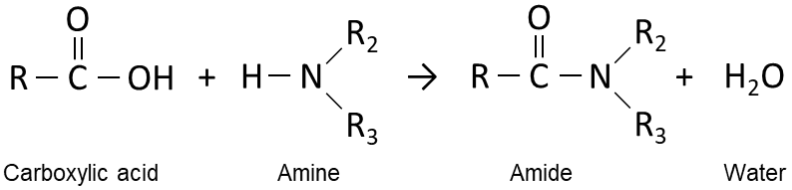

Figure 2-21: Formation of an amide by the condensation of carboxylic acid with an amine.

Other possible ways to form amides include the transition-metal catalysed hydrolysis reaction of nitriles [124] or the acylation of amines by stoichiometric amounts of alcohols producing amides and molecular hydrogen [125].

2.3.3 Nitriles

Nitriles are an important group of valuable chemicals used for pharmaceuticals, agricultural and fine chemicals. The functional group of a nitrile is the triple bonded N-atom to a C-atom (-CN). A ‘’green chemistry’’ way (without forming a large amount of inorganic salts) of producing nitriles is the transition-metal catalyzed dehydration of amides or the oxidative reaction of alcohols and ammonia, with only water as a side product (Figure 2-22) [126].

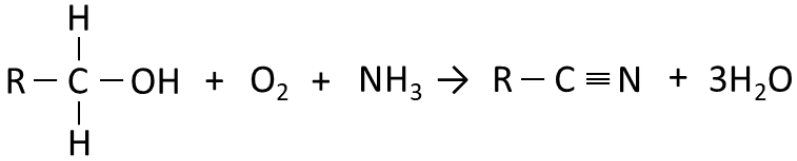

Figure 2-22: Formation of nitriles by the oxidative reaction of alcohols and ammonia.

2.3.4 NH_3 Co-feeding

In the current industrial way of producing N-containing compounds chemical intermediates are required as the process is composed of two steps: 1) synthesis of the chemical intermediate and 2) the conversion reaction of the intermediate into the N-containing compound. Therefore the formation of N-containing compounds in a single reaction was investigated as it could be economically more favourable [10]. The co-feeding of ammonia to a stream of synthesis gas over a heterogenous catalyst has been studied previously by Rottig (1958) [114] using a precipitated iron/copper catalyst impregnated with potassium. The process conditions used were a pressure of 30 bar and temperatures between 180 – 210 °C. He found mainly aliphatic primary amines. Kölbel *et al.* (1975) [127], [128] used iron catalysts promoted with potassium. The FT reaction was performed in a fixed-bed reactor. Steam was used as reactant instead of hydrogen at Kölbel-Engelhardt conditions. The formed N-containing compounds mainly consisted of primary amines. Claeys *et al.* (2011) [8] presented the formation of nitrogen or phosphorous containing species by co-feeding ammonia or phosphine to the synthesis gas mixture at a certain temperature (160–400 °C) and pressure range (1-50 bar). Linear nitriles, amides or formamides or linear phosphorus containing compounds, in the case of co-feeding phosphorus gas, are observed to form. Catalysts include cobalt, iron, ruthenium, rhodium or bulk iron modified with a promoter. The composition of the synthesis gas can be in a range of 0.5-5:1 H_2 to CO. However, other combinations of H_2, CO, H_2O and CO_2, are also possible. With the formation of the N-containing compounds, the concentration of oxygenates decreases. This suggests that the N-containing compounds are formed at the expense of the oxygenated compounds or their precursors. Consistently, an increase in olefins is observed upon addition of ammonia.

Henkel (2012) [10] studied the effect of co-feeding 5.0 vol.% ammonia over unpromoted and promoted iron and cobalt catalysts. The influence of ammonia on the CO conversion of unpromoted and potassium promoted iron-based catalysts (2.0 and 5.0 wt.% K-promotion) was tested by the addition of NH_3 after 240 minutes time on stream. While the activity was decreasing with time on stream (especially in the case of the potassium promoted samples), the deactivation could still be related to classic mechanisms such as carbon deposition etc. and was not clearly induced by ammonia.

Co-feeding of ammonia also influenced the product distribution (Figure 2-23). As the potassium promoted samples form oxygenated products during the ammonia-free Fischer-Tropsch

reactions, the N-containing compounds are formed in the presence of ammonia instead of the previously formed oxygenates [10]. However, the unpromoted samples (red lines), do not produce a significant amount of oxygenates. When ammonia is introduced to the unpromoted samples, no N-containing compounds were observed. This confirms that a high selectivity towards oxygenates is required to be able to form N-containing compounds by co-feeding NH_3.

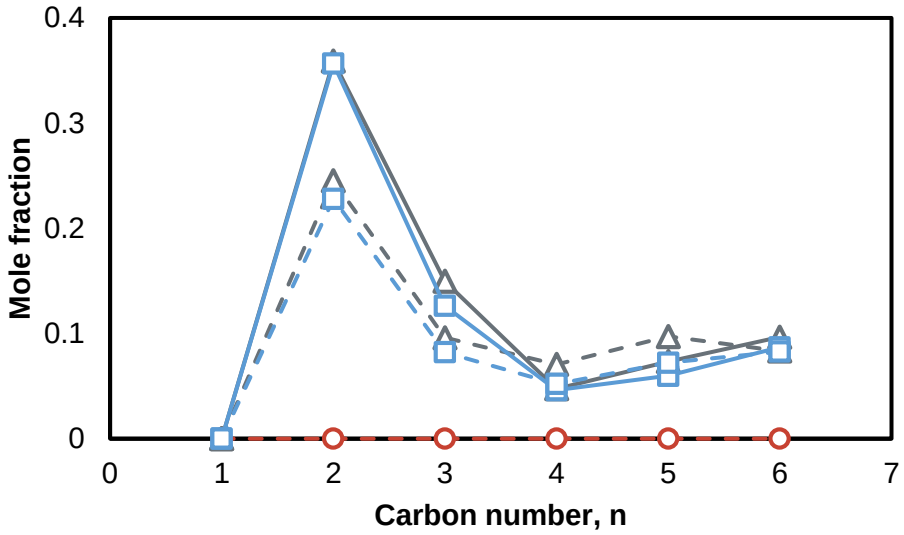

Figure 2-23: Mole fraction of oxygenates (solid lines) and amines/nitriles (dashed lines) in all linear organic products during FT runs on 0 (red circles), 2 (grey triangles) and 5 (blue squares) wt.% potassium promoted iron catalysts with and without co-feeding NH_3. Process conditions applied: T = 270 °C, P = 4 bar, GHSV = 1920 h^{-1}, H_2:CO = 2:1. Figure is adapted from Henkel (2012) [10].

The effect of ammonia over a platinum promoted cobalt/alumina catalyst was studied by Rao Pendyala *et al.* (2017) [115] using a continuously stirred tank reactor (CSTR). The ammonia was co-fed in the form of NH_4OH and NH_3. It must be noted that the authors were predominantly interested in the poisoning effect of small concentrations of ammonia in the feed stream rather than in detailed changes in selectivity. A significant ‘’step decrease’’ in CO conversion was observed as 1 ppm (0.0001 vol.%) of NH_4OH was co-fed into the reactor. Upon increasing the amount of ammonia (up to 1200 ppm = 0.12 vol.%), the activity of the catalysts did not show a significant further drop in conversion (Figure 2-24). Addition of NH_3 showed a slightly larger initial drop in CO conversion, however, it continues to follow similar trends as observed with NH_4OH co-feeding. Removal of the ammonia from the feed did not restore previous activity levels. Therefore, it is suggested that 1 ppm is sufficient to block certain active sites and allow the deactivation of the catalyst. An excess amount of ammonia does not harm the catalyst further. Simultaneously, it was observed that the chain growth probability increases in the presence of ammonia. Again, increasing the amount of ammonia did not show any further effect. In agreement with Claeys *et al.* (2011) [8], the olefin/paraffin ratio increased upon addition of ammonia.

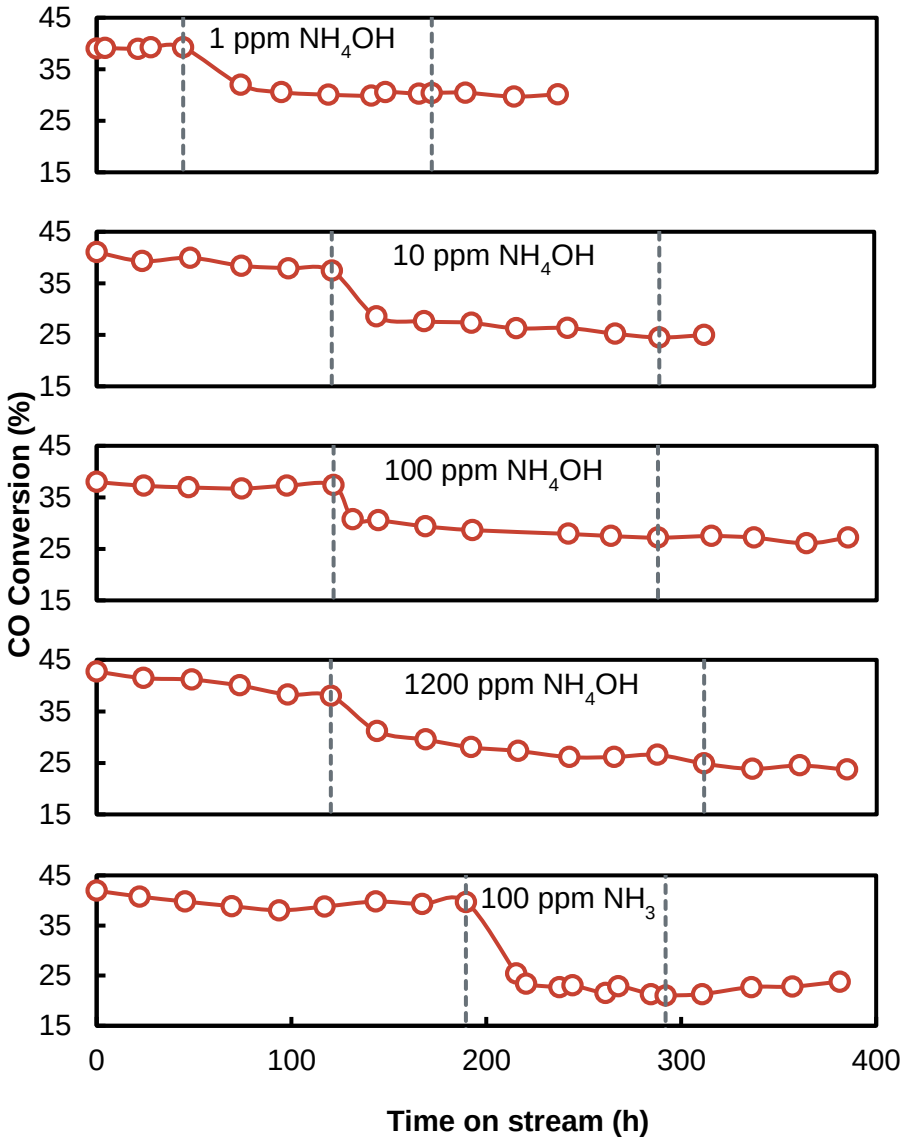

Figure 2-24: Effect of ammonia addition (between the two dashed lines) on the activity of a Pt-Co/Al_2O_3 catalyst. Conditions: T = 220 °C, P = 1.9 MPa, H_2/CO = 2, SV = 3-5 SL/h/g_{cat}. Figure is adapted from Rao Pendyala et al. (2017) [115].

Sango *et al.* (2015) [14] studied the formation of nitrogen containing compounds by co-feeding different amounts of ammonia to a potassium promoted iron catalyst in a slurry reactor. With time on stream the conversion decreases (Figure 2-25). Again, this cannot be directly related to the addition of ammonia up to a concentration of 10% in the feed. At 10% deactivation is slightly accelerated. Upon removal of the ammonia, a slight increase in CO conversion was observed. Having a closer look at the activity, the conversion to hydrocarbons (amended for the water-gas-shift reaction) does not change significantly. Hence, it is believed that the ammonia poisons the active sites, however, the poisoning of sites responsible for the WGS reaction is reversible, where for the sites responsible for hydrocarbon formation it is not.

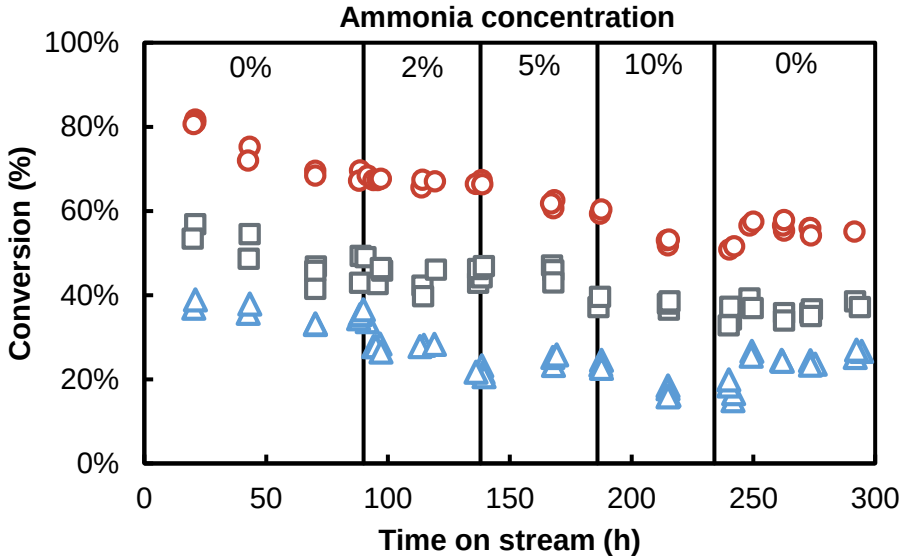

Figure 2-25: Effect of different concentrations of ammonia on the CO conversion (red circles), CO conversion to hydrocarbons (grey squares) and H_2 conversion (blue triangles) of a potassium promoted iron catalyst in a slurry reactor. Figure is adapted from Sango et al. (2015) [14].

Formation of N-containing compounds has shown the same dependency as previously reported by Claeys *et al.* (2011) [8] and Henkel (2012) [10]. Amines', nitriles' and amides' formation is accompanied with a significant reduction of the oxygenate selectivity (Figure 2-26 and Figure 2-27). Only the methyl ketones are not affected by the presence of ammonia.

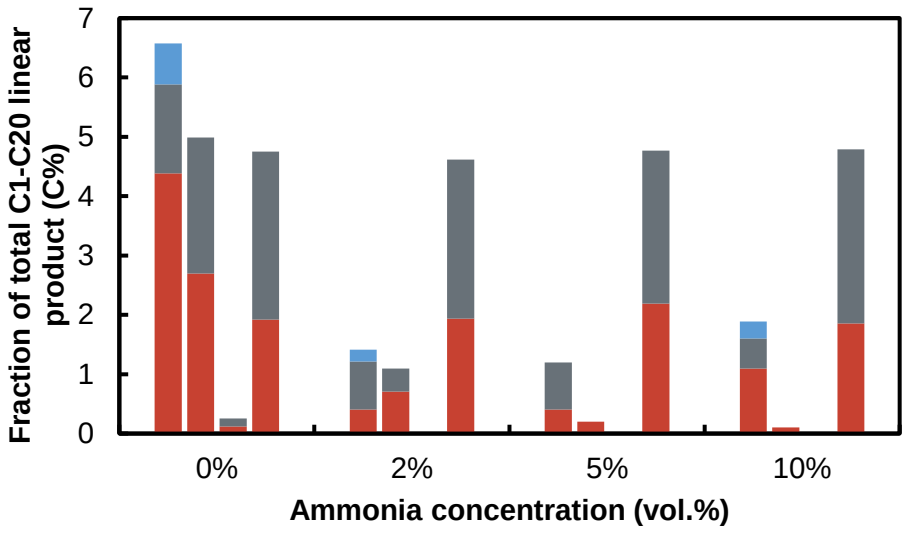

Figure 2-26: Distribution of the formed oxygenates in relation to the co-feeding of different amounts of ammonia over a potassium promoted iron catalyst in a slurry reactor. From left to right within one series; alcohols, aldehydes, carboxylic acids and methyl-ketones. With C_2-C_5 fraction (red), C_6-C_{12} fraction (grey) and C_{13}-C_{20} fraction (blue). Figure is adapted from Sango et al. (2015) [14].

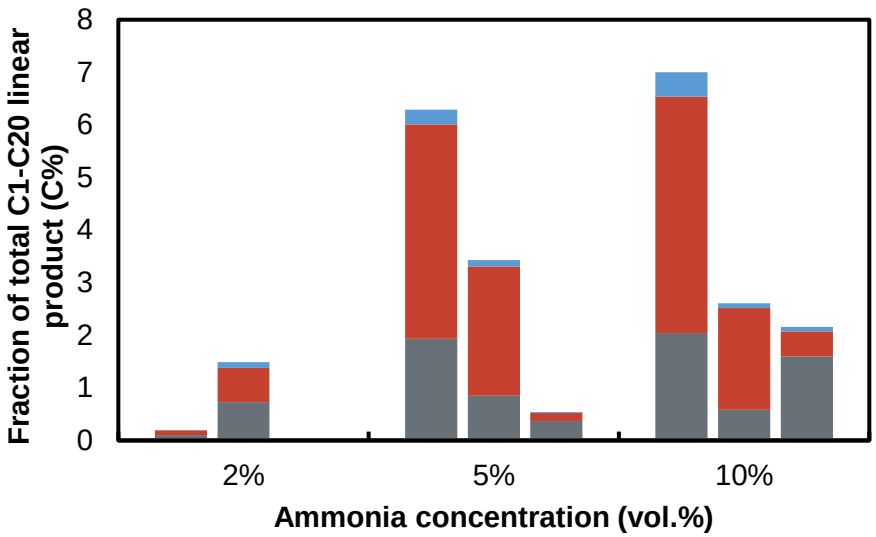

Figure 2-27: Formation of N-containing compounds upon addition of ammonia to the feed-gas over a potassium promoted iron catalyst in a slurry reactor. From left to right within one series; amines, nitriles and amides. With C_2-C_5 fraction (red), C_6-C_{12} fraction (grey) and C_{13}-C_{20} fraction (blue). Figure is adapted from Sango et al. (2015) [14].

As linear α-olefins have been shown to be able to re-adsorb on the catalyst, as discussed earlier, and the olefin content has been shown to increase upon the addition of ammonia, the study of Rausch *et al.* (2016) [129] investigates the impact of ammonia on product selectivity, focusing on the olefin content, using iron- and cobalt-based catalysts. The reaction using 30 wt.% Co/SiO_2 was carried out in a slurry reactor at 240 °C at 12 bar with a syngas flow rate of 150 mL/min and a H_2 to CO ratio of 2, which changed upon the addition of ammonia (0-26 vol.%). In a fixed bed reactor 15 wt.% Co/SiO_2 and 15 wt.% Fe/SiO_2 were investigated at reaction temperatures of 170 °C for cobalt and 300 °C for iron catalyst. A total syngas flow rate of 10 mL/min was used and remained constant during co-feeding of ammonia, by replacing the inert gas (N_2) which was co-fed in the experiments without NH_3.

The cobalt catalyst in the fixed bed reactor shows a much lower olefin to paraffin ratio than the iron catalyst, in the absence of ammonia. This indicates that the cobalt catalyst undergoes more secondary reactions hydrogenating the unsaturated hydrocarbons. The increase in olefin content upon co-feeding NH_3 was more significant for the 15 wt.% Co/SiO_2 catalyst than for the 15 wt.% Fe/SiO_2 catalyst (Figure 2-28). A possible reason behind the different behaviours of the two catalysts could be the actual adsorption of CO and NH_3 on the different catalytic surfaces. It was found in a temperature programmed desorption experiment with CO and NH_3 that NH_3 at 300 °C is already desorbed from the iron surface. However, no research has been done yet when NH_3 is present in the synthesis gas mixture, as this can change the adsorption/desorption behaviour through lateral interactions.

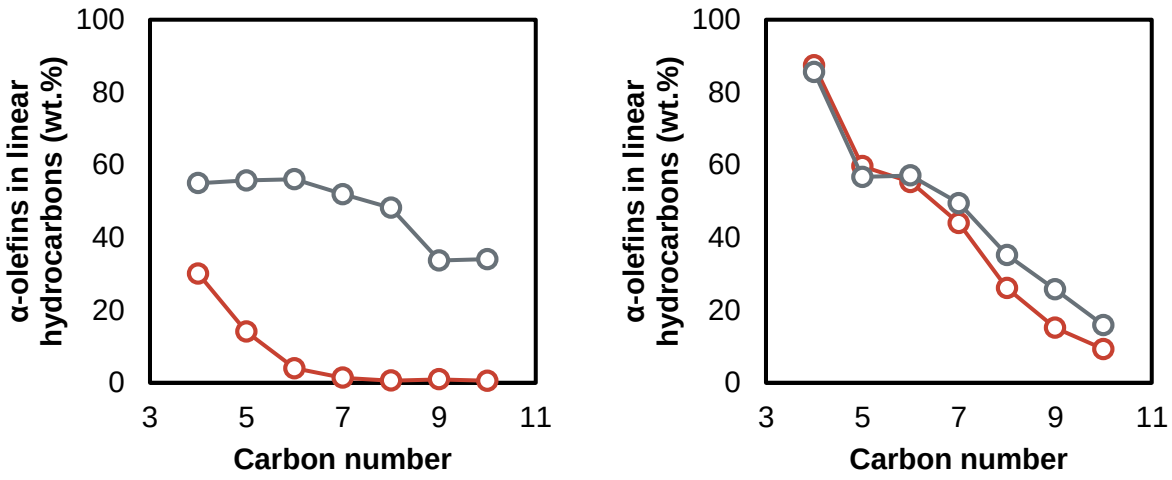

Figure 2-28: Influence of NH_3 (0 vol.% in red and 25 vol.% in grey) on the selectivity towards olefins (wt.%) during FTS using in the left figure 15 wt.% Co/SiO_2 and in the right figure 15 wt.% Fe/SiO_2 in a fixed bed reactor (T_{cobalt} = 170 C, T_{iron} = 300 C, P = 5 bar, H_2:CO:X = 2:1:1 with X = N_2 or NH_3, GHSV = 545 h^{-1}. Figure is adapted from Rausch et al. (2016) [129].

Fischer *et al.* (2016) [9] observed the formation of acetonitrile in the presence of ammonia in the feed gas over an alumina supported iron/rhodium alloy (Figure 2-29). The product distribution before and after the addition of ammonia is very similar. However, a significant drop in CO conversion was observed from 27.1% to 12.7% upon addition of ammonia. Removal of ammonia did not show a significant recovery (13.6%).

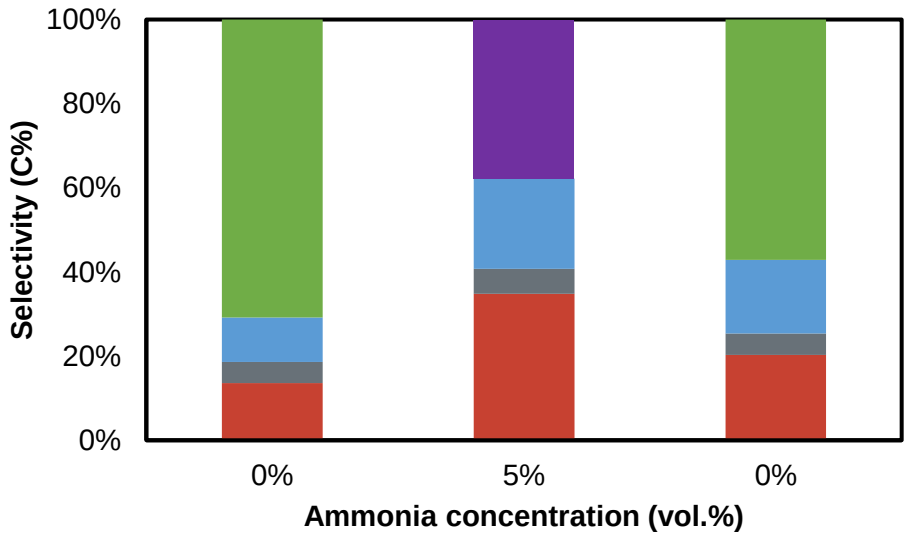

Figure 2-29: Product distribution before and after the addition of ammonia over an alumina supported iron/rhodium alloy. Methane (red), C_{2+} paraffins (grey), olefins (blue), oxygenates (green) and acetonitrile (purple). Figure adapted from Fischer et al. (2016) [9].

The exact mechanism for the formation of N-containing compounds is still very much unknown. It is unclear if the N-containing compounds are formed by the reaction of ammonia with carbonaceous surface precursors of oxygenates or if oxygenates are re-adsorbed onto the surface following secondary reactions in a hydroamination type mechanism (Figure 2-30). Proposed mechanisms for the formation of oxygenates include the the addition of a surface hydroxyl species into an alkyl species introduced by Johnston and Joyner (1993) [49] or the CO-insertion method proposed by Pichler and Schulz (1970) [59].

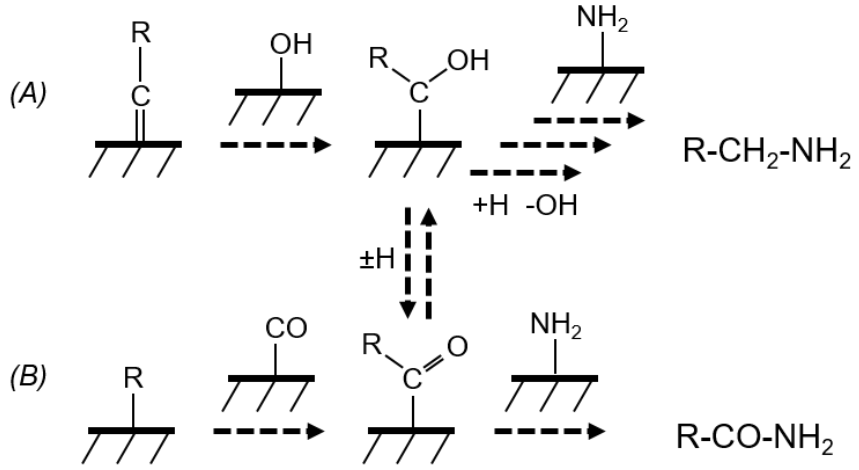

Figure 2-30: Proposed reaction mechanism of the formation of N-containing compounds at the expense of the earlier formed oxygen containing surface species originating either from the incorporation of (A) hydroxyl species [49] or (B) CO insertion [59] to a growing chain or via re-adsorption of oxygenates. Figure is adapted from Sango et al. (2015) [14].

Recently de Vries (2017) [15] studied the pathway to the formation of N-containing compounds when ammonia is co-fed during the FTS, providing fundamental insight to the mechanistic route to the formation of the products. In agreement with what was reported earlier by Sango *et al.* (2015) [14], the iron catalysts are much more resistant to NH_3 poisoning compared to cobalt catalysts. 1 vol.% NH_3 was co-fed with the synthesis gas during Fe-based FTS in a slurry reactor at 250 °C, pressure of 5 bar, H_2 to CO ratio of 2 and a space velocity of 2250 mL/h/g_{cat}. No major changes were observed regarding the catalyst activity. Overall oxygenate selectivity decreased upon the addition of ammonia (Table 2-3). Interestingly, the formed N-containing compounds consist only out of amines and amides. No nitriles were identified (Table 2-4). Thus, it is suggested that the primary formed nitriles and amines undergo secondary reactions to form secondary or tertiary amines.

Table 2-3: Oxygenate distribution with and without ammonia co-feeding using an Fe-based catalyst in a slurry reactor. Process conditions: T = 250 °C, P = 5 bar, GHSV = 2250 mL/h/g_{cat}, H_2:CO = 2, 1 vol.% NH_3. Table adapted from de Vries (2017) [15].

Oxygenates	Selectivity (C wt.%)	
	No NH_3	NH_3
n-alcohols (C_{1-17})	7.89	3.43
Carboxylic acids (C_{2-12})	0.50	0.02
Ketones (C_{3-11})	1.20	0.84
Aldehydes (C_{2-11})	0.88	0.00

Table 2-4: Selectivity towards N-containing compounds during NH_3 co-feeding in the FTS using an Fe-based catalyst in a slurry reactor. Process conditions: T = 250 °C, P = 5 bar, GHSV = 2250 mL/h/g_{cat}, H_2:CO = 2, 1 vol.% NH_3. Table adapted from de Vries (2017) [15].

N-containing compounds	Selectivity (%)
Primary amines (c_{2-7})	0.97
Secondary amines (C_{4-11})	0.20
Amides (C_{4-11})	0.15
Nitriles	0.00

Besides the experimental study, de Vries (2017) [15] also studied the role of NH_2 in the reaction mechanism towards FTS products on a Fe(100) surface, including N-containing compounds, using DFT calculations. Previously, Henkel (2012) [10] and Sango (2013) [130] suggested that NH_2 is inserted during chain growth in the final step, forming primary amines. In addition, de Vries (2017) [15] found that NH_2 has a significant higher activation barrier (E_a = 1.44 eV) for the reaction $NH_2 \rightarrow NH + H$ and thus it can get stuck on the Fe(100) surface. The previous stated hypothesis that NH_2 could be inserted into a growing chain is supported by results obtained, showing that NH_2 and CO can form certain 'islands' on the surface and therefore have NH_2 adsorbates available to react with the growing carbon chains. Finally, a suggestion was made that when the NH_2 and CO are close to one another, it lowers the activation energy for CO dissociation, following an increased formation of C atoms on the surface of the catalyst. Quick removal of the oxygen atom would improve the formation of amines.

2.4 β-Mo_2C as a catalyst for FTS

Transition metal carbides/nitrides or oxycarbides have shown promising results and high activity for CO hydrogenation [131]. These materials are generally very hard, refractory, resistant to corrosion and have high melting points (up to 3000 °C). Their physical properties are more related to ceramics, however their catalytic properties are similar to those of the noble metals [131].

Molybdenum is such a transition metal. Metallic molybdenum dissociates a CO molecule at room temperature and usually has very low surface areas of <1 m^2/g [131], however, molybdenum carbide adsorbs the CO in a molecular state. [132, 133]. Additionally, molybdenum carbide has been shown to have a high tolerance to sulphur poisoning, which makes it an interesting catalyst for the Fisher-Tropsch synthesis [134].

Previous investigations using Mo-based catalysts for CO hydrogenation towards higher alcohols are mostly focused on the sulfide, carbide or nitride form. Alkali promoted Mo_2S has been shown to produce an ASF-like product distribution, reaching a total oxygenate selectivity of about 70-80% (CO_2-free basis), whereof 50% of the total oxygenates is methanol. Process conditions applied are relatively high temperatures (270-330 °C) and elevated pressures (10-28 bar). However, the hydrocarbon selectivity is still between 15-30% and CO_2 is a major product due to the water-gas-shift reaction. Co-feeding H_2S into the reactor is required as it decreases hydrogenation and increases selectivity to higher alcohols. H_2S in the feed in turn also leads to the undesired formation of sulfided products [22].

Potassium promoted Mo_2N was investigated by Zaman *et al.* (2017) [135] under varying process conditions and promoter content (wt.%). The unpromoted catalyst showed a significantly higher hydrocarbon selectivity than the promoted samples. A maximum oxygenate selectivity was detected over the 0.03 wt.% K/Mo potassium promoted sample. Increasing the promoter loading decreased oxygenate selectivity and increased hydrocarbon formation. CO conversion did not change significantly upon the addition of potassium (Figure 2-31). CO_2 selectivities were observed between 50-60% in a temperature range of 275-325 °C on unpromoted samples and between 40-50% for the promoted samples.

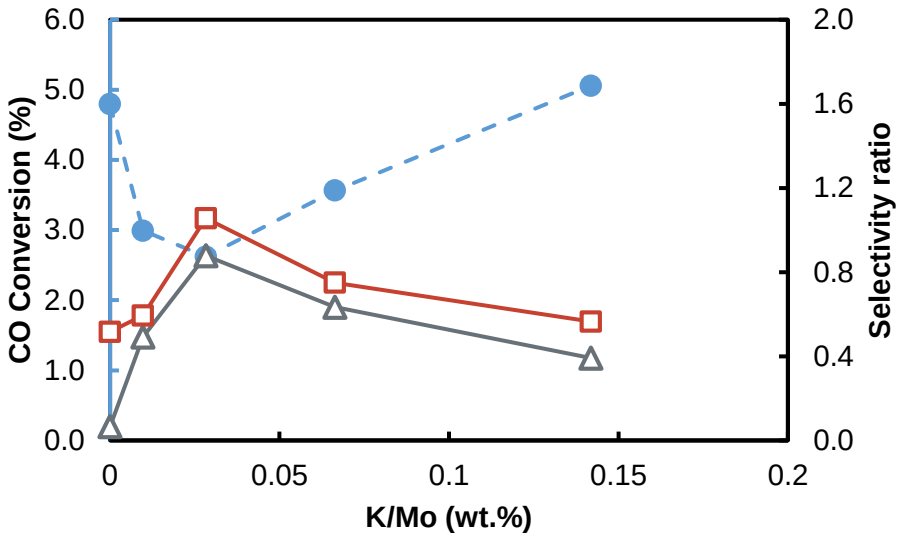

Figure 2-31: Influence of potassium promotion on the ratio oxygenates/hydrocarbons (grey), total C_{2+} oxygenates/methanol (red) and CO conversion (blue) on Mo_2N at 300 °C, 70 bar, GHSV of 60000 h^{-1} and H_2:CO ratio of 1. Figure is adapted from Zaman et al. (2017) [135].

Mo_xC has two common allotropes (Table 2-5). The hexagonal close packed structure (also referred to as β-Mo_2C) and the face-centered cubic structure (also referred to as α-MoC_{1-x}).

Table 2-5: Comparison of the hcp and fcc crystal structures of molybdenum carbide, [a] for x = 0.5. Table is adapted from Lee et al. (1988) [136].

Comparison of Structure	α-MoC_{1-x}	β-Mo_2C
Morphology	Plate-like	Random
Crystallographic arrangement of Mo atoms	FCC	HCP
Nearest neighbors		
Mo-C	3[a]	3
Mo-Mo	12	12
Distances (pm)		
Mo-C	212	209
Mo-Mo	299	296

Both types of crystal structures show high activity and produce mainly short chain hydrocarbons under Fischer-Tropsch conditions [21, 101, 134, 137, 138]. Ranhotra *et al.* (1987) [139] compared the two different crystal structures of molybdenum carbide with Mo_2N (fcc) for CO hydrogenation (Table 2-6). The activities of the catalysts were compared at a fixed CO conversion of 1.5%, varying the GHSV per catalyst to reach these conversions. It can be observed that the Mo_2C (fcc) and Mo_2N (fcc) show higher steady state activity (roughly double) than the Mo_2C (hcp). However, the Mo_2C (hcp) shows slightly more chain growth than the other two catalysts.

Table 2-6: CO hydrogenation over the α- and β-Mo_2C as well as Mo_2N. Comparing activity and selectivity. Reaction conditions: T = 300 °C, H_2:CO = 1:3. Table is adapted from Ranhotra et al. (1987) [139].

	Mo_2C (hcp)	Mo_2C (fcc)	Mo_2N (fcc)
N_{CH4} x 10^3 (s^{-1})	27.4	46.0	50.1
S_{CH4} (%)	76.9	83.7	83.5
S_{C2H4} (%)	5.2	1.2	1.5
S_{C2H6} (%)	15.6	14.3	14.0
S_{C3H6} (%)	1.1	0.0	0.0
S_{C3H8} (%)	1.3	0.9	1.0

Alkali promotion has been shown to enhance the selectivity towards oxygenates on a β-Mo_2C catalyst (Figure 2-32). Woo *et al.* (1991) [20] performed the reaction with a β-Mo_2C and found similar selectivities towards oxygenates in general and specifically C_{2+} oxygenates, however, at much higher CO conversions. An optimum loading seems to be prevalent like in the Mo_2N studies reported by Zaman *et al.* (2017) [135] however, the CO conversion of the Mo_2N is lower (3%) than the β-Mo_2C (10-14%) thus making it difficult to compare. Perhaps at lower space velocities, the Mo_2N catalyst would achieve higher conversion levels, therefore more potassium promotion would be possible, allowing for a direct comparison.

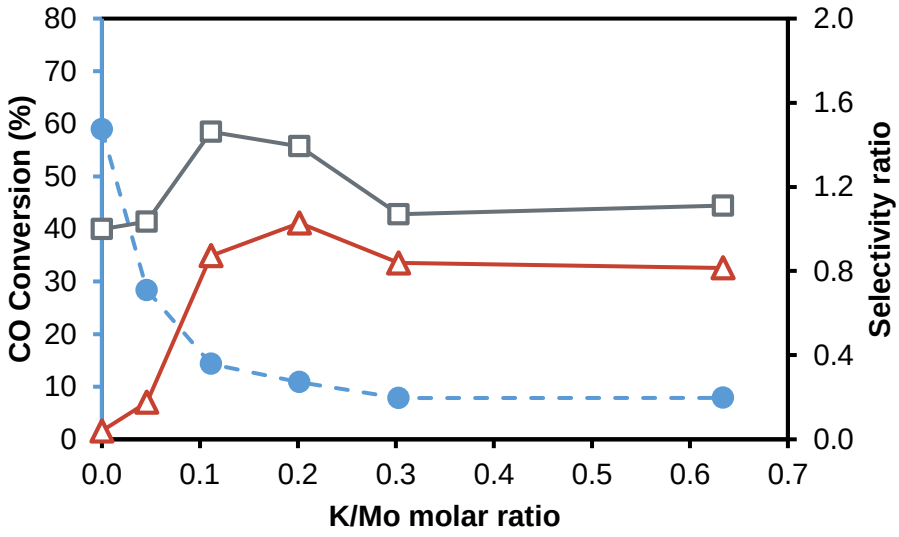

Figure 2-32: Influence of potassium promotion on the ratio oxygenates/hydrocarbons (red triangles), total C_{2+} oxygenates/methanol (grey squares) and CO conversion (blue circles) on β-Mo_2C at T = 300 °C, P = 80 bar, GHSV = 3400 L/kg_{cat}/h and H_2:CO ratio of 1. Figure is adapted from Woo et al. (1991) [20].

The two different crystal structures were compared by Xiang *et al.* (2006) [21], in the presence of different amounts of K_2CO_3. Again, it was shown that the unpromoted samples have a high activity while forming predominantly hydrocarbons. Upon promotion, the samples showed a significant shift in selectivity towards oxygenates (Figure 2-33). Overall, the hcp-crystal structure of

molybdenum carbide showed a higher oxygenate selectivity and chain growth than the fcc-crystal structure.

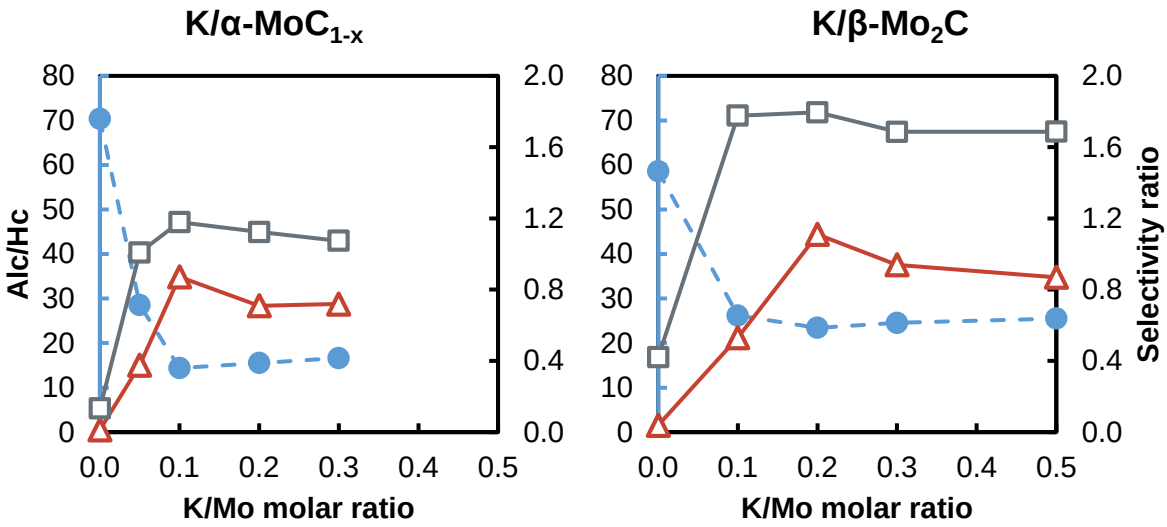

Figure 2-33: Effect of potassium on the ratio of oxygenates/hydrocarbons (red triangles), total C_{2+} oxygenates/methanol (grey squares) and CO conversion (blue circles) of both crystal structures at T = 300 °C, P = 80 bar, GHSV = 2000 h^{-1} and H_2:CO = 1. Figure is adapted from Xiang et al. (2006) [21].

In a report by Xiang *et al.* (2008) [140] higher alcohol synthesis (HAS) was studied over four potassium promoted β-Mo_2C catalysts, with three of them also being promoted with Co, Ni or Fe. The Fe/K-, Co/K- and Ni/K-promoted catalysts show a decrease in the formation of C_1 and C_2 alcohols, but an increase in the formation of C_{3+} alcohols, specifically butanol, compared to the K-promoted β-Mo_2C catalyst (Figure 2-34). The selectivity towards methane reduced significantly with the additional promotion, especially in the case of Fe. Nickel had the largest increase in CO conversion and higher alcohol selectivity. A decrease in CO conversion was observed for the iron-promoted catalyst (Table 2-7). Just like the earlier mentioned articles, WGS activity for the unpromoted sample is high, with CO_2 selectivities of around 50%. Unfortunately, no data was provided of the CO_2 selectivity of the promoted samples.

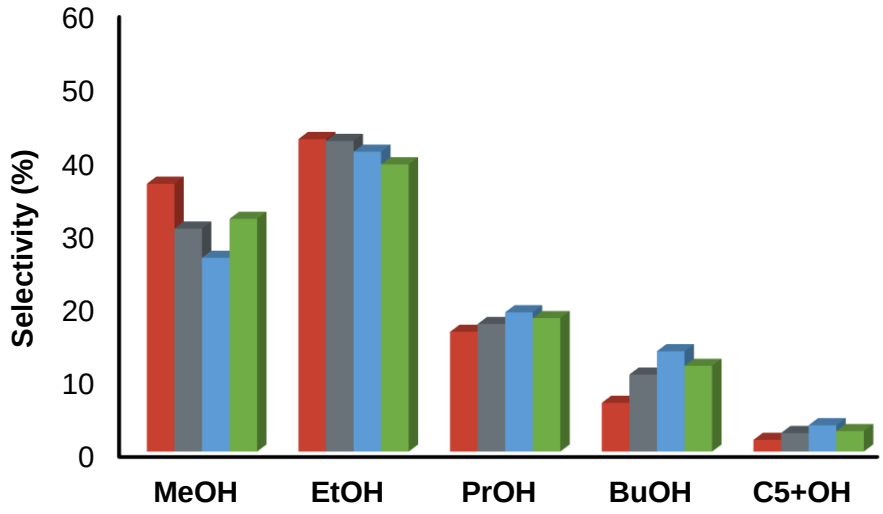

Figure 2-34: The distribution of the formed alcohols over the K/β-Mo_2C (red), K/Co/β-Mo_2C (grey), K/Ni/β-Mo_2C (blue) and K/Fe/β-Mo_2C (green) samples. Selectivities are CO_2-free. Figure is adapted from Xiang et al. (2008) [140].

Table 2-7: Catalytic performance of CO hydrogenation over the β-Mo_2C samples. Reaction conditions: T = 300 °C, P = 80 bar, GHSV = 2000 h^{-1}, H_2:CO = 1. Selectivities are free of CO_2. Figure adapted from Xiang and Zou (2013) [103].

Catalyst	X_{CO} (%)	STY (g/L/h)		Selectivity (C%)	
		ROH	C_{2+}OH	Alc.	HC
K/β-Mo_2C	23.41	122.06	65.93	52.60	47.40
K/Co/β-Mo_2C	40.76	156.43	99.58	42.59	57.41
K/Ni/β-Mo_2C	73.00	324.21	206.13	44.91	55.09
K/Fe/β-Mo_2C	22.01	75.15	42.46	41.95	58.05

Based on the results obtained by Xiang *et al.* (2008) [141], which still reported a selectivity towards hydrocarbons of 47.4 C% (CO_2-free) for a potassium promoted β-Mo_2C sample and an increased hydrocarbon selectivity to max 64.3 C% (CO_2-free) after promotion with nickel (1/4 – 1/10 Ni/Mo ratio), Wu *et al.* (2013) [102] studied the effect of β-Mo_2C-based catalysts on high surface area support materials. The precursor solution of ammonium molybdate was added to the support materials, activated carbon (AC), carbon nanotubes (CNTs) and titanium dioxide after aging, drying and calcining, the samples were carburized and subsequently promoted with potassium via impregnation. Comparing to the potassium promoted bulk carbide, TiO_2 showed the only increase in selectivity to higher alcohols (from ~30% to ~35% at 250 °C), but the selectivity

towards hydrocarbons remained similar (~50% to ~47% at 250 °C). TiO_2 was very unstable during high temperature carburization (750 °C), causing a loss of surface area, however a recent study of the same authors has shown that the required carburization temperature decreases with a decrease in particle size of the oxide precursors [142]. Therefore, if the carburization temperature could be below the phase transformation temperature of TiO_2 of 550 °C, the support could still be interesting for higher alcohol synthesis using β-Mo_2C. The AC-supported sample presented the highest total alcohol production (74.2 C% at 250 °C), however, methanol was the major product (62% at 250 °C). The CNT-supported catalysts produced predominantly hydrocarbons (~40 C% at 250 °C) and methanol (~41 C% at 250 °C). With increasing temperature, the production of methanol and higher alcohols decreased.

2.4.1 Synthesis of β-Mo_2C

The conventional preparation techniques for the preparation of molybdenum carbide involve the reaction of the metal, metal hydride or metal oxide with a reducing atmosphere containing carbon at very high reaction temperatures, above 1200 °C for Mo_xC. This method results in very low surface areas and therefore is not suitable for catalytic reactions. Another metallurgical way of preparing Mo_xC involves the reaction of the metal or oxide precursors with a carburizing gas containing hydrocarbons or CO, resulting again in very low surface areas. A synthetic method using reacting metal halides or metal carbonyl precursors in different atmospheres, such as H_2, hydrocarbons or an inert gas, resulting in a compound mixture of molybdenum carbide and molybdenum oxycarbide with surface areas of about 20-60 m^2/g is also reported [143, 144].

Until now, the most successful method of preparing β-Mo_2C with a high surface area (51 m^2/g) is proposed by Oyama (1981) [145], [146], a temperature programmed reaction (TPRe) of MoO_3 with a 20% CH_4/H_2 mixture. The following section will outline in detail the preparation of the MoO_3 and the effect of different preparation conditions for the synthesis of β-Mo_2C (hcp-phase).

2.4.1.1 Preparation of MoO_3

Yin *et al.* (1993) [147] studied the thermal decomposition of ammonium molybdate $(NH_4)_6Mo_7O_{24}{\cdot}4H_2O$ to MoO_3 studying the product using X-ray diffraction. The ammonium molybdate was exposed to a series of temperatures from room temperature up to 450 °C. It was found that the molybdenum salt precursor can be decomposed completely by heating in air (calcining) at 450 °C giving off NH_3 and H_2O. The following intermediates were observed with an increasing content of molybdenum: $(NH_4)_4Mo_5O_{17}$, $(NH_4)_2Mo_4O_{13}$, $(NH_4)_2Mo_{14}O_{43}$ and $(NH_4)_2Mo_{22}O_{67}$ and eventually forming the final product MoO_3.

Kim *et al.* (2016) [148] recently patented the formation of MoO_3 nanoparticles in a uniform size range by dissolving a molybdenum salt in a polar solvent first, followed by ultrasonication, preparing an aerosol. Subsequently, the synthesized aerosol is sprayed to a preheated reactor in the presence of a carrier gas. The particles are obtained by the decomposing at high temperature, dispersed into a second polar solvent followed by a solvothermal reduction reaction.

2.4.1.2 Preparation of β-Mo_2C

β-Mo_2C can be prepared by TPRe of its precursor oxide with a carbonaceous reducing gas mixture, such as CH_4 or C_2H_6 in H_2. The conditions used, such as the heating rate, the final temperature, the flow rate of the gases and the composition of the gas mixture, during the temperature programmed reaction determines the properties of the formed transition metal carbide.

Lee *et al.* (1987) [143] studied the reduction of MoO_3 under flowing H_2 while heating at 1 °C/min to 730 °C (Figure 2-35). Water formation was observed upon the reduction of the oxide. The first peak corresponds to the reduction from MoO_3 to MoO_2, followed by the second peak assigned to the reduction from MoO_2 to metallic Mo. Subsequently, the same experiment was performed, substituting the H_2 gas with 20% CH_4 in H_2 (Figure 2-36). A similar shape as in Figure 2-35 was observed for the water formation, during the reduction of the trioxide to the dioxide. The consumption of CH_4, starting at around ±580 °C is associated to the formation of the carbide [136, 143].

The described method is currently widely utilized with slight variations for the formation of the hexagonal phase of molybdenum carbide [20, 101, 103, 131, 149-151]. Mo *et al.* (2016) [101] studied the effect of the different carburization conditions on the synthesis of β-Mo_2C. The following variations were used synthesizing 22 different samples:

- Carburization gas: 20-100% CH_4 in H_2, 10% C_2H_6 in H_2, 5% C_4H_{10} in H_2, 20% CO in H_2.
- Heating rate: 1 and 7 °C/min.
- Final temperature: 550, 630, 700, 760, 800 °C.
- Holding time: 5 and 10 hours.

The effect of the different carburization conditions was analyzed by means of X-ray diffraction (XRD). The effect of the different carbon sources used resulted mostly in a decrease in average crystallite size (peak broadening) with increasing carbon number of the carbon source. Increasing holding time in turn increased the crystallite size. The effect of carburization temperature was most significant. At 550 °C the carbide was not formed, although MoO_3 reduced to MoO_2. From 630 °C onwards the carbide was formed, however, with increasing temperature it shows significant increases in XRD reflex intensities, indicating an increase in crystallite size. With increasing carburization temperatures, carbon deposition on the surface of the catalyst in the form of graphite has been observed [80, 101, 143, 152].

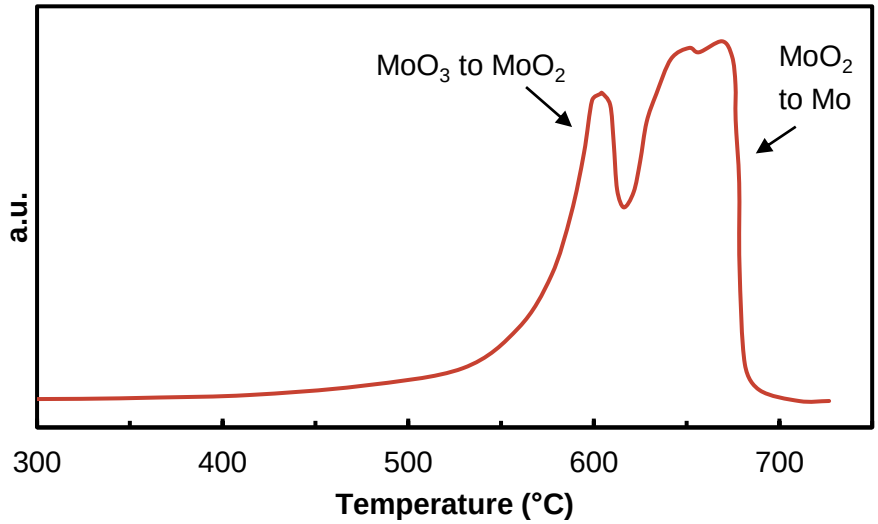

Figure 2-35: Temperature programmed reduction of MoO_3 in H_2 while heating with 1 °C/min to 730 °C. Conditions: 0.5 g MoO_3, GHSV ± 11 L/h/g_{cat}. Figure is adapted from Lee et al. (1987) [143].

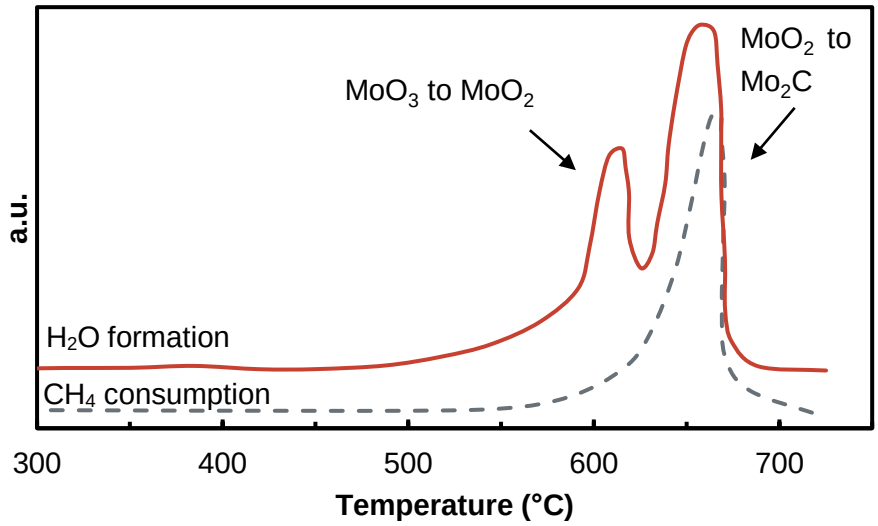

Figure 2-36: Temperature programmed reaction of MoO_3 with 20%CH_4/H_2 gas while heating with 1 °C/min to 730 °C. Conditions: 0.5 g MoO_3, GHSV ± 11 L/h/g_{cat}. Figure is adapted from Lee et al. (1987) [143].

The effect of methane concentration was investigated by increasing the amount of CH_4 in the H_2 mixture. Increasing the methane concentration to 50% results in no significant changes to the carbide phase compared to a sample treated in 20% methane, however slight peak broadening was observed. Increasing the concentration further (80% CH_4/H_2) yielded a mixture of β-Mo_2C (hcp) and α-MoC_{1-x} (fcc). In pure CH_4 the MoO_3 only reduces to Mo_4O_{11}.

3 Proposed work

3.1 Objectives

The aim of the present study is to perform the Fischer-Tropsch process over a potassium promoted hexagonal phase molybdenum carbide catalyst with the focus on the formation of oxygenates. Subsequently, in the presence of ammonia, it is envisaged that these oxygenates are replaced by valuable amines, nitriles and amides. To do so, a suitable catalyst composition (e.g. catalyst promoter and synthesis conditions) must be found, prepared and tested. Different concentrations of the alkali promoter potassium will be added and studied. To summarize, the objectives of this study are:

- Prepare a hexagonal phase molybdenum carbide catalyst (β-Mo_2C) using the temperature programmed reaction method with 20% CH_4 in H_2.
- Investigate the effect of carburization temperature and varying reaction conditions on the activity and selectivity in the Fischer-Tropsch synthesis.
- Subsequently, promote the optimized catalyst with different levels of potassium to investigate its effect on the activity and selectivity (oxygenates in particular) in the Fischer-Tropsch synthesis.
- Investigate the effect of different process conditions on the formation of higher alcohols using the promoted catalysts in the Fischer-Tropsch synthesis.
- Co-feeding of NH_3-gas to the optimized oxygenate yielding potassium promoted molybdenum carbide catalyst to investigate the formation of nitrogen-containing compounds.

3.2 Hypothesis

The promotion of β-Mo_2C with potassium will increase the selectivity towards long chained oxygenates in the Fischer-Tropsch synthesis. Potassium promotion reduces the catalyst's hydrogenation ability and therefore secondary reactions converting the formed oxygenates and olefins into paraffins are suppressed.

In general, the formation of oxygenates in the Fischer-Tropsch synthesis is favoured at low temperatures and elevated pressures. However, as higher alcohols are thermodynamically more stable than methanol, an increase in temperature favours the formation of higher alcohols. On the other hand, an increase in temperature also enhances the formation of hydrocarbons, with predominantly methane as the major product class.

Co-feeding of ammonia to the identified catalyst (highest oxygenate selectivity) in the Fischer-Tropsch synthesis leads to the formation of nitrogen-containing compounds, at the expense of oxygenates formed in the absence of ammonia.

3.3 Key questions

Some specific key questions can be asked associated with this study based on the previous described project objectives and hypothesis:

- What is the effect of different carburization conditions, e.g. temperature, on the catalytic performance during CO hydrogenation?
- How do different levels of potassium promotion affect the selectivity towards oxygenates?
- What kind of oxygenates can be formed using β-Mo_2C as a catalyst?
- What is the effect of different process conditions, e.g. temperature, pressure, space velocity and H_2:CO ratio, on the formation of these oxygenates?
- Do nitrogen-containing compounds form in the presence of ammonia over the β-Mo_2C based Fischer-Tropsch synthesis?

4 Experimental Methodology

4.1 Catalyst preparation

The preparation of a hexagonal molybdenum carbide (β-Mo_2C) catalyst is based on the method reported by Lee *et al.* (1987) [143]. The conditions for the temperature programmed reaction of MoO_3 with a 20% CH_4/H_2 mixture were varied to be able to observe its influence on the characteristics of the catalyst and its performance in the Fischer-Tropsch synthesis. The following section will explain the preparation of the MoO_3 and the different preparation conditions for the synthesis of the β-Mo_2C sample.

4.1.1 Preparation of MoO_3

Based on the literature all samples prepared for catalyst testing were obtained by heating ammonium molybdate ($(NH_4)_6Mo_7O_{24}\cdot 4H_2O$, >81.5%, SAARCHEM PTY LTD) in a calcination oven (Nabertherm, LT 5/12) in an air atmosphere. Samples were placed into a ceramic crucible and heated to 500 °C at a heating rate of 10 °C/min holding for 5 hours [137, 147, 153]. After conclusion, the oven was set to cool down to room temperature. The sample was removed from the oven and crushed using a mortar and pestle to a fine powder.

4.1.2 Preparation of β-Mo_2C

The hexagonal phase of β-Mo_2C was formed by slowly heating the oxide precursor, MoO_3, in a gaseous mixture of 20% CH_4 in H_2 (AFROX). The reaction was performed, by placing 2-3 gram of the oxide precursor in a double walled quartz tube (15 mm i.d, Glasstech, Inc) inside a tube furnace (Elite TSV12/38/250) (see Figure 4-1). The catalyst bed was loaded on top of a plug of quartz wool to make sure the catalyst bed was positioned in the middle of the furnace. A small plug of quartz wool was inserted above the catalyst to prevent the catalyst from being carried with the gas out of the reactor.

All FT-tested catalysts were prepared by an *in situ* carburization method. Instead of a quartz tube, a ¼" stainless-steel U-tube reactor was employed and the total mass of the MoO_3 precursor was decreased to ±1 g. A detailed explanation of the reactor setup is given in chapter 4.3.1. The variation of the carburization conditions for the FT-tested samples will be specified in chapter 4.3.2.

In general, the final carburization temperature was set between 630 and 1000 °C with heating rates varying between 1-10 °C/min up to a temperature of 400/450 °C(as no reaction occurs up to ±450 °C [143]). A heating rate of 1-2 °C/min was set from 400/450 °C onwards to the final carburization temperature, holding the final temperature for between 2 to 5 hours. At temperatures of ≥ 760 °C, carbon deposition in the form of graphite takes place [101].

After the carburization reaction, the catalyst was cooled to room temperature. Before the catalyst was exposed to air, the catalyst underwent a post-treatment passivation with 50 mL/min/g_{cat} of 1% O_2 in N_2 (AFROX) for 1 hour at room temperature. This treatment should form a thin oxide layer on the surface of the catalyst and therefore prevent the catalyst from oxidizing upon exposure to air. After the catalyst was prepared, passivated and cooled down, the catalyst was ready for further investigations. In general, the passivation step was completed for all catalysts, prepared in the quartz tube and stainless-steel U-tube, required for catalyst characterization and promotion purposes. However, an *in situ* sample was prepared, therefore not passivated before being exposed to testing conditions, to study the passivation effect on the activity and selectivity of the catalyst (see 4.3.2).

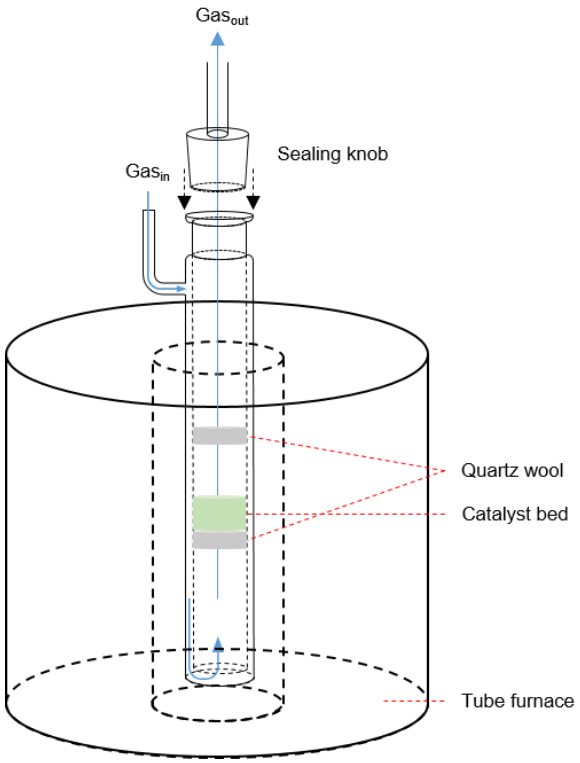

Figure 4-1: Illustration of the carburization set-up used for the synthesis of β-Mo_2C. Quartz tube dimensions: i.d. = 15 mm, o.d. = 22 mm, length tube 300 mm.

4.1.3 Catalyst promotion, drying and calcining

The preparation of the promoted samples was achieved by a wetness impregnation method. The catalysts were weighed out and the Mo content of the sample was calculated (under the assumption that the mass difference between the bulk carbide and the oxide of the passivation layer is negligible). The addition of potassium was based on a K/Mo ratio of 2.5 wt.%, 5.0 wt.% and 7.5 wt.%. Potassium carbonate (K_2CO_3, SAARCHEM) was dissolved in a few drops of distilled water, until a clear solution was obtained. Subsequently, the β-Mo_2C sample was added to the K_2CO_3-solution while stirring slowly, forming a smooth suspension. Once mixed properly, the

suspension was dried in a drying oven for about 1 to 2 hours at 120 °C. The dried sample was then calcined at 500 °C for 2 hours at a heating rate of 5 °C/min in the calcination rig (Figure 4-1) or *in situ* under 50 mL/min/g_{cat} of argon [21]. After calcination, the catalyst was ready for catalyst characterization/testing.

4.2 Catalyst characterization

Catalyst characterization was performed before and after catalyst testing. Before catalyst testing, it was made sure the desired phase was formed, analyzed using X-ray Diffraction (XRD). The influence of the different carburization conditions on the characteristics of the catalyst were analyzed using transmission electron microscopy (TEM), X-ray photoelectron spectroscopy (XPS), XRD and Raman spectroscopy. Temperature programmed hydrogenation (TPH) was used to analyze the reduction/methanation behavior of the graphite encapsulated catalysts. The metal loadings of the different catalysts were measured via inductively coupled plasma optical emission spectrometry (ICP-OES).

4.2.1 XRD analysis

X-ray diffraction (XRD) measurements were used to analyze the crystalline phases of the components of the catalysts. The obtained diffraction patterns were compared with reference data files reported in a database (ICDD PDF_2). The analysis was carried out in a D8 Advance Bruker laboratory X-ray diffractometer operated at 35 kV and 40 mA with a cobalt source (λ = 1.78897 Å) and position sensitive detector (LynxEye E 1D mode). The scan range was set from 20° to 120° 2Θ, with a step size of 0.043° and a time per step of 0.75s. Total scan time was 29 minutes and 50 seconds.

4.2.2 TEM analysis

Transmission electron microscopic (TEM) images of the prepared catalysts were taken with a Tecnai F20 transmission electron microscope equipped with a field emission gun (operated at 200 kV). The obtained images can be analyzed to identify the crystal phase of the catalyst, obtain particle size estimations as well as observations regarding morphology and formed layers/components on the catalyst. The catalyst samples were suspended in acetone in an ultrasonic bath. A droplet of the suspension was transferred onto holey carbon coated copper grids and dried prior to the viewing in the TEM.

4.2.3 XPS analysis

X-ray photoelectron spectroscopy (XPS) was carried out to observe the elemental composition on the surface of the catalyst. The measurements were carried out under a Kratos Axis Ultra DLD photoelectron spectrometer utilizing Al radiation (1486.6 eV photon energy). All data was acquired at a pass energy of 40 eV for high resolution spectra and 160 eV for survey scans. Step size was 0.1 eV for high resolution scans and 1 eV for the survey scans. Charge compensation was achieved using the Kratos immersion lens system and all spectra subsequently calibrated to the C 1s line taken to be 284.8 eV. XPS analysis can be conducted for the determination of the chemical and electronic state of the elements on the surface (first 10 nm) of the examined material. The analysis is performed by the irradiation of the material with a beam of X-rays, with

a known photon-energy (in this case Al radiation of 1486.6 eV). The X-rays excite the atoms and subsequently the electrons jump out of their shells into the ultra-high vacuum (UHV) chamber. In the UHV the electrons are sent through to a kinetic energy analyzer. With the known photon-energy of the X-rays and the measured kinetic energies, the binding energy can be calculated. The obtained binding energies are specific for each element which makes it possible to identify the elements present on the surface of the sample. Data analysis was completed with the CasaXPS software (v2.3.17 PR1.1) applying sensitivity factors from the manufacturer.

4.2.4 Raman analysis

Raman spectroscopy was performed to analyze the surface of the catalyst to observe any carbon deposition (graphitic/amorphous) and observe the formed oxide layer, MoO_x, as these are strong Raman scatterers. The analysis was carried out with a Renishaw inVia Raman Microscope equipped with a green laser. The software used for data analysis is WiRE 3.4 HF5925 build 2377. The measurements were completed setting the laser power between 20-60 MW. Raman spectra were recorded of the differently prepared samples to observe the effect of the different carburization temperatures on the surface of the catalysts.

4.2.5 Temperature programmed hydrogenation (TPH)

TPH experiments were performed studying the removal of the deposited carbon species on the surface of the catalyst, formed during the high temperatures of carburization. According to literature [101], four types of carbon can form the catalyst's surface; adsorptive, carbidic, pyrolytic or graphitic carbon. The desorption temperatures of these four types vary between 200 to 800 °C. Therefore, the TPH experiment was completed by analyzing the β-Mo_2C sample inside the calcination rig (Figure 4-1), which was equipped with a GC-TCD (Varian CP-4900) to monitor the CH_4 formation. The sample was heated to 800 °C under a hydrogen flow of ±150 mL/min/g_{cat} using a ramp rate of 1 °C/min. The CH_4 formation and consumption of hydrogen was monitored by the GC-TCD which thus indicated if carbon was removed from the surface. No internal standard was added to the gas stream, therefore no quantitative analysis was possible.

4.2.6 ICP-OES

Inductively coupled plasma optical emission spectrometry (ICP-OES) measurements on the samples were conducted by means of a Varian OES 730 Series spectroscope. ICP-OES analysis was performed to determine the metal loadings of potassium as well as molybdenum content in the catalysts. The instrument was equipped with a radial torch configuration and scandium as an internal standard. This method can be used to quantify small traces of metals in the catalyst as it is highly sensitive. Sample preparation is completed by a typical acid digestion in 3 mL of HCL, 3 mL of HF and a few droplets of HNO_3 in a reactor containing bi-distilled water. The process continued by heating the mixture to 130 °C, stirring for an hour and then cooling under a jet of

water. Residue is avoided by the addition of 60 mL of H_3BO_3 while stirring. After filtration, the solution is injected into the spectroscope.

4.2.7 In situ powder X-ray diffraction (in situ PXRD)

In situ PXRD measurements were performed in a XRK900 Anton Paar reaction cell attached to a laboratory XRD (Bruker D8 Advance) operated at 47 kV and 35 mA equipped with a molybdenum source (λ = 0.7107 Å) and a position sensitive detector (Bruker AXS Vantec). The samples were analyzed with a scan range of 13° to 40° 2Θ with step size: 0.0287° and z-drive of -1.95. Time per step was 0.2s, and scan time 5.0 minutes. The obtained diffraction patterns were compared to reference patterns recorded in the ICDD PDF-2 and analyzed using Rietveld refinement techniques.

4.3 Catalyst testing

4.3.1 Test unit and reactor set-up

An illustration of the test unit set-up is shown in Figure 4-2. The synthesis gas, a mixture of H_2 and CO (both from Air Liquide, 99.999% purity), was fed into the reactor using mass flow controllers (Brooks Instruments) which were calibrated before use. The NH_3 was co-fed using a 10% NH_3/H_2 mixture (AFROX) to be able to co-feed the ammonia at pressures above the vapor pressure of pure ammonia. All feed gas lines are joined into one inlet line flowing into the U-tube reactor (1/4" stainless steel, ID of 3.8 mm). An insulated stainless-steel block with six heating cartridges and a centrally located thermocouple was placed around the reactor for heating purposes. The fixed-bed reactor (Figure 4-3) was tightly packed with quartz wool on both sides of the catalyst bed, to prevent the catalyst from moving out of the isothermal zone. The inlet side of the catalyst bed was packed with silicon carbide (average particle size ~ 1 mm) which acts as a gas pre-heating zone. Again, the silicon carbide was tightly packed with quartz wool. The reactor outlet gas was led through a hot trap (190 °C) and was subsequently split via bleeding valves into a stream for the online 2D gas chromatography (see section 4.4.2), a stream to an ampoule sampler to take gas samples in a glass ampoule [154] for offline flame ionization gas chromatography (see section 4.4.2) analysis (Figure 4-4) and a main gas stream leading to the back pressure regulator. The latter was subsequently cooled in a cold trap (17 °C) to condense any high boilers as well as water. After pressure drop via a back-pressure regulator (GO Instruments, BP60-1A11CEK1Q1 up to maximum of 69 bar) the line continued to a three-way valve that sent the tail gas to a bubble flow meter (to analyze the flow rate of the gas) or to an online gas chromatogram equipped with a thermal conductivity detector (GC-TCD) for permanent gas analysis (see section 4.4.1) purposes. The reactor inlet and outlet lines were heated (red lines in Figure 4-2) to 190 °C and the sample lines to 180 °C to minimize the temperature gap between the inlet gas and the reactor and to prevent product condensation (which leads to blockage in the case of wax formation) in the outlet lines. The unit was also equipped with a by-pass line to allow the gas to by-pass the reactor joining the line just before the back-pressure regulator. This was used to stabilize flows at the required pressure, before the FT-reaction takes place.

4.3.2 Generalized experimental procedure

Prior to the Fischer-Tropsch experiments, the catalyst samples were treated in 50 mL/min/g_{cat} hydrogen at atmospheric pressure at 400 °C with a ramp rate of 5 °C/min for 4.5 hours to reduce the catalyst and to remove the oxide layer formed during the passivation step (see section 4.1.2). Exception was made for one *in situ* prepared non-promoted catalyst, which did not require reduction as it was not passivated. After reduction, the temperature was cooled to reaction temperature under argon or nitrogen flow. The reactor was pressurized to the required reaction pressure in a nitrogen or argon atmosphere. Once the reactor pressure was reached and stabilized, the vessel was isolated via the bypass and the reaction gases were set at the required

flow rates. The by-pass was then pressurized with the mixture of gases and left overnight to stabilize. The reaction was started by switching back to the reactor.

In case of NH_3 co-feeding, the argon flow rate is reduced in accordance with the NH_3 to be added so as to keep the partial pressure of hydrogen and carbon monoxide stable. A second external standard (nitrogen or argon) is co-fed to the exit line of the reactor, from the beginning of the experiment, for quantitative analysis (see 4.4.1).

Upon termination of the reaction, the reactive gas flows are shut off, followed by de-pressurizing of the reactor and set to cool down to room temperature under argon flow. Once room temperature is reached, the argon flow is shut off and the catalyst can be unloaded, without any post FT-run passivation method. After the experiment, the catalyst is exposed to post FT-run characterization.

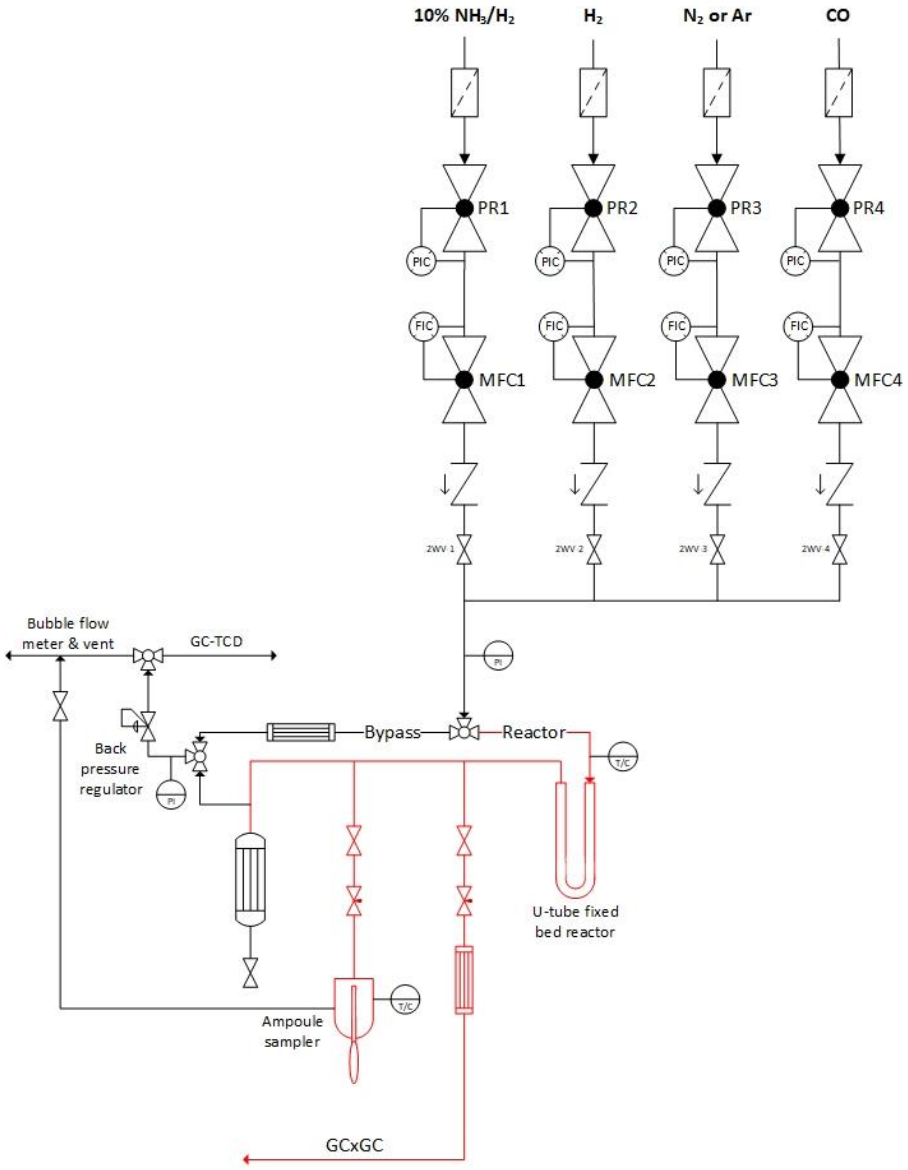

Figure 4-2: Illustration of the rig set-up used for catalyst testing. Red lines are heated lines.

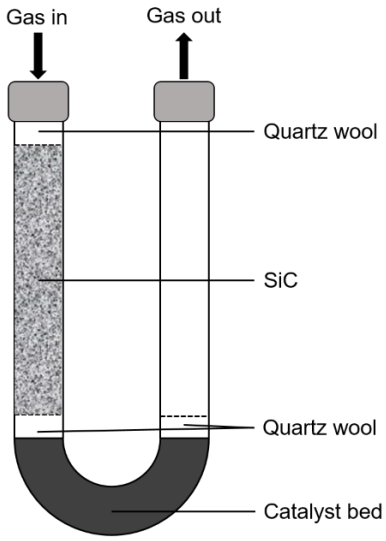

Figure 4-3: Illustration of the U-tube reactor, used for catalyst testing.

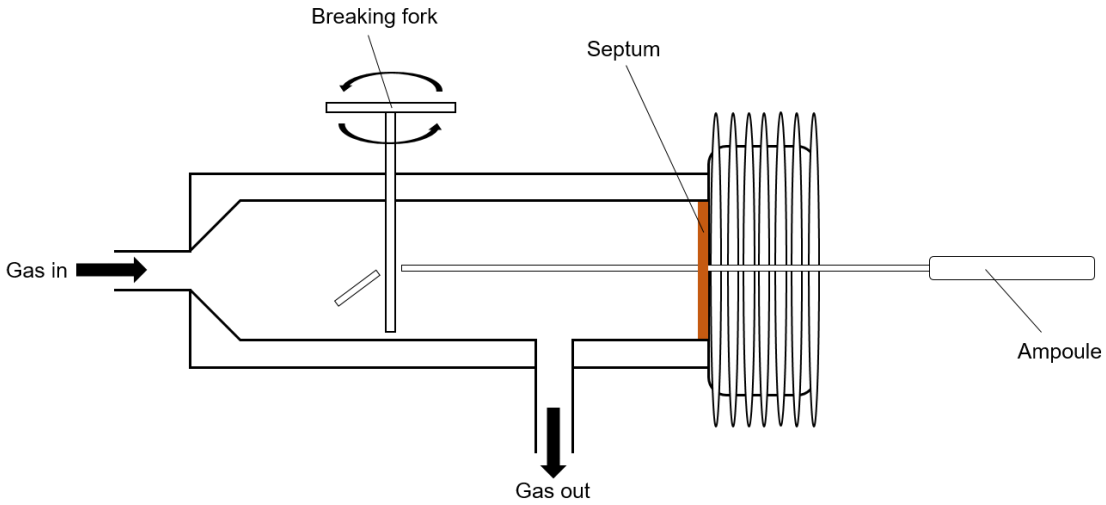

Figure 4-4: Schematic overview of the ampoule sampling technique for off-line gas analysis.

*4.3.3 **Specific experimental procedure***

The more specific preparation and testing conditions used for each FT-run are described in Table 4-1. A first set of Fischer-Tropsch experiments was performed inside the reaction tube to analyze the influence of the carburization temperature during catalyst synthesis and the passivation procedure of the catalyst on its activity and product selectivity under typical FT-conditions. Based on the obtained results it was decided which catalyst synthesis routine and reaction conditions was taken for further testing with potassium promotion. Eventually the catalyst with optimum potassium promotion was used for the FT-product upgrading, co-feeding NH_3:

Table 4-1: Specific preparation and testing conditions for all catalyst's that are tested for Fischer-Tropsch reaction.

Catalyst preparation				Catalyst testing			
FT run	T_{carb} °C	Passivation yes/no	Promotion wt. %	Reduction °C; h	Space velocity L/h/g_{cat}	$T_{reaction}$ °C	Pressure bar
1.1	630	no	n/a	n/a	16.0	240-300	33
1.2	630	yes	n/a	400; 4.5	9.6-16.0	260-280	33
1.3	760	no	n/a	600; 2.5	8.0-16.0	280-300	33
2.0	630	yes	n/a	400; 4.5	8.4-33.6	240-300	33-43
2.1	630	yes	5	400; 4.5	8.4	260-350	45
2.2	630	yes	7.5	400; 4.5	8.4	260-350	45
2.3	630	yes	2.5	400; 4.5	8.4	260-350	45
3.1	630	yes	5	400; 4.5	8.4	300	45-65
4.1	630	yes	5	400; 4.5	8.4	300	45
4.2	630	yes	5	400; 4.5	8.4	300	45
4.3	630	Yes	5	400; 4.5	8.4	300	45
4.4	630	Yes	5	400; 4.5	8.4	300	45

FT run 1.1*: In situ* prepared catalyst.

- An un-promoted, non-passivated, *in situ* prepared (prepared inside the U-tube reactor and not exposed to air before reaction) catalyst was tested for its activity in the Fischer-Tropsch reaction. Conditions applied were following literature reports [20, 21, 101] and set as followed: T = 280 °C, P = 33 bar and SV = 16 L/h/g_{cat}, and thereafter varied per obtained activity/selectivity (Table 4-1).

FT run 1.2: Passivated catalyst.

- Sample was prepared inside the U-tube reactor and directly after carburization, sample was quenched to room temperature and passivated with 50 mL/min/g_{cat} of 1% O_2 in N_2 gas for 1 hour, a required step for further promotion with potassium. After completion of the passivation step, the catalyst was heated at 5 °C/min to 400 °C to be reduced for 4.5 hours under 50 mL/min/g_{cat} of H_2 prior to reaction. At first, the same reaction conditions were applied as FT run 1.1 and set as followed: T = 280 °C, P = 33 bar and SV = 16 L/h/g_{cat}, and thereafter conditions were varied as per obtained activity/selectivity (Table 4-1).

FT run 1.3: Graphite capsulated catalyst.

- Based on theoretical calculations from Lee *et al.* (1987) [143] and experimental data shown by Mo *et al.* (2016) [101] increasing the carburization temperature while using 20% CH_4/H_2 as carburization gas mixture (>760 °C), graphite carbon is deposited on the

surface of the catalyst. To study the effect the graphitic carbon has on the catalytic activity and selectivity, a catalyst was prepared inside the U-tube reactor, using the same conditions as before, however with a final temperature of 760 °C. No passivation was conducted. Based on the earlier obtained TPH results, the catalyst was reduced at 600 °C for ±2.5 hours under 50 mL/min/g_{cat} of H_2 prior to reaction. Formation of CH_4 was monitored using a GC-TCD to stop the reduction/methanation step as soon as the CH_4 formation subsided, i.e. most of the deposited carbon was removed from the catalyst's surface. Reaction was started using the same starting conditions as FT run 1.1 and 1.2 and were set as followed: T = 280 °C, P = 33 bar and SV = 16 L/h/g_{cat}. Thereafter conditions were varied per obtained results activity/selectivity (Table 4-1).

FT run 2.0: Passivated ''baseline'' catalyst.

- Based on the obtained results from the previous three runs, it was decided to continue with the passivated catalysts to conduct further testing. The preparation of the catalyst was the same as in FT run 1.2. It was of interest to investigate the influence of a wide range of process conditions on the activity and selectivity of the catalyst. Starting conditions were set as followed: T = 240 °C, P = 33 bar and SV = 34 L/h/g_{cat}. Thereafter, a space velocity sweep (8-34 L/h/g_{cat}), followed by temperature sweep (240-300 °C) and finally a pressure sweep (33-43 bar) was applied (Table 4-1).

FT run 2.1 - 2.3: Potassium promoted catalysts.

- To upgrade the Fischer-Tropsch product spectrum towards a higher selectivity of oxygenates, passivated catalysts were promoted with K_2CO_3. An optimum amount of potassium promotion must be determined, as literature has shown it to exhibit a maximum regarding desired selectivity and activity [19-21]. The catalysts were prepared following the same preparation method as FT run 1.2. However, after the passivation step, catalysts were removed from the U-tube reactor and promoted (see section 4.1.3 for details). The catalysts were tested in the following order; 5.0 wt.% K/Mo (FT run 2.1), 7.5 wt.% K/Mo (FT run 2.2) and 2.5 wt.% K/Mo (FT run 2.3) promotion. All catalysts were exposed to the starting conditions set as followed: T = 260 °C, P = 45 bar and SV = 8 L/h/g_{cat}. A constant space velocity and pressure was maintained, but a temperature sweep (260-350 °C) was applied to observe the influence of temperature on the formation of higher oxygenates in relation to the activity of the catalyst.

FT run 3.1: Influence of pressure on 5.0 wt.% K/Mo promoted catalyst.

- The catalyst was prepared using the same preparation method as FT run 1.2, promoted with 5.0 wt.% K/Mo. The sample was exposed to the same space velocity as previous promoted samples at a reaction temperature of 300 °C. Pressure range of 45-65 bar was applied, to study the effect of total pressure on the formation of oxygenates and activity of the catalyst.

FT run 4.1: 4.7 vol.% NH_3 co-feeding

- The same catalyst as in FT 3.1 was used, promoted with 5.0 wt.% K/Mo. The catalyst was first exposed to the same FT conditions applied in FT run 3.1 and were set as followed: T = 300 °C, P = 45 bar and SV = 8 L/h/g_{cat}. Pressure was maintained at 45 bar throughout the run. The internal reference gas was replaced with N_2. An external reference gas (Ar) was added to the outlet stream, to allow for immediate quantitative analysis of the reactor outlet flows during stabilization of the feed composition. The catalyst was exposed to these 'normal FT conditions' (no NH_3 co-feeding) until CO conversion was stable. Upon stable CO conversion, ±4.7 vol.% of NH_3 (calculated based on total feed gas) was co-fed to the reactor at the expense of the internal standard, to keep partial pressures of H_2 and CO constant. After one hour of ammonia co-feeding a blockage of the reactor was observed, increasing the total pressure of the system, which lead to the premature termination of the experiment.

FT run 4.2: 1.5 vol.% NH_3 co-feeding

- As quantitative analysis was still difficult, as stabilization of the flows usually takes up to 12 hours and due to the loss of product gas towards the online GCxGC, the test unit was adjusted to add a second internal standard (Ar), which will allow for accurate calculations at any point during the run. The same catalyst was used as in FT run 3.1, promoted with 5.0 wt.% K/Mo. The catalyst was again exposed to normal FT conditions, set as follows: T = 300 °C, P = 45 bar and SV = 8 L/h/g_{cat} until stable CO conversion. Upon stable CO conversion, ±1.5 vol.% NH_3 was co-fed to the reactor. Blockage occurred after a few hours, however, accurate quantitative analysis of the products was successful with the help of the 2nd internal standard.

4.4 Product analysis

Product analysis is completed with three different gas-chromatographic (GC) techniques. The inorganic permanent gases and methane are analyzed and quantified using a GC equipped with three columns and thermal conductivity detectors (GC-TCD). The organic compounds are analyzed using an offline GC equipped with a flame ionization detector (FID) and online using the GCxGC (2D) equipped with a time of flight (TOF) and a flame ionization detector. All three analyzing techniques will be discussed in detail in the following section.

4.4.1 Analysis of inorganic compounds

An online micro GC (Varian CP-4900) equipped with three different dedicated thermal conductivity detectors (TCD) and columns was used for the analysis of permanent gases (for exact configuration see Appendix A). A TCD analyses the difference between the gases based on the thermal conductivity of each gas compared to a reference gas (carrier gas, in this case H_2 or Ar). The set-up was used to quantify the gases Ar, N_2, CO, H_2, CH_4 and CO_2.

Table 4-2: Column selection for the GC-TCD to analyse the inorganic gases.

TCD Column	Carrier Gas	Elutes in order of increasing retention time			
20m molecular sieve (MS5A) Plot	H_2	Ar	N_2	CH_4	CO
10m molecular sieve (MS5A) Plot	Ar	H_2	CO		
10m PorapakQ	H_2	Mix[a]	CH_4	CO_2	

[a]Mixture of Ar, N_2 & CO not retained in column

Ar/N_2 (Air Liquide, 99.999% purity) was used as an internal standard/reference gas, as it does not react with the catalyst and therefore can be used for quantitative analysis purposes. The concentration of the reference gas is a known concentration that stays stable during the entire reaction. The concentration of the reactants (CO and H_2) and products (CH_4, CO_2) can therefore be calculated in relation to their specific response factors and the concentration of the internal standard.

The concentration of the reactants or the products can be expressed in the following equation:

$$f_A \cdot \frac{[A]}{A_A} = f_B \frac{[B]}{A_B} \quad (4\text{-}1)$$

Where, f_x is the response factor of species x, $[x]$ the concentration of species x and A_x the peak area of species x obtained in the TCD-chromatogram.

The calibration of the GC-TCD (see Appendix C, Table 9-3) is required to calculate a response factor for each compound as a function of a specific reference gas. Calibration is completed by analyzing a mixture of the above gases with a known concentration of each compound. The response factors can subsequently be calculated with the following equation:

$$f_{Af(IS)} = \frac{f_A}{f_{IS}} = \frac{[IS] \cdot A_A}{A_{IS} \cdot [A]} \quad (4\text{-}2)$$

Where, IS is the internal standard and the A is the compound to be analyzed. By restructuring of equation (4-2) it is possible to calculate the concentration of the compound to be analyzed:

$$[A] = \frac{1}{f_{Af(IS)}} \cdot \frac{[IS] \cdot A_A}{A_{IS}} \quad (4\text{-}3)$$

4.4.2 Analysis of organic compounds

The organic products in the Fischer-Tropsch product spectrum are sampled using a glass ampoule technique and are analyzed offline using a GC Varian 3900 (for detailed conditions, see Appendix B) equipped with a flame ionization detector (FID). The FID is specific to the formed organic products. The different organic compounds elute at different retention times, depending on their interactions with the column lining (the stationary phase). The strength of the signal is related to the number of carbon atoms in the molecule and whether these carbon atoms are bonded to an oxygen atom. Kaiser (1969) [155] published a theoretical method calculating an increment in the response factors to account for these different oxygenates. Response factors for carbon atoms bonded only to hydrogen or other carbon atoms were allocated an increment of 1. Carbon atoms with one single bonded oxygen are assigned an increment of 0.55. Carbon atoms with a double bonded oxygen atom do not give any response. Using this method, the response factors can be calculated for each compound produced during the FTS and is as follows:

$$f_i = \left(\frac{N_{C,i}}{N_{C(noO)} + 0.55(N_{C(C-O)}) + 0(N_{C(C=O)}} \right) \quad (4\text{-}4)$$

Where, f_i is the response factor for a specific compound i, $N_{C,i}$ is the total number of carbon atoms in the compounds i, $N_{C(noO)}$ is the number of carbon atoms without bonds to oxygen, $N_{C(C-O)}$ is the number of carbon atoms single bonded to an oxygen atom and $N_{C(C=O)}$ is the number of carbon atoms double bonded to an oxygen atom, giving:

$$f_i = \left(\frac{N_{C,i}}{N_{C(noO)} + 0.55(N_{C(C-O)})} \right) \quad (4\text{-}5)$$

The calculation of the response factors for the nitrogen-containing compounds is based on a method described by Sango (2013) [130]. C_8 amine and nitrile response factors were calculated based on using 1-octene as the reference and hexane as a solvent. An injection containing a known concentration of C_8 amine and 1-octene was injected into the GC-FID and the corresponding area was linked to the molar carbon ratio of each compound relative to 1-octene. Thus, an observed carbon number can be calculated and the response factor would then be related to the actual number of carbons divided by the observed number of carbons (Table 4-3 for amine, Table 4-4 for nitrile). Amide response factors are estimated based on the functional

groups. The influence of these groups does not extend to more than one carbon; therefore, the C_{obs} is always one carbon lower than the actual carbon number.

Table 4-3: Calibration for amine FID response factor. Table is adapted from Sango (2013) [130].

Component	n_i / n_{octene}	Area				C_{obs}	f_i
		A1	A2	A3	Average		
1-octene	1	3.04E+08	4.39E+08	5.14E+08	4.19E+08	8	1.00
C8 amine	1.031	2.98E+08	4.22E+08	4.90E+08	4.03E+08	7.46	1.07

Table 4-4: Calibration for nitrile FID response factor. Table is adapted from Sango (2013) [130].

Component	n_i / n_{octene}	Area				C_{obs}	f_i
		A1	A2	A3	Average		
1-octene	1	6.97E+08	6.19E+08	7.03E+08	6.73E+08	8	1.00
C8 nitrile	0.993	7.04E+08	6.52E+08	6.87E+08	6.81E+08	8.15	0.98

With C_{obs} as the observed carbon number calculated as follows:

$$C_{obs} = \left(\frac{A_{average,i}}{n_i / n_{octene}}\right) / A_{average,octene} \cdot C_{n,i} \quad (4\text{-}6)$$

With $A_{average,i}$ for the average area obtained from the FID of the compound i, which is amine or nitrile. n is the molar carbon ratio and C_n is the actual carbon number. Thereafter, the response factor can be calculated:

$$f_i = \frac{C_{n,i}}{C_{obs,i}} \quad (4\text{-}7)$$

Each compound can be identified by comparison with known spectra or by calculation of its specific Kovats retention index number. Kovats indices [156] are specific values for each compound in the Fischer-Tropsch product spectra. In general, the n-paraffins start with a Kovats index of 100 for methane (C_1), 200 for ethane (C_2), 300 for propane (C_3) and so on. Upon identification of the retention times of the paraffins in the spectra, all other Kovats indices can be calculated for the other compounds by the following formula for isothermal chromatography:

$$KI = 100 \cdot \left[n + (N - n)\frac{\log(RT_{unknown}) - \log(RT_n)}{\log(RT_N) - \log(RT_n)}\right] \quad (4\text{-}8)$$

Where, KI is the Kovats index, RT is the retention time of the unknown peak, the smaller carbon number (n) and the larger carbon number $(N, with\ N = n + 1)$ of the n-paraffin peak.

For non-isothermal chromatography, the Kovats indices can be calculated by the following formula:

$$KI = 100 \cdot \left[n + (N - n)\frac{RT_{unknown} - RT_n}{RT_N - RT_n}\right] \quad (4\text{-}9)$$

In this study, the temperature program is both isothermal and non-isothermal during the entire analysis, therefore the isothermal formula was chosen, which could lead to some variations in the actual retention time of certain products.

From a known product spectrum and with the help of mass spectroscopy, the Kovats indices [156] of most the Fischer-Tropsch products are calculated (see Appendix D and Appendix E) and therefore a retention time can be calculated, to find the product in the obtained spectra from sample analysis.

Subsequently, the molar flowrate of each FT-product can be calculated using methane as the internal standard (its concentration is obtained from the GC-TCD). With the following formula, the molar flow rate can be calculated:

$$\dot{n}_i = \left(\frac{N_{CH_4}}{N_i}\right) \cdot \left(\frac{f_i \cdot A_i}{f_{standard} \cdot A_{CH_4}}\right) \cdot \dot{n}_{CH_4} \quad (4\text{-}10)$$

Or only based on carbon:

$$\dot{n}_{iC} = N_{CH_4} \cdot \left(\frac{f_i \cdot A_i}{f_{standard} \cdot A_{CH_4}}\right) \cdot \dot{n}_{CH_4} \quad (4\text{-}11)$$

Where, $\dot{n}_i$ is the molar flow rate of compound i, $\dot{n}_{iC}$ is the molar flow rate of compound i on carbon basis, N_{CH_4} is the number of carbon atom in CH_4.

4.4.3 Conversion, yield and selectivity

The activity of a catalyst in the Fischer-Tropsch synthesis is usually expressed as the amount of carbon monoxide converted in relation to the amount of carbon monoxide fed into the reactor, also known as the CO conversion (X_{CO}):

$$X_{CO}(\%) = \frac{(\dot{n}_{CO,in} - \dot{n}_{CO,out})}{\dot{n}_{CO,in}} \cdot 100\% \quad (4\text{-}12)$$

Where, X_{CO} is the conversion of CO, $\dot{n}_{CO,in}$ is the molar flow rate of CO into the reactor an $\dot{n}_{CO,out}$ is the molar flow rate of CO out of the reactor. In the presence of high WGS-activity, the CO conversion is an incorrect indication to the formation of actual FT-products. Therefore, the CO conversion to FT-product can be calculated as followed:

$$X_{CO\ to\ HC}(\%) = \frac{\left(\dot{n}_{CO,in} - \dot{n}_{CO,out}\right) - \dot{n}_{CO_2,out}}{\dot{n}_{CO,in}} \cdot 100\% \quad (4\text{-}13)$$

The yield of a compound can be expressed as the ratio of the molar flowrate of the compound formed to the molar flow rate of CO fed into the reactor and can be calculated as followed:

$$Y_{i,} = \frac{\dot{n}_{i,}}{\dot{n}_{CO,in}} \quad (4\text{-}14)$$

Or using carbon as a basis:

$$Y_{i,C} = \frac{\dot{n}_{i,C}}{\dot{n}_{CO,in}} \quad (4\text{-}15)$$

Where, Y_i is the yield of compound i, $Y_{i,C}$ is the yield of compound i on a carbon basis. The selectivity of a compound can therefore be calculated as a ratio of the yield of the compound to the CO conversion:

$$S_i = \frac{Y_i}{X_{CO}} \quad (4\text{-}16)$$

Or on a carbon basis:

$$S_{i,C} = \frac{Y_{i,C}}{X_{CO}} \quad (4\text{-}17)$$

All selectivities towards CH_4 and CO_2 presented in the results section are calculated based on 'carbon balance corrected' selectivities. The carbon balance is very sensitive to the CO conversion measured, especially at low conversions. Under these conditions, slight changes in the integration boundaries of the GC-TCD have significant impact on the apparent CO conversion in turn affecting the ability to close the carbon balance as well as the values for the CH_4 and CO_2 selectivity, directly extracted from the GC-TCD data. Therefore, to ''correct'' the calculated selectivities towards CO_2 and CH_4, they are divided by the carbon balance calculated (see Appendix G, Table 9-6). Selectivities towards the other organic products are not affected as they are generally presented as ratios. This process is conducted for all results presented to maintain consistency, but both the original and carbon balance corrected data is available in the figures and in Appendix G, Table 9-6.

5 Results and discussion

In the following section a detailed characterization of the prepared catalysts is given (chapter 5.1). Activity and selectivity trends are presented and discussed in the absence and presence of ammonia (chapter 5.2). Finally, the phase composition of the spent catalyst is reported (chapter 5.3).

5.1 Catalyst characterization

Lee *et al.* (1987) [143] published theoretical equilibrium relationships at atmospheric pressure for the carburization of Mo^0 with methane (reaction 5.1) and the decomposition of methane to carbon and hydrogen (reaction 5.2) (Figure 5-1). In between the two equilibrium equations the β-Mo_2C phase is proposed to be formed. At higher temperatures, graphitic carbon is deposited on the surface of the catalyst, while below the equilibrium line of reaction 5.1, the carbide does not form [143].

$$CH_4 + 2Mo \leftrightarrow Mo_2C + 2H_2 \quad (5.1)$$
$$CH_4 \leftrightarrow C + 2H_2 \quad (5.2)$$

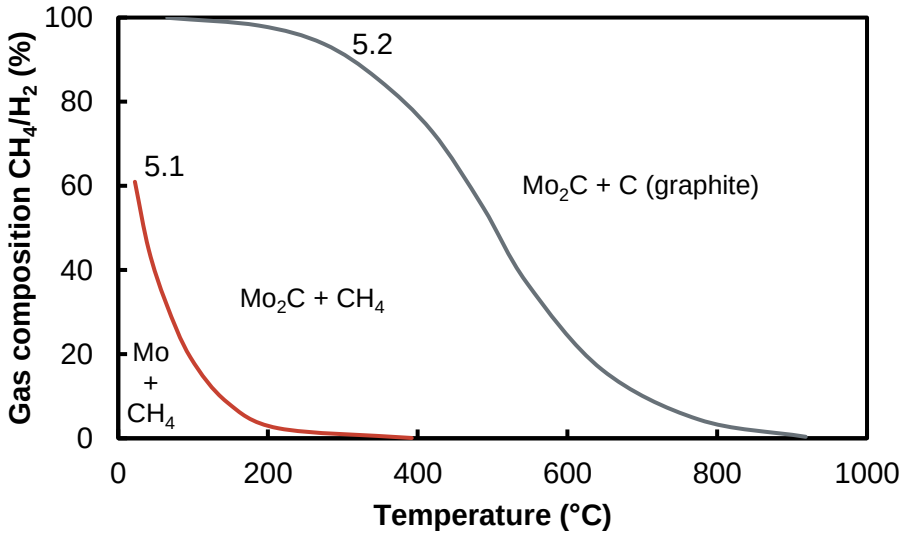

Figure 5-1: Equilibrium calculations for the two reactions; reaction 5.1 (red) and reaction 5.2 (grey). Figure is adapted from Lee et al. (1987) [143].

Mo *et al.* (2016) [101] studied the effect of carburization conditions on the formation of the β-Mo_2C from the precursor MoO_3, using different gas compositions and temperatures. While using 20% CH_4 in H_2 as the gas mixture, it was found that the carbide forms at 630 °C onwards with a ramp rate of 1 °C/min and 5 hours holding time at the final temperature. Below that temperature, the trioxide is only reduced to the dioxide (MoO_2) shown by both Raman and XRD. Analysis of the sample treated at a maximum temperature of 630 °C showed the presence of MoO_3, which is associated with the passivation layer applied after carburization to protect the carbide phase.

However, at temperatures of 760 °C and onwards, graphitic carbon was observed in Raman, which could indicate that the bulk β-Mo_2C (as shown in the XRD patterns) is encapsulated in a layer of graphitic carbon, thin enough not to be observed with XRD.

5.1.1 Effect of carburization temperature on the characteristic of β-Mo_2C

Based on the published results discussed above, three catalysts were prepared using 20% CH_4/H_2 at three different temperature zones, i.e. 630-650 °C, 750-760 °C and 1000 °C at a heating rate of 0.5 to 1 °C/min holding for 2 to 5 hours to observe the effect of the different carburization conditions on the phase composition of the catalyst (Table 5-1). XRD-analysis (Figure 5-2) was performed to determine the composition and the crystalline phase of the catalysts. The average crystallite sizes were also determined using Rietveld refinement [157]. At the temperatures 630 (A1) and 650 °C (A2 and A3) the sample re-oxidized if not passivated. The average crystallite size of β-Mo_2C at the 630 °C carburized sample was 35.0±0.3 nm. The samples prepared at 750 (B1) and 760 °C (B2), showed that the passivation step is not required and that both samples are stable in air. The average crystallite size is different for each sample (20.3 and 38.8 nm), which is possibly due to the difference in holding time (2 and 5 hours). The 1000 °C samples showed that the sample consists of 97.17 wt.% β-Mo_2C, with an average crystallite size of 63.6±0.6 nm, balanced by MoO_2. However, this is believed to be a residual of MoO_2 that is not carburized yet, rather than re-oxidized due to the small crystallite size of the MoO_2 phase. In sample A2, a sample prepared *in situ* in the XRD at 650 °C and subsequently exposed to air, MoO_2 exhibited a bimodal crystallite size distribution. The large crystallite sizes are believed to be formed during the spiking temperature of the sample upon exposure to air, i.e. re-oxidation of the carbide phase, sintering the catalyst particles. The small crystallite sized MoO_2 is identified as oxide fractions which did not entirely carburize yet. Sample A3, a sample was prepared *in situ* in the XRD at 650 °C, passivated and subsequently reduced under hydrogen for 4.5 hours at 400 °C. After cooling down to room temperature, the sample was exposed to air. Again, the sample was observed not to be entirely stable in air as 5.50% of the carbide re-oxidized to MoO_2.

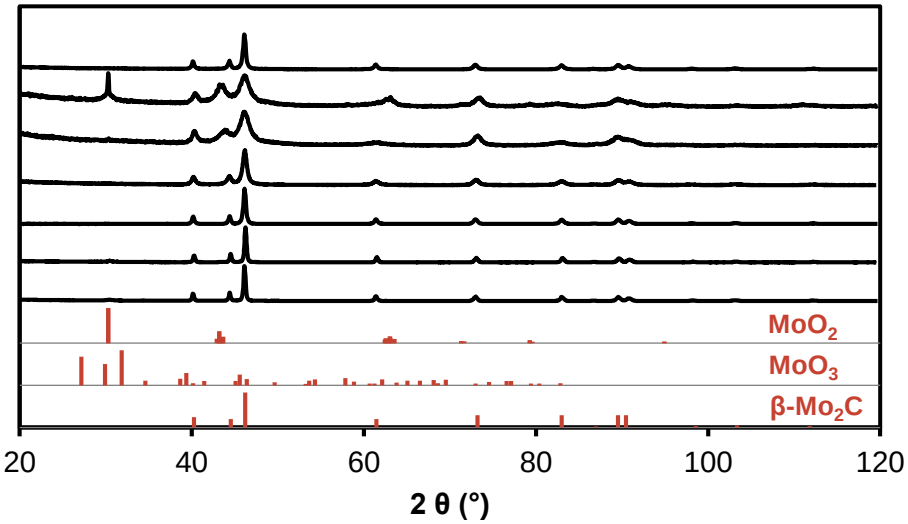

Figure 5-2: XRD analysis of samples from top to bottom A1, A2, A3, B1, B2, C1 and C2 (black). Reference patterns of MoO_2, MoO_3 and β-Mo_2C in red. X-ray source: cobalt.

Table 5-1: Effect of different catalyst preparation conditions on the composition and crystalline phase of the catalyst, defined by XRD using Rietveld refinement.

Sample	T_{final} (°C)	Ramp (°C/min)	Holding time (h)	Bulk composition (wt.%)		Crystallite size (nm)
A1[b]	630[c]	1	5	β-Mo_2C	100.00	35.0 ± 0.3
A2[a]	650	1	5	β-Mo_2C	53.52	8.0 ± 0.1
				MoO_2 (a)	36.38	9.9 ± 0.9
				MoO_2 (b)	10.10	93.9 ± 23.8
A3[a]	650	1	5	β-Mo_2C	100	8.4 ± 0.1
B1[b]	750[c]	0.5	2	β-Mo_2C	100.00	20.3 ± 0.1
B2[b]	760	1	5	β-Mo_2C	100.00	38.8 ± 0.2
C1[b]	1000[c]	0.7	2	β-Mo_2C	n/a	n/a
C2[b]	1000	0.7	2	β-Mo_2C	97.17	63.6 ± 0.6
				MoO_2	2.83	12.7 ± 1.4

a) *In situ* XRD samples, will be discussed in detail in section 5.1.4
b) Prepared in calcination rig, see Figure 4-1.
c) Passivated prior to exposure to air atmosphere.

Transmission electron microscopy (TEM) of samples A1, B2 and C1 showed clear differences specifically on the edges of the particles. Sample A1 (Figure 5-3) showed a dense clustered particle without any clear graphite deposition or oxide formation. With an increase in carburization temperature to 760 °C, sample B2, the formation of an unevenly distributed layer of a few nanometers thickness at the edge of the particles is observed (Figure 5-4). The thickness of the

layer increases with increasing carburization temperature as is observed from the TEM images of sample C1 (Figure 5-5), suggesting this constitutes the graphite layer reported in literature [101, 143]. The sample was exposed to passivation conditions, however, as for sample A1, this does not reflect in the TEM images taken.

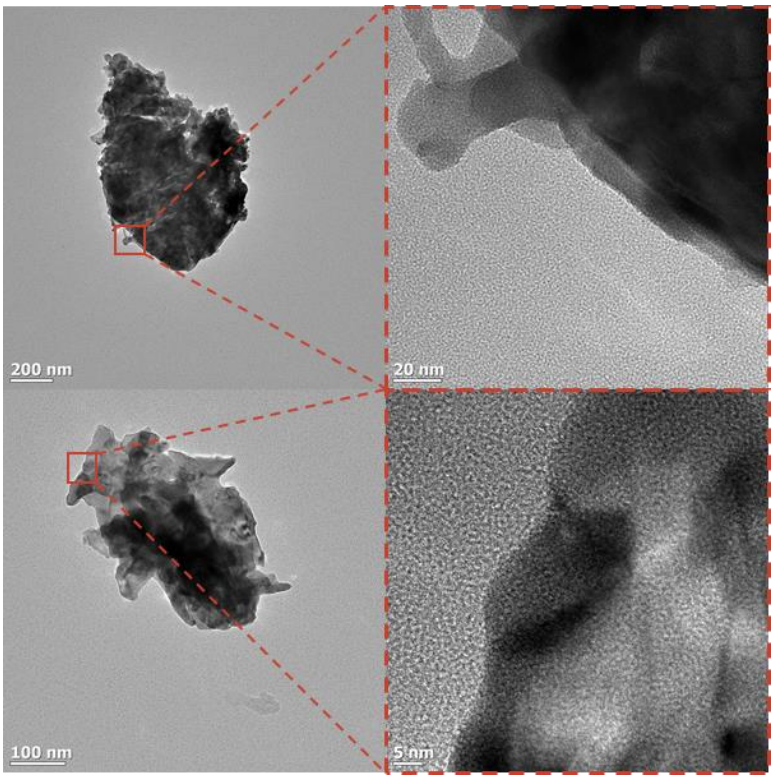

Figure 5-3: TEM image of two different particles from sample A1, carburized at 630 °C after passivation. No obvious oxide or graphite layer is visible around the catalyst.

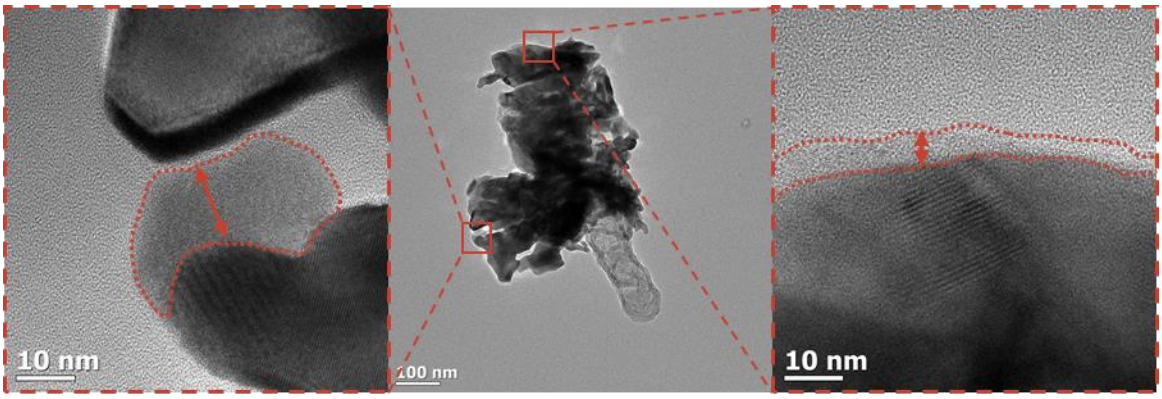

Figure 5-4: TEM image of a particle from sample B2, carburized at 760 °C without passivation. An unevenly distributed layer is observed on the edges of the particle. The dotted lines and the arrows in the pictures indicate the observed layer.

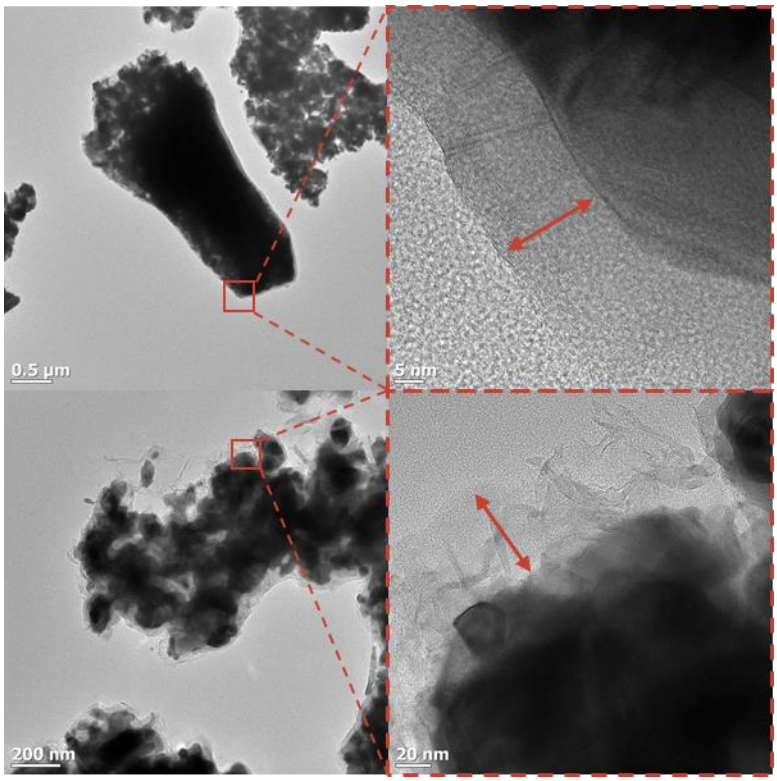

Figure 5-5: TEM image of sample C1, carburized at 1000 °C with subsequent passivation. The thickness of the layer observed as in Figure 5-4 increased.

Graphitic carbon, amorphous carbon as well as molybdenum oxide are strong Raman scatterers [101]. Raman spectroscopy (Figure 5-6) of the samples A1, B2, C2 as well as the precursor MoO_3 confirmed the hypothesis that the observed layer in the TEM images for samples B2 and C1 is graphitic carbon, shown by the D- and G-band at approximately 1347 and 1588 cm^{-1} respectively [158]. Interestingly, all samples show MoO_3 as well. This indicates that, even though the bulk catalyst is β-Mo_2C, the surface is covered with a layer of MoO_3 after passivation (A1) and even in the absence of passivation (samples B2 and C2). An increase in graphitic carbon depositions with increasing carburization temperature is also confirmed by the increased intensities of the D- and G-band (at 1347 and 1588 cm^{-1}, respectively) between samples B2 and C2, while no carbon peaks are observed in sample A1 (Figure 5-7). This shows that while the carbon layer coating of the high temperature carburized samples prevents bulk oxidation after exposure to atmospheric air, it does not completely protect the β-Mo_2C. Possibly the diffusion of O_2 to the carbide surface is limited by the C-coating resulting in a mild passivation treatment, similar to the one applied to sample A1, i.e. exposure to 1% O_2 in N_2 at room temperature.

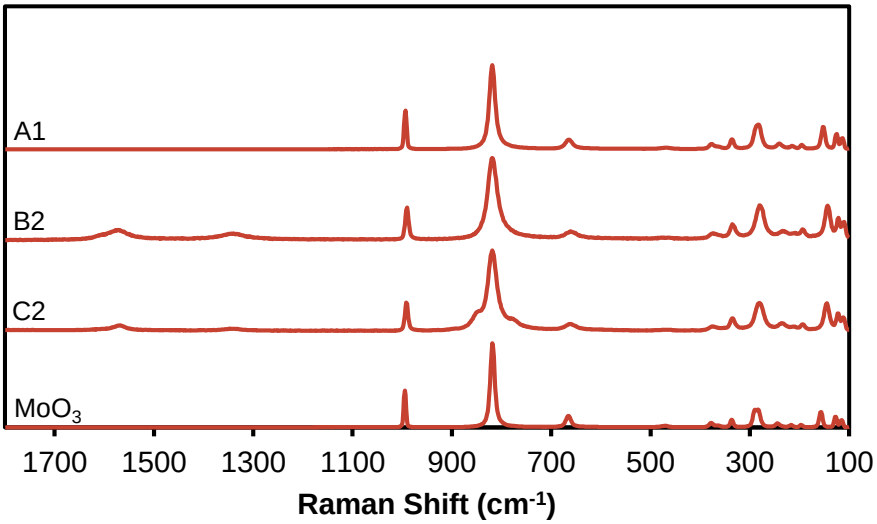

Figure 5-6: Raman spectra of samples A1 (630 °C), B2 (760 °C), C2 (1000 °C) and MoO_3. All samples show similar Raman scattering to MoO_3, however sample B2 and C2 show the specific scattering for graphitic carbon at 1347 and 1588 cm^{-1}.

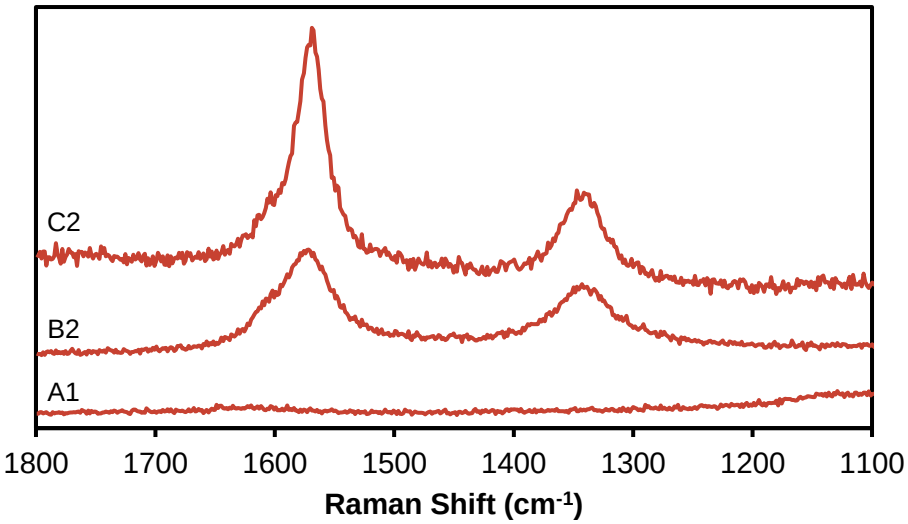

Figure 5-7: Raman spectra showing difference between D- and G-band intensities of the samples A1 (630 °C, no graphite visible), B2 (760 °C) and C2 (1000 °C).

5.1.2 Graphitic layer removal by temperature programmed hydrogenation

The surface structure of any catalyst is of course key to its performance. As it is proposed that the actual carbide phase is responsible for the desired catalytic activity, the samples carburized at 760 °C and 1000 °C, i.e. the samples covered by a graphitic carbon layer, were treated in a hydrogen stream to investigate the possibility of the removal of the carbon layer. A temperature programmed hydrogenation (TPH) reaction was carried out inside the calcination rig (Figure 4.1).

The possible formation of CH_4 was monitored with an online GC-TCD (Varian CP-4900 – see chapter 4.2.5). Both samples B2 and C2 underwent multiple methanation reactions at temperatures up to 800 °C. In a first TPH of sample B2 (Figure 5-8) the temperature was set to reach 800 °C at 5 °C/min. The GC-TCD analysis was started at 200 °C. At approximately 620 °C the initial formation of CH_4 was observed indicating the removal of the carbon layer, with a maximum at roughly 700 °C, upon which the formation rate started decreasing. At 800 °C, the methanation reaction was completed.

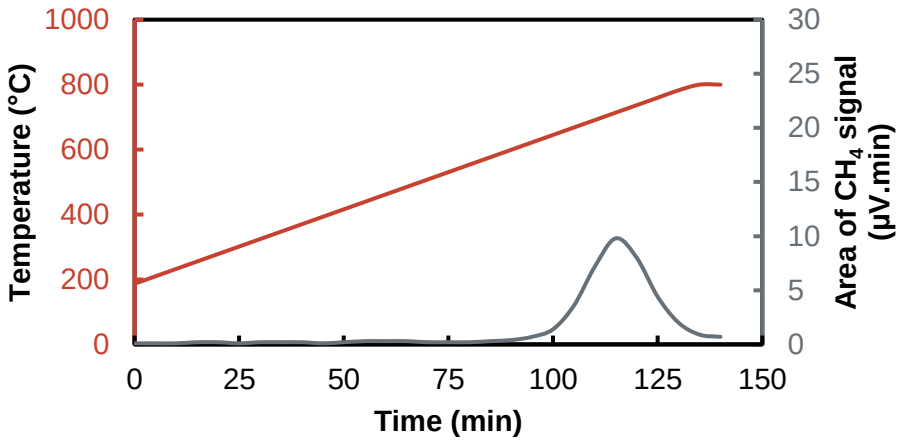

Figure 5-8: TPH run 1 profile of sample B2. Red line is the temperature profile and the grey line is the formation of CH_4 indicated with the area obtained from the GC-TCD. T_{final} = 800 °C, ramp rate = 5 °C/min, H_2 SV ~ 9 L/h/g_{cat}.

A second TPH analysis was performed for the samples B2 (Figure 5-9) and C2 (Figure 5-10). For both analyses, the temperature was set to 550 °C at 10 °C/min and thereafter at 1 °C/min to 800 °C. For sample B2, the formation of CH_4 was first detected at 555 °C, peaked at ±660 °C and declined while still heating to 800 °C. The analysis was stopped as soon as no CH_4 was detected in the off gas anymore. The CH_4 formation for sample C2 started at roughly 660 °C and continued up to 800 °C peaking after 295 minutes holding time. No methane was detected after 455 min at 800 °C. A significantly higher amount of CH_4 was formed during the treatment of sample C2 with a total area of 3571 µV compared to 222.5 from sample B2. This is in line with the thickness of the graphite layer observed in the TEM images and the intensity of the D- and G-band in the Raman spectra.

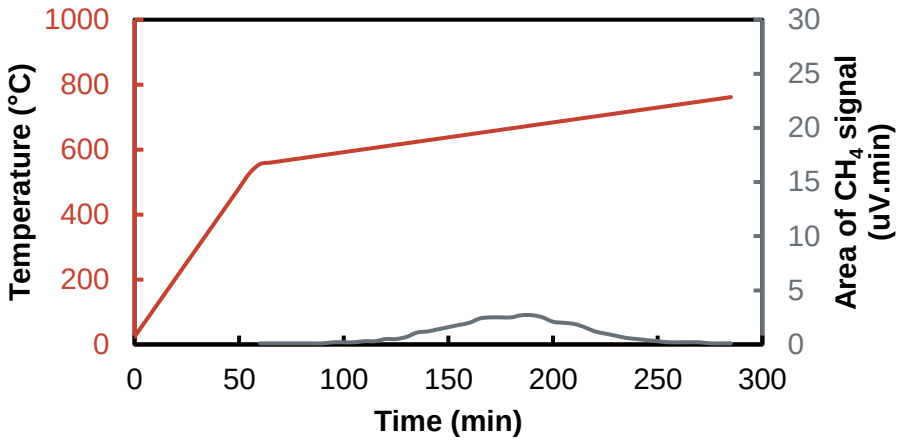

Figure 5-9: TPH run 2 profile of sample B2. Red line is the temperature program and the grey line is the formation of CH_4 indicated with the area obtained from the GC-TCD. T_{final} = 800 °C, ramp rate <550 °C = 10 °C/min; >550 °C = 1 °C/min, H_2 SV ~ 9 L/h/g_{cat}.

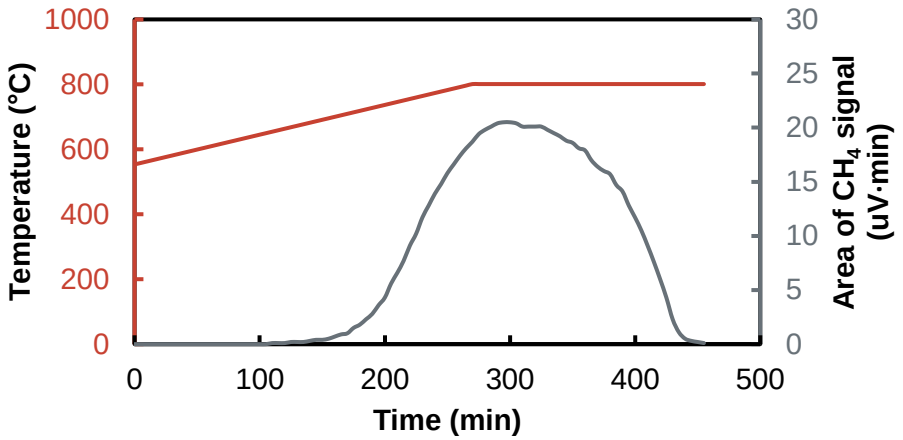

Figure 5-10: TPH run 2 profile of sample C2. Red line is the temperature program and the grey line is the formation of CH_4 indicated with the area obtained from the GC-TCD. T_{final} = 800 °C, ramp rate = 1 °C/min, H_2 SV ~ 9 L/h/g_{cat}.

Surprisingly, upon exposure to air, the materials after the hydrogenation treatment did not show any oxidation of the bulk catalyst to MoO_2 or MoO_3, as shown by XRD analysis (Figure 5-11). Either the carbon layer is not completely removed, or/and the previously identified oxide layer is not reduced in the TPH treatment and therefore still acts as barrier against bulk oxidation.

TEM images were taken of the hydrogen treated samples B2 and C2. No evidence of a carbon layer was observed for both samples (Figure 5-12). In addition, Raman spectroscopy was performed. Comparison of the spectra before and after TPH also confirmed the significant reduction of carbon deposits while no change in the oxide contribution to the spectrum was observed (Figure 5-13).

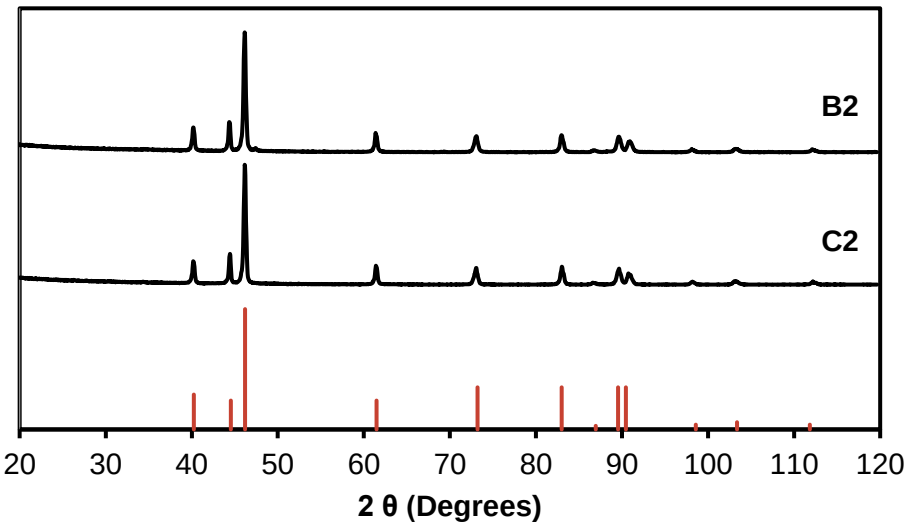

Figure 5-11: XRD analysis of samples B2 and C2 (black) after the temperature programmed hydrogenation treatment. β-Mo_2C reference in red. X-ray source: cobalt.

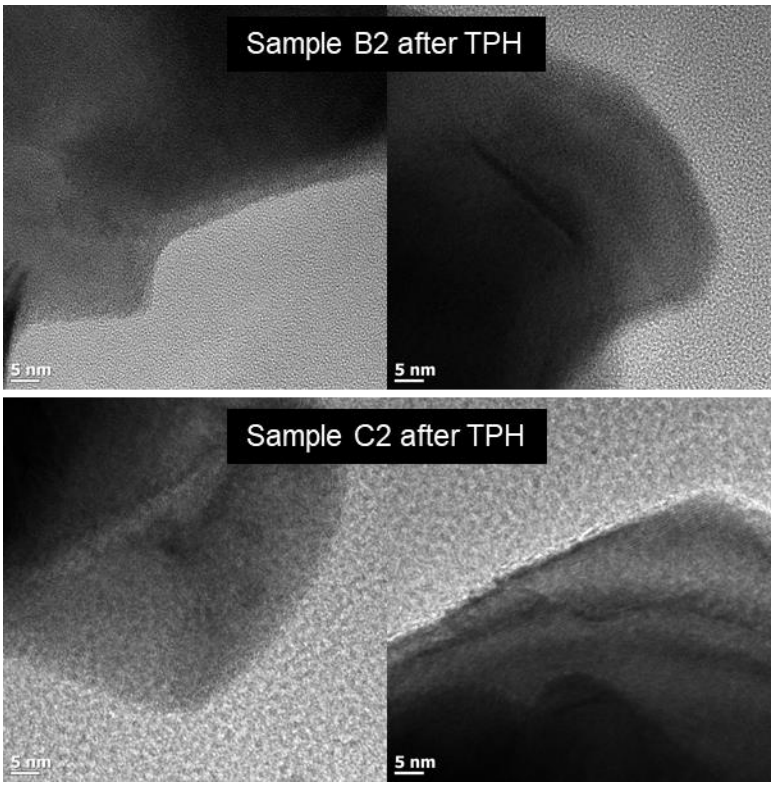

Figure 5-12: TEM images taken after the TPH run 2 reactions (Figure 5-9 and Figure 5-10) on sample B2 and C2. No graphite or oxide layer was observed.

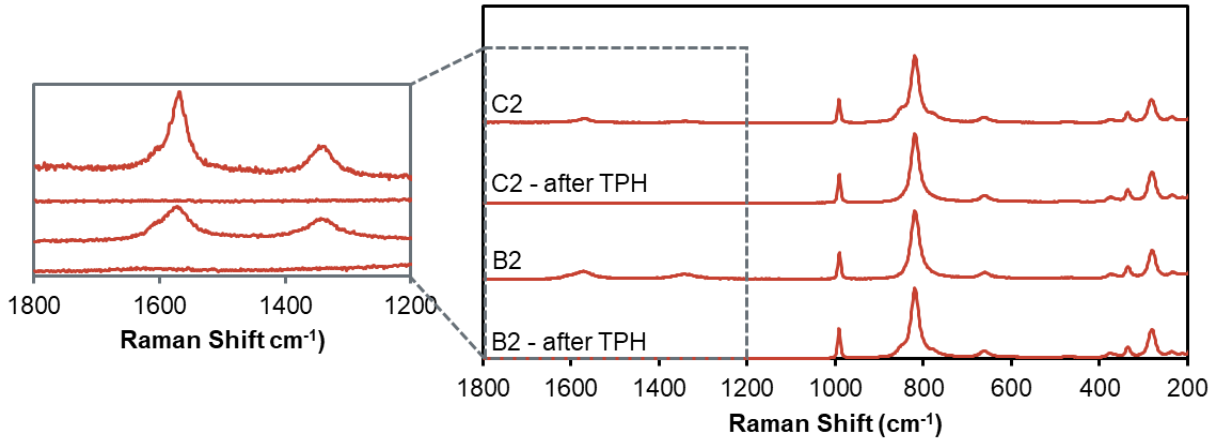

Figure 5-13: Raman spectroscopy of the samples before and after TPH showing the removal of the deposited graphite layer. Note: normalized data shown in figure on the right, original data shown in figure on the left.

5.1.3 Surface composition analysis after TPH

To investigate what exactly keeps the hydrogen treated samples from oxidizing, the composition of the surfaces of the carburized samples and hydrogen treated samples were studied using XPS. Consistent with the TEM images, Raman and TPH profiles, the XPS analysis confirmed that the carbon content on the surface of the catalyst increased with increasing carburization temperature. However, after the hydrogen treatment, the carbon content decreased and thus the oxygen content increased relatively (Figure 5-14). It is proposed that a limited amount of oxygen can diffuse through the graphitic layer on the carbide surface, resulting in a MoO_3 layer around the bulk β-Mo_2C.

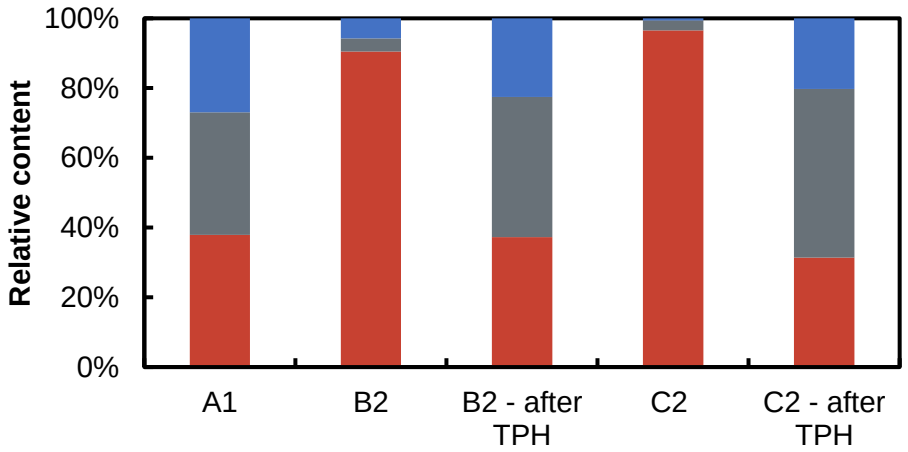

Figure 5-14: XPS analysis of C 1s (red), O 1s (grey) and Mo 3d (blue) on the samples A1, B2, B2 after TPH, C2 and C2 after TPH. All percentages presented are relative to each other.

Focusing just on the carbon content (Figure 5-15) it was observed that B2 and C2 exhibit mainly graphitic carbon on the surface, increasing in concentration with temperature, consistent with all previous analysis. However, on sample A1 graphitic carbon was also detected, suggesting that carbon deposition already happens at temperatures as low as 630 °C during the carburization process, but not to such an extent that it is visible in TEM or Raman analysis. The graphitic carbon, together with the carbidic carbon, makes up 80% of the carbonaceous composition on the surface of the catalyst. Other carbon phases that were observed include single and double bonded carbon to oxygen and saturated graphitic carbon. The temperature programmed hydrogenation of samples B2 and C2 decreased the graphitic phase, indicating that approximately 54-65% of the graphite layer is removed. Simultaneously, the single and double bonded oxygen to carbon compounds increased relatively. It is also observed that the ratios between the other carbon species (without the graphitic carbon) change upon the TPH treatment, which could indicate that not only graphitic carbon is removed. For example, the ratio between the carbide of sample B2 and the C-O is ±1, however, after TPH the ratio increased to ±3. This could indicate the removal of the C-O species during the TPH treatment. After TPH treatment both the overall surface composition regarding C, O and Mo as well as the C speciation of the samples B2 and C2 are comparable to sample A1 after carburization and passivation.

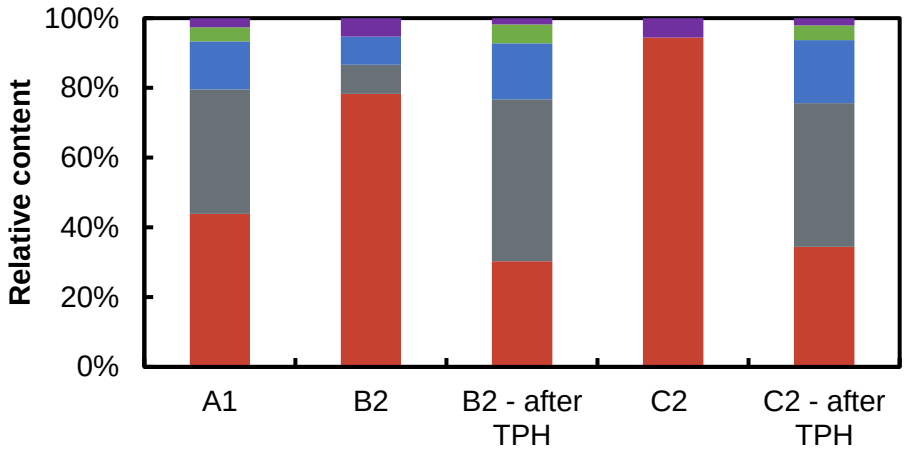

Figure 5-15: XPS analysis of graphite (red), carbide (grey), C-O (blue), C=O (green) and saturated graphite (purple) on the samples A1, B2, B2 after TPH, C2 and C2 after TPH. All percentages presented are relative to each other.

From the described characterization the following conclusions can be drawn. The graphitic capsulated catalyst, carburized at temperatures ≥760 °C, is apparently stable in air and can be treated with hydrogen at temperatures above 600 °C to remove most of the graphitic carbon layer as CH_4. However, after TPH the catalysts are still stable in air. It is therefore proposed that an oxide layer forms even in the presence of the graphitic over layer. Probably due to transport limitations this process is slow and mild and does not lead to bulk oxide formation. This passivation layer seems very resistant to hydrogenation as TPH treatment at 800 °C does not

result in its reduction. However common activation/reduction procedures for passivated β-Mo_2C catalysts reported in the literature only involve a hydrogen treatment at 400-450 °C [18, 101, 102, 139].

5.1.4 In situ XRD carburization of MoO_3 to β-Mo_2C

Utilizing high temperature *in situ* XRD analysis, the carburization at 650 °C followed by passivation and reduction as well as direct exposure to air was studied. The carburization of the catalyst (sample A3) (Figure 5-16) proceeds via the reduction of MoO_3 to MoO_2 before yielding β-Mo_2C. Using Rietveld refinement techniques, the detailed bulk phase transitions can be elucidated in great detail, showing the initial reduction from MoO_3 to MoO_2 to start between 490-510 °C yielding 99.9% MoO_2 at 640 °C (Figure 5-17). Carburization is first detected at 640 °C, reaching a pure β-Mo_2C phase after 2.5 hours at 650 °C.

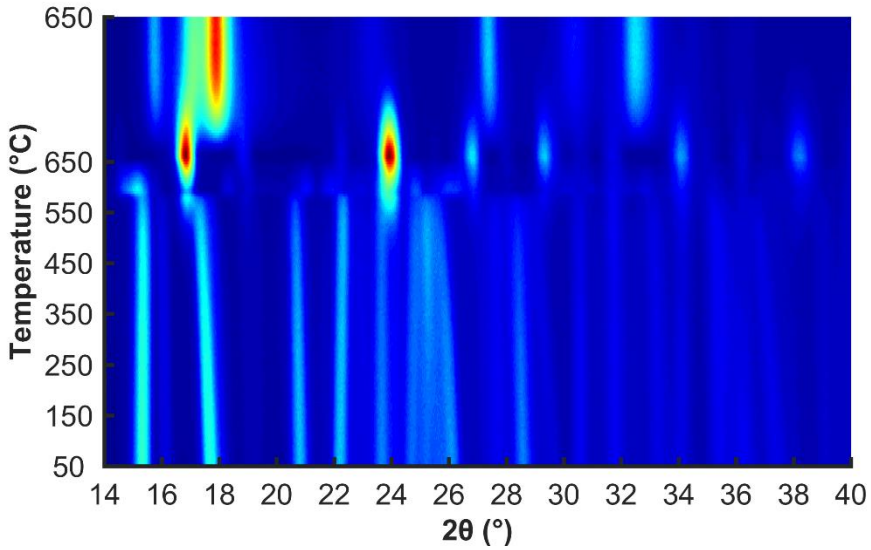

Figure 5-16: On top view of diffraction patterns collected during an in situ carburization experiment of sample A3 displaying phase transformation from MoO_3 to MoO_2 and finally β-Mo_2C. Conditions: T_{ramp} = 1 °C/min, T_{final} = 650 °C, SV = ±21 L/h/g_{cat}, carburization mixture: H_2 / CH_4 / N_2 = 9% / 2% / 89%, P = 1 atm, 1 scan per 5 minutes, total of 181 scans, step size 0.0287° and time per step is 0.2 seconds. X-ray source: molybdenum.

Besides the phase composition, the crystallite sizes of the different phases as a function of time on stream were determined (Figure 5-18). During the initial heating, the crystallite size of MoO_3 decreases gradually from 25 nm to 21 nm. This could be associated to an artifact originating in the slight shift in position of some reflexes due to thermal expansion (Figure 5-16). The reduced oxide phase (MoO_2) showed a decrease in size to approximately 15 nm. Initially β-Mo_2C is formed at about 5 nm increasing upon carburization to about 8.4 nm.

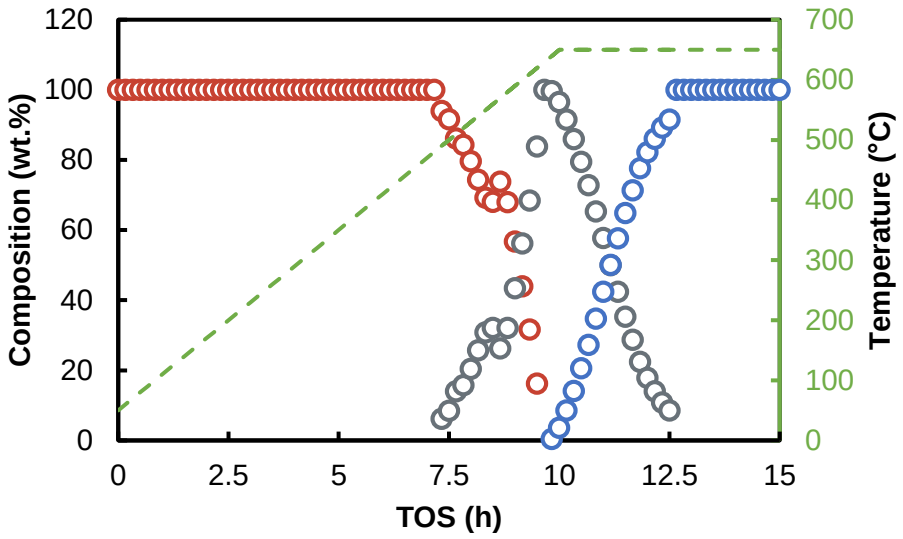

Figure 5-17: Composition of the catalyst calculated using Rietveld refinement of the in situ XRD carburization sample A3. Phases shown: MoO_3 (red), MoO_2 (grey) and β-Mo_2C (blue). Conditions: T_{ramp} = 1 °C/min, T_{final} = 650 °C, SV = ±21 L/h/g_{cat}, carburization mixture: H_2 / CH_4 / N_2 = 9% / 2% / 89%, P = 1 atm, 1 scan per 5 minutes, total of 181 scans.

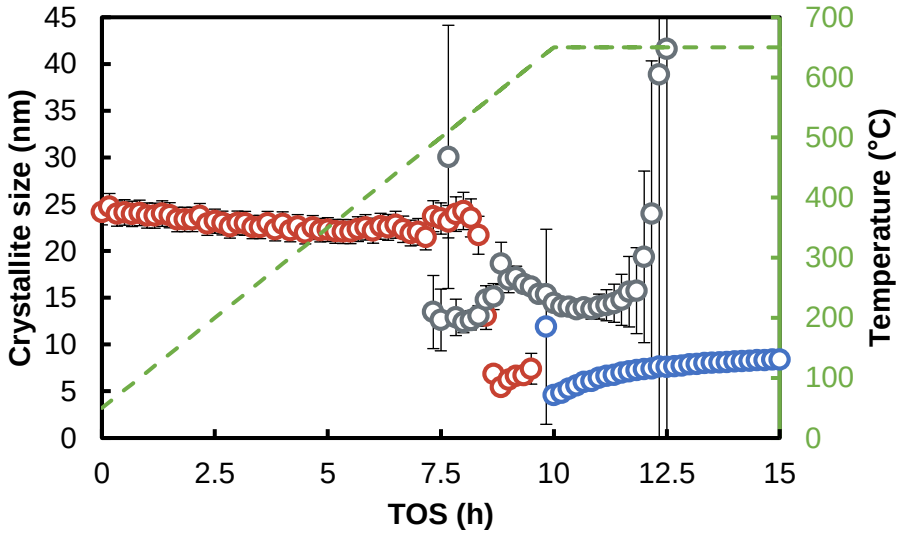

Figure 5-18: Crystallite sizes of the catalyst calculated using Rietveld refinement of the in situ XRD carburization sample A3. Phases shown: MoO_3 (red), MoO_2 (grey) and β-Mo_2C (blue). Conditions: T_{ramp} = 1 °C/min, T_{final} = 650 °C, SV = ±21 L/h/g_{cat}, carburization mixture: H_2 / CH_4 / N_2 = 9% / 2% / 89%, P = 1 atm, 1 scan per 5 minutes, total of 181 scans. Note that error bars for most refinements are so small that they are covered by the data markers.

The sample is cooled in N_2 to 50 °C and exposed for 1 hour to 1% O_2 in N_2 for passivation. No apparent changes in the bulk composition were observed.

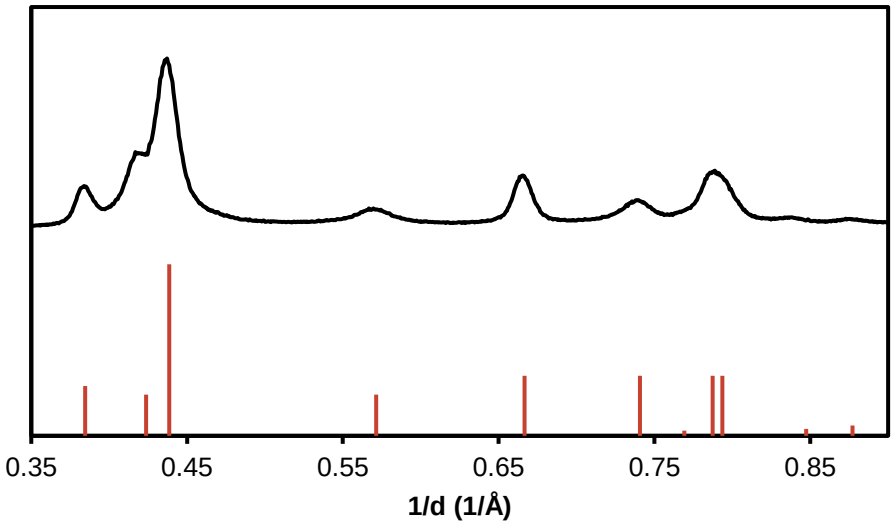

Figure 5-19: XRD diffraction pattern after in situ passivation for 1 hour in 1% O_2 in N_2. With β-Mo_2C reference pattern in red.

The passivated sample was subsequently reduced at 400 °C in a hydrogen atmosphere (Figure 5-20), again not showing any apparent changes in phase or crystallite size.

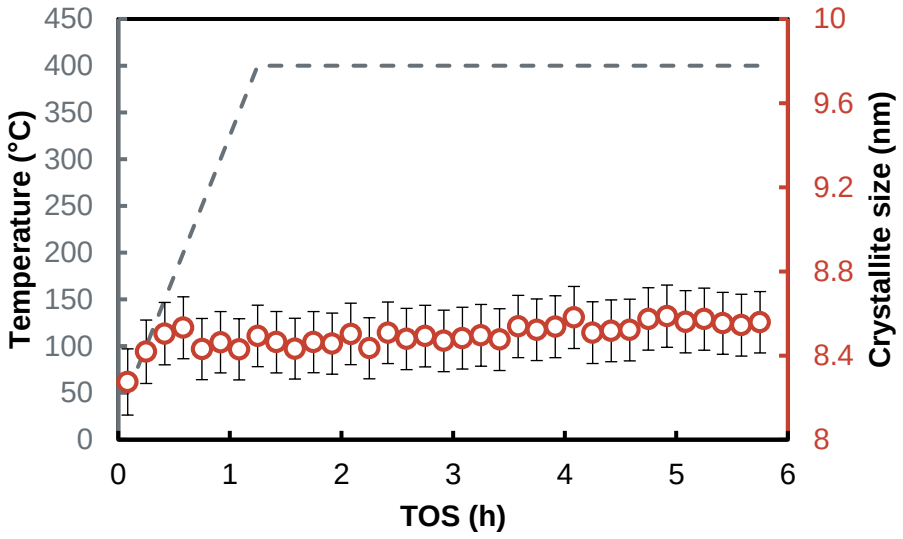

Figure 5-20: Crystallite sizes of β-Mo_2C (red circles) as a function of time and temperature (grey dashed line), with the calculated errors during the in situ XRD reduction of sample A3 using Rietveld refinement. Conditions: T_{ramp} = 5 °C/min, T_{final} is 400 °C, SV = 3 L/h/g_{cat}, P = 1 atm, 1 scan per 5 minutes, total of 69 scans.

After reduction, the sample is cooled to room temperature and removed from the *in situ* cell and therefore exposed to air. Subsequent analysis in air at higher resolution (Figure 5-15), showed the presence of a small amount of MoO_2. The composition of the sample was calculated to be 94.50 wt.% β-Mo_2C (with a crystallite size of 8.6±0.1 nm) and 5.50 wt.% MoO_2 (with a crystallite size of 14.3±5.1 nm). The MoO_2 is suggested to be a consequence of unsuccessful carburization due to the thick catalyst bed in the *in situ* XRD sample holder, rather than that it is re-oxidized upon contact with air, supported by the small crystallite size which is similar to that of MoO_2 in Figure 5-18.

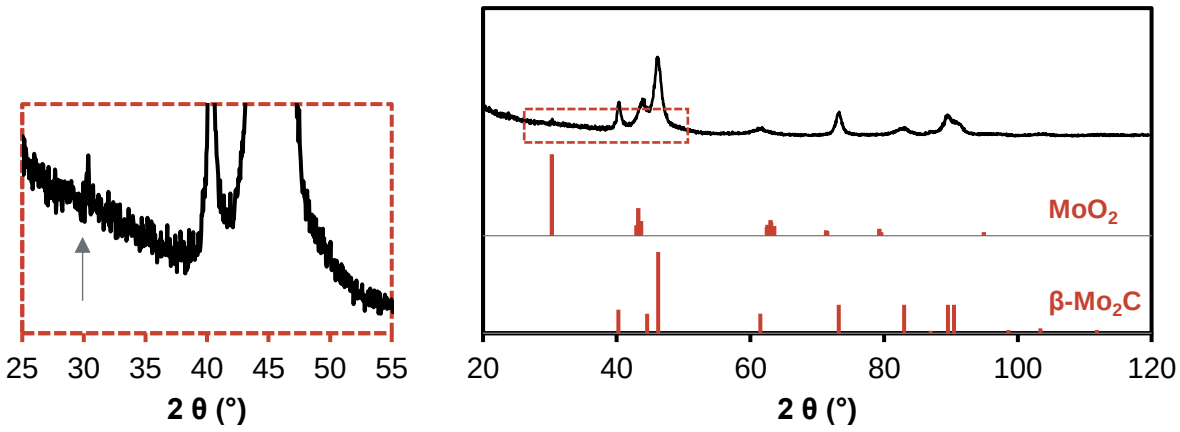

Figure 5-21: XRD diffraction pattern of the in situ XRD prepared sample A3 (black) and the reference patterns of MoO_2 and β-Mo_2C (red). A zoom-in is presented on the left showing the 2Θ area from 25 to 55°. X-ray source: cobalt.

A second sample (A2) was carburized in the *in situ* XRD to be exposed to air atmosphere at room temperature (25-30 °C) immediately after carburization. The process of carburization was very reproducible and the obtained sample contained 100% β-Mo_2C with an average crystallite size of 8.6 nm (see Appendix F Figure 9-1, Figure 9-2, Figure 9-3).

Upon exposure to air, the sample started glowing clearly indicating a spontaneous and exothermic reaction in contact with oxygen. Subsequent XRD analysis confirmed of the presence of MoO_2 in the bulk sample with two distinctly different average crystallite sizes: 9.9±0.9 nm and 93.9±23.8 nm (Figure 5-11). Raman spectroscopy indicated that the surface of both catalysts prepared in the *in situ* XRD, i.e. the sample directly exposed to air after carburization as well as the sample passivated, reduced and then exposed to air, still show the typical MoO_3 Raman spectrum, a phase not detected in XRD (Figure 5-22).

In summary, from the *in situ* XRD analysis it can be confirmed that β-Mo_2C is formed under the applied carburization conditions, however it requires passivation to be stable upon exposure to air. The catalyst is required to be stable in air for potassium promotion. However, all three catalysts were prepared for catalyst testing to study the effect of the carburization protocols on

the performance of the catalyst in CO hydrogenation. Eventually, the passivated samples were used for potassium promotion, as will be explained in section 5.2.5.

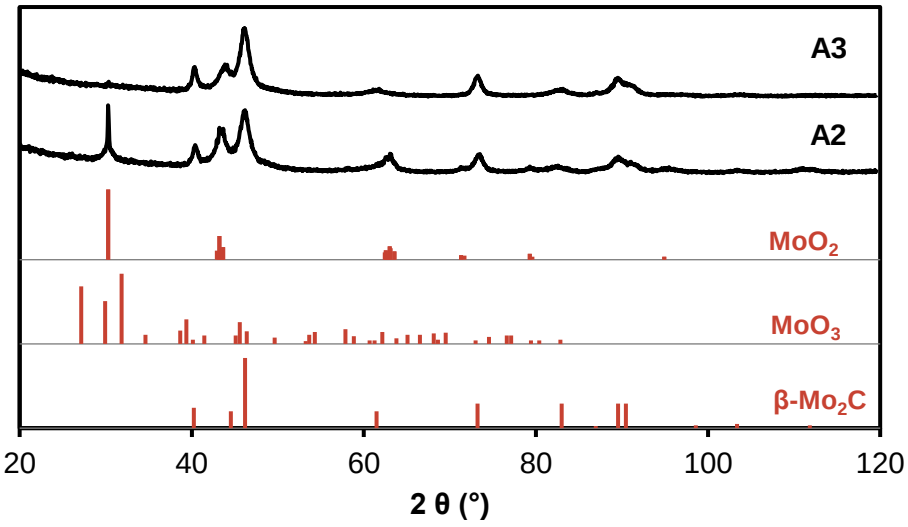

Figure 5-22: XRD analysis of sample A3 and A2 (black) after being exposed to air. Reference patterns (red) of MoO_2. MoO_3 and β-Mo_2C. X-ray source: cobalt.

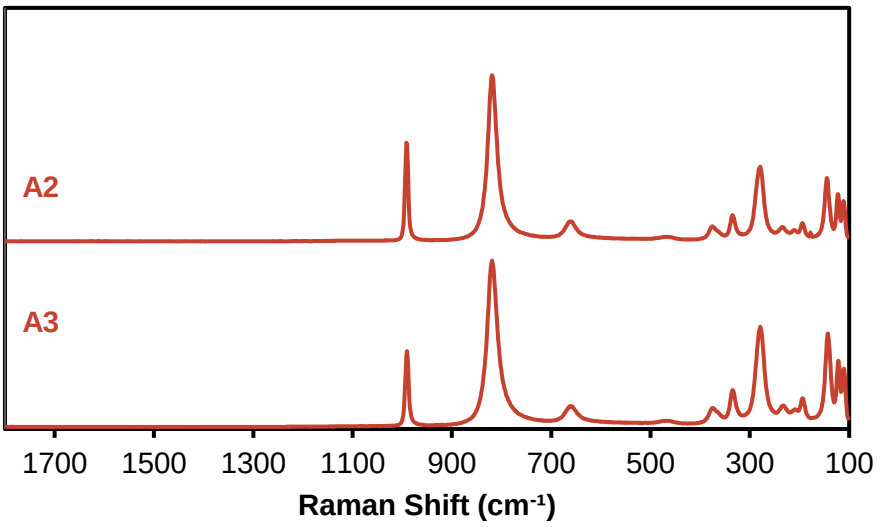

Figure 5-23: Raman scattering of the in situ XRD samples A2 and A3. Both samples display the MoO_3 Raman scattering.

5.1.5 Difference between catalyst preparation in calcination rig and testing unit

All previous samples are prepared in the calcination rig, as mentioned in section 4.1.2. However, in section 5.2.2 an *in situ* prepared catalyst will be discussed regarding its performance in the FTS. Thus, the catalyst needs to be carburized *in situ*, i.e. a catalyst is prepared inside the reactor

of the reaction unit (Figure 4.3) under the same carburization conditions as sample A1 (which was prepared in the calcination rig) at 630 °C. XRD analysis (Figure 5-24) confirmed a successful *in situ* synthesis, however, the catalyst showed much smaller crystallite sizes (average of 12 ± 0.1 nm) than the catalyst prepared in the calcination rig (average of 35 ± 0.3 nm). A possible reason for the larger crystallite sizes obtained in the calcination rig is an uneven isothermal zone resulting in temperature spikes or inferior hydrodynamic flow patterns resulting in local hotspots. Based on this finding, all catalysts prepared for the FT testing were prepared inside the testing unit, to keep the preparation method and crystallite sizes comparable over all experiments.

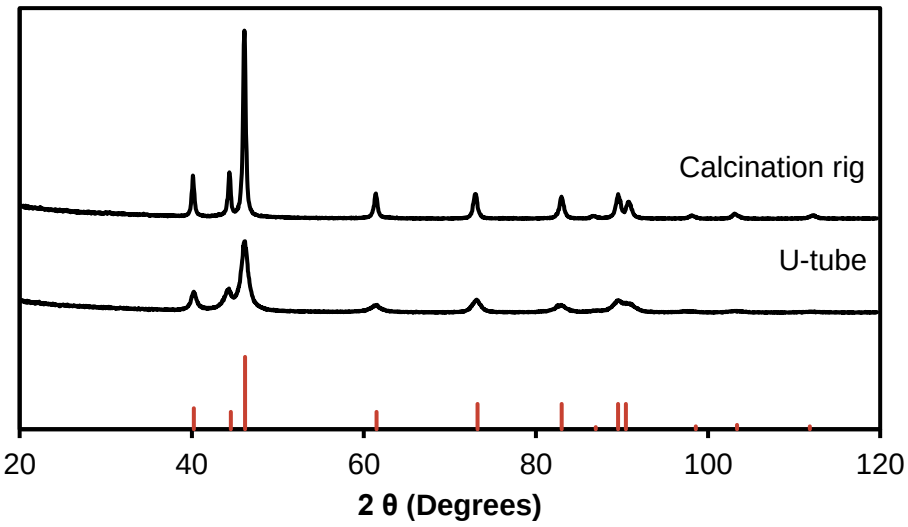

Figure 5-24: XRD diffractograms of the two different samples prepared inside the calcination rig and the U-tube reactor. X-ray source: cobalt.

5.1.6 Composition analysis on potassium promoted β-Mo_2C

Literature commonly reports potassium promotion to improve the catalytic performance of Mo_2C catalysts in synthesis gas conversion reactions [19-21, 153]. Three samples were prepared with potassium promotion; 2.5 wt.% (F), 5.0 wt.% (D) and 7.5 wt.% (E) (see section 5.2.9, 5.2.7 and 5.2.8 for the testing results of these samples). All three samples were analyzed with ICP-OES to confirm the K/Mo loading (Table 5-2). Unfortunately, for samples D and E insufficient sample was available to analyze before FT testing so only data from the spent catalyst (indicated by an asterisk) is available. D* was identified with a slightly higher potassium loading (6.2 wt. instead of 5.0 wt.), where E* seemed to contain of a lower amount of potassium (5.4 wt.% instead of 7.5 wt.%). The data for sample F before (1.9 wt.%) and after FT testing, F*, (1.8 wt.%) suggests that no significant loss of potassium is expected during FT reaction. G was prepared for the high pressure run in a different batch and showed again a slightly lower potassium amount than initiated (4.3 wt.% instead of 5.0 wt.%) and after FT testing the loading dropped to 3.9 wt.%. From the presented results it is observed that the initially added amount of potassium to the sample is

not fully impregnated into the sample and that some potassium gets lost upon the drying or calcination process. In subsequent sections, the below described potassium promoted samples will all be referred to be their loading as quantified after FT testing.

Table 5-2: ICP-OES analysis results of the potassium promoted samples and an unpromoted sample.

Sample name	*Theoretical wt.% K/Mo*	*ICP-result wt.% K/Mo*
Un-promoted	0.0%	0.0%
D - 6.2 wt.% K/Mo*	5.0%	6.2%
E - 5.4 wt.% K/Mo*	7.5%	5.4%
F - 1.9 wt.% K/Mo	2.5%	1.9%
F - 1.8 wt.% K/Mo*	2.5%	1.8%
G - 4.3 wt.% K/Mo	5.0%	4.3%
G - 3.9 wt.% K/Mo*	5.0%	3.9%

**spent sample, analyzed after FT*

5.2 Catalyst testing

5.2.1 Effect of surface composition on the activity and product distribution of the catalysts

The first set of experiments (FT 1) was performed testing three different synthesis routes described previously (Chapter 5.1) under FT-conditions to understand the activity of β-Mo_2C and the effect of the carburization temperature on the activity and product selectivity of the catalyst. For all experiments conducted a summary is presented and eventually an overall comparison of related experiments is provided.

5.2.2 FT run 1.1: In situ prepared β-Mo_2C

A β-Mo_2C catalyst was prepared *in situ*, i.e. inside the U-tube reactor, without passivation or reduction and exposed to FT conditions right after the carburization. The sample was exposed to the same carburization conditions as A1, i.e. 630 °C as the final temperature, ramping rate of 1 °C/min and holding time of 5 hours. The starting conditions of the FT-reaction were chosen at T = 280 °C, P = 33 bar, H_2 to CO ratio of 1 and GHSV of 16 L/h/g_{cat} (Table 4.1). The catalyst showed high activity from the start stabilizing at a CO conversion of 85% after ±6 hours time on stream (TOS). A CH_4 selectivity of 37 C% and CO_2 selectivity of 33 C% was observed at this CO conversion level. After 7.5 hours TOS, the temperature was lowered to 260 °C which resulted in a significant drop in the CO conversion to 16% at a total of 13 hours TOS. At this stage CO_2 and CH_4 selectivity were 31 C% and 27 C%, respectively. At 15 hours TOS, the temperature was further decreased to 240 °C, reaching a steady state CO conversion as low as 4%, after a total of 23.5 hours TOS. Simultaneously, the CH_4 selectivity dropped to 24 C% and the CO_2 selectivity to 22 C%. Via a subsequent increase in reaction temperature first to 260 and then 280 °C, after 25 hours TOS, the stability of the catalyst was tested. Even though the activity reaches levels close to the initial performance (85% vs 72% CO conversion), the catalyst has deactivated slightly over TOS requiring higher reaction temperature by about 20 °C to achieve a comparable conversion with 88%, after 95 hours TOS (Figure 5-25). CH_4 and CO_2 selectivity also reached similar levels to the initial performance with 37 C% vs 39 C% for CH_4 and 33 C% vs 35 C% for CO_2 (Figure 5-26).

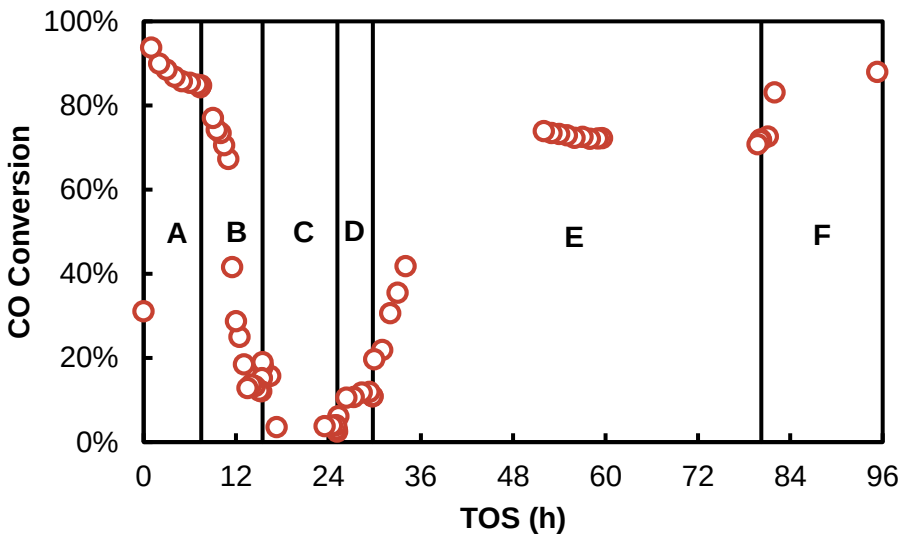

Figure 5-25: CO conversion from FT 1.1 obtained with TOS, varying conditions indicated by: A) 280 °C; B) 260 °C; C) 240 °C; D) 260 °C; E) 280 °C and F) 300 °C. Process conditions: P = 33 bar, H_2 to CO ratio = 1 and GHSV = 16 L/h/g_{cat}.

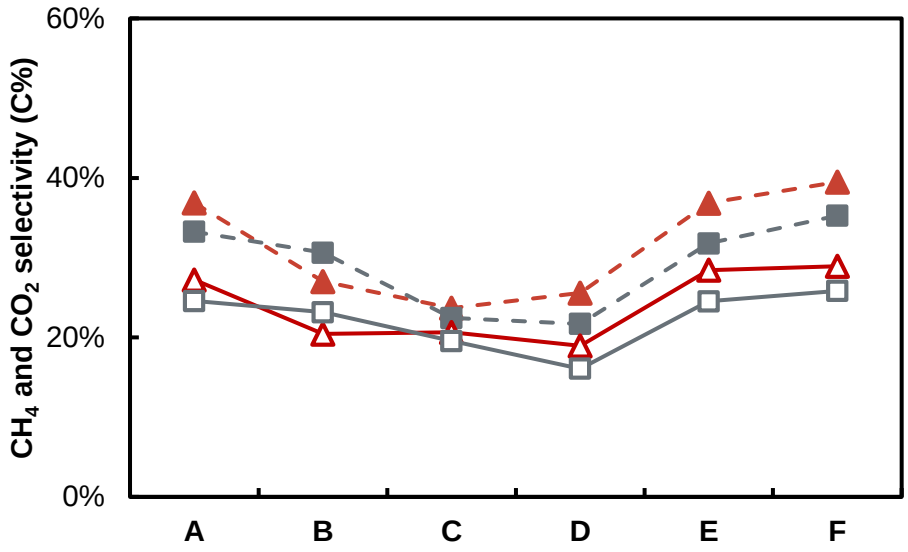

Figure 5-26: CH_4 (red triangles) and CO_2 (grey squares) selectivity, presenting original data (open symbols, solid lines) and carbon balance corrected (solid symbols, dashed line) from FT 1.1 obtained with TOS, varying conditions indicated by: A) 280 °C; B) 260 °C; C) 240 °C; D) 260 °C; E) 280 °C and F) 300 °C. Process conditions: P = 33 bar, H_2 to CO ratio = 1 and GHSV = 16 L/h/g_{cat}.

The organic products were analyzed using an offline GC-FID. All selectivities are calculated in C% and on a CO_2-free basis. The main products are hydrocarbons (HC) but at lower CO conversion the oxygenate (OX) selectivity increases. Oxygenate to total organic product ratio (HC and OX) was observed at 0.21 and 0.14 for conditions C and D, respectively (hydrocarbons including the paraffins and olefins, branched and linear; oxygenates including the alcohols,

aldehydes, carboxylic acids and ketones). For all conditions, the linear alcohols over total oxygenates ratio is ≥99 C%, with a methanol content between 0.67 (condition C) and 0.92 (condition A). The balance being C_2-C_4 alcohols reaching its peak at the lowest tested reaction temperature (Figure 5-27).

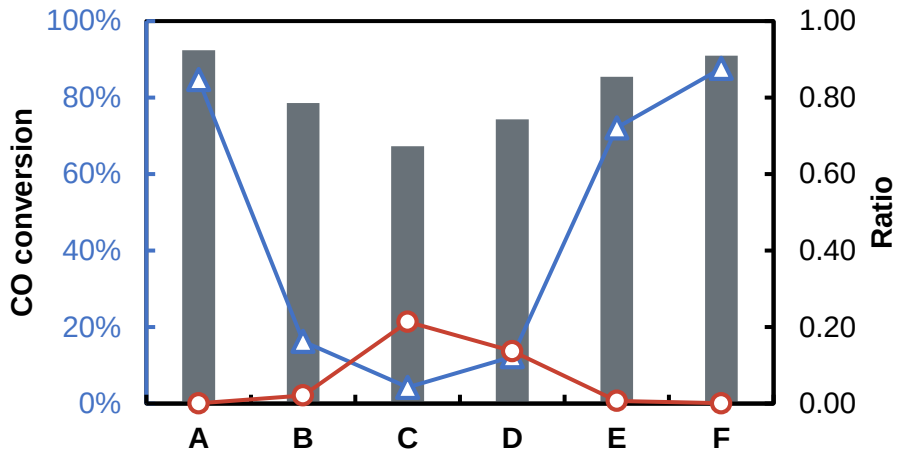

Figure 5-27: Organic product analysis obtained from FT 1.1 varying conditions indicated by: A) 280 °C; B) 260 °C; C) 240 °C; D) 260 °C; E) 280 °C and F) 300 °C. With oxygenate to total organic product (olefins, paraffins and oxygenates) ratio (red circles), MeOH to total oxygenate ratio (grey bars) and CO conversion (blue triangles). Process conditions: P = 33 bar, H_2 to CO ratio = 1 and GHSV = 16 L/h/g_{cat}.

A decrease in temperature slightly enhances the linear paraffins chain growth, shown by the increase in the α-value from 0.34 at 280 °C to 0.44 at 240 °C. Returning to higher temperatures decreases the α-value to 0.33 at 300 °C. The olefin content was not significant enough during condition A, E and F indicating a very strong hydrogenation activity at reaction temperatures of 280 °C and above, therefore for conditions B, C and D only the chain growth probability for linear olefins was calculated. No significant difference was observed between the three conditions, with α-values of 0.30, 0.30 and 0.29, respectively. The chain growth probability of oxygenates is based on the linear alcohols. The observed α-values are 0.17, 0.19, 0.16 and 0.12 for conditions B, C, D, E. The oxygenate content in condition A and F is not significant enough to calculate its chain growth probability (Figure 5-28).

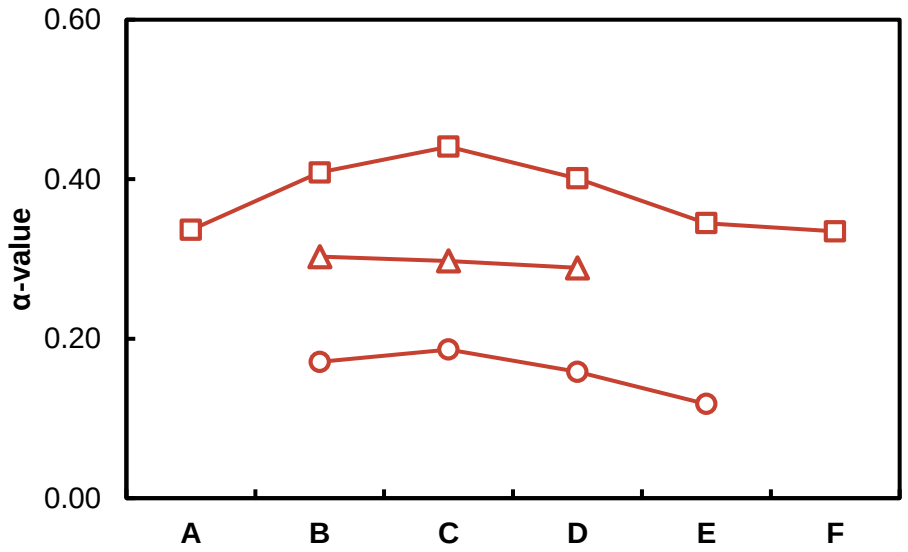

Figure 5-28: Chain growth probability calculated for the linear products from FT 1.1 of the product classes C_3-C_8 paraffins (squares), C_3-C_8* olefins (triangles) and C_2-C_6* alcohols (circles) varying conditions indicated by: A) 280 °C; B) 260 °C; C) 240 °C; D) 260 °C; E) 280 °C and F) 300 °C. Process conditions: P = 33 bar, H_2 to CO ratio = 1 and GHSV = 16 L/h/g_{cat} (* = if possible).*

5.2.3 FT run 1.2: Passivated β-Mo_2C

To study the effect of passivation and subsequent reduction on the catalyst's activity and product selectivity, the same catalyst employed in FT 1.1 (see chapter 5.2.2) was prepared and subsequently passivated (see chapter 4.1.2). As described previously, the passivation step is essential to allow an additional wet impregnation with a promotor after the carburization. Prior to reaction it was attempted to remove as much of the passivation layer as possible in a process similar to treatments described in the literature [18, 101, 102, 139] namely a hydrogen reduction step (4.5 hours in hydrogen at 400 °C). The same initial FT conditions were chosen as in experiment FT 1.1, i.e. T = 280 °C, P = 33 bar, H_2 to CO ratio of 1 and GHSV of 16 L/h/g_{cat}. Thereafter, conditions were changed based on the catalyst performance (see Table 4.1).

The catalyst showed lower activity than the *in situ* prepared catalyst at the initial conditions (T = 280 °C, P = 33 bar and SV = 16 L/h/g_{cat}). After an initial conversion of over 80% it quickly loses activity and reaches an apparent steady state after 9 hours TOS at a CO conversion of 46%, with a CH_4 selectivity of 24 C% and CO_2 selectivity of 53 C%. Trying to increase the CO conversion, the space velocity was lowered to 9.6 L/h/g_{cat} after 11.5 hours TOS. This increased the conversion slightly to 55% after 21 hours TOS. CH_4 and CO_2 selectivity were measured to be 25 C% and 45 C%, respectively. Decreasing temperature to 260 °C dropped the CO conversion to 15% (Figure 5-29). CH_4 and CO_2 selectivity dropped to 20 C% and 40 C%, respectively (Figure 5-30). The passivation/reduction treatment therefore seems to reduce the overall catalysts' activity and specifically the CO hydrogenation activity from approximately 70% of the converted CO forming

hydrogenated products to about 50%. It can be hypothesized that the introduced oxidic surface sites which are not fully removed by the hydrogen treatment support the water-gas-shift reaction and therefore not only lead to an increased CO_2 selectivity but also to an increased concentration of H_2.

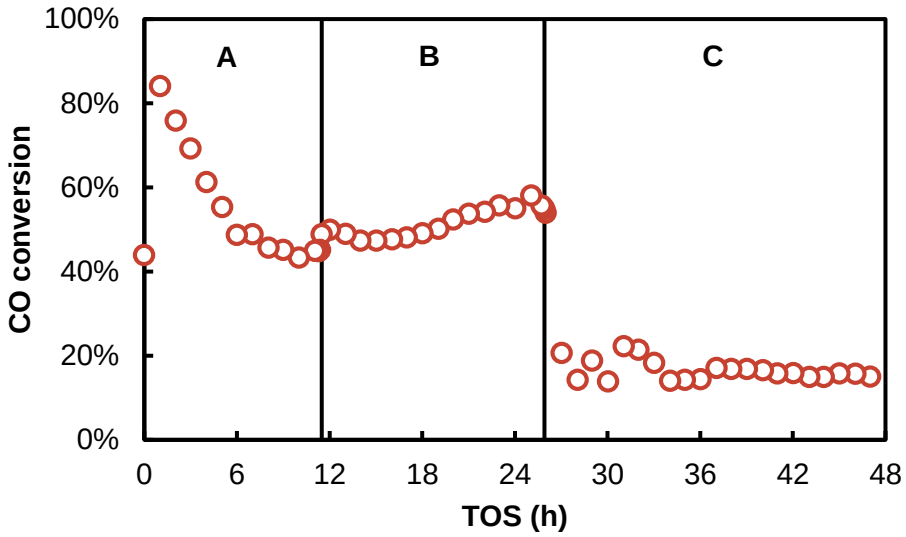

Figure 5-29: CO conversion from FT 1.2 obtained with TOS, varying conditions as indicated: A) 280 °C and 16 L/h/g_{cat}; B) 280 °C and 9.6 L/h/g_{cat}; C) 260 °C and 9.6 L/h/g_{cat}. Process conditions: P = 33 bar and H_2 to CO ratio = 1.

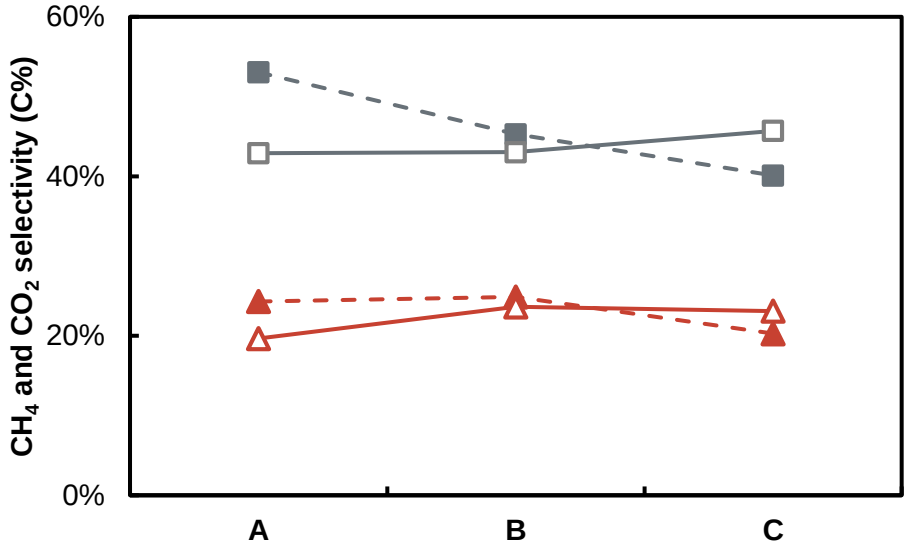

Figure 5-30: CH_4 (red triangles) and CO_2 (grey squares) selectivity, presenting original data (open symbols, solid lines) and carbon balance corrected (solid symbols, dashed line) from FT 1.2 obtained with TOS, varying conditions as indicated: A) 280 °C and 16 L/h/g_{cat}; B) 280 °C and 9.6 L/h/g_{cat}; C) 260 °C and 9.6 L/h/g_{cat}. Process conditions: P = 33 bar and H_2 to CO ratio = 1.

The analysis of the organic products showed that hydrocarbons were again the dominating product class with oxygenate to total organic product ratios between 0.01 and 0.16. The primary oxygenated product was methanol with a methanol to total oxygenate ratio of ±0.8. As 100% of the oxygenate fraction are alcohols, the balance of the total oxygenates are C_2-C_4 alcohols (Figure 5-31).

Interestingly, comparing the pristine β-Mo_2C catalyst of the experiment FT 1.1 with the passivated and reduced sample under similar conditions, i.e. at 260 °C (condition B in FT 1.1 and condition C in FT 1.2), it is evident that at similar conversions (the lower activity of the passivated and reduced catalyst is countered by a lower space velocity) the oxygenate selectivity is significantly higher in experiment FT 1.2 (oxygenate to total organic product ratio of 0.16 vs. 0.02 with a very comparable oxygenate composition) (Figure 5-31).

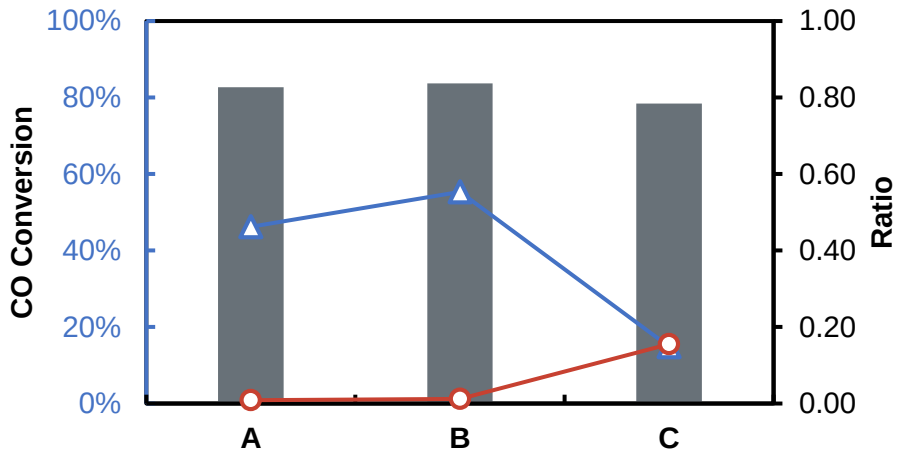

Figure 5-31: Organic product analysis obtained from FT 1.2 varying conditions indicated by: A) 280 °C and 16 L/h/g_{cat}; B) 280 °C and 9.6 L/h/g_{cat}; C) 260 °C and 9.6 L/h/g_{cat}. With oxygenate to total organic product (olefins, paraffins and oxygenates) ratio (red circles), MeOH to total oxygenate ratio (grey bars) and CO conversion (blue triangles). Process conditions: P = 33 bar and H2 to CO ratio = 1.

Initially, the drop in space velocity from 16 to 9.6 L/h/g_{cat} did not change the chain growth probability much for the paraffins (from 0.35 to 0.34) and olefins (from 0.23 to 0.24). Upon the decrease in temperature to 260 °C the α-values increase slightly, from 0.34 to 0.38 (paraffins) and 0.24 to 0.27 (olefins). Interestingly the chain growth probability was not affected by the increased WGS activity and the associated higher H_2 concentration. A possible reason for this behavior is that CO oxidation is taking place, in the form of the Mars-Van Krevelen type mechanism by means of the oxidic surface of the catalyst. However, this has not been previously reported to take place over MoO_3 or MoO_2. The chain growth probability for linear alcohols could only be calculated for conditions C, as condition A and B did not form sufficient amount of oxygenates. The α-value for linear alcohols at condition C was observed at 0.14. Comparing condition B in FT 1.1 and condition C in FT 1.2 at similar conversion levels, the chain growth

probabilities are also very similar, with 0.41 vs 0.38 for paraffins, 0.30 vs 0.27 for olefins and 0.17 vs 0.14 for alcohols.

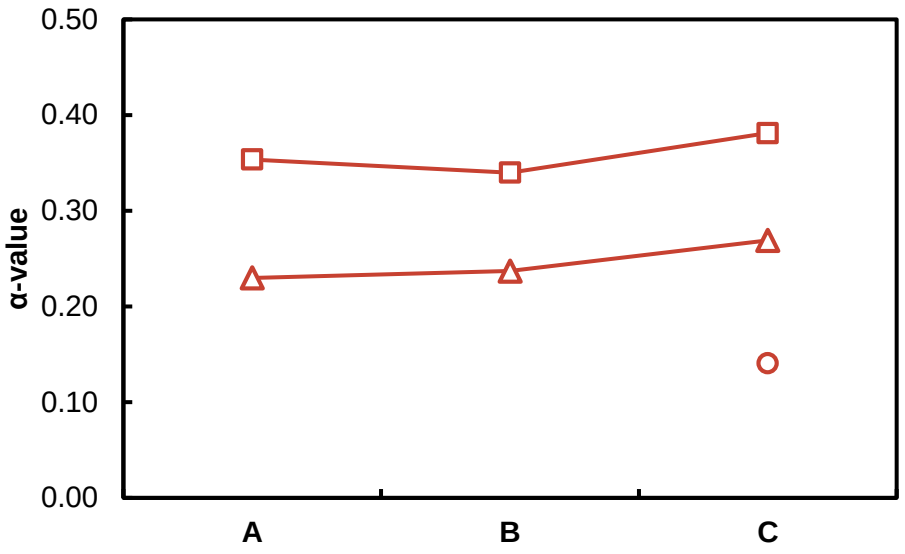

Figure 5-32: Chain growth probability calculated for the linear products from FT 1.2 of the product classes C_3-C_8 paraffins (squares), C_3-C_8* olefins (triangles) and C_2-C_6* alcohols (circles) varying conditions indicated by: A) 280 °C and 16 L/h/g_{cat}; B) 280 °C and 9.6 L/h/g_{cat}; C) 260 °C and 9.6 L/h/g_{cat}. Process conditions: P = 33 bar and H_2 to CO ratio = 1 (* = if possible).*

5.2.4 FT run 1.3: Graphite encapsulated β-Mo_2C

As previously described in the literature [101] and shown in detail for the present catalyst system in section 5.1.2, an increase in carburization temperature increases carbon deposition on the catalyst. This layer becomes so thick that it protects the catalyst from bulk oxidation once exposed to air possibly by transport limitations of oxygen to the β-Mo_2C surface. Removal of this layer via hydrogenation forms CH_4 and could possibly result, if conducted *in situ* and without exposure to air (see section 5.1.2), in a 'cleaner' carbide phase on the surface of the catalyst. With a cleaner carbide phase, it means that if the freshly prepared and temperature programmed hydrogenated catalyst does not come into contact with air, the MoO_3 layer - indicated by the Raman spectra in section 5.1.2 - could be absent.

A catalyst was prepared *in situ* at 760 °C in the U-tube reactor. Prior to testing, the graphite layer was removed under H_2 at 600 °C for ±2.5 hours at a GHSV 9 L/h/g_{cat}. The formation of CH_4 was monitored by a GC-TCD, to stop the hydrogenation process as soon as the graphite layer is removed (Figure 5-33). A sharp increase of CH_4 concentration was measured in the reactor outlet gas after less than 10 minutes TOS. After about 20 minutes a decrease in CH_4 concentration was interpreted as the hydrogenation of the graphite layer concluding. However, after about 85 minutes a slow increase in CH_4 formation was observed. To make sure that all graphite was removed the treatment was continued for an additional 55 minutes. However, no drop or sudden

increase was observed, therefore the hydrogenation was stopped, to prevent over-reduction/decomposition of the carbide phase itself.

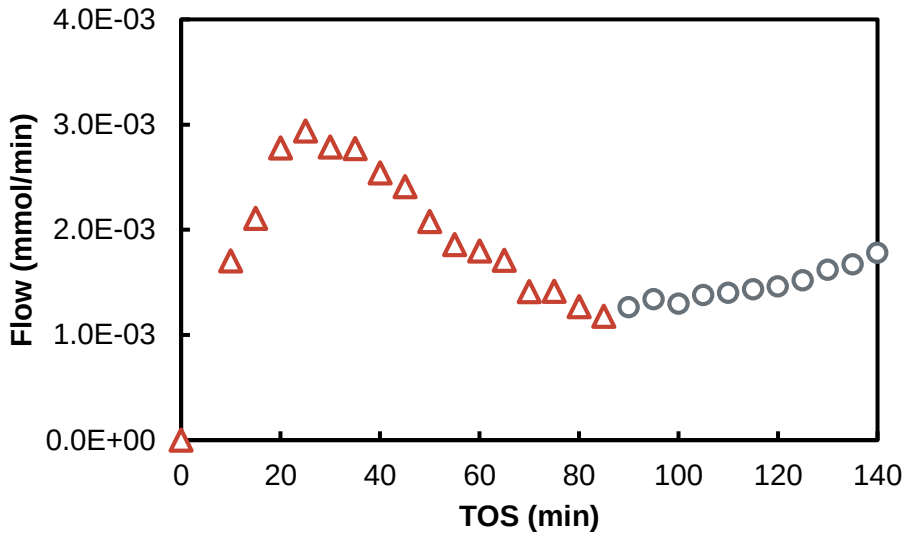

Figure 5-33: TPH reaction on the in situ prepared sample at 760 °C prior to reaction, indicating the initial graphite removal (red triangles) followed by the proposed partial decomposition of the β-Mo_2C (grey circles). Reaction conditions: T = 600 °C, P = 1 atm, GHSV = 9 L/h/g_{cat}.

After the hydrogenation step, the catalyst testing started using the same reaction conditions as FT 1.1 and 1.2, i.e. T = 280 °C, P = 33 bar, H_2 to CO ratio of 1 and GHSV of 16 L/h/g_{cat}. A CO conversion below 3% was observed for the first hour, therefore the conditions were adjusted. Space velocity was dropped from 16 to 12 L/h/g_{cat} resulting in an increased CO conversion of 9% after 15 hours TOS with the selectivities to CH_4 and CO_2 at 24 C% and 31 C%, respectively. Interestingly the CO conversions seems to gradually increase with time on stream. After 15.5 hours TOS, a further decrease in space velocity (8 L/h/g_{cat}) showed a small increase in the CO conversion, to 12% after 19 hours TOS. CO_2 and CH_4 selectivities were recorded at 20 C% and 29 C%. Subsequently, at 20 hours TOS, the temperature was increased to 300 °C. A significant jump in the steady state CO conversion was observed, again increasing with time on stream, reaching 45% after 36 hours TOS. CH_4 and CO_2 selectivities increased simultaneously to 27 C% and 41 C%, respectively. The apparent increase in activity indicates the presence of a possible formation process on the surface of the catalyst taking place. The nature of this process is at this stage unknown but is possibly associated with an *in situ* carburization or further carbon removal. A subsequent decrease in temperature after ±41 hours TOS (280 °C), led to a drop in the steady state CO conversion to 20% at 48 hours TOS, which is still higher than the first time the catalyst experienced these conditions (Figure 5-34). The CH_4 and CO_2 selectivity at these conditions were 32 C% and 51 C%, respectively (Figure 5-35).

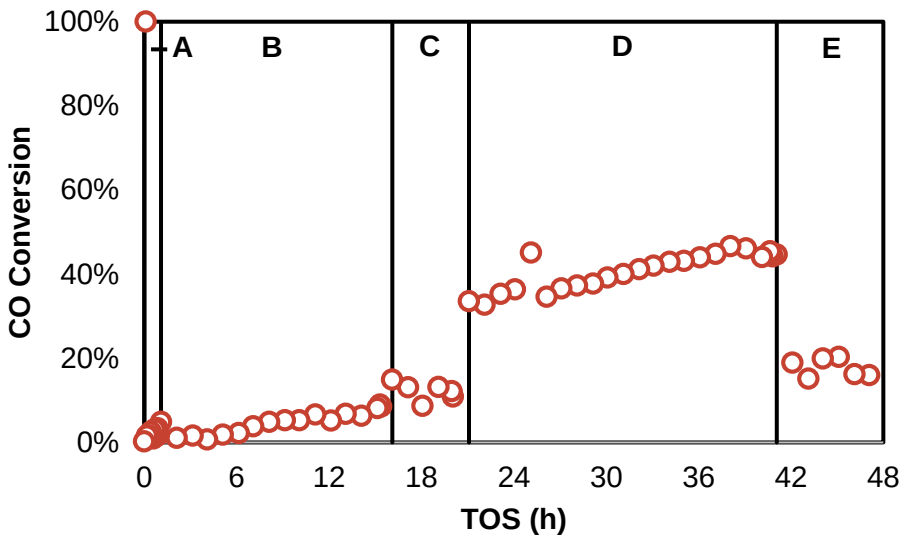

Figure 5-34: CO conversion from FT 1.3 obtained with TOS, varying conditions as indicated: A) 280 °C and 16 L/h/g_{cat}; B) 280 °C and 12 L/h/g_{cat}; C) 280 °C and 8 L/h/g_{cat}, D) 300 °C and 8 L/h/g_{cat} and E) 280 °C and 8 L/h/g_{cat}. Process conditions: P = 33 bar, H_2 to CO ratio = 1.

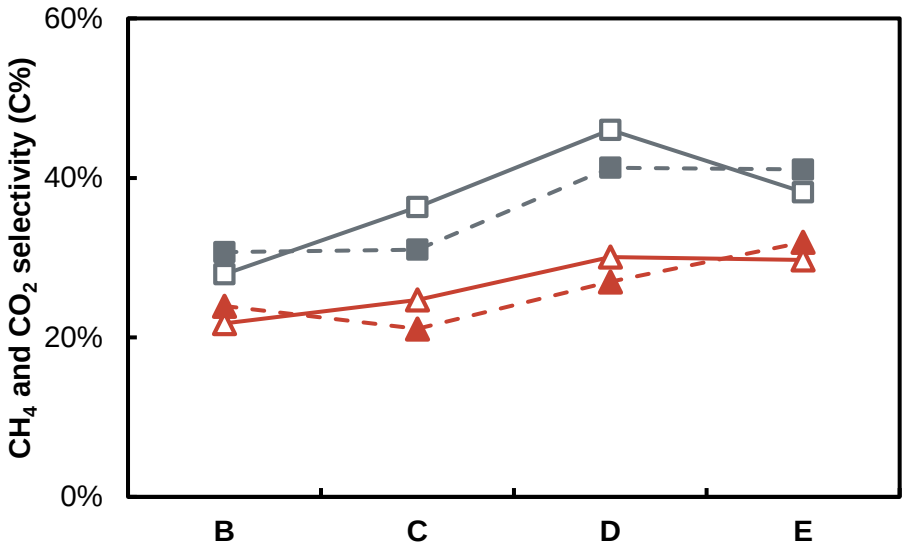

Figure 5-35: CH_4 (red triangles) and CO_2 (grey squares) selectivity, presenting original data (open symbols, solid lines) and carbon balance corrected (solid symbols, dashed line) from FT 1.3 obtained with TOS, varying conditions as indicated: B) 280 °C and 12 L/h/g_{cat}; C) 280 °C and 8 L/h/g_{cat}, D) 300 °C and 8 L/h/g_{cat} and E) 280 °C and 8 L/h/g_{cat}. Process conditions: P = 33 bar, H_2 to CO ratio = 1.

The analysis of the organic products has shown an oxygenate to total organic product ratio between 0.08 and 0.29. Although direct comparison of the experiments FT 1.1 and 1.2 with the present catalyst is difficult due to the lack of similar conversions at comparable reaction conditions, it is evident that a very high content of oxygenates was achieved. Even at CO conversions of 45% at 300 °C the oxygenate to total organic product fraction was 0.08. This is

significantly higher than the other three samples at comparable conversions or reaction temperatures. However, returning to 280 °C in condition E also shows that the oxygenate selectivity reduces drastically (0.29 in condition C and 0.13 in condition E). This could be the effect of catalyst deactivation at 300 °C or an effect associated with the observed gradual increase in activity and hypothesized surface 'reconstruction'. Methanol is the dominant formed oxygenated product with methanol to total oxygenate fractions of 0.65 to 0.73. No organic product analysis was performed on condition A.

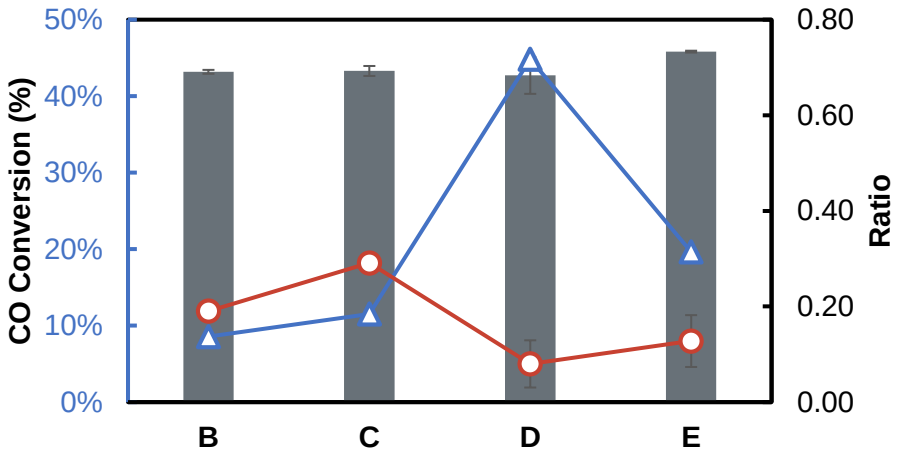

Figure 5-36: Organic product analysis obtained from FT 1.3 varying conditions indicated by: B) 280 °C and 12 L/h/g_{cat}; C) 280 °C and 8 L/h/g_{cat}, D) 300 °C and 8 L/h/g_{cat} and E) 280 °C and 8 L/h/g_{cat}. With oxygenate to total organic product (olefins, paraffins and oxygenates) ratio (red circles), MeOH to total oxygenate ratio (grey bars) and CO conversion (blue triangles). Process conditions: P = 33 bar, H_2 to CO ratio = 1.

The primary organic products are still mainly short chain paraffins, as is indicated by the chain growth probability of the linear paraffins (α-value of ±0.4), which decreases with increasing temperature. The chain growth probability of the linear olefins remained relatively stable (±0.3), as did the α-value for the linear alcohols (±0.16). Overall, in comparison to the previous two runs, the chain growth probabilities towards all three product classes are similar.

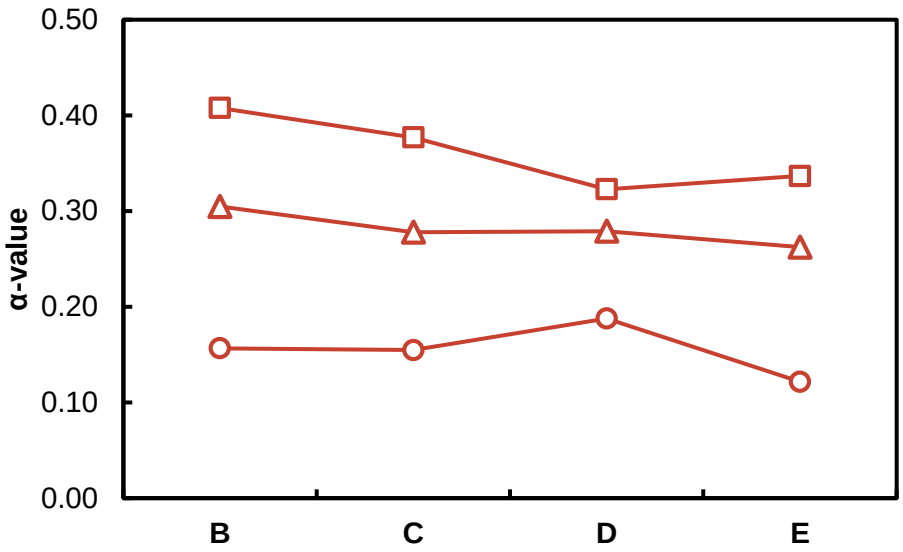

Figure 5-37: Chain growth probability calculated for the linear products from FT 1.3 of the product classes C_3-C_8 paraffins (squares), C_3-C_8* olefins (triangles) and C_2-C_6* alcohols (circles) varying conditions indicated by: B) 280 °C and 12 L/h/g_{cat}; C) 280 °C and 8 L/h/g_{cat}, D) 300 °C and 8 L/h/g_{cat} and E) 280 °C and 8 L/h/g_{cat}. Process conditions: P = 33 bar, H_2 to CO ratio = 1 (* = if possible).*

5.2.5 Effect of carburization conditions on the activity and selectivity of the catalysts

In comparison of the three tested catalysts some general conclusions can be drawn which are mostly well documented in the literature for unsupported Mo_xC catalysts. All three catalysts produce mainly hydrocarbons with a rather small chain growth probability. An increase in oxygenate selectivity was observed with a decrease in CO conversion. Within the oxygenated products, methanol was the most favourable product to be formed. Besides hydrogenation, all catalysts display a high activity for the WGS reaction (or the earlier mentioned CO oxidation reaction). The *in situ* catalyst showed the highest catalytic activity, however, passivation of the catalyst is required for the promotion of the catalyst with potassium. Promotion of the catalyst prior to carburization (co-precipitation) has been reported by Kojima and Aika (2001) [159] and is reported to change the carburization process and enhance the formation of metallic molybdenum [21]. The sample undergoing a passivation/reduction treatment showed reduced CO conversion but at the same time at very comparable conditions an increased oxygenate selectivity. It also had the highest tendency to produce CO_2, i.e. the highest WGS activity, which might be associated to residual MoO_x phases after the relatively mild reduction. The catalyst carburized at 760 °C exhibiting a graphite layer had, after removal of this layer, the lowest catalytic activity with a surprisingly high oxygenate selectivity – although a direct comparison of the catalytic performance is difficult and the stability of the catalyst regarding selectivity is uncertain. As addition of potassium to the catalyst has shown to negatively impact the catalytic activity [20] while significantly improving the oxygenate selectivity, the disadvantage of the deactivation outweighs the possible selectivity advantages. Therefore, further detailed studies on catalyst

activity and selectivity as a function of reaction conditions, potassium loading and ammonia co-feeding were conducted with passivated and subsequently reduced catalysts.

5.2.6 FT run 2.0: ''baseline'' catalyst

Based on above described findings, a β-Mo_2C catalyst carburized at 630 °C combined with a passivation and subsequent activation in hydrogen (see section 4.3.2 and 5.2.5) was reproduced and exposed to a variety of process conditions: a space velocity sweep between 8-34 L/h/g_{cat} (conditions A-D), a temperature sweep between 240-300 °C (conditions D-I) and finally a pressure sweep between 33-43 bar (conditions I-L). The main objective was to identify parameters enhancing the oxygenate yield for further testing in the presence of potassium promotion.

To avoid catalyst deactivation due to harsh conditions, the present experiment was started with the potentially mildest conditions within the specified range. The catalyst was exposed to a space velocity of 34 L/h/g_{cat}, temperature of 240 °C and absolute pressure of 33 bar. A low CO conversion of 1.7% was measured after 3.5 hours TOS (condition A in Figure 5-38) with a CH_4 and CO_2 selectivity of 21 C% and 19 C%, respectively. Upon lowering the SV stepwise to 8 L/h/g_{cat} (conditions B to D in Figure 5-38) the CO conversion only marginally increased to 2%. With the change in SV, the CH_4 selectivity marginally decreased to 20, 19 and 19 C% for conditions B, C and D respectively. The CO_2 selectivity remained relatively stable and only showed a significant increase at the lowest SV to 25 C%.

At the lowest SV, after 43 hours TOS, the reactor temperature was gradually increased to 300 °C (conditions D to G in Figure 5-38). The CO conversion increased from 2 to 5, 14 and 34%. This is lower than the conversions observed for a similar catalyst at similar conditions discussed earlier (Figure 5-30) and is probably associated to the different 'history' of reaction conditions the catalyst experienced. Interestingly, the CH_4 selectivity remained nearly constant over the whole temperature range (19, 18, 21, 22 C% respectively with increasing temperature from 240 °C to 300 °C). At the same time, the water-gas-shift activity increased from 25 C% CO_2 selectivity to 31, 39 and 45 C%. To test for catalyst deactivation or change in performance induced through the high temperature condition, the reaction temperature was reduced stepwise to 260 °C yielding 7% CO conversion. The CH_4 selectivities were again constant at 22, 21 and 21 C% with decreasing temperature from 300 to 280 and 260 °C. CO_2 selectivities decreased from 45 C% to 37 and 31 C%. It can therefore be concluded that the catalyst's performance was not altered through the exposure to the 300 °C condition, showing similar if not slightly higher conversion and selectivity (conditions E vs I in Figure 5-38 and Figure 5-39). A minor effect on the composition of the oxygenate fraction was observed (Figure 5-39) and will be discussed later.

The last condition sweep was increasing the pressure to 38 bar and 43 bar and subsequently returning to 33 bar (conditions I to L in Figure 5-38). Increase of pressure did not have a significant effect on the CO conversion which was recorded as 7, 6, 5, and 4%, respectively. In terms of

selectivity towards CH_4 and CO_2 the values stayed relatively stable with CH_4 at 21, 20, 18 and 18 C% and CO_2 31, 30, 28 and 28 C%.

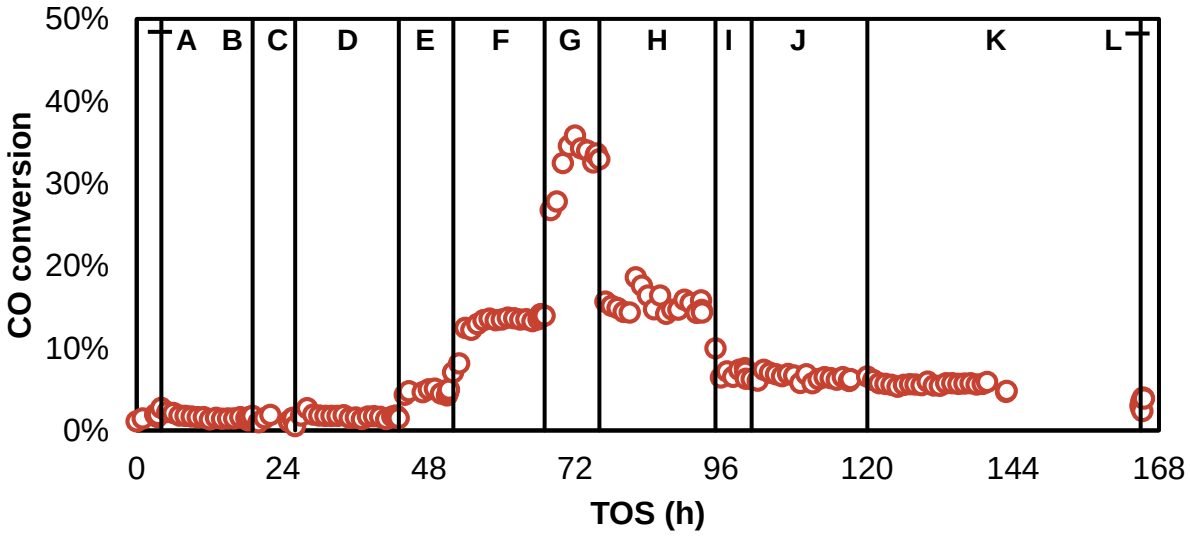

Figure 5-38: CO conversion from FT 2.0 obtained with TOS, varying conditions as indicated: At 240 °C and 33 bar: A) 34 L/h/g_{cat}, B) 25 L/h/g_{cat}, C) 17 L/h/g_{cat}, D) 8 L/h/g_{cat}. At 33 bar and 8 L/h/g_{cat}: E) 260 °C, F) 280 °C, G) 300 °C, H) 280 °C, I) 260 °C. At 260 °C and 8 L/h/g_{cat}: J) 38 bar, K) 43 bar, L) 33 bar.

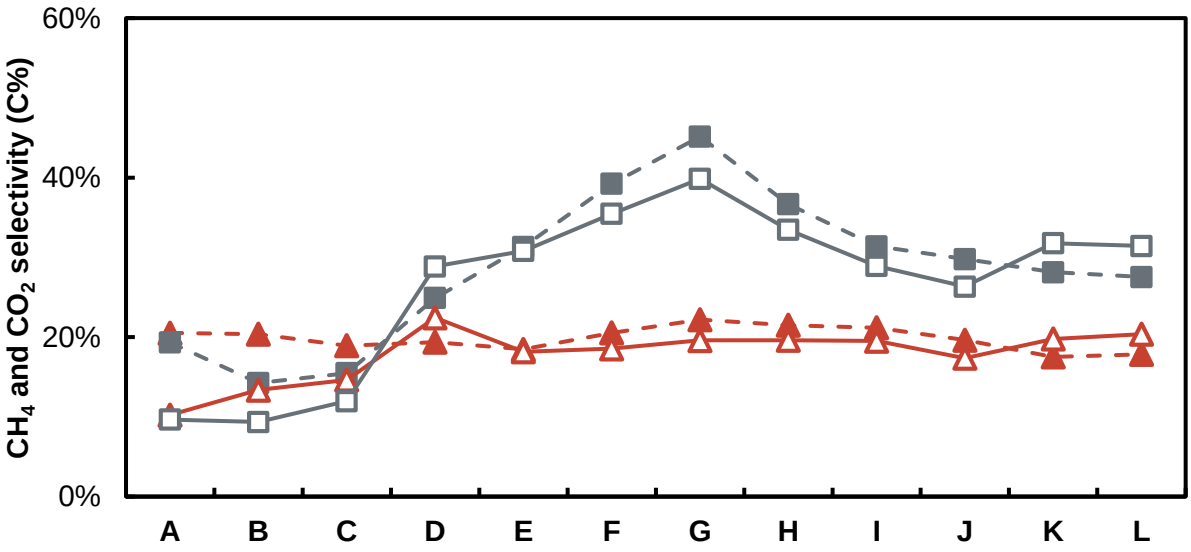

Figure 5-39: CH_4 (red triangles) and CO_2 (grey squares) selectivity, presenting original data (open symbols, solid lines) and carbon balance corrected (solid symbols, dashed line) from FT 2.0 obtained with TOS, varying conditions as indicated: At 240 °C and 33 bar: A) 34 L/h/g_{cat}, B) 25 L/h/g_{cat}, C) 17 L/h/g_{cat}, D) 8 L/h/g_{cat}. At 33 bar and 8 L/h/g_{cat}: E) 260 °C, F) 280 °C, G) 300 °C, H) 280 °C, I) 260 °C. At 260 °C and 8 L/h/g_{cat}: J) 38 bar, K) 43 bar, L) 33 bar.

The analysis of the organic products showed an initially stable oxygenate to total organic product (HC and OX) ratio of 0.31, 0.33 and 0.34 with decreasing SV. Only at the lowest SV (condition D) the ratio dropped to 0.27. This drop is paralleled by an increase in CO_2 selectivity but cannot be explained as calculation artifact as the hydrocarbon selectivities are reported as CO_2 free. An increase in temperature (conditions E-G) above 260 °C resulted in a decrease in the oxygenate to total organic product ratio from 0.27 (conditions D & E) to 0.19 (condition F) and finally 0.10 (condition G). This is paralleled with the previously described increase in CO conversion and CO_2 selectivity. A subsequent return of the temperature to 260 °C increases the oxygenate to hydrocarbon ratio back to 0.27. The change in pressure, from 33 to 43 bar, did not influence the total oxygenate selectivity, with the ratio towards hydrocarbons remaining relatively stable between 0.25 and 0.29 (Figure 5-40).

The hydrocarbon product class can be divided into paraffins and olefins. The two different groups can be expressed as linear olefin to linear paraffin ratio (O/P), calculated exemplary for the C_3 fraction. The O/P ratio is an indication to what extent secondary hydrogenation reactions are taking place. The effect of the different conditions applied on this ratio is significant and starts with 1.06 at condition A. The drop in space velocity showed a small increase followed by a decrease (1.26, 1.20 and 0.85 for conditions B, C and D, respectively). Upon the increase in temperature, the olefin content decreased significantly from 0.85 to 0.59, 0.24 and 0.13 at conditions D to G, respectively. The decrease in temperature had a reversible impact and from condition G to I the olefin to paraffin ratio was observed at 0.13 to 0.20 and 0.30. The increase in pressure to 43 bar increased the olefin content to 0.45 (condition J) and 0.61 (condition K). Upon the dropping the pressure to 33 bar a ratio of 0.75 was recorded (Figure 5-40). This is higher than the starting point of the pressure sweep (condition I) as well as the initial exposure to 260 °C during the temperature sweep (condition E).

The change in conditions had a slight effect on the product distribution within the oxygenates, however the major oxygenated product class remained alcohols with above 94 C%, balanced by aldehydes, carboxylic acids and ketones. From conditions A-D the methanol fraction of the total oxygenates is approximately 0.50. The methanol content increases with temperature from 0.49 to 0.52, 0.60, and 0.64 at 260, 280 and 300 °C, respectively. A subsequent decrease in temperature showed a slight drop in methanol content from 0.64 to 0.62 at 260 °C, which is higher than the initial value at these reaction conditions (0.52). Increasing pressure showed a decrease in methanol content, from 0.62 to 0.52 at 43 bar. However, this proved non-reversible and remained at 0.52 upon reduction of the pressure to 33 bar (Figure 5-40). This trend is qualitatively comparable to the described olefin to paraffin ratio with both product classes, oxygenates and olefins prone to secondary reactions such as hydrogenation. Why the activity of the sites responsible for these secondary reactions does change with TOS, i.e. does not reach the same values as during previous exposure to the same reaction conditions, is unknown at this stage.

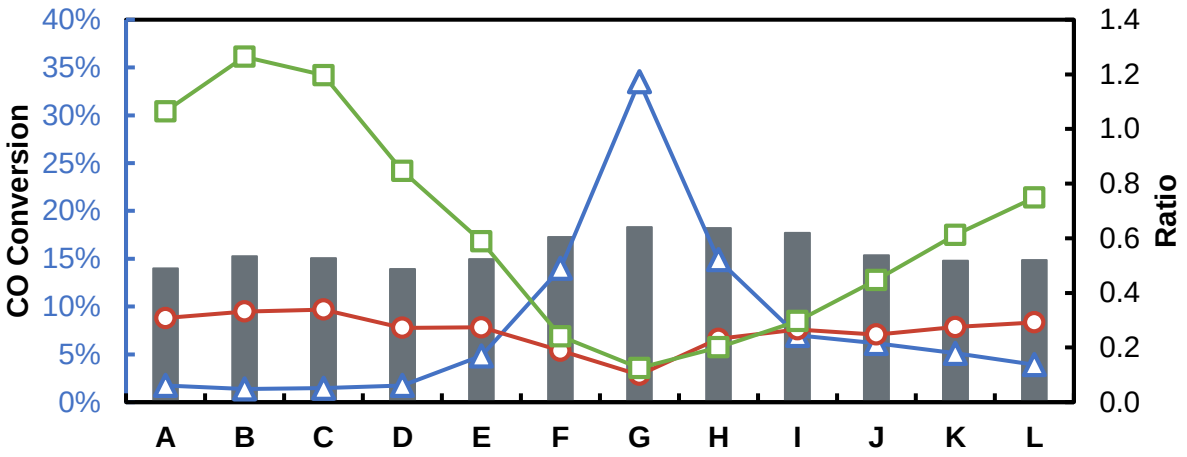

Figure 5-40: Organic product analysis obtained from FT 2.0 as a function of process conditions indicated as: At 240 °C and 33 bar: A) 34 L/h/g_{cat}, B) 25 L/h/g_{cat}, C) 17 L/h/g_{cat}, D) 8 L/h/g_{cat}. At 33 bar and 8 L/h/g_{cat}: E) 260 °C, F) 280 °C, G) 300 °C, H) 280 °C, I) 260 °C. At 260 °C and 8 L/h/g_{cat}: J) 38 bar, K) 43 bar, L) 33 bar. With oxygenate to total organic product (olefins, paraffins and oxygenates) ratio (red circles), MeOH to total oxygenate ratio (grey bars), CO conversion (blue triangles) and C_3-olefin to C_3-paraffin ratio (green squares).

While oxygenate fractions of close to 50 C% are obtained at low conversion conditions, the major product class remains the short chained hydrocarbons. Chain growth probability of the different product classes (linear paraffins, linear olefins and linear alcohols) was not much affected by the change in conditions (Figure 5-41). The SV sweep resulted in α-values for linear paraffins, from A-D, of 0.49, 0.48, 0.50 and 0.49, for linear olefins 0.31, 0.32, 0.31 and 0.31 and for linear alcohols 0.23, 0.23, 0.21 and 0.26. Increasing temperature (conditions D-G) decreases the α-values of the linear paraffins from 0.49 to 0.44, 0.39 and 0.36 for the linear olefins from 0.31 to 0.30, 0.30 and 0.27 and for linear alcohols from 0.26 to 0.23, 0.21 and 0.25. This apparent increase in hydrogenation activity is in line with the observed trends in olefin and oxygenate content. A subsequent decrease in temperature (G-I) increases the α-values for the linear paraffins from 0.36 to 0.40 and 0.43 and for the linear olefins from 0.27 to 0.29 and 0.31 and for the linear alcohols from 0.25 to 0.21 and 0.19. The applied pressure sweep (conditions I-L) also influenced the α-value for linear paraffins slightly from 0.43 to 0.47, 0.49 and 0.50 and for the linear olefins from 0.31 to 0.31, 0.27 and 0.30 and for the linear alcohols from 0.19 to 0.22, 0.22 and 0.24.

The focus of the project is not only to increase the total oxygenate selectivity but also to study the effect of the different process conditions on the oxygenate distribution, such as alcohols, aldehydes, ketones and carboxylic acids. During FT run 2.0, alcohols are the dominant formed class of oxygenates, with contents between 94 C% (condition L) and 99 C% (condition H). The second group of oxygenates are the aldehydes, with values between 1 C% (condition H) and 5 C% (condition G). only small traces of ketones and carboxylic acids are observed, up to 1 C% maximum (Figure 5-42).

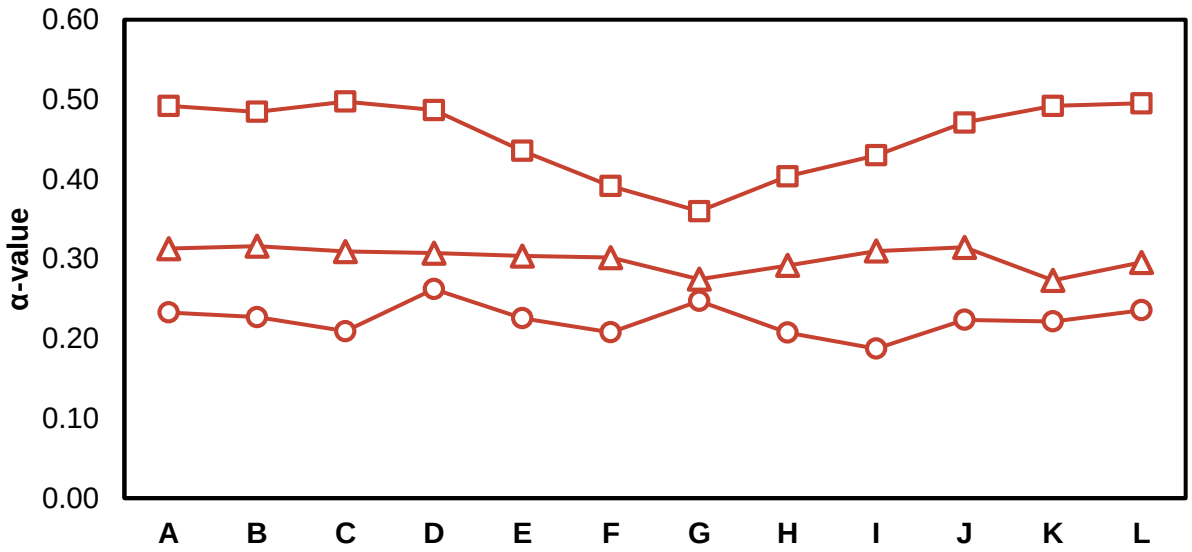

Figure 5-41: Chain growth probability calculated for the linear products from FT 2.0 of the product classes C_3-C_8 paraffins (squares), C_3-C_8* olefins (triangles) and C_2-C_6* alcohols (circles) varying conditions at 240 °C and 33 bar indicated by A) 34 L/h/g_{cat}, B) 25 L/h/g_{cat}, C) 17 L/h/g_{cat}, D) 8 L/h/g_{cat}. At 33 bar and 8 L/h/g_{cat}: E) 260 °C, F) 280 °C, G) 300 °C, H) 280 °C, I) 260 °C. At 260 °C and 8 L/h/g_{cat}: J) 38 bar, K) 43 bar, L) 33 bar (* = if possible).*

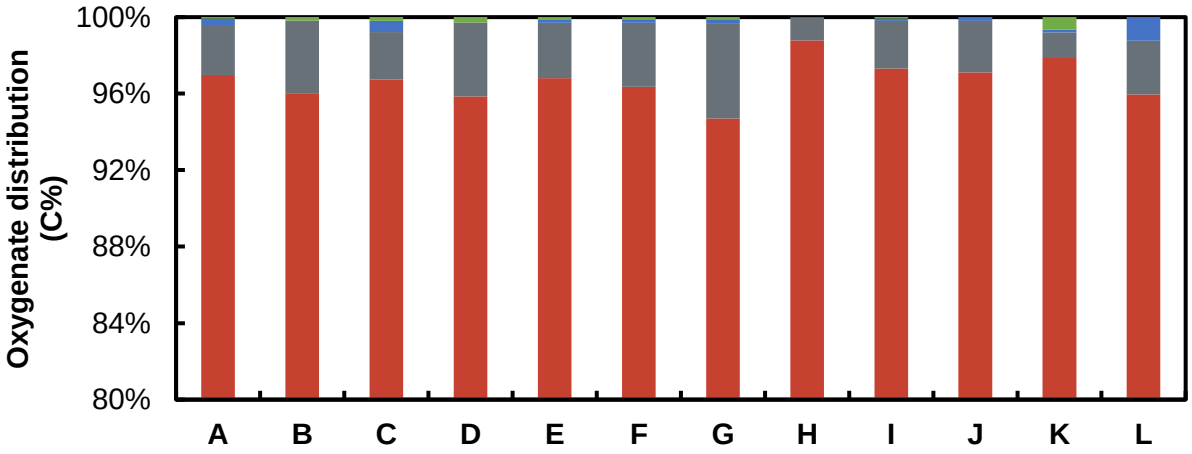

Figure 5-42: Oxygenate distribution of FT run 2.0 with the product classes alcohols (red), aldehydes (grey), carboxylic acids (blue) and ketones (green) as a function of different process conditions: at 240 °C and 33 bar indicated by A) 34 L/h/g_{cat}, B) 25 L/h/g_{cat}, C) 17 L/h/g_{cat}, D) 8 L/h/g_{cat}. At 33 bar and 8 L/h/g_{cat}: E) 260 °C, F) 280 °C, G) 300 °C, H) 280 °C, I) 260 °C. At 260 °C and 8 L/h/g_{cat}: J) 38 bar, K) 43 bar, L) 33 bar.

Alcohols dominate the oxygenate slate; therefore, it is interesting to study the effect of different process conditions on the formation of C_1, C_2, C_3 and C_4 linear alcohols. On average, methanol is the most favourably formed alcohol, with a content (in the alcohol fraction) between 50 C% (condition D) and 67 C% (condition G). Thereafter, ethanol is the second most favourable alcohol, with values between 19 C% (condition G) and 33 C% (condition A). The influence of different

parameters is the most significant with a change in temperature. Upon increasing temperature, the methanol content increases, significantly, from 53 C% (condition E) to 67 C% (condition G), whereas the ethanol content drops from 30 C% to 19 C%, respectively.

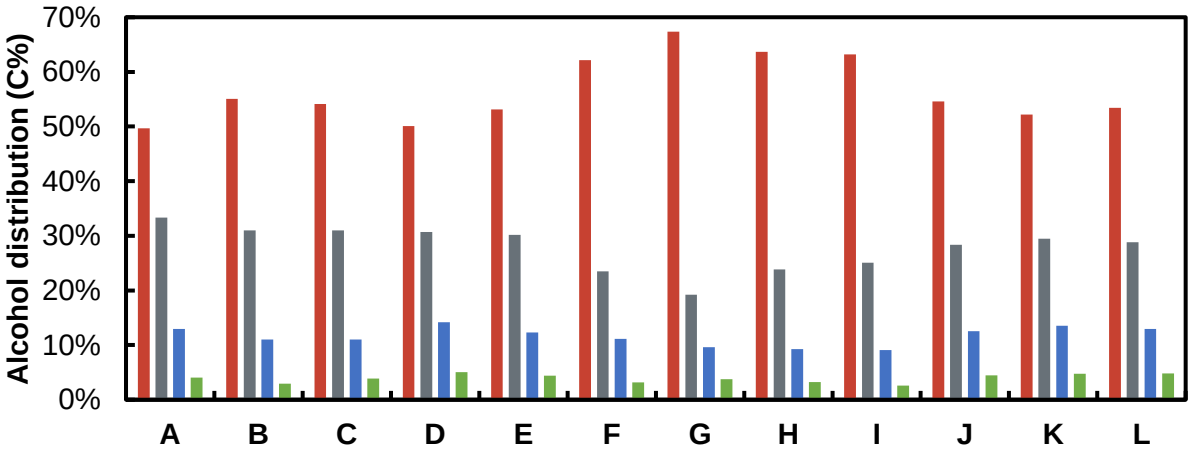

Figure 5-43: Alcohol distribution of FT run 2.0 with methanol (red), ethanol (grey), propanol (blue) and C_{4+} alcohols (green) as a function of a variation of process conditions: at 240 °C and 33 bar indicated by A) 34 L/h/g_{cat}, B) 25 L/h/g_{cat}, C) 17 L/h/g_{cat}, D) 8 L/h/g_{cat}. At 33 bar and 8 L/h/g_{cat}: E) 260 °C, F) 280 °C, G) 300 °C, H) 280 °C, I) 260 °C. At 260 °C and 8 L/h/g_{cat}: J) 38 bar, K) 43 bar, L) 33 bar.

5.2.7 FT run 2.1: D - 6.2 wt.% K/Mo promoted β-Mo_2C*

Based on the obtained results from the first set of FT experiments, the promoted catalysts – potassium promotion is widely reported to increase oxygenate selectivity [18, 21, 102] – were tested using process conditions resulting in a reasonable catalytic activity and oxygenate selectivity. However, as potassium is also known to deactivate the catalyst [21], conditions which result in appreciable catalytic performance regarding CO conversion were chosen. Since temperature has been shown to have the most significant influence on both, the activity and oxygenate selectivity, it was the only parameter varied. As the influence of pressure in the present study was minimal and in the literature [17, 18] pressures up to 100 bar were used which in turn are reported to be beneficial for the oxygenate selectivity, the pressure was set at the highest pressure that is technically possible, of 45 bar. Space velocity was maintained at 8 L/h/g_{cat}.

A catalyst was prepared using the same method as described in section 5.2.3. After the passivation step the catalyst was removed from the reactor and subsequently promoted via wetness impregnation with K_2CO_3 (as described in section 4.1.3) with an ICP-determined loading of 6.2 wt.% K/Mo of the spent sample (Table 5-2). The catalyst was calcined at 500 °C for 4.5 hours in argon with a GHSV of 4 L/h/g_{cat}, reduced in the reactor unit and exposed to the reaction conditions, i.e. T = 260 °C, P = 45 bar, H_2 to CO ratio of 1 and GHSV of 8 L/h/g_{cat}. A stable CO conversion as low as 1% was obtained after 7 hours TOS. CH_4 and CO_2 selectivity at this low conversion are 14 C% and 46 C%, respectively. In comparison to the unpromoted catalyst

(section 5.2.6) the reported effects of potassium promotion can be confirmed, namely a decreased conversion [20, 21] (1% vs. 5%), a decreased CH_4 selectivity [20] (14 C% vs 18 C%), and an increased WGS activity [20] (CO_2 selectivity of 46 C% vs. 31 C%). An increase in temperature to 280 °C, increased the CO conversion to 4% after 28 hours TOS. With this increase in CO conversion, the selectivities towards CH_4 and CO_2 were not significantly influenced and remained around 11 C% and 48 C%, respectively. Another step increase in temperature to 300 °C, increased CO conversion further to 6%. The selectivity towards CH_4 was 10 C%, the CO_2 selectivity increased to 52 C%. As CO conversion was still low compared to the unpromoted samples at similar conditions, the temperature was increased once more to 320 °C. CO conversion reached 10% at an apparent steady state. Selectivity did not change significantly with CH_4 at 10 C% and CO_2 at 54 C%. To test if any catalyst deactivation has happened over TOS or due to the applied conditions, the temperature was reduced to 280 °C. The CO conversion dropped to 2% while the selectivity towards CH_4 remained relatively stable at 10 C% and CO_2 decreased to 45 C%. While in relative terms, the catalyst's CO conversion dropped significantly from 4% during the initial exposure to 280 °C to 2%, this should be regarded as similar due to the expected associated error in the determination of the conversion specifically at low levels. CH_4 and CO_2 selectivities remain stable confirming an absence of deactivation. Assured of the catalyst's stability an even higher reaction temperature of 350 °C was set. This increase in temperature led to an increase in CO conversion to 17%. A subsequent increase in selectivity towards CO_2 was observed, reaching 52 C% which is not higher than the selectivity recorded at 300 and 320 °C. CH_4 increased by 2 C%-points to 12 C%. Again, reversibility was tested by dropping the reaction temperature to 280 °C. The run ended with a CO conversion of 2% (Figure 5-44). Which indicates, no significant catalyst deactivation took place at the high temperatures. Correspondingly, selectivities returned to their approximate initial values of 9 C% and 42 C% for CH_4 and CO_2, respectively (Figure 5-45).

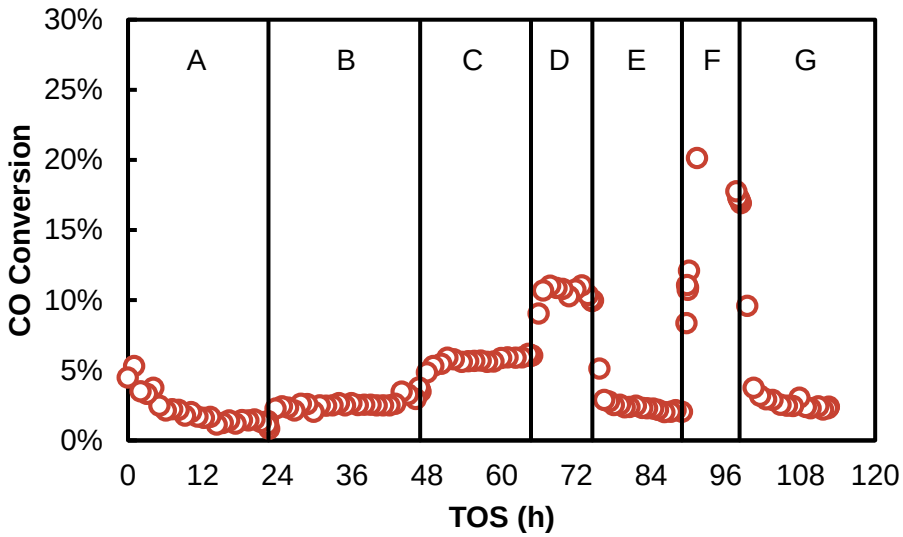

Figure 5-44: CO conversion from FT 2.1 obtained with TOS, varying conditions as indicated: A) 260 °C, B) 280 °C, C) 300 °C, D) 320 °C, E) 280 °C, F) 350 °C and G) 280 °C. Process conditions: P = 45 bar, H_2 to CO ratio = 1 and GHSV = 8 L/h/g_{cat}.

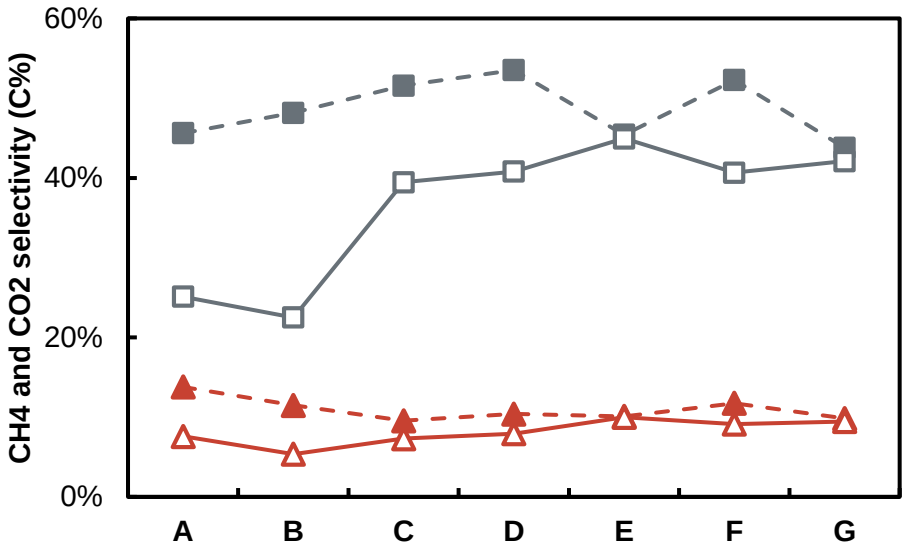

Figure 5-45: CH_4 (red triangles) and CO_2 (grey squares) selectivity, presenting original data (open symbols, solid lines) and carbon balance corrected (solid symbols, dashed line) from FT 2.1 obtained with TOS, varying conditions as indicated: A) 260 °C, B) 280 °C, C) 300 °C, D) 320 °C, E) 280 °C, F) 350 °C and G) 280 °C. Process conditions: P = 45 bar, H_2 to CO ratio = 1 and GHSV = 8 L/h/g_{cat}.

Analysis of the organic products was again conducted using an offline GC-FID (Figure 5-46). The 6.2 wt.% K/Mo promotion was found to have a significant effect regarding the product selectivity. Compared to the unpromoted sample (Figure 5-40) the oxygenate selectivity is significantly higher at overall lower CO-conversions. But even at 260 °C, with comparable conversions of 5 and 2% for the unpromoted and promoted catalyst respectively (condition E of the unpromoted catalyst in

Figure 5-39 and condition A in Figure 5-42), the oxygenate to hydrocarbon ratio is by 17%-points higher. It must be noted that the CO_2 selectivity is also higher in the promoted catalyst (46 vs 31 C%) levelling the observed increase in oxygenate selectivity somewhat. An increase in temperature from 260 to 280, 300 and 320 °C (conditions A-D) showed an oxygenate to hydrocarbon ratio of 0.57, 0.50, 0.54 and 0.47, respectively. The decrease to 280 °C (condition E) showed an increase in the oxygenate content to 0.67 which is significantly higher than the oxygenate fraction during initial exposure to the same reaction conditions (0.50 at condition B). This has been observed for the unpromoted sample, albeit at a much lower level (comparison condition F to H in Figure 5-39) and disappearing fully upon further reduction in reaction temperature to 260 °C. The subsequent increase to 350 °C (condition F) expectedly reduced the oxygenates selectivity to a level similar to that measured at 320 °C. Importantly, and in line with previous reports in the literature [20, 21], the fraction of methanol in the oxygenates is reduced drastically with the introduction of potassium promotion. Levels of 0.28, 0.24, 0.20, 0.20, 0.25 and 0.20 as the conditions change from A-F, respectively, are half to a third of those found over the unpromoted catalyst. It is interesting to see that the methanol content decreases with an increase in temperature, as suggested in section 2.2.3.1 (Figure 5-46).

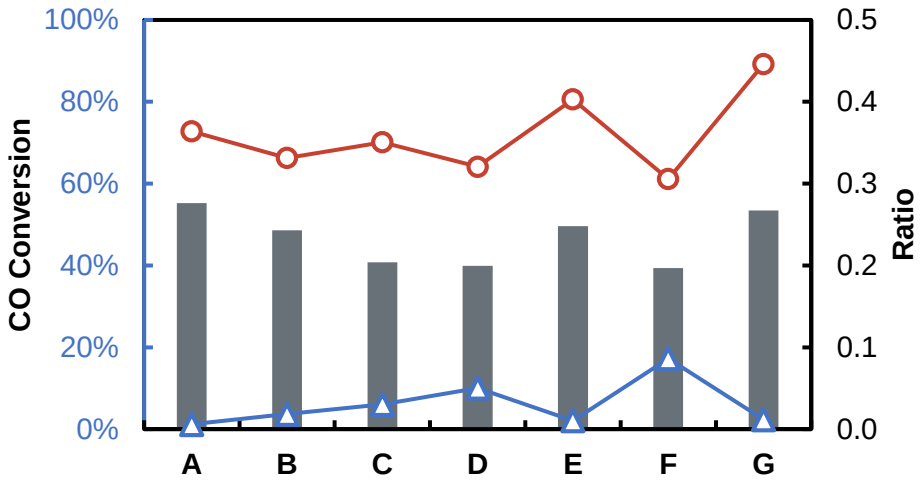

Figure 5-46: Organic product analysis obtained from FT 2.1 varying conditions indicated by: A) 260 °C, B) 280 °C, C) 300 °C, D) 320 °C, E) 280 °C, F) 350 °C and G) 280 °C. Process conditions: P = 45 bar, H_2 to CO ratio = 1 and GHSV = 8 L/h/g_{cat}. With oxygenate to total organic product ratio (red circles), MeOH to total oxygenate ratio (grey bars) and CO conversion (blue triangles).

The formed hydrocarbon product also shows a significant increase in the olefin content compared to the unpromoted sample in FT 2.0 in line with reported promoter effects of alkali metals [160] suppressing secondary hydrogenation reactions. It was observed that the C_3-linear olefin to C_3-linear paraffin ratio (O/P) increases with temperature, from 2.43 to 2.97 and 3.50, conditions A-C respectively. Upon a further increase to 320 °C, condition D, a drop to 2.93 was observed. The return to 280 °C (condition E) yielded an O/P ratio of 3.40, also higher than the initial value at this reaction temperature. A subsequent increase to 350 °C (condition F) increased the O/P ratio to

3.58. Finally, the temperature was again dropped to 280 °C (condition G) and found a O/P ratio of 3.12 (see Appendix H, Figure 9-4). The O/P ratio is not only significantly higher than for the unpromoted catalyst but also follows an opposing trend with temperature, namely increasing with increasing temperature.

To account for the significantly shifted product selectivity upon promotion, the chain growth probability is calculated based on linear paraffins, linear olefins and linear alcohols (Figure 5-47). The α-values for linear paraffins are, from A-G, 0.41, 0.54, 0.51, 0.49, 0.54, 0.51 and 0.58, respectively. For the linear olefins, the observed α-values are from condition A-G: 0.43, 0.49, 0.47, 0.45, 0.50, 0.45 and 0.50, respectively. Finally, for the linear alcohols, the α-values are determined as 0.26, 0.27, 0.29, 0.27, 0.32, 0.24 and 0.40. In summary, the chain growth probability towards the hydrocarbons is slightly enhanced upon the promotion with potassium with the effect of temperature being negligible. However, the chain growth probability of the linear alcohols increased on each return to 280 °C compared to its precedent at the same conditions.

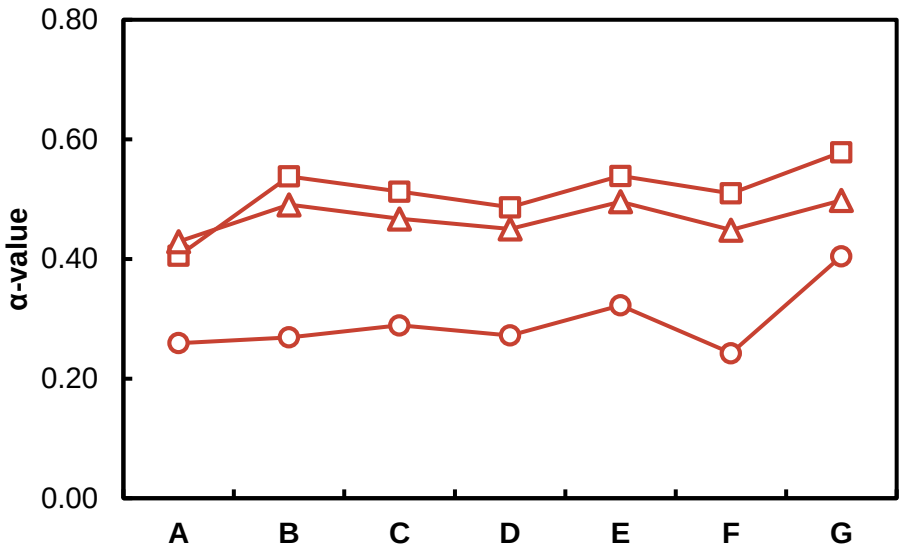

Figure 5-47: Chain growth probability calculated for the linear products from FT 2.1 of the product classes C_3-C_8 paraffins (squares), C_3-C_8* olefins (triangles) and C_2-C_6* alcohols (circles) varying conditions indicated by: A) 260 °C, B) 280 °C, C) 300 °C, D) 320 °C, E) 280 °C, F) 350 °C and G) 280 °C. Process conditions: P = 45 bar, H_2 to CO ratio = 1 and GHSV = 8 L/h/g_{cat} (* = if possible).*

The promotion with potassium showed a significant increase in oxygenate selectivity in comparison to the unpromoted samples. It is observed that the alcohols are still the primary formed products (between 59 C% at condition A and 90 C% at condition F), followed by aldehydes (between 8 C% at condition F and 37 C% at condition A) and some small traces of carboxylic acids (up to 2 C% at condition A) and ketones (up to 6 C% at condition E). In the unpromoted catalyst, over 90 C% of the oxygenates were alcohols, independent of reaction conditions. The increase in temperature showed a significant increase in alcohol content, mostly at the expense of the aldehydes. From conditions A to D, the alcohol selectivity increased from 59 C% to 86 C%,

respectively. Returning to 280 °C at condition E the alcohol concentration remained slightly higher than the initial value at the same conditions (78 C% vs 70 C%). An increase to 350 °C at condition F, increased the alcohol selectivity to its maximum in this run, 90 C%. Finally, back to 280 °C, the alcohol content dropped to 82 C%, which is again higher than the initial values at the same process conditions (Figure 5-48) indicating that a change in the catalyst's surface is taking place with TOS resulting in a slight shift in selectivity. Whether this change is related to phase or physical changes or rather with an accumulation of surface species is not known at this stage.

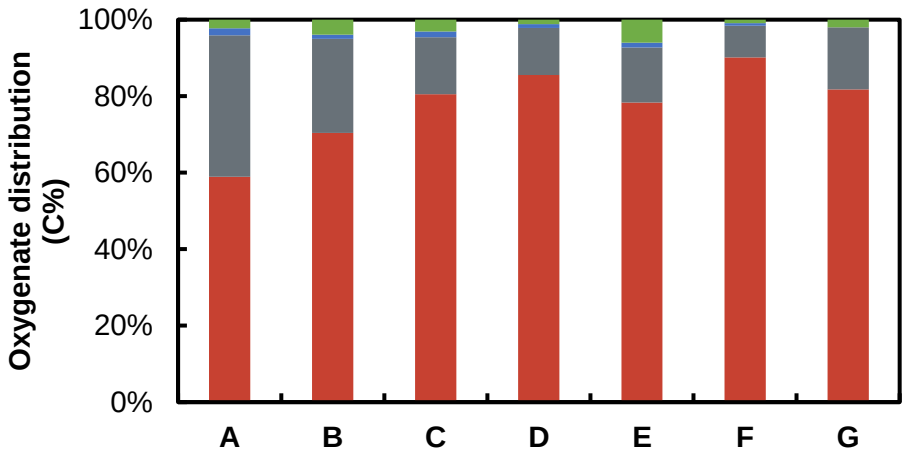

Figure 5-48: Oxygenate distribution of FT run 2.1 with the product classes alcohols (red), aldehydes (grey), carboxylic acids (blue) and ketones (green) as a function of temperature: A) 260 °C, B) 280 °C, C) 300 °C, D) 320 °C, E) 280 °C, F) 350 °C and G) 280 °C. Process conditions: P = 45 bar, H_2 to CO ratio = 1 and GHSV = 8 L/h/g_{cat}.

A closer look on the C_1-C_{4+} alcohols (Figure 5-49) reveals that different to the unpromoted sample, an increase in temperature leads to a significant decrease in methanol formation (from 47 C% at 260 °C to 23 C% at 320 °C) and an increase in ethanol selectivity (from 39 C% at 260 °C to 53 C% at 320 °C). Also, propanol (from 8 C% at 260 °C to 16 C% at 320 °C) and C_{4+} alcohols (from 6 C% at 260 °C to 11 C% at 300 °C) show an increase in concentration upon the increase in temperature. A subsequent decrease in temperature to 280 °C showed similar results to the initial values at these conditions. Increasing to 350 °C led to a more significant drop in the methanol content to 21 C%, where ethanol increased to its maximum of 55 C%. Propanol and C_4 alcohols were observed at 16 C% and 8 C%, respectively. A final drop in temperature to 280 °C showed again similar results to the initial values at these conditions, except ethanol is slightly lower and C_{4+} alcohols slightly higher, as supported by the increase in chain growth probability (Figure 5-49).

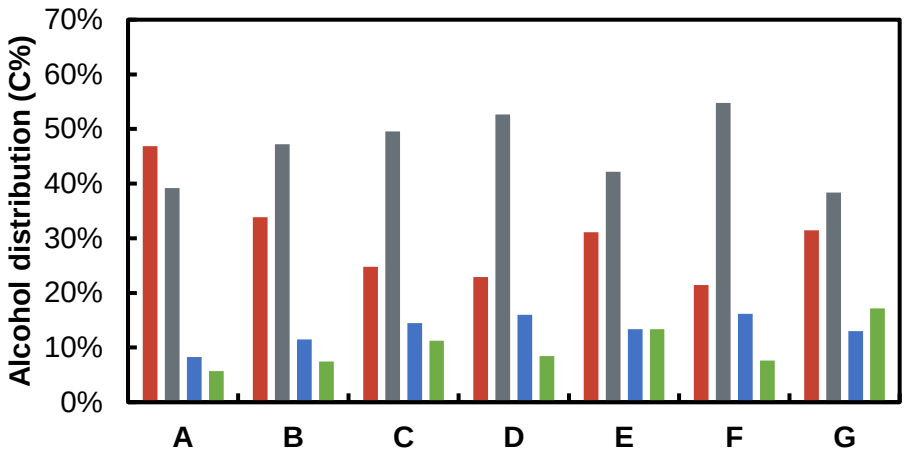

Figure 5-49: Alcohol distribution of FT run 2.1 with methanol (red), ethanol (grey), propanol (blue) and C_{4+} alcohols (green) as a function of temperature: A) 260 °C, B) 280 °C, C) 300 °C, D) 320 °C, E) 280 °C, F) 350 °C and G) 280 °C. Process conditions: P = 45 bar, H_2 to CO ratio = 1 and GHSV = 8 L/h/g_{cat}.

5.2.8 FT run 2.2: E - 5.4 wt.% K/Mo promoted β-Mo_2C*

The second promoted sample was E* - 5.4 wt.% K/Mo (Table 5-2) prepared using the same method as FT run 2.1 and the same initial reaction conditions were chosen, i.e. T = 260 °C, P = 45 bar, H_2 to CO ratio of 1 and GHSV of 8 L/h/g_{cat}. The CO conversion at condition A was comparable to the previous run with 2% after 20 hours TOS (Figure 5-50), however at a lower CH_4 (11 C%) and a higher CO_2 (59 C%) selectivity (Figure 5-51). An increased temperature (280 °C) led to an increased CO conversion of 5% at steady state after 38 hours TOS. The selectivity towards CH_4 remained stable at 10 C% and CO_2 dropped to 51 C% respectively now very comparable to the 6.2 wt.% K/Mo catalyst. Upon a further increase in temperature to 300 °C (condition C), the CO conversion jumped to 11% followed by a slow decrease and settled at 8% after 53.5 hours TOS. For neither the unpromoted nor the D* - 6.2 wt.% K/Mo sample was this fast jump followed by a slower decrease in CO conversion upon a temperature increase previously observed. Selectivities of CH_4 and CO_2 remained similar at 11 C% and 51 C% at the end of the condition. Subsequent temperature increases result in a very similar catalytic response, an initial jump in CO conversion with increasing temperature, followed by a gradual decrease. Condition E was stopped too early and therefore not allowed to stabilize fully. While the peak activity of the present catalyst was significantly higher at each condition compared to the D* - 6.2 wt.% K/Mo sample, the stabilized CO conversion is very comparable. To study catalyst deactivation the temperature was decreased back to 280 °C (condition F). It seems that the catalyst was slightly deactivated over time on stream or due to the reaction conditions as the CO conversion obtained was 2% compared to the initial 6% at condition B. CH_4 as well as CO_2 selectivity were also recorded to be lower at 11 and 48 C% respectively. Overall both the CO conversion as well as the CH_4 and CO_2 selectivity are very comparable to the previously

discussed promoted sample with the difference that from 300 °C onwards, the CO conversion spikes upon the temperature increase before stabilizing.

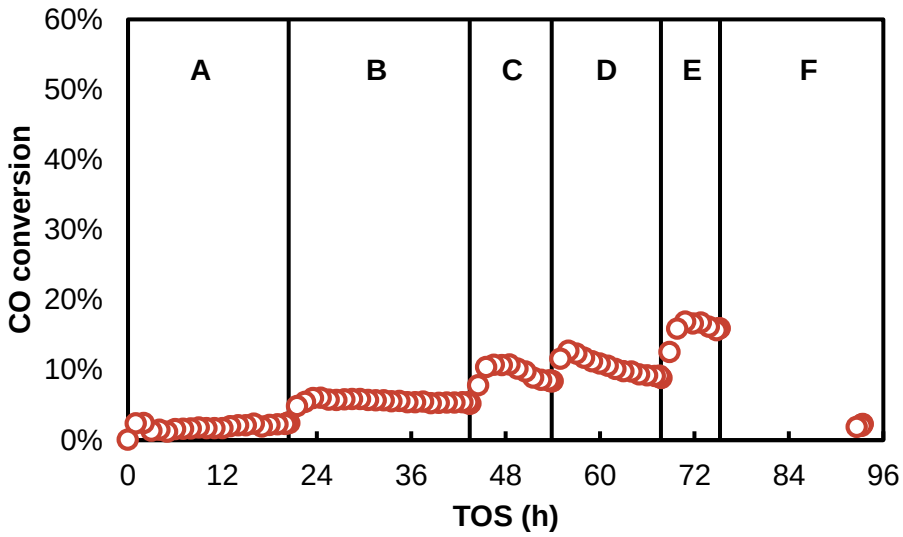

Figure 5-50: CO conversion from FT 2.2 obtained with TOS, varying conditions as indicated: A) 260 °C, B) 280 °C, C) 300 °C, D) 320 °C, E) 350 °C and F) 280 °C. Process conditions: P = 45 bar, H_2 to CO ratio = 1 and GHSV = 8 L/h/g_{cat}.

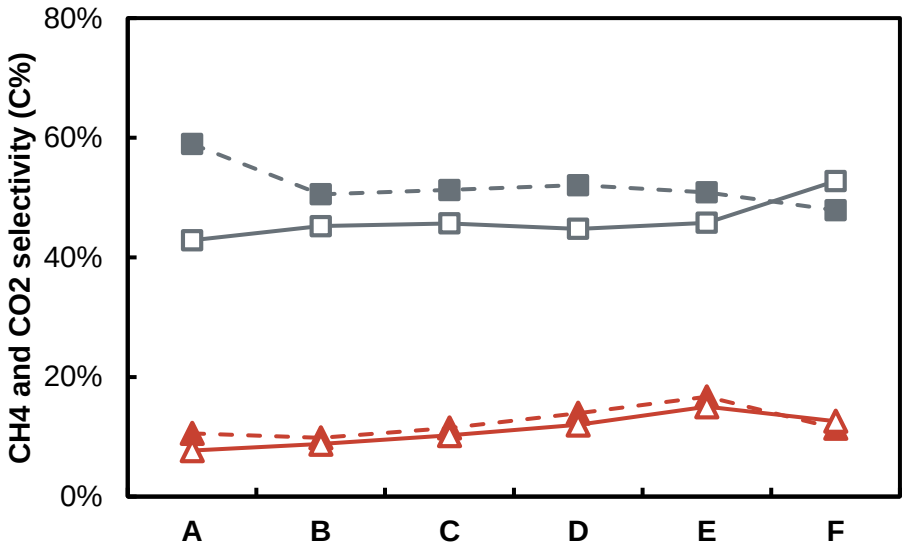

Figure 5-51: CH_4 (red triangles) and CO_2 (grey squares) selectivity, presenting original data (open symbols, solid lines) and carbon balance corrected (solid symbols, dashed line) from FT 2.2 obtained with TOS, varying conditions as indicated: A) 260 °C, B) 280 °C, C) 300 °C, D) 320 °C, E) 350 °C and F) 280 °C. Process conditions: P = 45 bar, H_2 to CO ratio = 1 and GHSV = 8 L/h/g_{cat}.

For condition A (260 °C), the oxygenate to total organic product ratio was 0.30. A slight increase was observed for condition B, 0.34, but subsequently the oxygenate selectivity dropped with the

increase in temperature (condition C, D and E) to 0.31, 0.25 and finally 0.22. A decrease in temperature back to 280 °C increased the oxygenate content to 0.31, which is slightly lower than the initial value of 0.34. Overall, the oxygenate selectivity decreased slightly with decreasing potassium concentration (Table 5-2). With an increase in temperature (conditions A-E) the methanol content within the total oxygenates was relatively constant without displaying the clear decreasing trend – although the lowest value was recorded for the highest reaction temperature – with increasing temperature previously observed (see Figure 5-42). The hydrocarbon product is mostly olefinic, with a clearly lesser hydrogenation activity compared to D* - 6.2 wt.% K/Mo (see Appendix H, Figure 9-5).

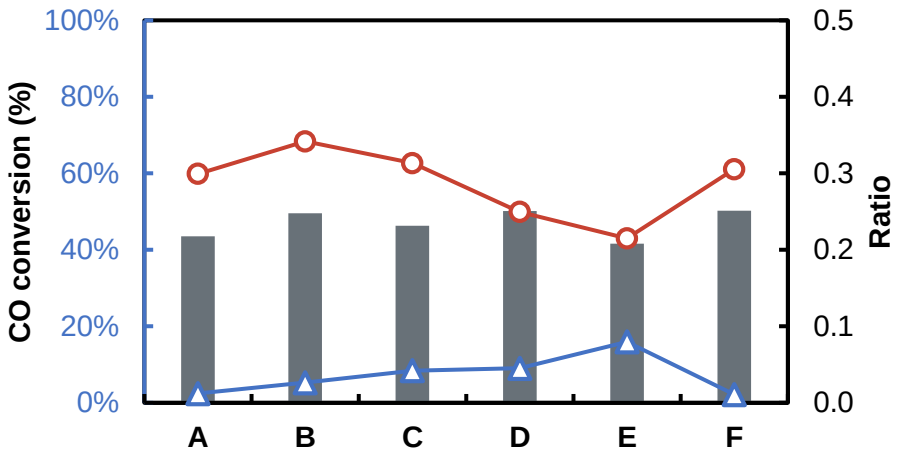

Figure 5-52: Organic product analysis obtained from FT 2.2 varying conditions indicated by: A) 260 °C, B) 280 °C, C) 300 °C, D) 320 °C, E) 350 °C and F) 280 °C. Process conditions: P = 45 bar, H_2 to CO ratio = 1 and GHSV = 8 L/h/g_{cat}. With oxygenate to total organic product ratio (red circles), MeOH to total oxygenate ratio (grey bars) and CO conversion (blue triangles).

The chain growth was again calculated for the three-different product classes (Figure 5-53), linear paraffins, linear olefins and linear alcohols. For all three product classes the α-value only changes marginally compared to the behavior of the highest promoted catalyst (D* - 6.2 wt.% K/Mo). Potentially the oxygenate fraction displays a slightly lower chain growth probability which is mirrored by the overall higher MeOH content (see Figure 5-46).

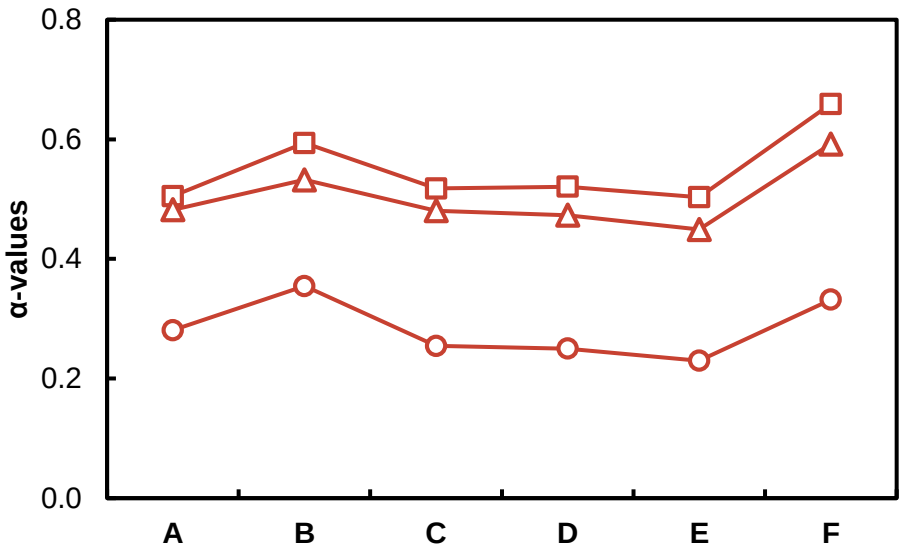

Figure 5-53: Chain growth probability calculated for the linear products from FT 2.2 of the product classes C_3-C_8 paraffins (squares), C_3-C_8* olefins (triangles) and C_2-C_6* alcohols (circles) varying conditions indicated by: A) 260 °C, B) 280 °C, C) 300 °C, D) 320 °C, E) 350 °C and F) 280 °C. Process conditions: P = 45 bar, H_2 to CO ratio = 1 and GHSV = 8 L/h/g_{cat} (* = if possible).*

The decrease in potassium promotion (from 6.2 wt.% to 5.4 wt.% K/Mo) showed some significant differences in the oxygenate product distribution. The major oxygenated product class remained alcohols, however now with 73 C% at the starting conditions (A). This is much higher than the 59 C% obtained at condition A during FT 2.1. Upon the increase in temperature the alcohol content increased to 94 C% at 280 °C (again significantly higher than 70 C% at the same conditions in FT 2.1). Thereafter, where in FT 2.1 the alcohol content increases with increasing temperature, during FT 2.2 the alcohol content decreases with increasing temperature to 85 C% at 350 °C. This is lower than in FT 2.1 at the same process conditions applied (90 C%). A subsequent drop in temperature back to 280 °C was followed by another decrease in alcohol content to 79 C%, which is much lower than the original value at the same conditions but similar to condition E and G of FT 2.1. The differences in alcohol content between FT 2.1 and FT 2.2 are mainly due to the decreased aldehyde formation at the lower potassium promoted sample E* in FT 2.2. The aldehyde content showed a more significant drop upon the increase in temperature than sample D*. Increasing to 280 °C dropped the aldehyde content by 16 C% points vs 12 C% points during FT 2.1. Upon a further increase in temperature, the aldehyde content surprisingly increased to about 13 C% at 350 °C, where FT 2.1 showed a decrease in aldehyde content with an increase in temperature. A subsequent return to 280 °C caused the aldehyde content to drop to 10 C%, which is higher than its original value at the same conditions. The carboxylic acids reached a maximum of 5 C% at condition F and the ketones had a maximum of 6 C% at the same condition. The sudden change in selectivity after returning to 280 °C is possibly again a restructuring effect

of the catalyst's surface at 350 °C, which could have had an influence on the surface of the catalyst.

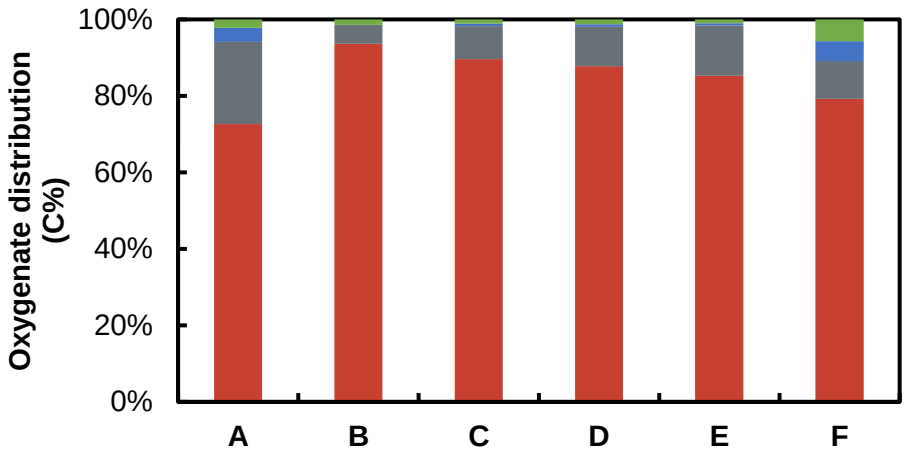

Figure 5-54: Oxygenate distribution of FT run 2.2 with the product classes alcohols (red), aldehydes (grey), carboxylic acids (blue) and ketones (green) as a function of temperature: A) 260 °C, B) 280 °C, C) 300 °C, D) 320 °C, E) 350 °C and F) 280 °C. Process conditions: P = 45 bar, H_2 to CO ratio = 1 and GHSV = 8 L/h/g_{cat}.

Within the alcohol fraction, the increase in temperature did not have as clear an effect as it had on the 6.3 wt.% K/Mo promoted sample (FT 2.1). The decrease in potassium promotion showed a significant decrease in methanol content (30 C% at FT 2.2 vs 47 C% at FT 2.1), compared to condition A. An increase in temperature decreased the methanol content by only 6 C% points to 24 C% at 350 °C, which is a small change compared to FT 2.1 where the methanol content dropped by 26 C% points from 260 °C to 350 °C. A subsequent decrease in temperature to 280 °C was followed by an increase in selectivity towards methanol to 31 C%, similar to the values observed during FT 2.1 at the same conditions.

The decrease in methanol was followed by an increase in ethanol from 47 C% to 53 C% at conditions A and E, respectively. Where the initial value of ethanol (condition A) is much higher than in FT 2.1 (39 C%), the ethanol content at condition E is similar to that of FT 2.1 at the same conditions. A subsequent decrease in temperature to 280 °C decreased the ethanol selectivity to 40 C% (38-42 C% at the same conditions in FT 2.1). In line with the lower methanol and higher ethanol content, propanol selectivity was higher overall than during FT 2.1. The change in temperature did not influence the formation towards propanol significantly and remained between 14-16 C%. C_{4+} alcohols fluctuated between 7 C% (condition E) and 15 C% (condition F). Besides condition B (13 C% vs 7 C%) and C (8 C% vs 11 C%), the other values are similar to that of FT 2.1.

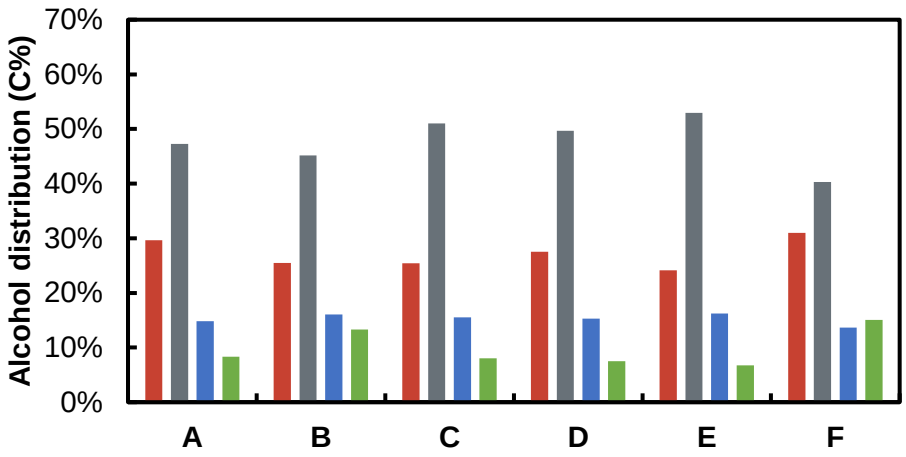

Figure 5-55: Alcohol distribution of FT run 2.2 with methanol (red), ethanol (grey), propanol (blue) and C_{4+} alcohols (green) as a function of temperature: A) 260 °C, B) 280 °C, C) 300 °C, D) 320 °C, E) 350 °C and F) 280 °C. Process conditions: P = 45 bar, H_2 to CO ratio = 1 and GHSV = 8 L/h/g_{cat}.

5.2.9 FT run 2.3: F - 1.8 wt.% K/Mo promoted β-Mo_2C*

The third potassium promoted sample was prepared using the same method as in FT run 2.1, but with 1.8 wt.% K (after FT) representing the lowest degree of promotion. Catalyst testing was started by exposing the catalyst to the same reaction conditions as in FT run 2.1 and FT run 2.2, i.e. T = 260 °C, P = 45 bar, H_2 to CO ratio of 1 and GHSV of 8 L/h/g_{cat}. As would be expected for a decreased amount of promotion, the catalyst displays a slightly higher activity regarding CO conversion. Interestingly, and like sample E* - 5.4 wt.% K/Mo, the conversion level increases rapidly upon an increase in reaction temperature followed by a steady decrease. While the initial jump is not as evident as in the case of the previous catalyst, the behavior is observed already at 280 °C. The slight increase in activity is paralleled by a decrease in CO_2 and an increase in CH_4 selectivity. As the catalyst showed signs of deactivation (the slow drop in CO conversion, Figure 5-56), the temperature was dropped to 280 °C resulting in a CO conversion of 1%, where initially (condition B) the conversion was 7%.

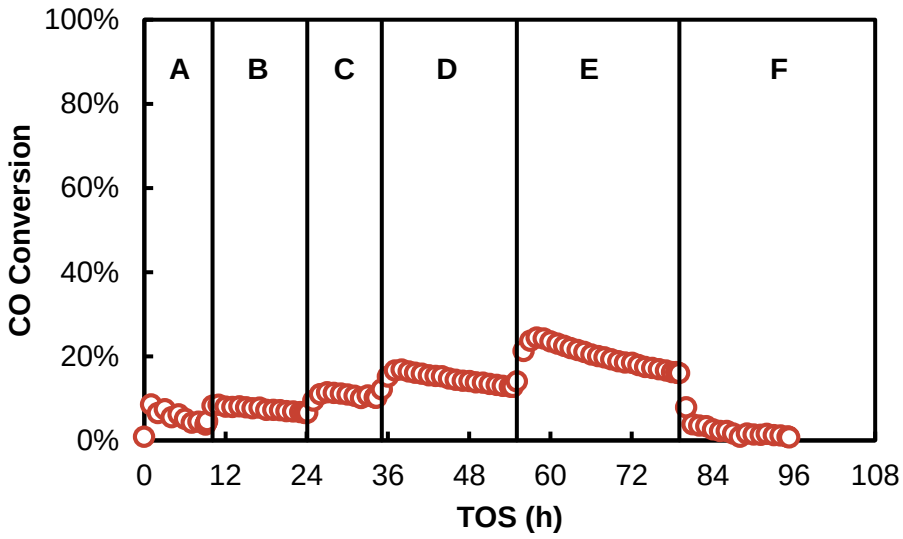

Figure 5-56: CO conversion from FT 2.3 obtained with TOS, varying conditions as indicated: A) 260 °C, B) 280 °C, C) 300 °C, D) 320 °C, E) 350 °C and F) 280 °C. Process conditions: P = 45 bar, H_2 to CO ratio = 1 and GHSV = 8 L/h/g_{cat}.

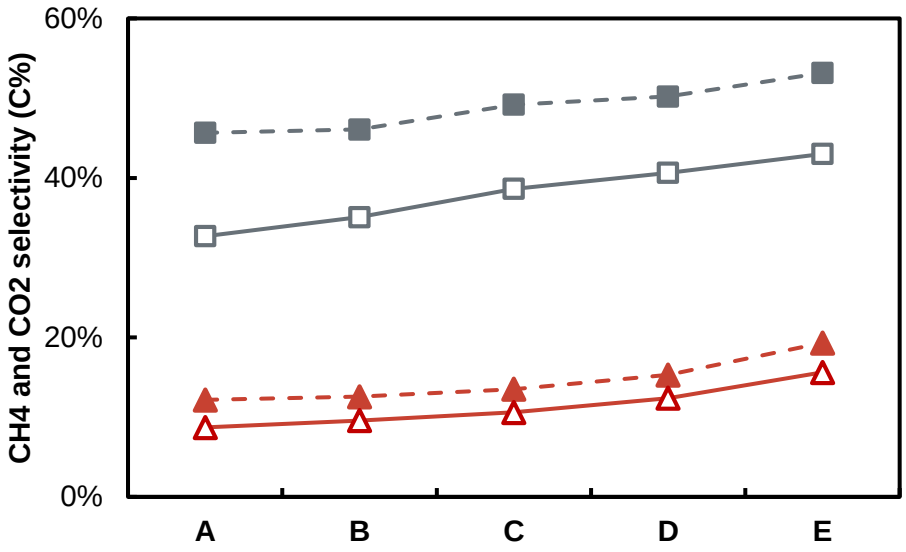

Figure 5-57: CH_4 (red triangles) and CO_2 (grey squares) selectivity, presenting original data (open symbols, solid lines) and carbon balance corrected (solid symbols, dashed line) from FT 2.3 obtained with TOS, varying conditions as indicated: A) 260 °C, B) 280 °C, C) 300 °C, D) 320 °C, E) 350 °C and F) 280 °C. Process conditions: P = 45 bar, H_2 to CO ratio = 1 and GHSV = 8 L/h/g_{cat}.

The oxygenate selectivity is surprisingly high for a lower potassium concentration in the catalyst with about 40 C% of the organic product. A maximum of 44 C% was obtained at 300 °C. A further increase in reaction temperature was detrimental. It must be noted though that the methanol content in the oxygenate fraction is the highest of all the promoted samples while still being approximately 50 C% lower than in the case of the unpromoted sample. No information about

condition F regarding organic product analysis is available due to the very low CO conversion. Increase in temperature from condition A-E was found to suppress the formation of methanol in comparison to the total oxygenates, with a methanol to total oxygenate ratio of 0.28, 0.32, 0.27, 0.25 and 0.20, respectively. An interesting trend was observed for the linear olefin to linear paraffin ratio with an increase in temperature. The olefin content started with a ratio of 2.67 at condition A followed by an increase to 2.88 at condition B. Thereafter, the O/P ratio was observed at 3.02, 2.70 and 2.45 for conditions C, D and E (see Appendix H, Figure 9-6).

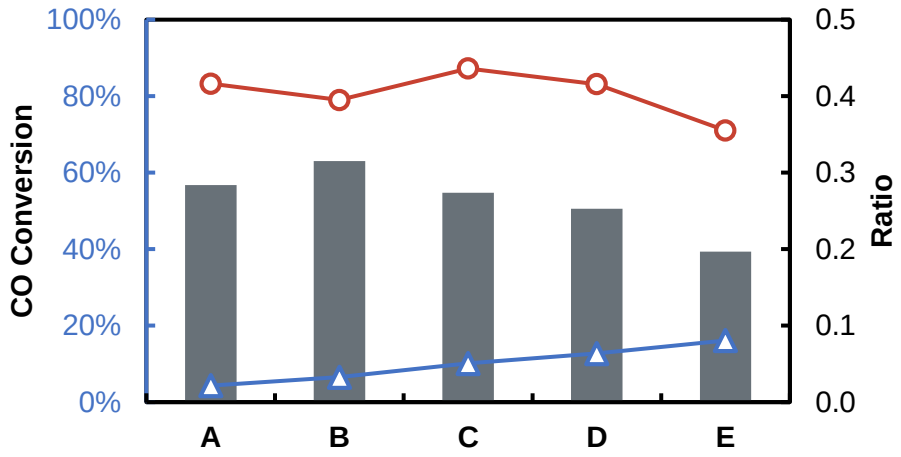

Figure 5-58: Organic product analysis obtained from FT 2.3 varying conditions indicated by: A) 260 °C, B) 280 °C, C) 300 °C, D) 320 °C and E) 350 °C. Process conditions: P = 45 bar, H_2 to CO ratio = 1 and GHSV = 8 L/h/g_{cat}. With oxygenate to hydrocarbon ratio (red circles), MeOH to total oxygenate ratio (grey bars), CO conversion (blue triangles).

The chain growth probabilities (Figure 5-59), towards linear paraffins, olefins and oxygenates are hardly distinguishable from previous runs in the presence of potassium.

A further drop in potassium promotion to 1.8 wt.% K/Mo showed a significantly higher alcohol content at the starting conditions of 86 C% vs 59 and 73 C% at FT 2.1 and 2.2, respectively. It can be suggested that the amount of potassium on the sample significantly influences the type of oxygenates formed. Thereafter, with an increase in temperature, the alcohol selectivity shows a similar trend to FT 2.2. The second biggest group of oxygenates are again the aldehydes, but at lower levels compared to FT 2.1 and 2.2, with a maximum of 13 C% (condition A). The decrease in potassium was shown to have a substantial influence on the formation of acids and ketones. Only small traces of carboxylic acids and ketones were observed, all below 1 C% (Figure 5-60).

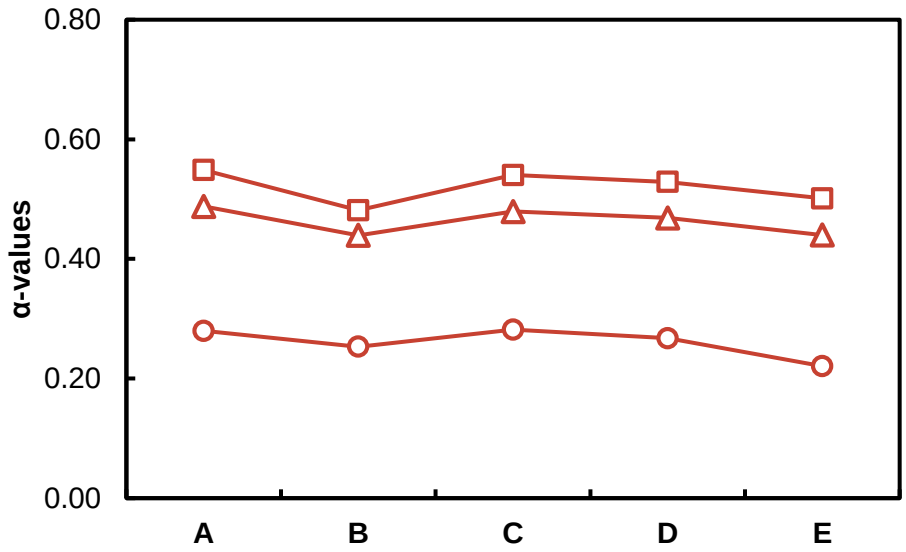

Figure 5-59: Chain growth probability calculated for the linear products from FT 2.3 of the product classes C_3-C_8 paraffins (squares), C_3-C_8* olefins (triangles) and C_2-C_6* alcohols (circles) varying conditions indicated by: A) 260 °C, B) 280 °C, C) 300 °C, D) 320 °C and E) 350 °C. Process conditions: P = 45 bar, H_2 to CO ratio = 1 and GHSV = 8 L/h/g_{cat} (* = if possible).*

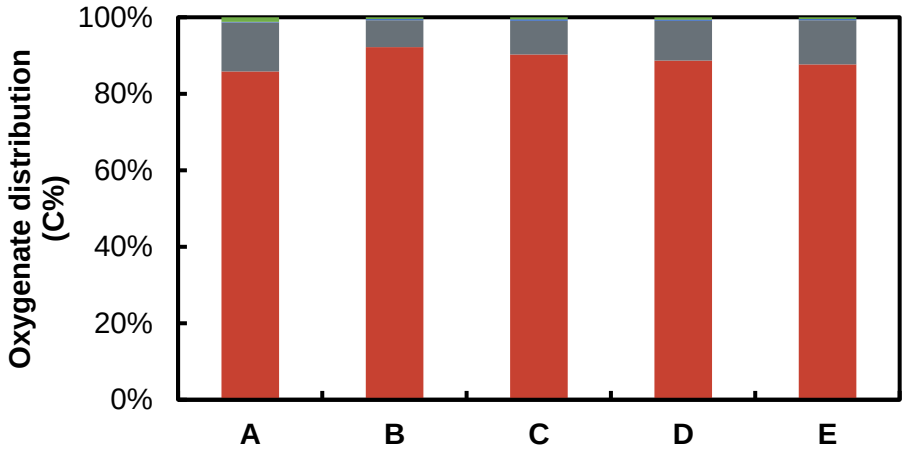

Figure 5-60: Oxygenate distribution of FT run 2.3 with the product classes alcohols (red), aldehydes (grey), carboxylic acids (blue) and ketones (green) as a function of temperature: A) 260 °C, B) 280 °C, C) 300 °C, D) 320 °C and E) 350 °C. Process conditions: P = 45 bar, H_2 to CO ratio = 1 and GHSV = 8 L/h/g_{cat}.

In line with the higher potassium promoted samples in FT 2.1 and 2.2, the methanol content decreases with an increase in temperature from 33 C% at 260 °C to 23 C% at 350 °C. The methanol selectivity at the starting condition is similar to that of FT 2.2, however very different to the 6.2 wt.% K/Mo promoted sample (47 C%). The ethanol selectivity was also very similar to that of FT 2.2 with an increase in ethanol selectivity from 48 C% at 260 °C to 53 C% at 350 °C with the latter being very comparable to the 55 C% of FT 2.1 under the same process conditions. The selectivity towards propanol and C_{4+} alcohols is very comparable to both FT 2.1 and FT 2.2. A

slight increase towards the formation of propanol was observed from 13 C% at 260 °C to 18 C% at 350 °C. The C_{4+} content decreased from 7 C% at 260 °C to 5 C% at 350 °C (Figure 5-61).

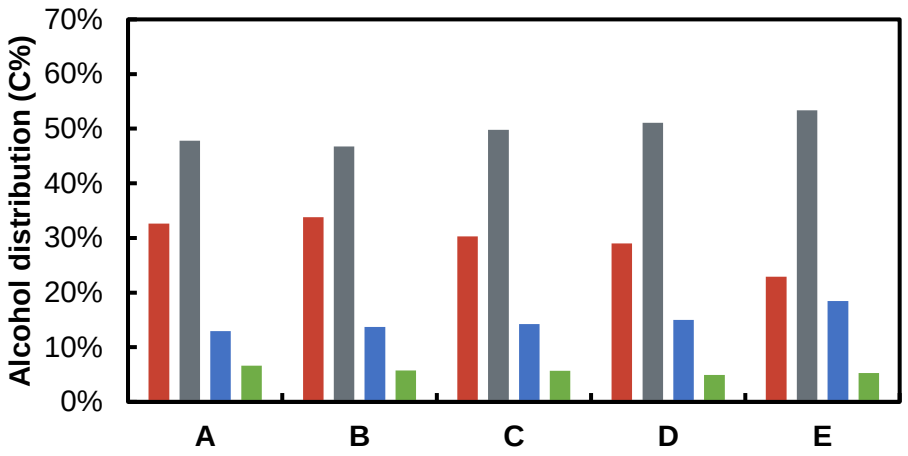

Figure 5-61: Alcohol distribution of FT run 2.3 with methanol (red), ethanol (grey), propanol (blue) and C_{4+} alcohols (green) as a function of temperature: A) 260 °C, B) 280 °C, C) 300 °C, D) 320 °C and E) 350 °C. Process conditions: P = 45 bar, H_2 to CO ratio = 1 and GHSV = 8 L/h/g_{cat}.

5.2.10 FT run 3.1: G - 3.9 wt.% K/Mo β-Mo_2C, high pressure sweep*

The conversion levels of all performed experiments on the potassium promoted samples described above are rather low (<20%) and it is of interest to find a way to increase these with measures beyond the reaction temperature. In the literature [18, 20, 21, 161] the reaction pressure applied is commonly above 45 bar, sometimes even reaching 100 bar, having a positive impact on total oxygenate selectivity. Therefore, the testing unit used for the present study was adjusted to perform experiments at pressures of up to 65 bar. To observe the effect of time on stream on the product selectivity, samples for offline GC-FID were taken at 3, 10 and 24 hours TOS at each pressure setting. At exactly 24 hours the pressure was increased in steps of 10 bar.

Observing the results from the GC-TCD, the CO conversion does not change much with the increase in pressure (Figure 5-62). The steady state CO conversions (after 24 hours on stream for each condition) were 8%, 8%, 9% and 6% at pressures of 45, 55, 65 and 45 bar, respectively. Simultaneously with the CO conversion, the CH_4 selectivity was relatively stable as well (Figure 5-63). CO_2 selectivity decreases slightly from 49 C% to 47 C%, 44 C% and 42 C%. After reverting to 45 bar, the CO conversion is slightly lower (Figure 5-62).

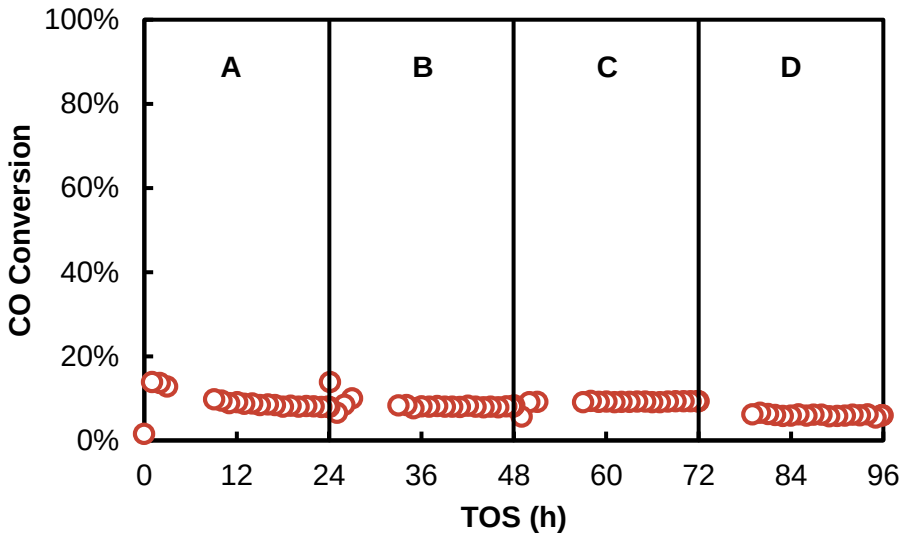

Figure 5-62: CO conversion from FT 3.1 obtained with TOS, varying conditions as indicated: A) 45 bar, B) 55 bar, C) 65 bar and D) 45 bar. Process conditions: T = 300 °C, H_2 to CO ratio = 1 and GHSV = 8 L/h/g_{cat}.

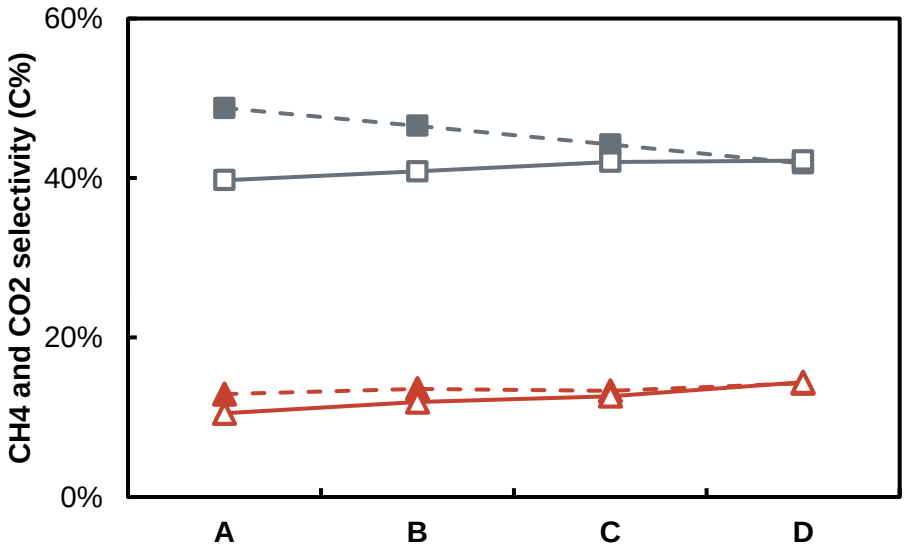

Figure 5-63: CH_4 (red triangles) and CO_2 (grey squares) selectivity, presenting original data (open symbols, solid lines) and carbon balance corrected (solid symbols, dashed line) from FT 3.1 obtained with TOS, varying conditions as indicated: A) 45 bar, B) 55 bar, C) 65 bar and D) 45 bar. Process conditions: T = 300 °C, H_2 to CO ratio = 1 and GHSV = 8 L/h/g_{cat}.

With time on stream at the different pressures several interesting observations can be made (Figure 5-64). While the conversion is hardly affected, the olefin to paraffin ratio decreases (see Appendix H, Figure 9-7), the oxygenate content increases and within the oxygenates the fraction of methanol also grows with the increase in reaction pressure. Only the oxygenate content displays a sharp dip at 3 hours TOS at each new pressure setting (conditions A1, B1 and C1).

This dip is followed by a gradual increase resulting in a steady increase of the oxygenate content with reaction pressure when comparing the performance data after 24 hours TOS at each condition (conditions A3, B3 and C3). It is proposed that the initial drop is an effect of the operation. To increase pressure the backpressure regulator of the test unit is closed further. This results in a stagnant atmosphere of reactive gases within the reactor until the new pressure set-point is reached. These stagnant conditions potentially result in high conversion conditions, might also initially reduce the observed oxygenate concentration. The steadily decreasing olefin to paraffin ratio (see Appendix H, Figure 9-7) with increasing reactor pressure might be an effect of the resulting increased hydrogen partial pressure which overcomes the previously reported suppression of secondary (hydrogenation-)reactions by the promoter.

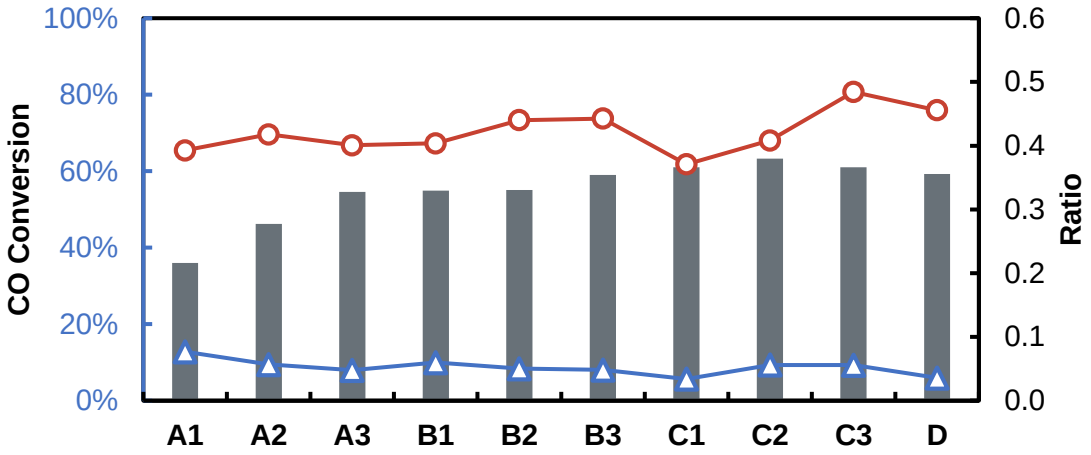

Figure 5-64: Organic product analysis obtained from FT 3.1 varying conditions indicated by: A) 45 bar, B) 55 bar, C) 65 bar and D) 45 bar. Process conditions: T = 300 °C, H_2 to CO ratio = 1 and GHSV = 8 L/h/g_{cat}. With oxygenate to total organic product ratio (red circles), MeOH to total oxygenate ratio (grey bars) and CO conversion (blue triangles).

No significant effect was observed regarding the chain growth probability remaining mostly stable at levels previously observed and discussed (see chapter 5.2.7).

Literature reports that an increase in pressure moves the position of the equilibrium to the side of the reaction with the least number of molecules [22]. Therefore, the formation of the overall products increases at higher pressures. However, the formation of oxygenates increases to a higher degree than that of the hydrocarbons due to the incorporation of O and the therefore lowered amount of product water, increasing the total oxygenate selectivity. From the data in Figure 5-66 it is observed that the formation of methanol is mostly influenced (from 33 C% to 36 C% of total oxygenates), which is in line with the observations in the literature over a methanol synthesis catalyst [110]. As CO conversion is relatively stable, a change in selectivity is therefore related to the change in conditions. Interestingly, the methanol was most influenced, by an increase, followed by ethanol (decrease) and then the rest of the higher alcohols (Figure 5-66). According to these results, a high pressure is favourable when higher oxygenate selectivity is

required, however, the methanol content does rise simultaneously. Interestingly, the increase in oxygenates is in line with the decrease in olefin content. Although both species are prone to secondary reactions.

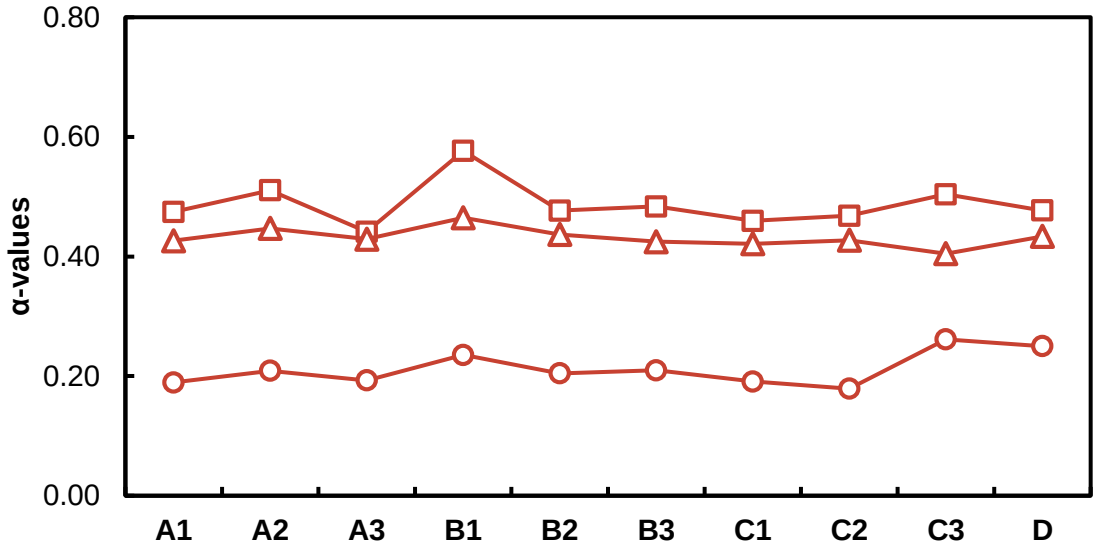

Figure 5-65: Chain growth probability in FT 3.1 calculated for the linear products of the product classes paraffins (squares), olefins (triangles) and alcohols (circles) varying conditions indicated by: A) 45 bar, B) 55 bar, C) 65 bar and D) 45 bar. Process conditions: T = 300 °C, H_2 to CO ratio = 1 and GHSV = 8 L/h/g_{cat}.

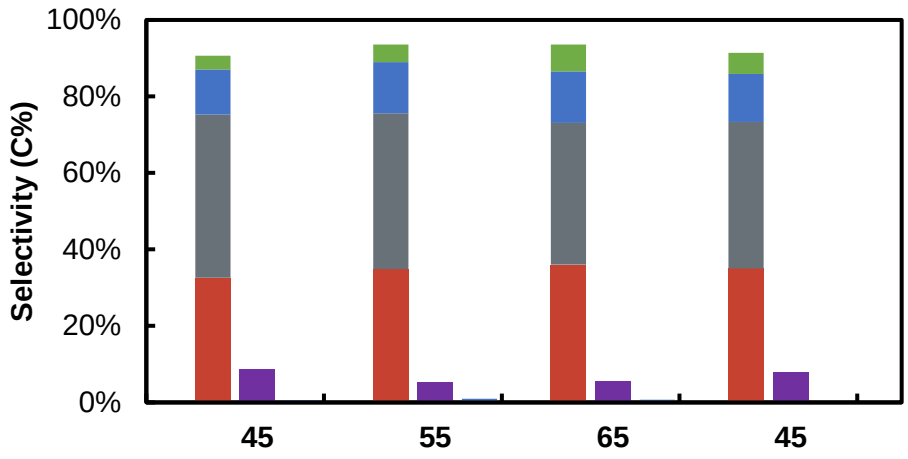

Figure 5-66: Oxygenate selectivity and linear alcohol distribution as a function of pressure, based on the 24 hours' TOS measurements in FT 3.1. With: methanol (red), ethanol (grey), propanol (blue) and C_{4+} alcohol (green). Other oxygenates are aldehydes (purple) and the other two groups ketones and carboxylic acids (too small to show).

5.3 Consolidation of catalytic performance of β-Mo_2C

Temperature has been shown to have a major influence on the CO conversion, an increase in temperature is followed by increase in CO conversion, therefore, principally all graphs presented below, as a function of the CO conversion, can be changed into a function of temperature or vice versa and would display similar trends.

5.3.1 Effect of potassium promotion on oxygenate formation over β-Mo_2C

The effect of potassium on the catalyst has been shown to be significant in various ways. One of the observations, which is in line with reports in the literature [20, 21], is that the CO conversion decreases upon promotion, however the amount of potassium, within the here studied boundaries, does not seem to influence the extent to which the catalytic activity decreases (Figure 5-68). The unpromoted sample shows a CO conversion up to 34% at 300 °C, while the three promoted samples all have shown a CO conversion at ≤10%, at the same reaction temperature. Paralleled by the decrease in CO conversion, the selectivity to methane decreased and to CO_2 increased, with the latter to a lesser degree for the promoted samples (Figure 5-67).

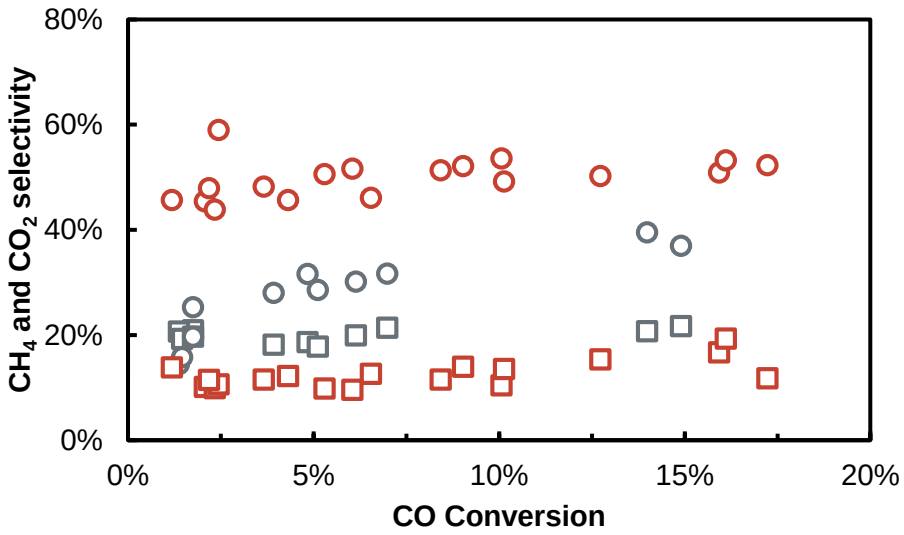

Figure 5-67: Carbon balance corrected CH_4 (squares) and CO_2 (circles) selectivities as a function of the CO conversion for the promoted samples (red) (FT 2.1-2.3) and the unpromoted sample (grey) (FT 2.0).

If both these undesired C_1 product species are excluded from the amount of converted CO, the conversions of the promoted samples at 300 °C are very similar to the conversion of the unpromoted sample at 280 °C (±6%) (Figure 5-68). The difference in oxygenate selectivity between these two points is significant (10 C% vs ±36 C%). A slight deactivation of the potassium promoted samples is observed during the testing routine. This seems to be enhanced by lower potassium content but is nearly absent in the unpromoted catalyst. This could indicate that the promoter undergoes some formation process under reaction conditions which is more prominent at low concentrations in the timeframes tested.

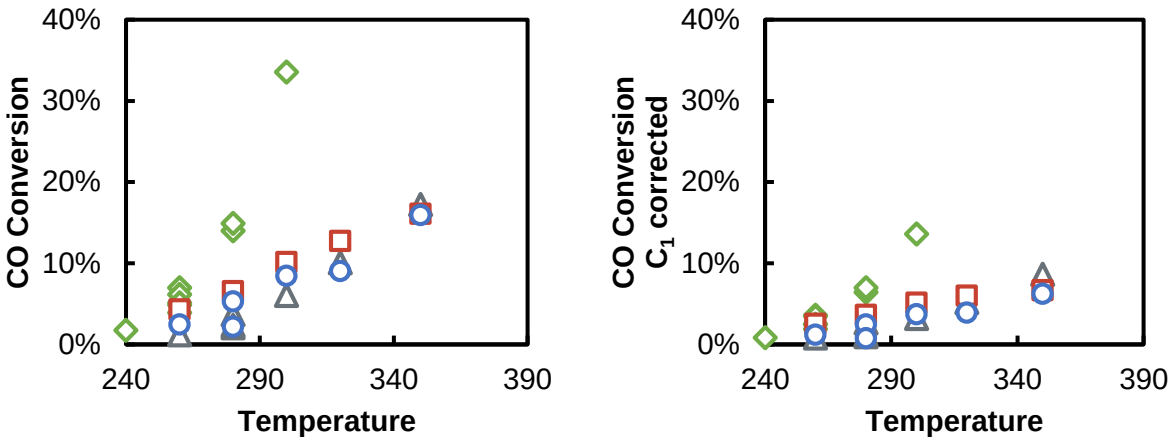

Figure 5-68: Effect of potassium promotion and temperature on the original (figure on the left) and the C_1-corrected (figure on the right) CO conversion over β-Mo_2C. The following samples are shown: FT 2.3 - 1.8 wt.% K/Mo (red squares), FT 2.1 - 6.2 wt.% K/Mo (grey triangles), FT 2.2 - 5.4 wt.% K/Mo (blue circles), FT 2.0 - unpromoted sample (green diamonds). Process conditions are specified in Table 4-1.

Besides the effect on the activity of the catalyst (WGS and chain growth), potassium promotion has also been shown to have a significant effect on the product selectivity. Where the unpromoted sample does not show a linear olefin to linear paraffin (exemplary for C_3) ratio of higher than 1.26 at very low conversions (±1%), the promoted samples lowest observed linear olefin to linear paraffin ratio is 2.43 at a similar CO conversion. The higher the CO conversion, the lower the linear olefin to linear paraffin ratio for all the unpromoted samples (Figure 5-69). However, this trend does not hold for the promoted samples. The hypothesized suppression of secondary hydrogenation reactions commonly described as the mechanism of potassium yielding higher olefin content [160] does not seem to be influenced by conversion levels nor reaction temperature.

The chain growth probability is a good parameter to explain the likelihood of forming longer chained products. An ASF-distribution can be defined for each group of products per sample, and from these plots a certain α-value can be calculated, indicating the chain growth probability. The α-values calculated for the **linear olefins** are above 0.4 for the promoted samples, and for the unpromoted samples below 0.4. Interestingly, the chain growth probability remains constant over all levels of CO conversion. The effect of potassium promotion on the chain growth probability of **linear paraffins** is less significant, however it also showed a small increase in the chain growth probability. The different levels of CO conversion seem to have more influence as well. A slight trend is visible with an increase in α-values with a decreasing CO conversion (Figure 5-71).

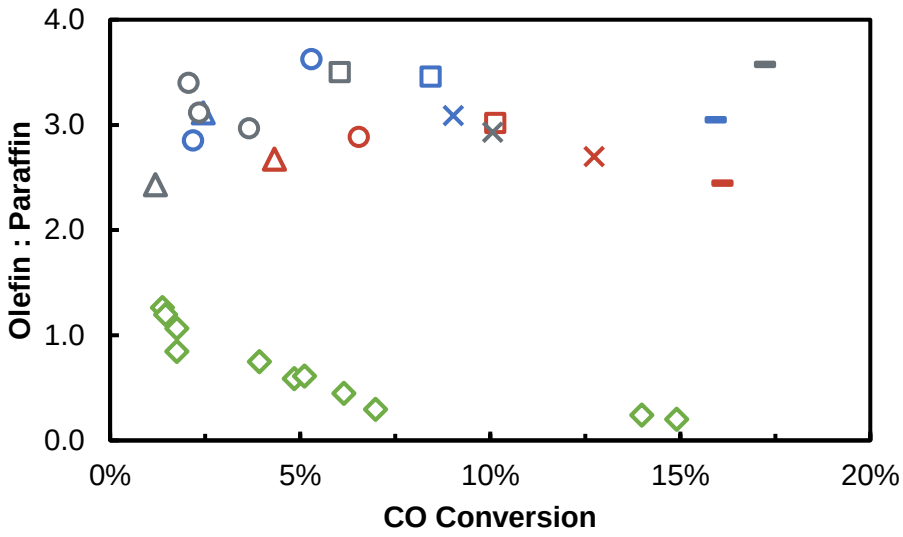

Figure 5-69: C_3-linear olefin to C_3-linear paraffin ratio of the following samples are shown: FT 2.3 - 1.8 wt.% K/Mo (red), FT 2.1 - 6.2 wt.% K/Mo (grey), FT 2.2 - 5.4 wt.% K/Mo (blue), at varying temperatures of 260 °C (triangles), 280 °C (circles), 300 °C (squares), 320 °C (crosses) and 350 °C (dashes), FT 2.0 - unpromoted sample (green diamonds).

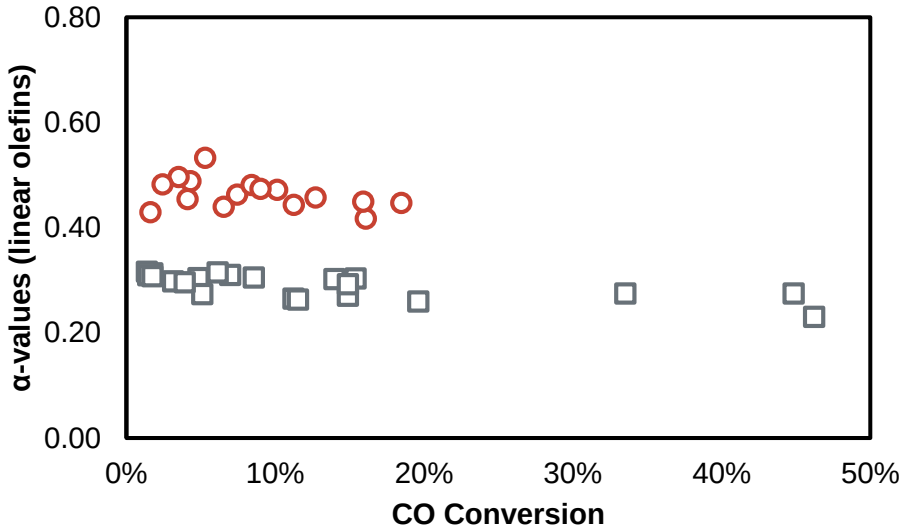

*Figure 5-70: Chain growth probability as a function of CO conversion towards **linear olefins** for promoted (red circles) and unpromoted (grey squares) samples.*

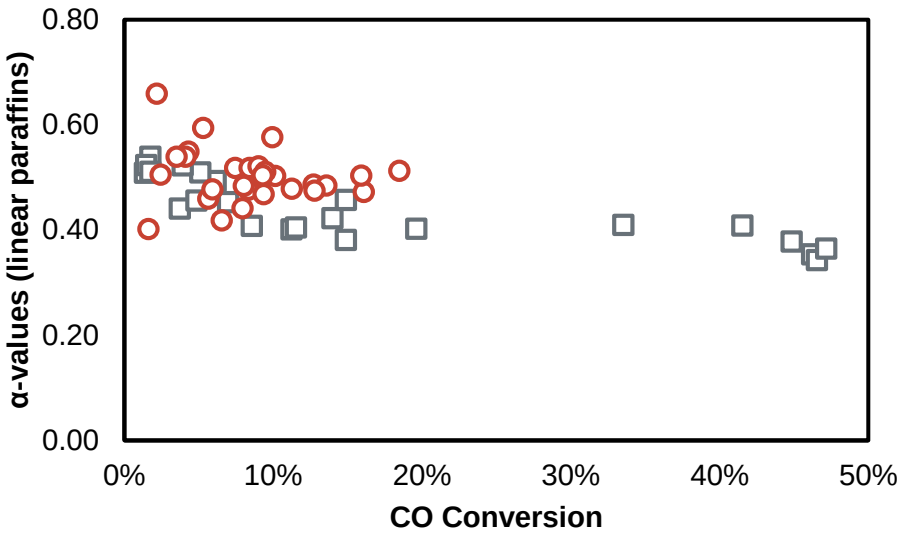

*Figure 5-71: Chain growth probability as a function of CO conversion towards **linear paraffins** for promoted (red circles) and unpromoted (grey squares) samples.*

The focus of the present study is the formation of oxygenates which was reported to be enhanced by potassium promotion [18-21, 102]. The unpromoted samples showed an increase in oxygenate selectivity upon a decrease in CO conversion, with a maximum content of oxygenates (CO_2-free) of around 35 C% at a CO conversion of approximately 1%. Over the promoted samples more oxygenates are formed, mostly above a 30 C% content, even at higher conversions of 16% which equates to reaction temperatures of up to 350 °C (Figure 5-72).

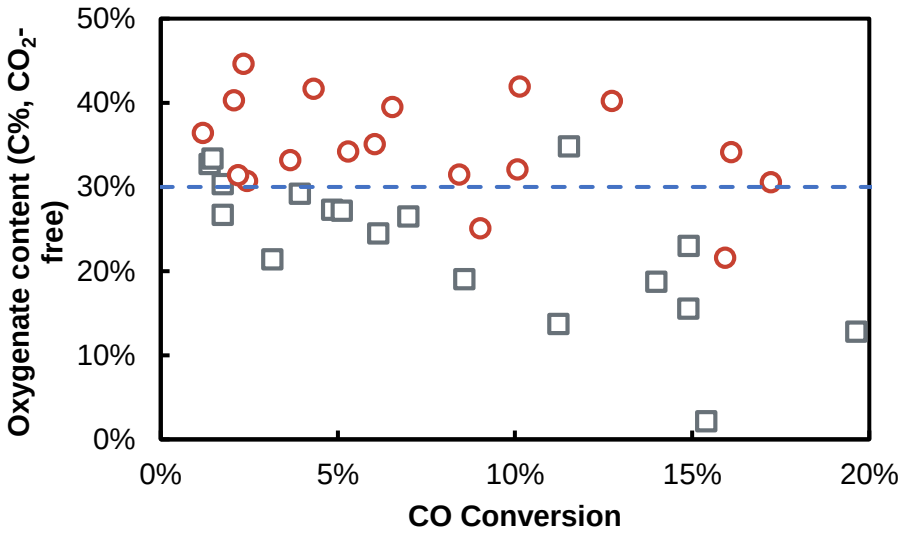

Figure 5-72: Oxygenate to total organic product ratios of the performed FT reactions with 1.8 wt.%, 6.2 wt.% and 5.4 wt.% K/Mo promoted samples combined from FT run 2.1 to 2.3 (red circles) compared to the unpromoted samples (grey squares) combined from FT run 1.1 to FT run 2.0.

Within the oxygenate fraction (Figure 5-73) all four main functionalities are detected: alcohols, aldehydes, carboxylic acids and ketones. The product is dominated by alcohols, for the unpromoted samples (≥94 C%) and the promoted samples (≥59 C%). While in the absence of potassium this fraction remains constant with increasing conversion, the promoted samples produce a significant number of aldehydes (up to 37 C% at 2% CO conversion), specifically at lower CO conversions. Small traces of ketones and carboxylic acids are formed, together ±10 C% at low CO conversions <5%. With increasing conversion, the content of aldehydes, ketones and carboxylic acids decreases and thus the remaining oxygenated product is dominated by alcohols.

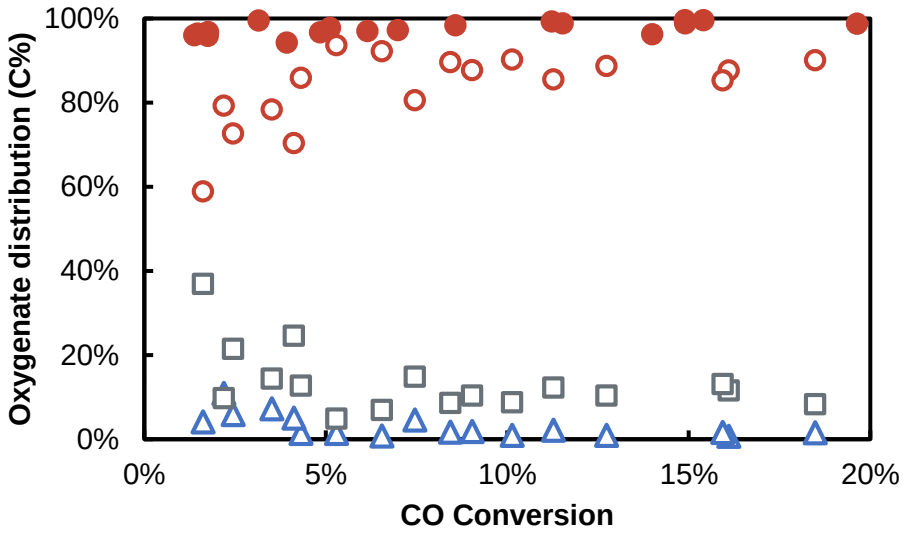

Figure 5-73: Distribution of the different product classes within the oxygenated compounds, comparison between promoted (open symbols) and unpromoted (solid symbols) samples, with alcohols (red circles), aldehydes (grey squares) and other oxygenated products such as ketones and carboxylic acids (blue triangles).

Within the oxygenate fraction, the unpromoted samples have been shown to form mainly methanol, up to a methanol to total oxygenate ratio of 0.92 at 85% CO conversion and a lowest ratio of 0.49 at 2% CO conversion. The promoted samples don't show a higher ratio than 0.32 which indicates that higher alcohols are more likely to be formed upon promotion with potassium (Figure 5-74). The chain growth probability of **linear alcohols** therefore expectedly also increases upon addition of potassium. However, the chain growth probability is still rather low, with a maximum observed chain growth probability around 0.4. This indicates that, even though it was observed that the methanol formation significantly decreases, the main alcohol products have chain lengths with carbon numbers between C_2-C_4.

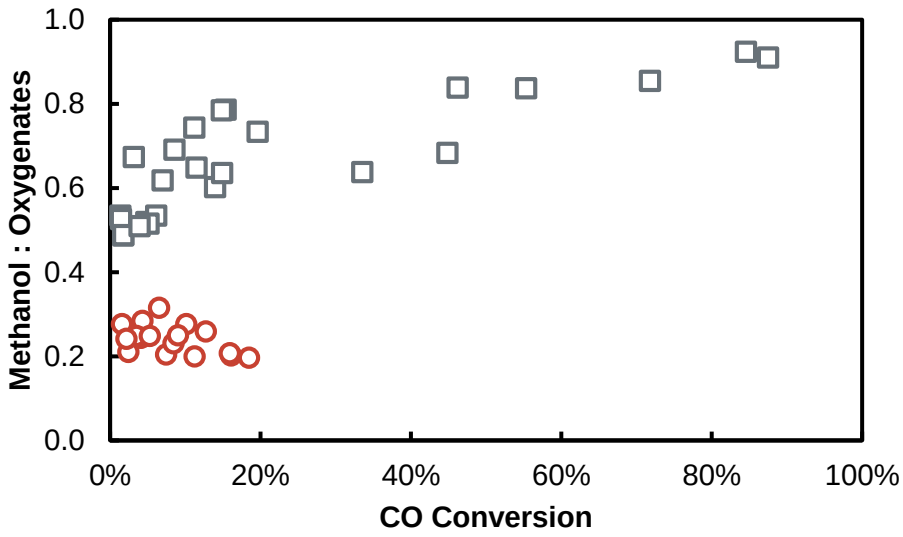

Figure 5-74: Methanol to oxygenate ratio of the promoted samples (red circles) and the unpromoted samples (grey squares).

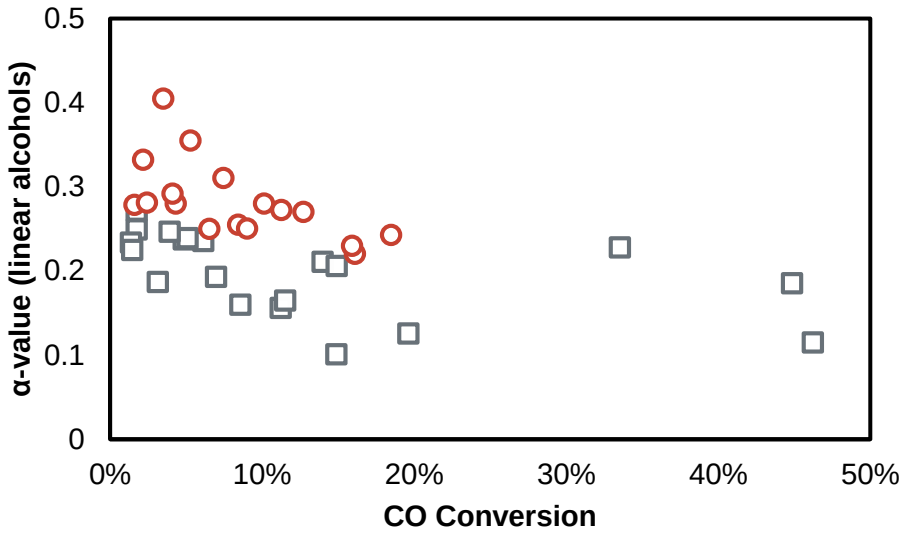

*Figure 5-75: Chain growth probability as a function of CO conversion towards **linear alcohols** for promoted (red circles) and unpromoted (grey squares) samples.*

A detailed product analysis confirms this. The promoted samples produced predominantly ethanol (up to 54 C%). It is observed that with an increase in CO conversion, the methanol content decreases, where ethanol and propanol increases. At the higher conversions, the selectivity towards methanol and propanol are almost equal. However, due to the domination of ethanol, the chain growth probability remains relatively low.

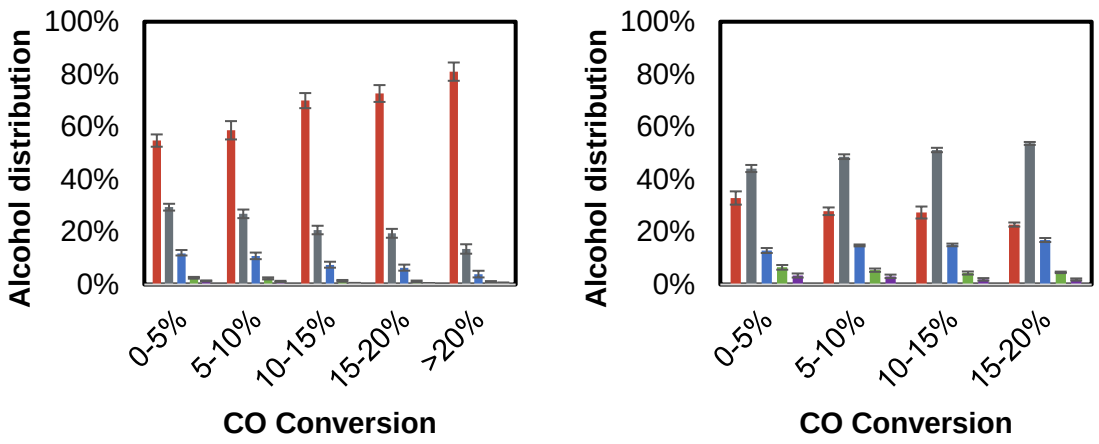

Figure 5-76: Alcohol distribution over the unpromoted samples (figure on the left) and the promoted samples (figure on the right) as a function of the CO conversion, with from left to right per series methanol (red, #1), ethanol (grey, #2), propanol (blue, #3), C_4 alcohols (green, #4) and C_{5+} alcohols (purple, #5).

5.3.2 ***Effect of temperature on oxygenate formation using β-Mo_2C***

Plotting the content per carbon number of linear alcohols as a function of reaction temperature (Figure 5-77) it can be observed that with an increase in temperature the methanol concentration decreases, ethanol increases, propanol increases and C_{4+}-alcohols show a slight decrease. Only data from the promoted samples are displayed. Based on these results, the theoretical equilibrium equations (in section 2.2.3.2) can only assist in the explanation for the formation of the short chain alcohols (C1-C3), as the higher alcohols differ from the theoretical calculations. Formation of the longer chained products is far more complicated and cannot be explained by only using the Gibbs free energy of formation.

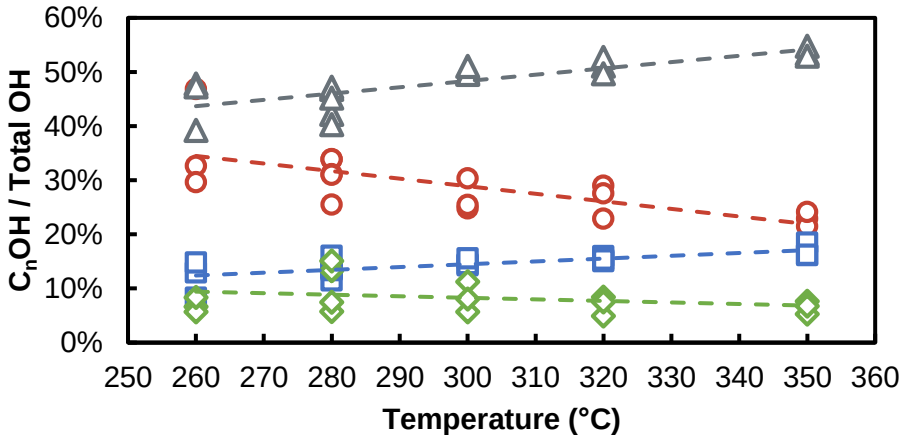

Figure 5-77: Alcohol distribution as a function of temperature during the K/Mo promoted samples, with methanol (red), ethanol (grey), propanol (blue) and C_{4+} alcohols (green).

5.4 Ammonia co-feeding during FTS

5.4.1 FT run 4.1: 4.7 vol.% NH_3 co-feeding

Based on the previous performance results (FT runs 2.0 to 3.1, see sections 5.2.6, 5.2.7, 5.2.8, 5.2.9 and 5.2.10) catalyst D* - 3.9 wt.% K/Mo was chosen to study the effect of ammonia co-feeding on the catalyst's stability and product spectrum. To obtain a reasonable conversion the reaction temperature was set at 300 °C at a pressure of 45 bar and a space velocity of 8 L/h/g_{cat}. Ammonia was co-fed in the form of a 10 vol.% NH_3 in H_2 mixture providing a constant H_2 and CO partial pressure and partially replacing the inert N_2 with ammonia (Table 5-3). This results in a concentration of ammonia in the total feed gas (CO, H_2, N_2 and NH_3) of 4.7 vol.%. As it is expected that the switch of feed gas composition will not result in an ideal step change due to back mixing and dead volumes in the testing set-up, an additional controlled flow of Ar was introduced into the reactor outlet gas after the pressure drop allowing to directly calculate conversions and selectivities via the online GC-TCD.

Table 5-3: Gas composition FT run 4.1 with and without co-feeding ammonia.

	Gas	*Vol.%*	*P_i (bar)*
Normal FT	H_2	43%	19.3
	CO	43%	19.3
	N_2	14%	6.4
NH_3 co-feeding	10% NH_3/H_2	47%	19.1 (H_2) / 2.1 (NH_3)
	CO	43%	19.3
	N_2	10%	4.5

Under standard FT conditions, i.e. in the absence of ammonia, a CO conversion of 17% was recorded (Figure 5-78). This is higher than for a similar catalyst at the same conditions, but after previous exposure to lower reaction temperatures (see FT run 2.1, section 5.2.7), but very comparable to the same catalyst directly exposed to 300 °C in FT run 3.1 (see section 5.2.10). CH_4 and CO_2 selectivity are also similar to this previous run with 12 C% and 50 C%, respectively. Upon co-feeding of ammonia, a step decrease in the CO conversion was observed (Figure 5-78) to about 13% while the CH_4 selectivity increased to 14 C% and CO_2 decreased (Figure 5-79) to 34 C% (after 45 min TOS) (Figure 5-80). The sudden sharp decrease could be a result of the reaction of unconverted ammonia with CO_2 to form ammonium carbonate in the exit lines of the testing unit. Although all lines are heated and ammonium carbonate has a melting temperature of only 58 °C and is reported to fully decompose at 120 °C [162], a line blockage has previously been observed in related reactions and was associated with the formation of the carbonate [8, 14]. After one hour on stream, the pressure of the reactor increased sharply and the reaction had to be terminated.

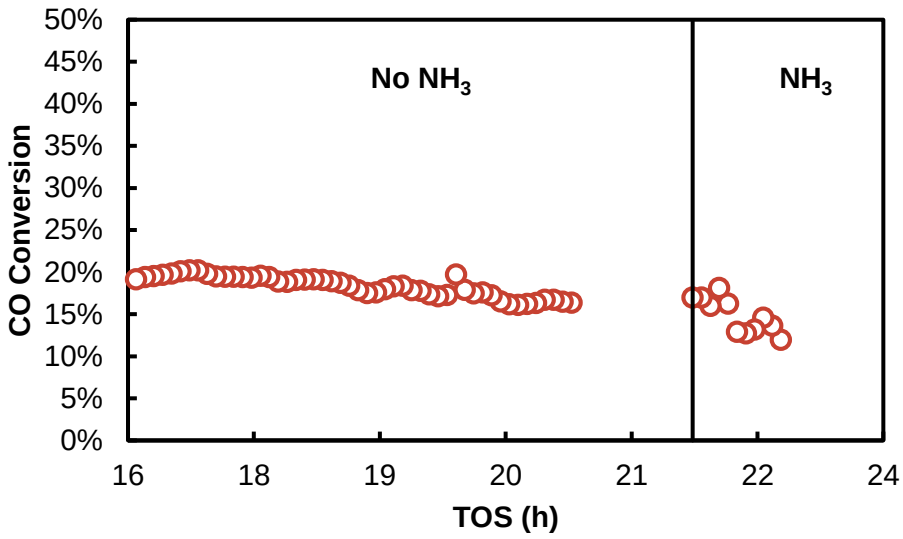

Figure 5-78: CO conversion from FT 4.1 obtained with TOS in the absence and presence of NH_3. Process conditions: T = 300 °C, P = 45 bar, H_2 to CO ratio = 1 and GHSV = 8 L/h/g_{cat}.

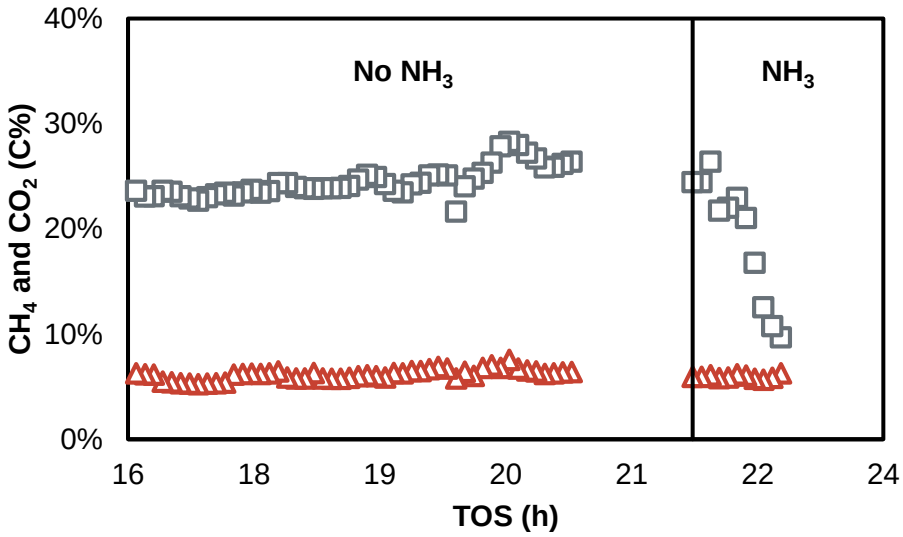

Figure 5-79: CH_4 (red triangles) and CO_2 (grey squares) selectivity from FT 4.1 in the absence and presence of ammonia. Process conditions: T = 300 °C, P = 45 bar, H_2 to CO ratio = 1 and GHSV = 8 L/h/g_{cat}.

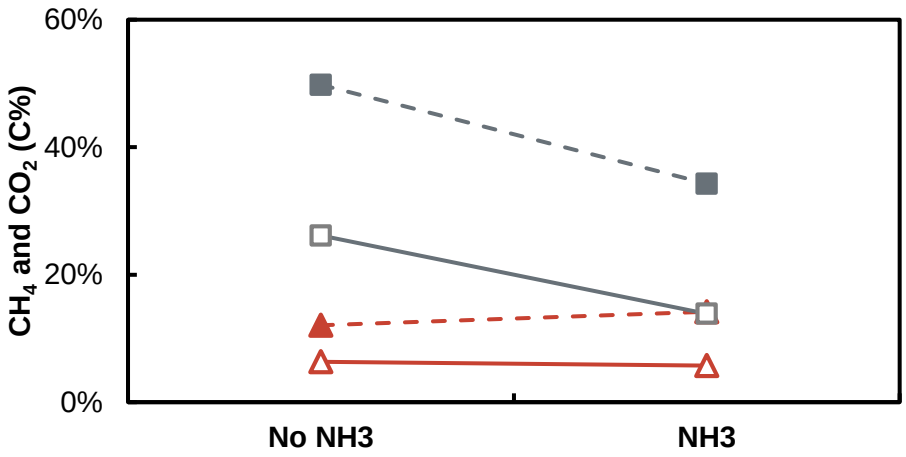

Figure 5-80: CH_4 (red triangles) and CO_2 (grey squares) selectivity from FT 4.1, presenting original data (open symbols, solid lines) and carbon balance corrected data (solid symbols, dashed line) obtained in the absence and presence of ammonia. Process conditions: T = 300 °C, P = 45 bar, H_2 to CO ratio = 1 and GHSV = 8 L/h/g_{cat}.

The organic products, both under standard FT conditions and after 45 minutes in the presence of ammonia, were analyzed as previously discussed using an offline GC-FID (see Figure 5-81) and in addition with GCxGC-FID/MS.

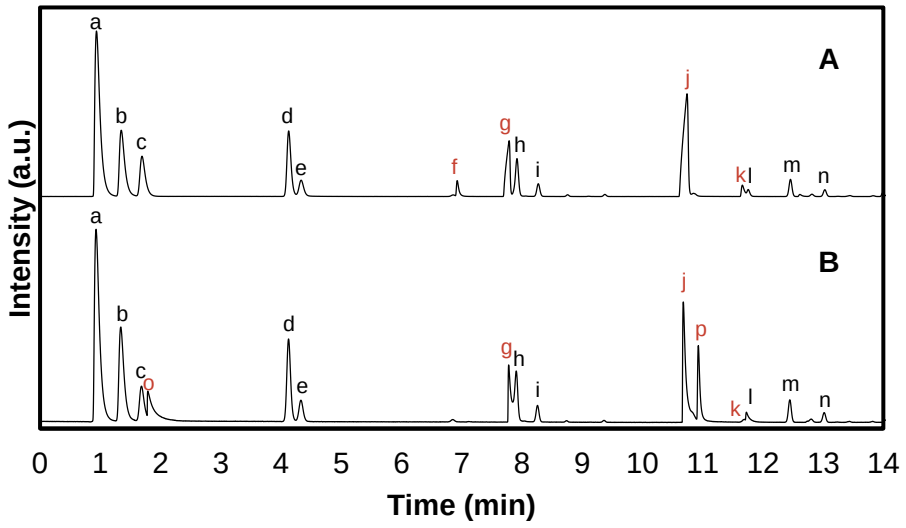

Figure 5-81: GC-FID chromatogram from FT 4.1 displaying a retention time of 0-14 min in the absence (A) and presence (B) of ammonia. With: a) methane, b) ethene, c) ethane, d) propene, e) propane, f) ethanal, g) methanol, h) butene (1), i) n-butane, j) ethanol, k) propanal, l) 2-me-butane, m) pentene (1), n) n-pentane, o) N-containing compound and p) acetonitrile.

GCxGC has the mayor advantage of being able to separate complex product mixtures on a second column (retention time on Y-axis) with differing polarity to the primary column (retention

time of X-axis). In combination with the associated TOF-MS, species can be identified before being quantified by the FID detector. One drawback of the technique is the inability to cool the GC oven resulting in no separation of small molecules. The first separated paraffin and olefin is the C_8 fraction, aldehyde and ketone the C_6 fraction and for the alcohols it is ethanol (see Figure 5-82). It is visible that in the absence of NH_3 the linear alcohols (dashed lines) are formed, starting with ethanol at the lowest retention time in both columns, and some aldehydes (arrows). After 45 minutes of ammonia co-feeding, the nitriles are appearing (circles) and the aldehydes are disappearing.

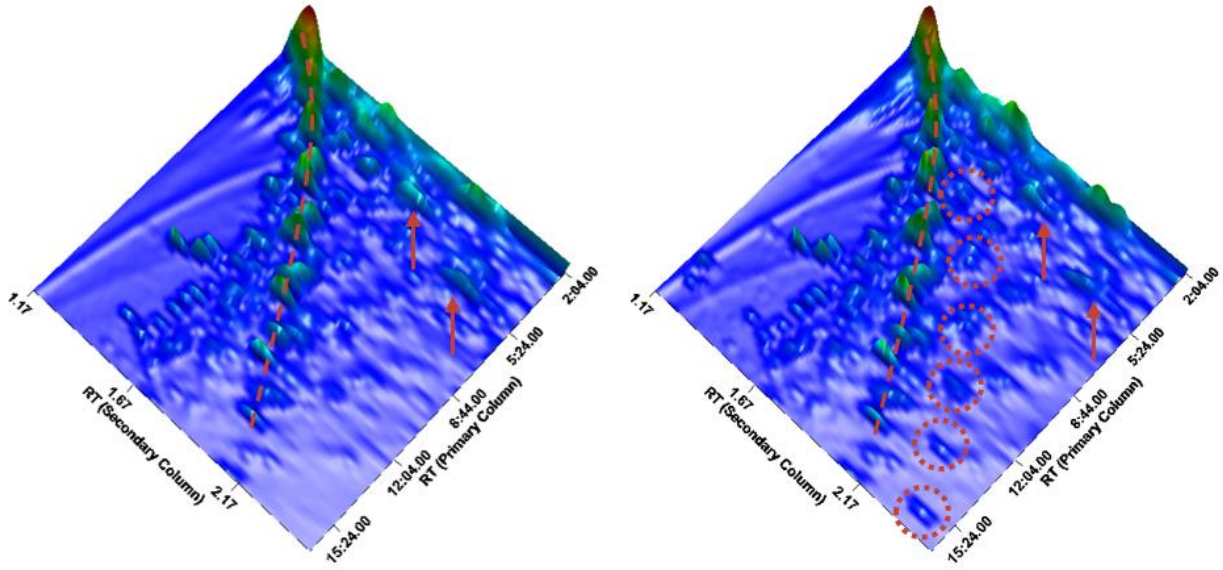

Figure 5-82: Image taken from the GCxGC analysis of FT 4.1 in the absence (left) and presence (right) of 4.7 vol.% NH_3 co-feeding. Dashed lines indicate the linear and branched alcohols, circles indicate the nitriles and the arrows indicate the aldehydes.

Upon addition of ammonia, the linear alcohol content in the total products decreases from 41.61 C% to 29.59 C%. Aldehydes were already a minor product group but further decrease from 3.57 C% to 2.13 C%. Ketones were not affected and stayed relatively constant at 1.05 C% and 1.64 C%. Olefins show a small increase in concentration, from 21.15 C% to 26.81 C% and the paraffins a small decrease from 30.92 C% to 29.14 C%. The C_3-olefin to C_3-paraffin ratio remains relatively constant at 3.4. The N-containing compounds consist mainly of nitriles (8.26 C%) with only a small trace of amides observed (0.11 C%) (see Table 5-4). Compared to previous studies [9, 10, 14, 129, 130] it is evident that β-Mo_2C displays a mixture of the previously described effects upon exposure to an ammonia bearing synthesis gas. An increase in olefin content was previously observed for a Co catalyst [129], however no nitrogen containing compounds were formed. Like iron catalysts [14, 130] and different from RhFe crystallites, the catalytic activity is not significantly affected by the ammonia. The nitrile heavy product spectrum resembles that reported for RhFe [9]. Lastly, while the alcohol concentration in the product does reduce, this reduction is to a much lower degree than reported for iron and RhFe [9, 14]. This indicates that molybdenum carbide

catalysts can either not activate NH_3 as efficiently as the Fe bearing catalysts or the incorporation of the N-bearing surface species is much slower/less efficient.

The linear alcohols are the most affected class of oxygenates upon co-feeding of ammonia, decreasing in concentration from 41.68 C% to 27.63 C%. Focusing on the linear alcohol distribution (Figure 5-83) it can be observed that the C_1-C_3 are the alcohols decreasing in concentration. Methanol decreased from 8.9 C% to 5.4 C%, ethanol from 15.7 C% to 10.6 C% and propanol from 10.2 C% to 2.5 C%.

Table 5-4: Product distribution in the absence and presence of NH_3 co-feeding from FT 4.1. Selectivities are CO_2-free selectivities (C%).

	No NH_3	*NH_3*
1-alcohols	41.61%	29.59%
branched	1.70%	2.30%
Aldehydes	3.57%	2.13%
Ketones	1.05%	1.64%
Olefins	21.15%	26.81%
Paraffins	30.92%	29.14%
Amides	n/a	0.11%
Nitriles	n/a	8.26%

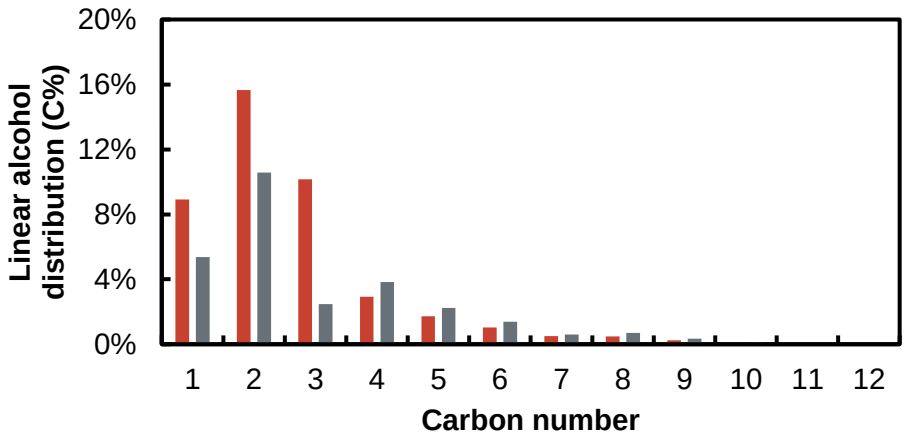

Figure 5-83: Linear alcohol distribution from FT 4.1 in the absence (#1, red) and presence (#2, grey) of ammonia. Process conditions: T = 300 °C, P = 45 bar, H_2 to CO ratio = 1 and GHSV = 8 L/h/g_{cat}.

5.4.2 FT run 4.2: 1.5 vol.% NH_3 co-feeding

In an attempt to extend the duration of the experiment, i.e. suppress or at least delay the formation of ammonium carbonate and the associated line blockage, the concentration of ammonia in the total feed gas was reduced from 4.7 to 1.5 vol.% at otherwise identical reaction conditions. Furthermore, to improve the ease of data analysis, the inert gas stream through the reactor now consisted of a mixture of N_2 and Ar. Only the N_2 flow was changed during the experiment when

introducing ammonia, leaving Ar as constant internal standard for quantification of the GC-TCD measurements (see Table 5-5).

Table 5-5: Gas composition FT run 4.2 with and without co-feeding ammonia.

	Gas	*Vol.%*	*P_i (bar)*
Normal FT	H_2	43%	19.3
	CO	43%	19.3
	N_2	7%	3.2
	Ar	7%	3.2
NH_3 co-feeding	10% NH_3/H_2	44.4%	19.3 (H_2) / 0.7 (NH_3)
	CO	43%	19.3
	N_2	5.6%	2.5
	Ar	7%	3.2

Again, the CO conversion after 30 hours TOS is comparable to previous runs with similar CH_4 and CO_2 selectivity at 15 C% and 48 C%, respectively. After 31.5 hours TOS, the ammonia was fed into the gas stream and the CO conversion decreased to 16% after about 50 minutes. Subsequently, the CO conversion started increasing again back to its original value after approximately 2.5 hours (Figure 5-84). Unfortunately, after about 3 hours TOS a pressure increase in the reactor was observed indicating the presence of a blockage and forced the shut-down of the experiment. After 1 hour TOS, the CH_4 and CO_2 selectivity showed a small increase to 17 C% and 50 C% (Figure 5-86), respectively. 2 hours later, after 3 hours of NH_3 co-feeding, the CO_2 selectivity showed the expected drop (Figure 5-85) as the blockage occurred, to about 43 C%. CH_4 stayed constant at 16 C% (Figure 5-86).

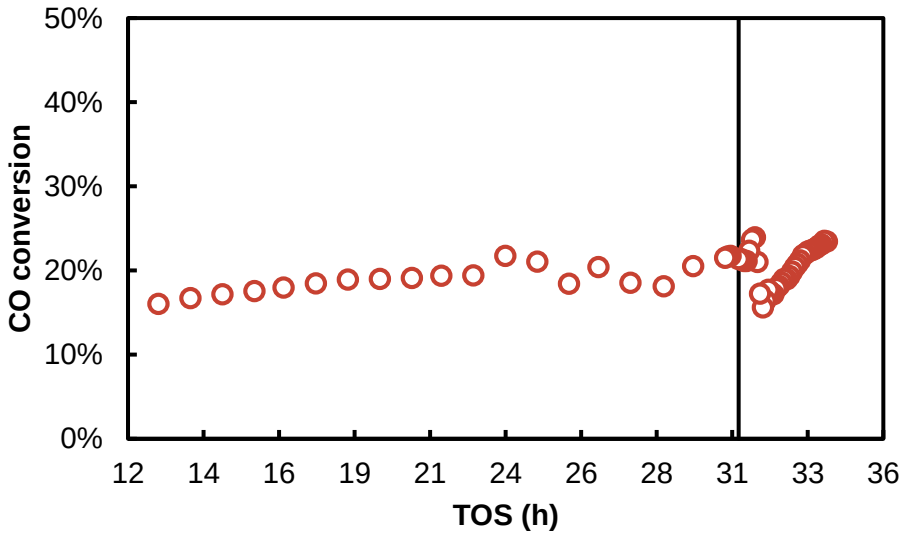

Figure 5-84: CO conversion from FT 4.2 obtained with TOS in the absence and presence of NH_3. Process conditions: T = 300 °C, P = 45 bar, H_2 to CO ratio = 1 and GHSV = 8 L/h/g_{cat}.

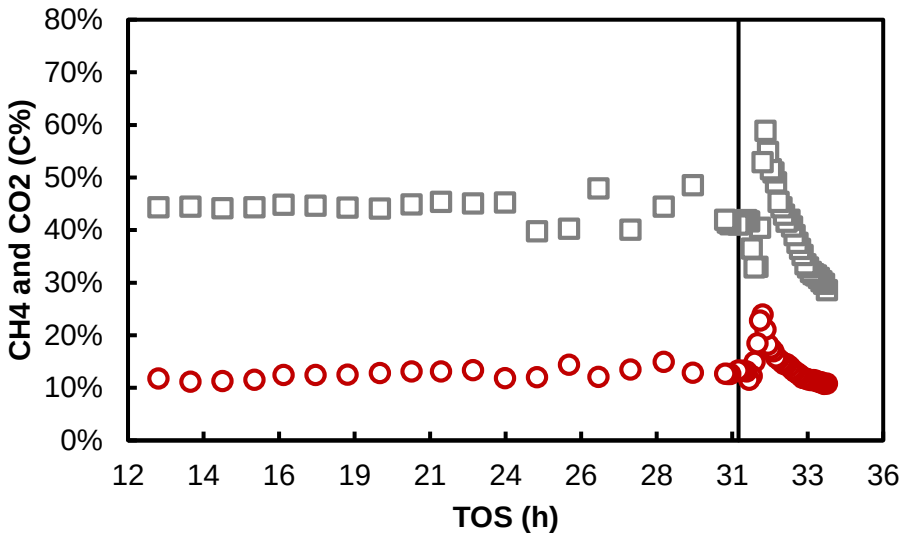

Figure 5-85: CH_4 (red triangles) and CO_2 (grey squares) selectivity from FT 4.2 in the absence and presence of ammonia. Process conditions: T = 300 °C, P = 45 bar, H_2 to CO ratio = 1 and GHSV = 8 L/h/g_{cat}.

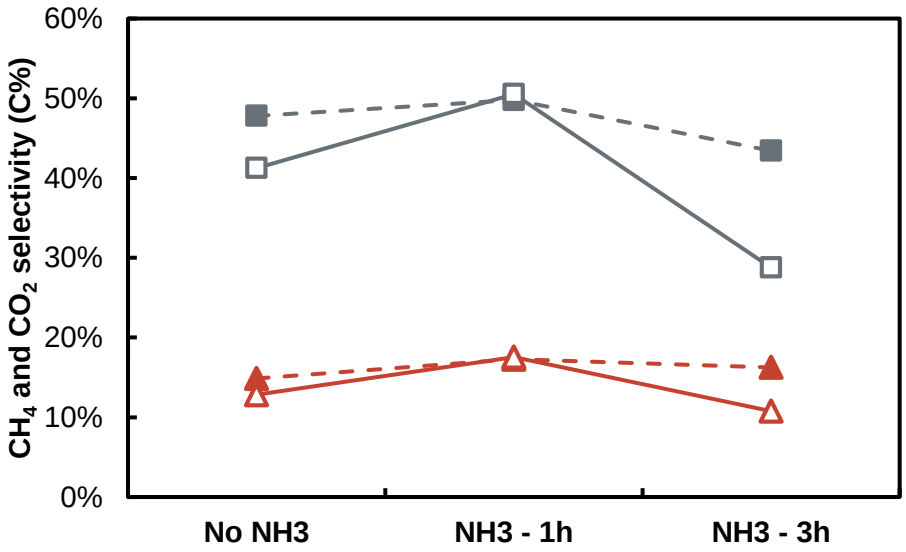

Figure 5-86: CH_4 (red triangles) and CO_2 (grey squares) selectivity from FT 4.2, presenting original data (open symbols, solid lines) and carbon balance corrected (solid symbols, dashed line) in absence and presence of ammonia. Process conditions: T = 300 °C, P = 45 bar, H_2 to CO ratio = 1 and GHSV = 8 L/h/g_{cat}.

The composition of the organic product was again analyzed using an offline GC-FID (see Figure 5-87) and in addition with GCxGC-FID/MS, in the absence of ammonia (see Appendix I, Figure 9-9), after 1 hour (see Appendix I, Figure 9-10) and after 3 hours (see Appendix I, Figure 9-11) of NH_3 co-feeding. Before ammonia was fed into the reactor the oxygenate to total organic product ratio was 0.42 with linear alcohols being the major oxygenated product (35.77 C%). Aldehydes (3.23 C%), branched alcohols (2.58 C%), ketones and carboxylic acids (together 0.64 C%) form

the rest of the oxygenated products. Upon 1 hour of co-feeding, the oxygenate to total organic product ratio decreased to 0.22. The linear alcohol content decreased to 21.02 C%, aldehydes decreased to 0.13 C%, branched alcohols to 0.23 C% and the concentration of ketones and carboxylic acids remained low. Nitriles are again the dominantly formed N-containing compounds, observed at 6.22 C% of the total organic products. A small trace of amides was observed with 0.03 C%. The decrease of the oxygenates led to an increase in olefins to 28.33 C% and a small increase in paraffins to 43.66 C%. The C_3-olefin to C_3-paraffin ratio increased from 3.29 to 3.53 (see Appendix H, Figure 9-8).

After 3 hours of ammonia co-feeding and after the observed increase in CO conversion, the product composition had not changed significantly. The oxygenate to total organic product ratio as well as the alcohol selectivity increased, reaching levels still lower than in the absence of ammonia. The aldehydes remain low and ketones remain unaffected. The latter was also observed in a previous study [9]. The C_3-olefin to C_3-paraffin ratio decreased, but remains elevated in comparison to the normal FT conditions (see Appendix H, Figure 9-8). The formation of N-containing compounds remained relatively stable with TOS with 6.62 C% nitriles and a small increase in amides to 0.16 C%.

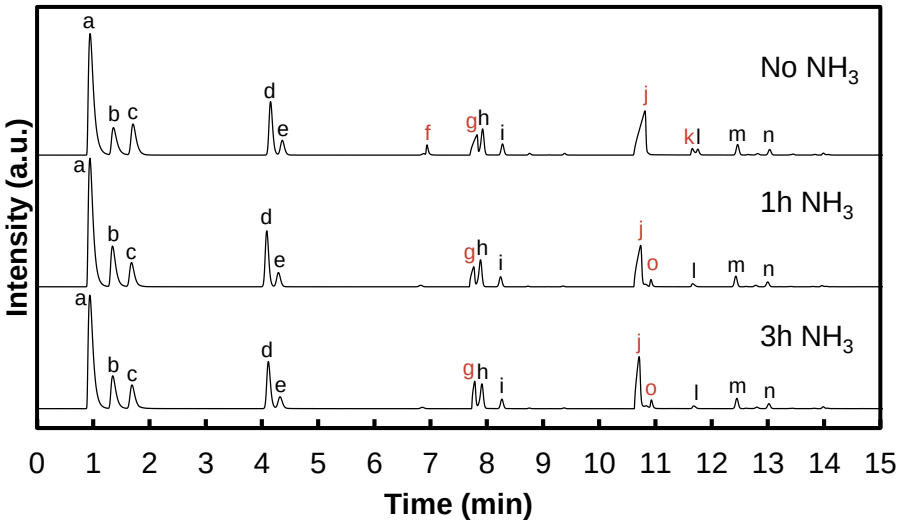

Figure 5-87: GC-FID chromatogram from FT 4.2 displaying a retention time of 0-15 min in the absence and presence (1h and 3h) of ammonia. With: a) methane, b) ethene, c) ethane, d) propene, e) propane, f) ethanal, g) methanol, h) butene (1), i) n-butane, j) ethanol, k) propanal, l) 2-me-butane, m) pentene (1), n) n-pentane and o) acetonitrile.

Table 5-6: Product distribution in the absence and presence of NH_3 co-feeding from FT 4.2. Selectivities are CO_2-free selectivities (C%).

	No NH_3	*1h NH_3*	*3h NH_3*
Linear Alcohols	35.77%	21.02%	30.94%
Branched Alcohols	2.58%	0.23%	1.99%
Aldehydes	3.23%	0.13%	0.28%
Ketones	0.58%	0.32%	0.43%
Carboxylic Acids	0.06%	0.06%	0.14%
Olefins	20.30%	28.33%	24.58%
Paraffins	37.47%	43.66%	34.86%
Nitriles	n/a	6.22%	6.62%
Amides	n/a	0.03%	0.16%

Like FT 4.1, the linear alcohol content was the most significantly influenced product class upon co-feeding ammonia, dropping in concentration from 30.03 C% to 19.90 C% after 1 hour and reaching 24.93 C% after 3 hours. A closer look on the linear alcohol distribution (Figure 5-88) reveals that the C_1 and C_2 alcohols are the affected species. Methanol decreases from 7.7 C% to 6.1 C% recovering fully after 3 hours TOS. Ethanol showed the most significant drop from 17.1 C% to 10.8 C%, followed by an increase to 14.4 C%, which is still lower than without co-feeding ammonia. It could be said from the two previous runs that the short chain alcohols are most influenced upon co-feeding of ammonia, which could explain that acetonitrile is the major nitrogen containing compound.

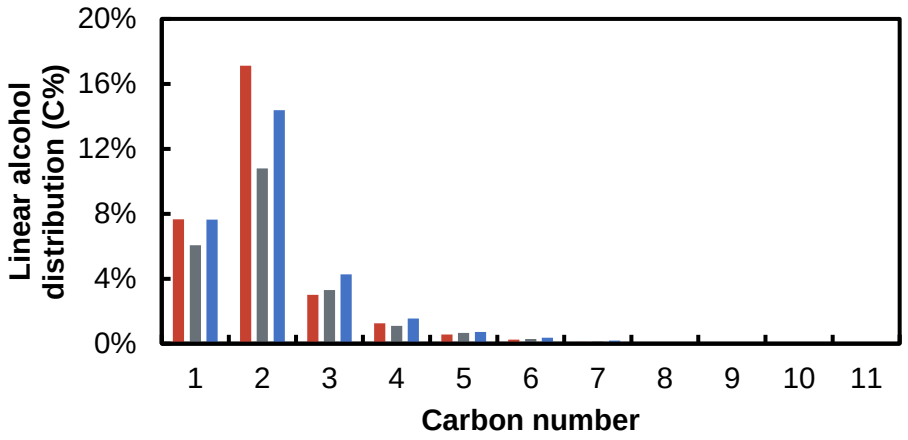

Figure 5-88: Linear alcohol distribution from FT 4.2 in the absence (red), 1 hour presence (grey) and 3 hours presence (blue) of ammonia. Process conditions: T = 300 °C, P = 45 bar, H_2 to CO ratio = 1 and GHSV = 8 L/h/g_{cat}.

5.4.3 Effect of NH_3 on the performance of K/β-Mo_2C in the FTS

A NH_3 conversion can be estimated based on the NH_3 fed into the reactor in relation to the formed N-containing compounds. After 45 minutes of ammonia co-feeding in FT 4.1, the ammonia conversion to nitriles and amides was 0.66%. At a lower concentration of ammonia in the feed gas, a significantly higher conversion of 7.70 to 8.08% can be calculated. In experiment FT 4.1 the ammonia to OH ratio (sum of alcohols, aldehydes and carboxylic acids formed in the absence of ammonia) was 7.2 mmoles of NH_3 per mmole of OH. In the presence of ammonia, the formed N-containing compounds, mainly nitriles and to some minor extent amides, amount to 0.0014 mmoles (Table 5-7). This equates to a calculated conversion of ammonia to N-containing product of only 0.66%. Clearly the ammonia in the gas stream is not the limiting factor in the formation of these compounds. The ratio of ammonia to OH at the reactor outlet, assuming no formation of ammonium carbonate in the hot reactor, has risen to 42.3 mmoles of NH_3 per mmole of OH. During FT 4.2, the ammonia is co-fed in a ratio of 1.1 mmoles of NH_3 per mmole of OH. The calculated ammonia conversion to product is 7.70 to 8.08 %. This equates to 4 times higher absolute NH_3 conversion compared to FT 4.1 at a higher NH_3 concentration. For FT 4.2 the ratio of ammonia to OH at the reactor outlet is around 1.4 mmoles NH_3 per mmole OH.

Besides the formation of ammonium carbonate, the dominant class of N-containing compounds formed are nitriles. The formed nitriles have an ASF-like distribution with an α-value of 0.56, assuming that acetonitrile is not a kinetically favoured product (Figure 5-89).

The nitrile fraction is dominated by acetonitrile with ≥58 C%, followed by propanenitrile with ≥21 C%. Thereafter the selectivity drops significantly towards C_{4+} nitriles (Figure 5-90).

Table 5-7: NH_3 conversion of FT run 4.1 and FT run 4.2.

FT Run	X_{CO}	NH_3 *in*	NH_3 *converted*	X_{NH3}
	(%)	(mmole)	(mmole)	(%)
FT 4.1	13.67%	0.21	0.0014	0.66%
FT 4.2 (1h)	17.4%	0.07	0.0052	7.70%
FT 4.2 (3h)	23.4%	0.07	0.0055	8.08%

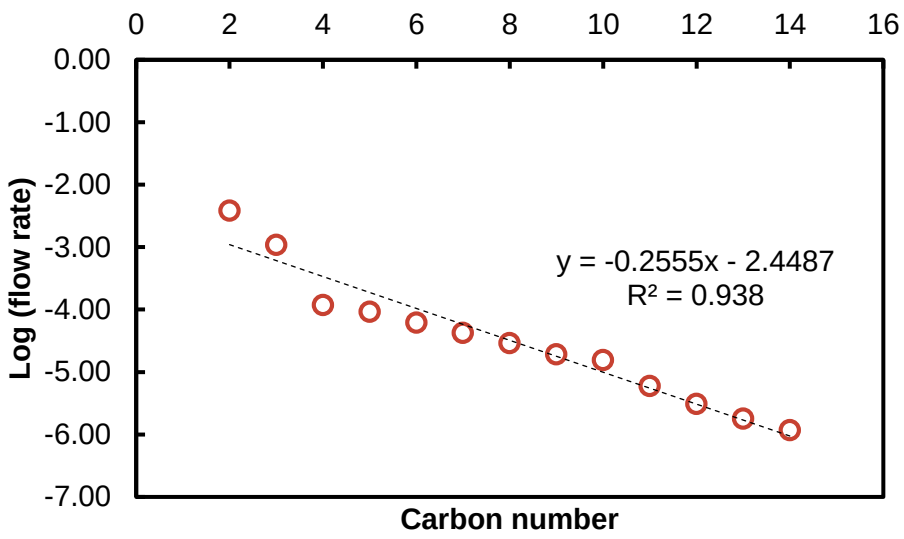

Figure 5-89: ASF-like distribution of nitriles formed during FT 4.2 after 3 hours of ammonia co-feeding. Process conditions: T = 300 °C, P = 45 bar, H_2 to CO ratio = 1 and GHSV = 8 L/h/g_{cat}.

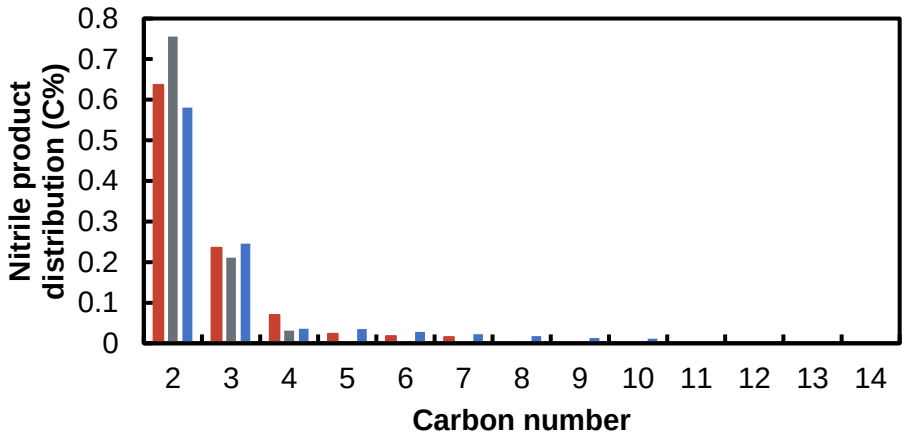

Figure 5-90: Nitrile product distribution of FT run 4.1 (red), FT run 4.2 after 1 hour (grey) and 3 hours (blue) of ammonia co-feeding. Process conditions: T = 300 °C, P = 45 bar, H_2 to CO ratio = 1 and GHSV = 8 L/h/g_{cat}.

The amides observed in FT run 4.1 also seem to follow an ASF-like product distribution (see Figure 5-91). Unfortunately, insufficient amides were formed to calculate the ASF-plot above C_4. The chain growth probability for the formation of amides based on the observed results is 0.22.

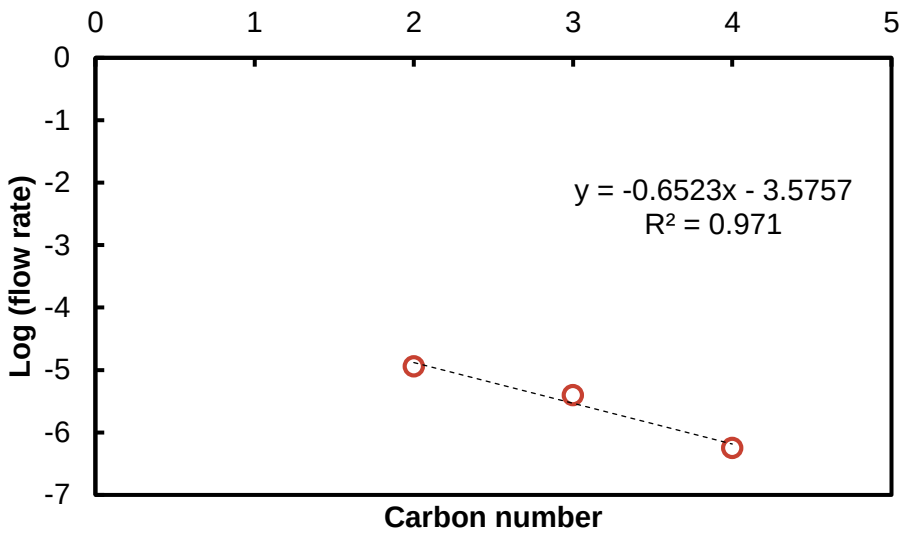

Figure 5-91: ASF-like distribution of amides formed during FT 4.1 with ammonia co-feeding. Process conditions: T = 300 °C, P = 45 bar, H_2 to CO ratio = 1 and GHSV = 8 L/h/g_{cat}.

Co-feeding of ammonia does not have a significant effect on the chain growth probability towards the linear alcohols (Figure 5-92). Before ammonia is added the α-value for linear alcohols is 0.34, after 1 hour of ammonia the α-value is 0.36 and after 3 hours of ammonia co-feeding, the α-value is 0.35. However, there is a slight difference in the C_2 group visible, which is in line with the earlier presented data in Figure 5-88.

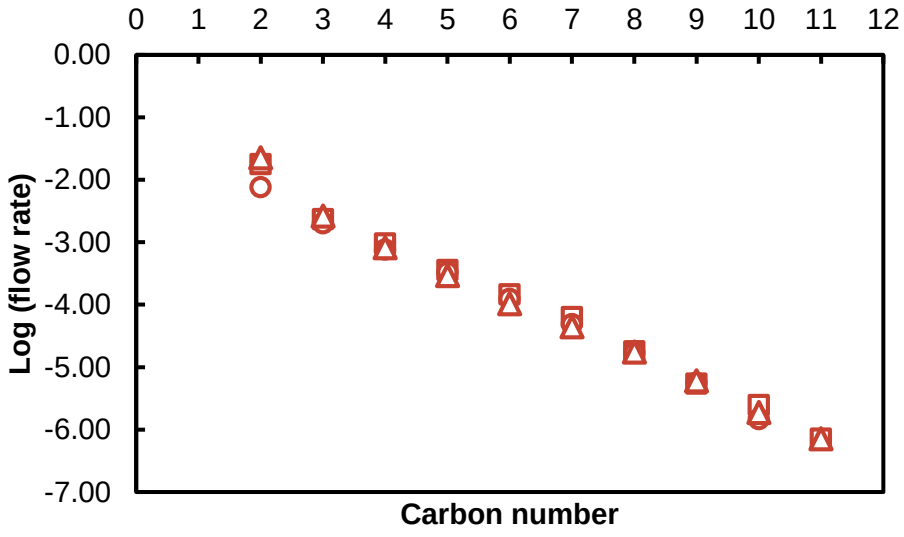

Figure 5-92: ASF-plots of linear alcohols from FT 4.2 before (triangles), after 1 hour (circles) and after 3 hours (squares) of ammonia co-feeding.

In summary, the formation of N-containing compounds is possible by co-feeding ammonia to synthesis gas over a potassium promoted β-Mo_2C. The activity of the catalyst is not seriously

affected. Predominantly nitriles, specifically C_2 and C_3 nitriles, are formed at the expense of the short chain linear alcohols. In this behavior the catalyst is similar to the reported FeRh system [9]. Besides the drop in oxygenate content and the formation of nitriles, the olefin to paraffin selectivity increases indicating the potential poisoning/blocking of reactive sites for the secondary hydrogenation reactions. The extent to which oxygenated products disappear in favour of N-containing compounds is significantly lower than for previously studied catalysts [9, 10, 14, 129, 130] and changes with TOS at least at low NH_3 concentrations. This could suggest a gradual formation of the catalyst in an ammonia bearing synthesis gas environment. Following an initial poisoning of sites responsible for oxygenate formation, slowly a mechanism develops yielding N-containing compounds. At high ammonia co-feeding (FT 4.1) the ammonia conversion to nitriles and amides was low at 0.66%. A lower level of ammonia co-feeding enhances the efficiency slightly and an ammonia conversion of ±8% was observed. However, the catalyst has a very high water-gas-shift activity and therefore, CO_2 is one of the main products. This product reacts most probably with unreacted ammonia forming ammonium carbonate, which results in reactor blockages. As the melting temperature of ammonium carbonate is 58 °C, the reaction probably mainly takes place at a cold spot in the reactor, such as the cold trap. However, the formed ammonium carbonate could not be collected and analyzed. Suppressing the WGS activity of the catalyst or feeding lower amounts of ammonia resulting in a 100% conversion of ammonia in the hot zone of the catalyst could circumvent this challenge.

5.5 Spent catalyst characterization

XRD analysis was performed after the reaction under FT conditions with the unpromoted, potassium promoted and samples exposed to ammonia co-feeding, to confirm that the phase of the catalyst remained stable. The catalysts were removed from the reactor and exposed to air without any post FT treatment. The first set of experiments (FT 1) did not show any oxidation and all catalysts were stable after being exposed to air after the FT reaction (Figure 5-93). What exactly prevents the re-oxidation observed for a fresh activated catalyst in these spent samples is unknown. A layer of oxide and/or carbon formed during the reaction or during exposure to air could be present. The sharp peak at around 70° is due to impurities in the sample.

The promoted samples also all show the β-Mo_2C phase independently of the reaction conditions and the presence or absence of ammonia. No obvious signs of oxidation were observed from the obtained XRD chromatograms (Figure 5-94 and Figure 5-95).

The crystallite sizes and phase compositions of the spent samples are defined by the Rietveld refinement technique. All catalyst were confirmed to consist of 100% β-Mo_2C. The *in situ* prepared sample at 630 °C (FT 1.1) has a crystallite size of 11.1±0.1 nm. This is very comparable to the sample prepared *in situ*, discussed in section 5.1.5. This confirms that the β-Mo_2C catalyst is resistant to sintering under FT conditions. The spent sample from FT 1.2, which is prepared inside the rig at 630 °C, followed by passivation and reduction, has a crystallite size of 12.0±0.1 nm. The sample prepared for FT 1.3, was carburized at 760 °C followed by a TPH treatment. The spent sample has a crystallite size of 20.1±0.3 nm. This is higher, due to the higher carburization temperatures.

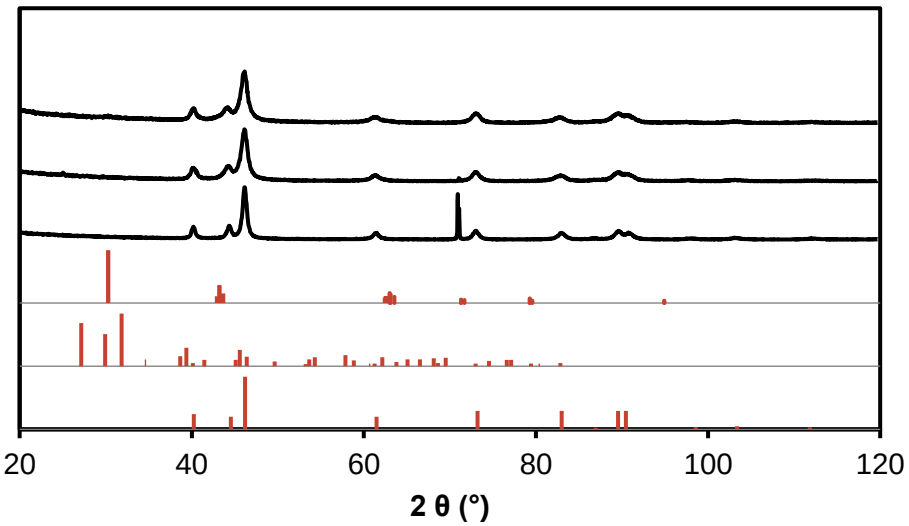

Figure 5-93: XRD-chromatograms of the spent samples (black) from top to bottom: FT 1.1, 1.2 and 1.3. With ref patterns (red) from top to bottom: MoO_2, MoO_3 and Mo_2C.

FT 2.0 was again a sample prepared *in situ*, passivated and reduced. The crystallite size of the spent sample is slightly smaller than FT 1.2, 8.1±0.1 nm, however still in a comparable range. The promoted samples all have again similar crystallite sizes for the spent samples. For FT 2.1, 2.2 and 2.3 the crystallite sizes are 10.9±0.1, 9.3±0.1 and 11.0±0.1 nm, respectively.

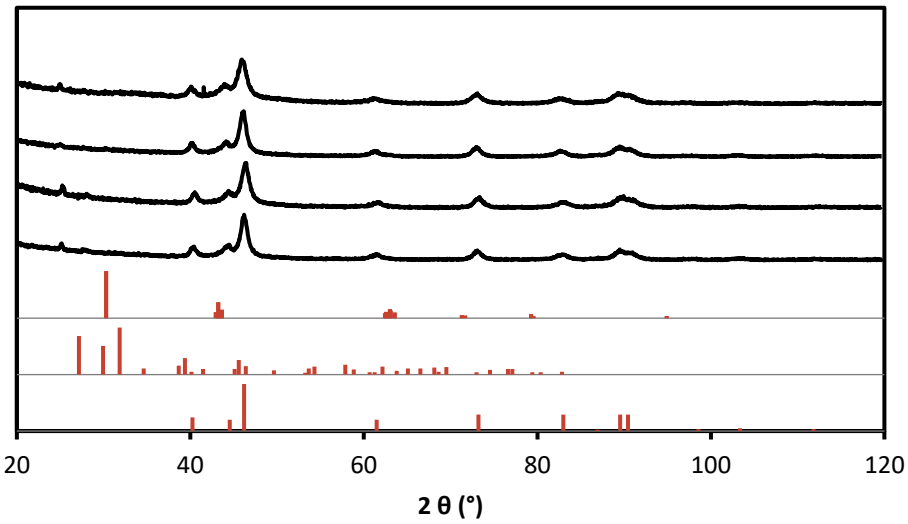

Figure 5-94: XRD-chromatograms of the spent samples (black) from top to bottom: FT 2.0 (unpromoted), FT 2.3 (F 1.8 wt.% K/Mo), FT 2.2 (E* 5.4 wt.% K/Mo) and FT 2.1 (D* 6.2 wt.% K/Mo). With reference patterns (red) from top to bottom: MoO_2, MoO_3 and Mo_2C.*

The XRD chromatograms of the two NH_3 co-fed samples seem to have a higher signal to noise ratio, this could indicate smaller crystallite sizes. Rietveld refinement confirmed crystallite sizes for the spent samples of FT 4.1 and 4.2 as 5.7±0.1 and 7.6±0.1 nm, respectively.

Previously it was shown that all samples show the pattern of MoO_3 in Raman spectroscopy, prior to being exposed to FT conditions. The high temperature (≥760 °C) carburized samples show the D- and G-bands at 1347 and 1588 cm^{-1} [101], respectively, indicating graphitic carbon on the surface of the catalyst (see Figure 5-13). After being exposed to FT conditions, the unpromoted sample (FT 2.0) was re-analyzed using the Raman spectroscopy and it was found that the previously recorded MoO_3 scattering disappeared but displaying a wide G-band peak at around 1588 cm^{-1}. Similar Raman scattering has been reported by Mo *et al.* (2016) [101] who suggested that carbon deposition on the catalysts has taken place. Sample D* - 3.9 wt.% K/Mo (spent sample from FT 3.1) was also analyzed using the Raman technique, which showed similar results as the spent unpromoted sample. Again, carbon deposition was observed in the form of the very weak D- and G-band that is visible in the spectrum, at 1347 and 1588 cm^{-1}, respectively. No MoO_3 scatters were observed. The last sample analyzed with the Raman spectroscope was the spent sample from FT 4.2. Again, even weaker D- and G-bands are observed indicating carbon deposition. The weakness of the peaks could be related to the duration and the harshness of the conditions applied of the run. However, no MoO_3 scatter peaks were observed (see Figure 5-96).

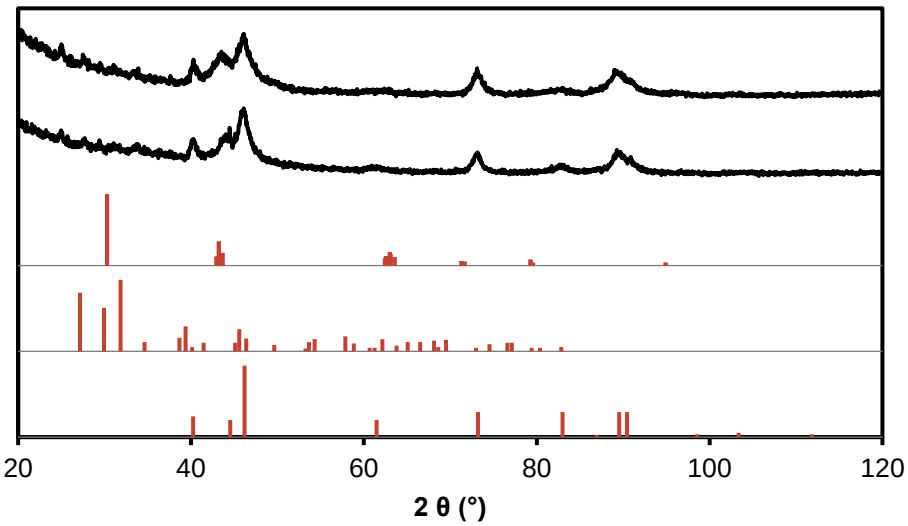

Figure 5-95: XRD-chromatograms of the spent samples (black) from top to bottom: FT run 4.1 and 4.2. With reference patterns (red) from top to bottom: MoO_2, MoO_3 and Mo_2C.

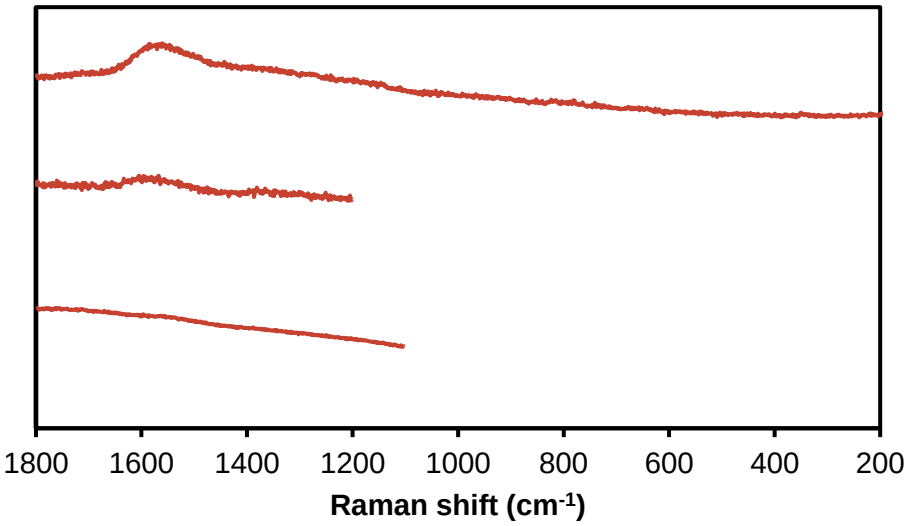

Figure 5-96: Raman spectra of the spent samples from top to bottom: FT 2.0, FT 3.1 and FT 4.2.

6 Conclusion

This study presents the use of unpromoted and potassium promoted β-Mo_2C catalyst in the Fischer-Tropsch synthesis with and without co-feeding of ammonia. The project can be divided into three main parts. The synthesis of β-Mo_2C, the effect of carburization protocols on the surface of the catalyst, its activity, and to a certain extent the selectivity, under a variety of FT process conditions. Furthermore, the promotional effect of potassium on the prepared β-Mo_2C catalysts was investigated regarding the activity, but most importantly the selectivity towards oxygenates, under a variety of FT process conditions. Finally, the co-feeding of NH_3 to the potassium promoted β-Mo_2C catalysts, to observe its effect on the catalyst activity and selectivity, mainly focusing on the formation of N-containing compounds. Based on previous research it was assumed that at reaction conditions achieving a high oxygenate selectivity would also achieve the highest possible selectivity towards N-containing compounds.

A hexagonal phase molybdenum carbide (β-Mo_2C) catalyst was synthesized using a temperature programmed reaction of MoO_3 with 20% CH_4 in H_2, a method previously described by Lee *et al.* (1987) [143], at three different carburization temperature ranges, i.e. 630-650 °C, 750-760 °C and 1000 °C. XRD analysis of the final carburized sample, after passivation, confirmed that the β-Mo_2C phase was formed. It was observed that the increase in temperature leads to an increase in carbon deposition, in the form of a graphite layer [101]. Raman and TEM analysis confirmed that the graphitic carbon was successfully removed by means of a temperature programmed hydrogenation reaction, forming CH_4. After the hydrogen treatment, the catalyst remained stable in air. *In situ* XRD analysis of the carburization of MoO_3 to β-Mo_2C confirmed that β-Mo_2C is formed at 650 °C. After carburization, the catalyst was exposed to an air atmosphere at room temperature and it was observed that the catalyst partially oxidizes to MoO_2. Passivation of the freshly carburized β-Mo_2C and subsequent reduction was performed and showed that the sample remained stable showing a β-Mo_2C phase. However, despite the carburization method used, all samples showed by means of Raman analysis - after the samples were exposed to air - Raman spectra indicating MoO_3.

Catalyst testing was performed in a fixed bed U-tube reactor. The formation of products was analyzed using online GC-TCD, offline GC-FID and online GCxGC. In the first set of experiments, the unpromoted samples prepared at different carburization temperatures (630 °C, with and without passivation, and 760 °C) were exposed to a variety of process conditions (T = 240-300 °C, P = 33 bar and SV = 8-16 L/h/g_{cat}). The catalyst prepared at 630 °C (*in situ*, without any passivation/reduction or exposure to air) showed higher CO hydrogenation activity than the passivated and subsequently reduced catalyst. However, passivation of the catalyst is required, to allow it to be removed from the reactor for promotion with K_2CO_3. The 760 °C prepared catalyst, after removal of the graphitic carbon on the surface, was shown to be the least active catalyst.

This supports the suggestion that either not all graphite is removed, or the graphitic carbon has changed the surface of the catalyst to such extent that it was irreversible.

All three unpromoted β-Mo_2C catalysts produce mainly hydrocarbons with small chain growth probabilities, which is well documented in the literature [20, 21, 139]. A decrease in CO conversion leads to an increase in oxygenate selectivity. It was also observed that the passivated sample (FT 1.2) shows higher oxygenate to total organic product ratios (0.16 at 15% CO conversion) than the *in situ* prepared sample (FT 1.1) at similar conversion levels (0.02 at 16% CO conversion). Therefore, it is suggested that the presence of MoO_3 on the surface of the catalyst has a significant influence on the formation of oxygenates. Within the formed oxygenates, the most favourable product formed was methanol. Besides CO hydrogenation, a high activity for the WGS was observed.

The second set of experiments were all performed using β-Mo_2C prepared at 630 °C, subsequently passivated, promoted with potassium and then reduced prior to exposure to FT conditions. All catalysts were tested at 45 bar with a space velocity of 8.4 L/h/g_{cat} and a temperature range of 260 °C to 350 °C. The promotion with potassium showed a significant increase in oxygenate selectivity, at all applied process conditions, compared to the unpromoted samples. However, the different promotion levels did not show significant differences regarding activity and selectivity during the testing under Fischer-Tropsch conditions. The CO conversion was affected upon promotion with the lowest level of potassium but did not decrease further at higher wt.% of potassium.

Besides the increase in total oxygenates, also an increase in higher oxygenates (C_{2+}) was observed for the potassium promoted samples, specifically the formation of ethanol in comparison to methanol. The effect of reaction temperature has been shown to influence the oxygenate selectivity significantly. An increase in temperature leads to a decrease in the methanol content, while increasing the ethanol selectivity. However, the increase in temperature also enhances the formation of hydrocarbons, therefore the total selectivity towards oxygenates decreased. Besides linear alcohols (which is the major class within the oxygenates) also aldehydes, ketones and carboxylic acids were observed. The formation of these classes is significantly reduced by an increase in temperature/CO conversion.

The effect of increasing pressure up to 65 bar was also investigated on a 3.9 wt.% potassium promoted β-Mo_2C catalyst and has been found to increase the total oxygenate selectivity, in particular towards methanol. However, the change in pressure had a much smaller effect than the change in temperature over the ranges investigated.

The third part of the project was the co-feeding of NH_3 during the FTS on a promoted β-Mo_2C catalyst. The formation of N-containing compounds was studied as well as the effects of ammonia on the catalyst's activity. The main N-containing product class that was observed upon the co-feeding of 1.5 vol.% and 4.7 vol.% NH_3 is nitriles, specifically C_2 and C_3 nitriles. Small traces of

amides were also observed. Besides the observation of N-containing compounds it was also confirmed that the formation of oxygenates decreases, supporting the suggestion made by among others Claeys *et al.* (2011) [8], Henkel (2012) [10], Sango (2013) [130] and de Vries (2017) [15] that the N-species are inserted into the earlier formed oxygenates or precursor species of these oxygenates.

Furthermore, Sango (2013) [130] has confirmed the formation of ammonium carbonate, upon co-feeding of NH_3, by the reaction with CO_2, resulting in a blockage in the reactor. During this study, a significant decrease in the selectivity towards CO_2 was observed simultaneously with a blockage in the reactor that occurred within 1-3 hours TOS of ammonia co-feeding. Therefore, it is assumed that the blockage was formed due to the formation of ammonium carbonate.

In the short period of NH_3 co-feeding a quick drop in CO conversion was observed, however this seemed to be recovered within an hour or two. Unfortunately, no long-term investigation on the effect of NH_3 on the potassium promoted β-Mo_2C was possible, as the blockage occurred during all experiments.

Besides the formation of N-containing compounds, the decrease in oxygenates, an increase in olefin content was observed upon co-feeding with ammonia. This is in line with the observations from Claeys *et al.* (2011) [8].

7 Future recommendations

The use of a potassium promoted β-Mo_2C has shown promising results in producing a high amount of oxygenates. However, more research should be conducted regarding the high activity towards WGS, by possibly varying the composition of the catalyst with different promoters. Optimization regarding specific surface area could be of interest in order to increase the activity of the catalyst, specifically for the potassium promoted samples. This could be done by varying the carburization conditions, starting with a lower average crystallite size of the precursor MoO_3, or supporting the oxidic precursor.

Perhaps the addition of other promoters could lead to an increase in the oxygenate selectivity. Specifically, an increase towards the formation of higher oxygenates is of interest, to observe the possible formation of longer chained N-containing compounds, upon the co-feeding of ammonia.

Suppressing the WGS activity would also be of interest for the ammonia co-feeding part, trying to prevent the blockage, formed by the reaction of CO_2 and NH_3.

In situ Raman analysis on the carburization reaction from MoO_3 to β-Mo_2C would be of interest to observe if MoO_3 would also be present in a freshly prepared β-Mo_2C sample, without being in contact with air. In general, the surface composition of the catalyst at the different stages of its life are of great interest.

8 References

[1] M. E. Dry, Catalysis Today, 2002, **71**, 227-241.

[2] D. Dillerop, H. van den Berg, and A. G. J. van der Ham, Industrial & Engineering Chemistry Research, 2010, **49**, 12529-12537.

[3] M. E. Dry, Applied Catalysis A: General, 1990, **138**, 319-344.

[4] H. Schulz, Topics in Catalysis, 2003, **26**, 73-85.

[5] E. van Steen and M. Claeys, Studies in Surface Science and Catalysis, 2004, **152**, 601-680.

[6] A. P. Steynberg and M. E. Dry, M. E. Dry, Ed. *Fischer-Tropsch Technology*. Elsevier Science & Technology Books, 2004.

[7] H. Schulz, Applied Catalysis A: General, 1999, **186**, 3-12.

[8] M. Claeys, E. van Steen, F. Roessner, and T. Sango, Process for the Production of Nitrogen or Phosphorus Containing Compounds from Synthesis Gas, 2011.

[9] N. Fischer, R. Henkel, H. Kotze, M. Furst, J. Olivier, J. Neethling, and M. Claeys, Catalysis Communications, 2016, **87**, 14-17.

[10] R. Henkel, The Influence of Ammonia on Fischer-Tropsch Synthesis and Formation of N-Containing Compounds, PhD, Institute for Pure and Applied Chemistry, Carl von Ossietzky Univeristat Oldenburg, Oldenburg, Germany, 2012.

[11] V. V. Ordomsky, A. Carvalho, B. Legras, S. Paula, M. Virginie, V. L. Sushkevich, and A. Y. Khodakov, Catalysis Today, 2016, **275**, 84-93.

[12] V. R. R. Pendyala, G. Jacobs, C. Bertaux, S. Khalid, and B. H. Davis, Journal of Catalysis, 2016, **337**, 80-90.

[13] A. Rawoot, The Production of Nitrogen-Containing Compounds Via a Modified Fischer-Tropsch Process, MSc, Chemical Engineering, University of Cape Town, Cape Town, 2016.

[14] T. Sango, N. Fischer, R. Henkel, F. Roessner, E. van Steen, and M. Claeys, Applied Catalysis A: General, 2015, **502**, 150-156.

[15] C. de Vries, Adding Ammonia During Fischer-Tropsch Synthesis: Pathways to the Formation of N-Containing Compounds., PhD, Chemical Engineering, University of Cape Town, Cape Town, 2017.

[16] A. Rawoot, The Production of Nitrogen-Containing Compounds Via a Modified Fischer-Tropsch Process, M.Sc., Department of Chemical Engineering, University of Cape Town, Cape Town, 2016.

[17] H. Al-Megren, T. Xiao, M. AlKinany, S. Aldree, Y. Huang, H. Chen, P. P. Edwards, and V. Kuznetsov, Applied Petrochemical Research, 2013, **3**, *3-4*, 71-77.

[18] J. M. Christensen, L. D. L. Duchstein, J. B. Wagner, P. A. Jensen, B. Temel, and A. D. Jensen, Industrial & Engineering Chemistry Research, 2012, **51**, *11*, 4161-4172.

[19] E. T. Liakakou and E. Heracleous, Catal Sci Technol, 2016, **6**, *4*, 1106-1119.

[20] H. C. Woo, K. Y. Park, Y. G. Kim, I. Nam, J. S. Chung, and J. S. Lee, Applied Catalysis, 1991, **75**, 267-280.

[21] M. L. Xiang, D. B. Li, W. H. Li, B. Zhong, and Y. H. Sun, Fuel, 2006, **85**, *17-18*, 2662-2665.

[22] P. Forzatti, E. Tronconi, and I. Pasquon, Catalysis Reviews - Science and Engineering, 1991, **33**, 109-168.

[23] F. Fischer, Industrial & Engineering Chemistry, 1925, **17**, *6*, 574-576.

[24] F. Fischer, National Petroleum News, 1926, **18**, 49.

[25] F. Fischer and H. Tropsch, Brennstoff-Chemie, 1926, **7**, 299-300.

[26] F. Fischer and H. Tropsch, Brennstoff-Chemie, 1926, **7**, 97-104.

[27] F. Fischer and H. Tropsch, Brennstoff-Chemie, 1928, **9**, 39.

[28] F. Fischer and H. Tropsch, Berichte der Deutschen Chemischen Gesellschaft B, 1926, **59B**, 830.

[29] F. Fischer and H. Tropsch, Berichte der Deutschen Chemischen Gesellschaft B, 1926, **59B**, 923.

[30] F. Fischer, H. Tropsch, and P. Dilthes, Brennstoff-Chemie, 1925, **6**, 265.

[31] F. Fischer, H. Tropsch, and W. Ter-Nedden, Berichte der Deutschen Chemischen Gesellschaft B, 1927, **60B**, 1330.

[32] P. Sabatier and J. B. Senderens, Comptes Rendus Hebdomadaires des Seances de l'Academie de Sciences, 1902, **134**, 514.

[33] P. Sabatier and J. B. Senderens, Comptes Rendus Hebdomadaires des Seances de l'Academie de Sciences, 1902, **134**, 689.

[34] K. Aasberg-Petersen, T. S. Christensen, I. Dybkjaer, J. Sehested, M. Ostberg, R. M. Coertzen, M. J. Keyser, and A. P. Steynberg, Stud Surf Sci Catal, 2004, **152**, 258-405.

[35] K. Aasberg-Petersen, I. Dybkjaer, C. V. Ovesen, N. C. Schjodt, J. Sehested, and S. G. Thomsen, Journal of Natural Gas Science and Engineering, 2011, **3**, *2*, 423-459.

[36] D. Chiche, C. Diverchy, A. C. Lucquin, F. Porcheron, and F. Defoort, Oil & Gas Science and Technology – Revue d'IFP Energies nouvelles, 2013, **68**, *4*, 707-723.

[37] H. Boerrigter, H. den Uil, and H. P. Calis, "Green Diesel from Biomass by Fischer-Tropsch Synthesis - New Insights in Gas Cleaining and Process Design," ECN Biomass, 2002.

[38] M. J. A. Tijmensen, A. P. C. Faaij, C. N. Hamelinck, and M. R. M. van Hardeveld, Biomass and Bioenergy, 2002, **23**, 129-152.

[39] N. E. Tsakoumis, M. Rønning, Ø. Borg, E. Rytter, and A. Holmen, Catalysis Today, 2010, **154**, *3-4*, 162-182.

[40] I. Wender, Fuel Processing Technology, 1996, **48**, 189-297.

[41] D. R. Lide, Ed. *CRC Handbook of Chemistry and Physics*, 84 ed. CRC Press, 2003-2004.

[42] J. L. Casci, C. M. Lok, and M. D. Shannon, Catalysis Today, 2009, **145**, *1-2*, 38-44.

[43] A. Y. Khodakov, W. Chu, and P. Fongarland, Chemical Reviews, 2007, **107**, 1692-1744.

[44] T. McMahon. (2017, 25 September 2017). *Historical Crude Oil Prices (Table)*. Available: https://inflationdata.com/Inflation/Inflation_Rate/Historical_Oil_Prices_Table.asp

[45] G. J. Hutchings, M. van der Riet, and R. Hunter, J. Chem. Soc., Faraday Trans. 1, 1989, **85**, *9*, 2875-2890.

[46] H. Shulz and M. Claeys, Applied Catalysis A: General, 1999, **186**, 71-90.

[47] X.-Q. Gong, R. Raval, and P. Hu, Molecular Physics, 2004, **102**, *9-10*, 993-1000.

[48] X.-Q. Gong, R. Raval, and P. Hu, Surface Science, 2004, **562**, *1-3*, 247-256.

[49] P. Johnston and R. W. Joyner, Studies in Surface Science and Catalysis, 1993, **75**, 165-180.

[50] H. Schulz, K. Beck, and E. Erich, in *Proceedings of the 9th International Congress on Catalysis*, Calgary, Canada, 1988, p. 829.

[51] H. Schulz, E. Erich, H. Gorre, and E. v. Steen, Catalysis Letters, 1990, **7**, 157-168.

[52] C. B. Lee and R. B. Anderson, in *Proceedings of the 8th International Congress on Catalysis*, Bruxelles, Belgium, 1985, p. II15.

[53] P. M. Maitlis, H. C. Long, R. Quyoum, M. L. Turner, and Z. Q. Wang, Chemical Communications, 1996, 1-8.

[54] P. M. Maitlis, R. Quyoum, H. C. Long, and M. L. Turner, Applied Catalysis A: General, 1999, **186**, 363-374.

[55] M. L. Turner, N. Marsih, B. E. Mann, R. Quyoum, H. C. Long, and P. M. Maitlis, Journal of the American Chemical Society, 2002, **124**, 10456-10472.

[56] H. H. Storch, N. Golumbic, and R. B. Anderson, John Wiley & Sons, 1951, 603.

[57] A. Sternberg and J. Wender, in *International Conference on Coordination Chemistry*, London, 1959, p. 53: Springer-Verlag Wien.

[58] S. Roginski, in *3rd International Congress on Catalysis*, Amsterdam, 1965, vol. 2, p. 939: North-Holland Publ.

[59] H. Pichler and H. Schulz, Chemie Ingenieur Technik, 1970, **42**, *18*, 1162-1174.

[60] J. P. Hindermann, G. J. Hutchings, and A. Kiennemann, Catalysis Reviews - Science and Engineering, 1993, **35**, *1*, 1-127.

[61] K. Takeuchi, T. Matsuzaki, T. Hanaoka, H. Arakawa, and Y. Sugi, Journal of Molecular Catalysis, 1989, **55**, 361-370.

[62] J. Stein and E. L. Muetterties, Chemical Reviews, 1979, **79**, 479-490.

[63] C. J. Weststrate, J. van de Loosdrecht, and J. W. Niemantsverdriet, Journal of Catalysis, 2016, **342**, 1-16.

[64] C. J. Weststrate, P. van Helden, and J. W. Niemantsverdriet, Catalysis Today, 2016, **275**, 100-110.

[65] C. J. Weststrate, I. M. Ciobîcă, A. M. Saib, D. J. Moodley, and J. W. Niemantsverdriet, Catalysis Today, 2014, **228**, 106-112.

[66] C. Ledesma, J. Yang, D. Chen, and A. Holmen, ACS Catalysis, 2014, **4**, *12*, 4527-4547.

[67] J. Happel, Chemical Engineering Science, 1978, **33**, *11*, 1567.

[68] P. Biloen, J. N. Helle, F. G. A. van den Berg, and W. M. H. Sachtler, Journal of Catalysis, 1983, **81**, 450-463.

[69] S. L. Shannon and J. G. Goodwin Jr, Chemical Reviews, 1995, **95**, 677-695.

[70] H. A. J. van Dijk, J. H. B. J. Hoebink, and J. C. Schouten, Chemical Engineering Science, 2001, **56**, 1211-1219.

[71] J. Yang, Y. Qi, J. Zhu, Y. Zhu, D. Chen, and A. Holmen, Journal of Catalysis, 2013, **308**, 37-49.

[72] M. Claeys, Selektivitat, Elementarschritte Un Kineische Modellierung Bei Der Fischer-Tropsch-Synthese, Ph.D., Universitat Fridericiana Karlsruhe, Karlsruhe, 1997.

[73] C. H. Bartholomew, Applied Catalysis A: General, 2001, **212**, 17-60.

[74] J. A. Moulijn, A. E. van Diepen, and F. Kapteijn, Applied Catalysis A: General, 2001, **212**, 3-16.

[75] M. Argyle and C. Bartholomew, Catalysts, 2015, **5**, *1*, 145-269.

[76] P. Forzatti and L. Lietti, Catalysis Today, 1999, **52**, 165-181.

[77] C. H. Bartholomew, Catalysis Reviews, 1982, **24**, *1*, 67-112.

[78] A. M. Saib, D. J. Moodley, I. M. Ciobîcă, M. M. Hauman, B. H. Sigwebela, C. J. Weststrate, J. W. Niemantsverdriet, and J. van de Loosdrecht, Catalysis Today, 2010, **154**, *3-4*, 271-282.

[79] J. M. Christensen, P. M. Mortensen, R. Trane, P. A. Jensen, and A. D. Jensen, Applied Catalysis A: General, 2009, **366**, *1*, 29-43.

[80] J. M. Christensen, A. D. Jensen, and P. A. Jensen, Catalytic Synthesis of Long-Chained Alcohols from Syngas, PhD, Department of Chemical and Biochemical Engineering, Technical University of Denmark, Denmark, 2011.

[81] C. H. Bartholomew, M. W. Stoker, L. Mansker, and A. Datye, *Studies in Surface Science and Catalysis*, vol. 126, B. Delmon and G. F. Froment, Eds.: Elsevier, 1999, pp. 265-272.

[82] N. Fischer, Preparation of Nano and Angstrom Sized Cobalt Ensembles and Their Performance in the Fischer-Tropsch Synthesis, Ph.D., Department of Chemcial Engineering, Univeristy of Cape Town, Cape Town, 2011.

[83] J. A. Schwarz, C. Contescu, and A. Contescu, Chemical Reviews, 1995, **95**, 477-510.

[84] R. D. Entenberg and A. L. Menard. Jr., Journal of Marketing, 1966, **30**, 28-32.

[85] A. Marin and D. Kodjak, "Relative Cancer Risk of Reformulated Gasoline and Conventional Gasoline Sold in the Northeast," Northeast States for Coordinated Air Use Management, 1998.

[86] J. Stolark, "Fact Sheet - a Brief History of Octane in Gasoline from Lead to Ethanol," Environmental and Energy Study Institute, 2016, Available: http://www.eesi.org/papers/view/fact-sheet-a-brief-history-of-octane.

[87] V. R. Surisetty, A. K. Dalai, and J. Kozinski, Applied Catalysis A: General, 2011, **404**, 1-11.

[88] A. P. Steynberg, R. L. Espinoza, B. Jager, and A. C. Vosloo, Applied Catalysis A: General, 1999, **186**, 41-54.

[89] V. Fattore, B. Notari, A. Paggini, and V. Lagana, Catalytic System for Producting Mixtures of Methanol and Higher Alcohols, Italy Patent 4,513,100, 1985.

[90] C. E. Hofstadt, K. Kochloefl, and O. Bock, Katalysator Zur Synthese Von Methanol Un Hohere Alkohole Enthaltenden Alkoholgemischen, Germany, 1981.

[91] P. C. Ellgen and M. M. Bhasin, Process for Producing Ethanol, Acetic Acid and/or Acetaldehyde, from Synthesis Gas, United States, 1978.

[92] M. Ichikawa, K. Shikakura, K. Sekizawa, and K. Tanaka, Process for Producing Oxygen-Containing Hydrocarbon Compounds, Japan, 1981.

[93] M. M. Bhasin, W. J. Bartley, P. C. Ellgen, and T. P. Wilson, Journal of Catalysis, 1978, **54**, 120-128.

[94] T. Hanaoka, H. Arakawa, T. Matsuzaki, Y. Sugi, K. Kanno, and Y. Abe, Catalysis Today, 2000, **58**, 271-280.

[95] P. Courty, D. Durand, A. Sugier, and E. Freund, Process for Manufacturing a Mixture of Methanol and Higher Alcohols from Synthesis Gas, France Patent 4,659,742, 1987.

[96] J. A. Dalmon, P. Chaumette, and C. Mirodatos, Catalysis Today, 1992, **15**, 101-127.

[97] N. D. Subramanian, G. Balaji, C. S. S. R. Kumar, and J. J. Spivey, Catalysis Today, 2009, **147**, *2*, 100-106.

[98] T. Matsuzaki, T. Hanaoka, K. Takeuchi, Y. Sugi, and M. Reinikainen, Catalysis Letters, 1991, **10**, 193-200.

[99] M. Gupta, M. L. Smith, and J. J. Spivey, ACS Catalysis, 2011, **1**, *6*, 641-656.

[100] G. J. Quarderer, R. R. Stevens, G. A. Cochran, and C. B. Murchison, Preparation of Ethanol and Higher Alcohols from Lower Carbon Number Alcohols, United States, 1989.

[101] T. Mo, J. Xu, Y. Yang, and Y. W. Li, Catalysis Today, 2016, **261**, 101-115.

[102] Q. X. Wu, J. M. Christensen, G. L. Chiarello, L. D. L. Duchstein, J. B. Wagner, B. Temel, J. D. Grunwaldt, and A. D. Jensen, Catalysis Today, 2013, **215**, 162-168.

[103] M. Xiang and J. Zou, Journal of Catalysts, 2013, **2013**, 1-5.

[104] I. Boz, M. Sahibzada, and I. S. Metcalfe, Industrial & Engineering Chemistry Research, 1994, **33**, 2021-2028.

[105] X. Xiaoding, E. B. M. Doesburg, and J. J. F. Scholten, Catalysis Today, 1987, **2**, 125-170.

[106] S. Shetty, A. P. J. Jansen, and R. A. van Santen, Journal of the American Chemical Society, 2009, **131**, 12874-12875.

[107] N. D. Subramanian, J. Gao, X. Mo, J. G. Goodwin Jr, W. Torres, and J. J. Spivey, Journal of Catalysis, 2010, **272**, *2*, 204-209.

[108] V. Subramani and S. K. Gangwal, Energy & Fuels, 2008, **22**, 814-839.

[109] K. Fang, D. Li, M. Lin, M. Xiang, W. Wei, and Y. Sun, Catalysis Today, 2009, **147**, *2*, 133-138.

[110] R. G. Herman, Catalysis Today, 2000, **55**, 233-245.

[111] M. Xu and E. Iglesia, Journal of Catalysis, 1999, **188**, 125-131.

[112] P. M. Brown and J. M. Maselli, Process for Preparaing N-Alkylamines, United States of America, 1973.

[113] W. Rottig, Process for the Catalytic Kohlenoxydhydrierung, Germany, 1954. Available: http://www.google.ch/patents/DE904891C?cl=en.

[114] W. Rottig, Catalytic Hydrogenation of Carbon Monoxide with Addition of Ammonia or Methylamine, Germany, 1958.

[115] V. R. Rao Pendyala, W. D. Shafer, G. Jacobs, M. Martinelli, D. E. Sparks, and B. H. Davis, RSC Adv., 2017, **7**, *13*, 7793-7800.

[116] W. P. Ma, G. Jacobs, D. E. Sparks, V. R. R. Pendyala, S. G. Hopps, G. A. Thomas, H. H. Hamdeh, A. MacLennan, Y. F. Hu, and B. H. Davis, Journal of Catalysis, 2015, **326**, 149-160.

[117] C. Gunanathan and D. Milstein, Angew Chem Int Ed Engl, 2008, **47**, *45*, 8661-4.

[118] A. Seayad, M. Ahmed, H. Klein, R. Jackstell, T. Gross, and M. Beller, Science, 2002, **297**, 1676-1678.

[119] A. A. Nunez Magro, G. R. Eastham, and D. J. Cole-Hamilton, Chem Commun (Camb), 2007, *30*, 3154-6.

[120] Y. Jin, D. Qian, and Q. Du, Industrial Crops and Products, 2013, **44**, 258-262.

[121] K. Granby and S. Fagt, Analytica Chimica Acta, 2004, **520**, *1-2*, 177-182.

[122] E. di Tomaso, M. Beltramo, and D. Piomelli, Nature, 1996, **382**, 677.

[123] E. Vitz, J. W. Moore, J. Shorb, X. Prat-Resina, T. Wendorff, and A. Hahn. (10 September 2017). *Textbook Maps, General Chemistry Textbook Maps, Chemprime, 8.18: Organic Nitrogen Compounds*. Available: https://chem.libretexts.org/

[124] C. J. Cobley, M. Van den Heuvel, A. Abbadi, and J. G. de Vries, Tetrahedron Letters, 2000, **41**, 2467-2470.

[125] C. Gunanathan, Y. Ben-David, and D. Milstein, Science, 2007, **317**, 790-792.

[126] T. Oishi, K. Yamaguchi, and N. Mizuno, Angew Chem Int Ed Engl, 2009, **48**, *34*, 6286-8.

[127] H. Kölbel, I. Abdulahad, and M. Ralek, Chemischer Informationsdienst, 1975, **6**, *49*,

[128] H. Kölbel and J. Trapper, Angewandte Chemie, 1966, **5**, *9*, 843-844.

[129] A. K. Rausch, L. Schubert, R. Henkel, E. van Steen, M. Claeys, and F. Roessner, Catalysis Today, 2016, **275**, 94-99.

[130] T. Sango, Nitrogen-Containing Compounds from Ammonia Co-Feed to the Fischer-Tropsch Synthesis, MSc, Department of Chemical Engineering, University of Cape Town, Cape Town, 2013.

[131] S. T. Oyama, Catalysis Today, 1992, **15**, 179-200.

[132] G. S. Ranhotra, G. W. Haddix, A. T. Bell, and J. A. Reimer, Journal of Catalysis, 1987, **108**, 24-39.

[133] G. Leclercq, M. Kamal, J. F. Lamonier, L. Feigenbaum, P. Malfoy, and L. Leclercq, Applied Catalysis A: General, 1995, **121**, 169-190.

[134] K. Z. Qi, G. C. Wang, and W. J. Zheng, Surface Science, 2013, **614**, 53-63.

[135] S. F. Zaman, N. Pasupulety, A. A. Al-Zahrani, M. A. Daous, S. S. Al-Shahrani, H. Driss, L. A. Petrov, and K. J. Smith, Applied Catalysis A: General, 2017, **532**, 133-145.

[136] J. S. Lee, L. Volpe, F. H. Ribeiro, and M. Boudart, Journal of Catalysis, 1988, **112**, 44-53.

[137] D. V. N. Vo and A. A. Adesina, Applied Catalysis A: General, 2011, **399**, *1-2*, 221-232.

[138] H. Kim, K. H. Lee, and J. S. Lee, Research on Chemical Intermediates, 2000, **26**, *5*, 427-443.

[139] G. S. Ranhotra, A. T. Bell, and J. A. Reimer, Journal of Catalysis, 1987, **108**, 40-49.

[140] M. L. Xiang, D. B. Li, H. C. Xiao, Z. L. Hanli, H. J. Qi, W. H. Li, B. Zhong, and Y. H. Sun, Fuel, 2008, **87**, *4-5*, 599-603.

[141] M. L. Xiang, D. B. Li, H. C. Xiao, J. L. Zhang, W. H. Li, B. Zhong, and Y. H. Sun, Catalysis Today, 2008, **131**, *1-4*, 489-495.

[142] Q. X. Wu, G. L. Chiarello, J. M. Christensen, B. Temel, J. D. Grunwaldt, and A. D. Jensen, "Active Carbon Supported Molybdenum Carbides for Higher Alcohols Synthesis from Syngas," presented at the SynFuel2012 Symposium, Munich, Germany, 29-30 June 2012, 2012.

[143] J. S. Lee, S. T. Oyama, and M. Boudart, Journal of Catalysis, 1987, **106**, 125-133.

[144] G. Poncelet, P. Grange, and P. A. Jacobs, *Preparation of Catalysts Iii Scientific Bases for the Preparation of Hetergeneous Catalysts*. 1982.

[145] S. T. Oyama, Ph.D., Chemical Engineering, Stanford University, Stanford, 1981.

[146] M. Boudart and L. Volpe, Journal of Solid State Chemistry, 1985, **59**, 348-356.

[147] Z. Yin, Q. Zhao, S. Chen, G. Liu, and S. Wang, Journal CSIMM, 1993, **24**, *4*, 541-546.

[148] J. Kim, S. H. Im, S. Ha, H. S. CHOI, W. S. Kim, S. P. Yoon, and J. Han, Method for Preparing Molybdenum Oxide Nanoparticles, 2016. Available: https://www.google.com/patents/US20160362303.

[149] K. Y. Park, W. K. Seo, and J. S. Lee, Catalysis Letters, 1991, **11**, 349-356.

[150] S. Ramanathan and S. T. Oyama, Journal of Physical Chemistry, 1995, **99**, 16365-16372.

[151] P. M. Patterson, T. K. Das, and B. H. Davis, Applied Catalysis A: General, 2003, **251**, *2*, 449-455.

[152] K. Oshikawa, M. Nagai, and S. Omi, Journal of physical Chemistry B, 2001, **105**, 9124-9131.

[153] S. W. Chiang, C. C. Chang, J. L. Shie, C. Y. Chang, D. R. Ji, and J. Y. Tseng, Journal of the Taiwan Institute of Chemical Engineers, 2012, **43**, *6*, 918-925.

[154] H. Schulz, W. Bohringer, C. Kohl, N. Rahman, and A. Will, DGMK Forschungsbericht, 1984, **3**, 320.

[155] R. Kaiser, Methoden der Physikalischen Analyse, 1969, **5**, 357.

[156] E. S. Kovats, Fresenius' Zeitschrift für analythische Chemie, 1961, **181**, 351-364.

[157] H. M. Rietveld, Journal of Applied Crystallography, 1969, **2**, 65-71.

[158] D. S. Knight and W. B. White, Journal of Materials Research, 1989, **4**, *02*, 385-393.

[159] R. Kojima and K. Aika, Applied Catalysis A: General, 2001, **219**, 141-147.

[160] H. F. Xiong, M. A. Motchelaho, M. Moyo, L. L. Jewell, and N. J. Coville, Fuel, 2015, **150**, 687-696.

[161] N. Wang, K. Fang, D. Jiang, D. Li, and Y. Sun, Catalysis Today, 2010, **158**, *3-4*, 241-245.

[162] J. E. J. House, Inorganic and Nuclear Chemistry Letters, 1980, **16**, 185-187.

9 Appendices

9.1 Appendix A

Table 9-1: GC-TCD operating settings

Model: GC-Model Varian CP-4900

	Channel 1	Channel 2	Channel 3
Column	molesieve (MS5A)	PorapakQ	molesieve (MS5A)
Column length	20 m	10 m	10 m
Carrier gas	H2	H2	Ar
Injection time	350 ms	350 ms	350 ms
Injector temperature	-	80 °C	-
Column oven temperature	80 °C	60 °C	`
Column pressure	1.5 bar	1 bar	1.5 bar
Stabilization time		5 s	
Sampling time		35 s	

9.2 Appendix B

Table 9-2: GC-FID operating settings

Model: GC-Model Varian 3900			
Detector	Flame ionization detector (FID)		
Detector temperature			200 °C
Injector temperature			200 °C
Split ratio			7
Column			
Column pressure			1.72 bar
Flame gas	H2		30 mL/min
Makeup gas	N2		25 mL/min
Air flow			300 mL/min
Temperature program	Ramp (°C/min)	Step (°C)	Time (min)
	-	-55	1.5
	9	0	0
	4	100	1
	4	200	2
	10	280	5
	20	150	-
Total time			80 min
Coolant			CO2 (liquid)

9.3 Appendix C

Table 9-3: TCD Calibration

Component	Conc. (%)	1	2	3	Average	fi (N2)	fi (Ar)
N2	5.0	1271.3	1270.1	1270.1	1270.5	1.00	0.93
Ar	9.5	2595.3	2592	2591.7	2593.0	1.07	1.00
CH4	15.5	3337.7	3335.9	3335.9	3336.5	0.85	0.79
CO	20.0	5007.3	5003.9	5006	5005.7	0.98	0.92
CO2	10.1	5686.5	5697.3	5694.5	5692.8	2.22	2.07
H2	39.9	46925.8	62306.1	52963.3	54065.1	5.33	4.96

9.4 Appendix D

Table 9-4: GC-FID Kovats indices/response factors

Name	KI	C_n	C=C	C-OH	R-CO-R	R-CO-H	f_i
Methane	100.00	1	0	0	0	0	1.00
Ethene	162.03	2	1	0	0	0	1.00
Ethane	200.00	2	0	0	0	0	1.00
Propene	294.11	3	1	0	0	0	1.00
Propane	300.00	3	0	0	0	0	1.00
2-Me-Propane	369.55	4	0	0	0	0	1.00
Ethanal	371.22	2	0	0	0	1	2.00
Methanol	386.69	1	0	1	0	0	1.82
Butene (1) & 2-Me-Propene (1)	392.97	4	1	0	0	0	1.00
Butadiene (1,3)	395.67	4	1	0	0	0	1.00
N-Butane	400.00	4	0	0	0	0	1.00
T-Butene (2)	412.95	4	1	0	0	0	1.00
C-Butene (2)	428.47	4	1	0	0	0	1.00
Ethanol	454.20	2	0	1	0	0	1.29
3-Me-Butene (1)	460.96	5	1	0	0	0	1.00
Propanone & Propanal	476.64	3	0	0	1	0	1.50
2-Me-Butane	477.42	5	0	0	0	0	1.00
Pentene (1)	490.45	5	1	0	0	0	1.00
2-Me-Butene (1)	496.37	5	1	0	0	0	1.00
N-Pentane	500.00	5	0	0	0	0	1.00
T-Pentene (2)	509.15	5	1	0	0	0	1.00
C-Pentene (2)	517.77	5	1	0	0	0	1.00
2-Me-Butene (2)	522.65	5	1	0	0	0	1.00
Propanol (1)	551.91	3	0	1	0	0	1.18
Acetic Acid	568.87	2	0	1	0	0	1.29

2-Me-Pentane	572.61	6	0	0	0	0	1.00
Butanone (2)	574.88	4	0	0	1	0	1.33
3-Me-Pentane	577.41	6	0	0	0	0	1.00
Butanol	578.81	4	0	0	0	1	1.33
2-Me-Pentene (1)	585.46	6	1	0	0	0	1.00
Hexene (1)	590.37	6	1	0	0	0	1.00
N-Hexane	600.00	6	0	0	0	0	1.00
T-Hexene (2)	603.85	6	1	0	0	0	1.00
C-Hexene (2)	611.97	6	1	0	0	0	1.00
Butanol (1)	639.16	4	0	1	0	0	1.13
Pentanone (2)	642.90	5	0	0	1	0	1.25
3-Me-Hexene (1)	643.89	7	1	0	0	0	1.00
2-Me-Hexane	656.96	7	0	0	0	0	1.00
Propionic Acid	658.10	3	0	1	0	0	1.18
Pentanal	661.51	5	0	0	0	1	1.25
3-Me-Hexane	669.19	7	0	0	0	0	1.00
2-Me-Hexene (1)	681.66	7	1	0	0	0	1.00
Heptene (1)	690.00	7	1	0	0	0	1.00
Z-Heptene (3)	696.54	7	1	0	0	0	1.00
N-Heptane	700.00	7	0	0	0	0	1.00
T-Heptene (2)	704.36	7	1	0	0	0	1.00
C-Heptene (2)	714.06	7	1	0	0	0	1.00
Butanoic Acid	745.19	4	0	1	0	0	1.13
Pentanol (1)	750.10	5	0	1	0	0	1.10
4-Me-Heptane	768.37	8	0	0	0	0	1.00
2-Me-Heptane	770.33	8	0	0	0	0	1.00
3-Me-Heptane	776.18	8	0	0	0	0	1.00
Hexanal	780.05	6	0	0	0	1	1.20
2-Me-Heptene (1)	785.82	8	1	0	0	0	1.00
Octene (1)	789.31	8	1	0	0	0	1.00
T-Octene (3)	794.68	8	1	0	0	0	1.00
T-Octene (4)	796.56	8	1	0	0	0	1.00
N-Octane	800.00	8	0	0	0	0	1.00
T-Octene (2)	802.93	8	1	0	0	0	1.00
C-Octene (2)	813.11	8	1	0	0	0	1.00
Hexanol (1)	850.80	6	0	1	0	0	1.08
2-Me-Octane & 4-Me-Octane	867.45	9	0	0	0	0	1.00
3-Me-Octane	875.13	9	0	0	0	0	1.00
Heptanal	883.08	7	0	0	0	1	1.17
Nonene (1)	889.63	9	1	0	0	0	1.00
Nonene (4)	894.83	9	1	0	0	0	1.00

N-Nonane	900.00	9	0	0	0	0	1.00
T-Nonene (2)	901.88	9	1	0	0	0	1.00
C-Nonene (2)	913.09	9	1	0	0	0	1.00
Heptanol (1)	952.30	7	0	1	0	0	1.07
4-Me-Nonane & 5-Me-Nonane	965.00	10	0	0	0	0	1.00
2-Me-Nonane	967.09	10	0	0	0	0	1.00
3-Me-Nonane	974.40	10	0	0	0	0	1.00
Decene (1)	989.51	10	1	0	0	0	1.00
T-Decene (4)	994.26	10	1	0	0	0	1.00
N-Decane	1000.00	10	0	0	0	0	1.00
C-Decene (2)	1013.72	10	1	0	0	0	1.00
4-Me-Decane	1060.18	11	0	0	0	0	1.00
5-Me-Decane	1063.53	11	0	0	0	0	1.00
2-Me-Decane	1066.86	11	0	0	0	0	1.00
3-Me-Decane	1074.24	11	0	0	0	0	1.00
Nonanal	1084.84	9	0	0	0	1	1.13
Undecene (1)	1089.92	11	1	0	0	0	1.00
Rest-C-11-Olefin	1093.53	11	1	0	0	0	1.00
N-Undecane	1100.00	11	0	0	0	0	1.00
C-Undecene (2)	1112.86	11	1	0	0	0	1.00
Dodecene (1)	1190.37	12	1	0	0	0	1.00
N-Dodecane	1200.00	12	0	0	0	0	1.00
C-Dodecene (2)	1214.46	12	1	0	0	0	1.00
Tridecene (1)	1290.65	13	1	0	0	0	1.00
N-Tridecane	1300.00	13	0	0	0	0	1.00
C-Tridecene (2)	1315.08	13	1	0	0	0	1.00
N-Tetradecane	1400.00	14	0	0	0	0	1.00
C-Tetradecene (2)	1415.21	14	1	0	0	0	1.00
N-Pentadecane	1500.00	15	0	0	0	0	1.00
N-Hexadecane	1600.00	16	0	0	0	0	1.00
N-Heptadecane	1700.00	17	0	0	0	0	1.00
N-Octadecane	1800.00	18	0	0	0	0	1.00
N-Nonadecane	1900.00	19	0	0	0	0	1.00

9.5 Appendix E

Table 9-5: GC-FID response factors N-containing compounds

Compound	C_n	C_{obs}	rf_z
Ethanamine	2	1.46	1.37
Ethanenitrile	2	2.15	0.93
Ethanamide	2	1.00	2.00
Propanamine(-1)	3	2.46	1.22
Propanenitrile	3	3.15	0.95
Propanamide	3	2.00	1.50
Butanamine(-1)	4	3.46	1.16
Butanenitrile	4	4.15	0.96
Butanamide	4	3.00	1.33
Pentanamine(-1)	5	4.46	1.12
Pentanenitrile	5	5.15	0.97
Pentanamide	5	4.00	1.25
Hexanamine(-1)	6	5.46	1.10
Hexanenitrile	6	6.15	0.98
Hexanamide	6	5.00	1.20
Heptanamine(-1)	7	6.46	1.08
Heptanenitrile	7	7.15	0.98
Heptanamide	7	6.00	1.17
Octanamine(-1)	8	7.46	1.07
Octanenitrile	8	8.15	0.98
Octanamide	8	7.00	1.14
Nonanamine(-1)	9	8.46	1.06
Nonanenitrile	9	9.15	0.98
Nonanamide	9	8.00	1.13
Decanamine(-1)	10	9.46	1.06
Decanenitrile	10	10.15	0.99
Decanamide	10	9.00	1.11
Undecanamine(-1)	11	10.46	1.05
Undecanenitrile	11	11.15	0.99
Undecanamide	11	10.00	1.10
Dodecanamine(-1)	12	11.46	1.05
Dodecanenitrile	12	12.15	0.99
Dodecanamide	12	11.00	1.09
Tridecanamine(-1)	13	12.46	1.04
Tridecanenitrile	13	13.15	0.99
Tridecanamide	13	12.00	1.08
Tetradecanamine(-1)	14	13.46	1.04
Tetradecanenitrile	14	14.15	0.99
Tetradecanamide	14	13.00	1.08

Pentadecanamine(-1)	15	14.46	1.04
Pentadecanenitrile	15	15.15	0.99
Pentadecanamide	15	14.00	1.07

9.6 Appendix F

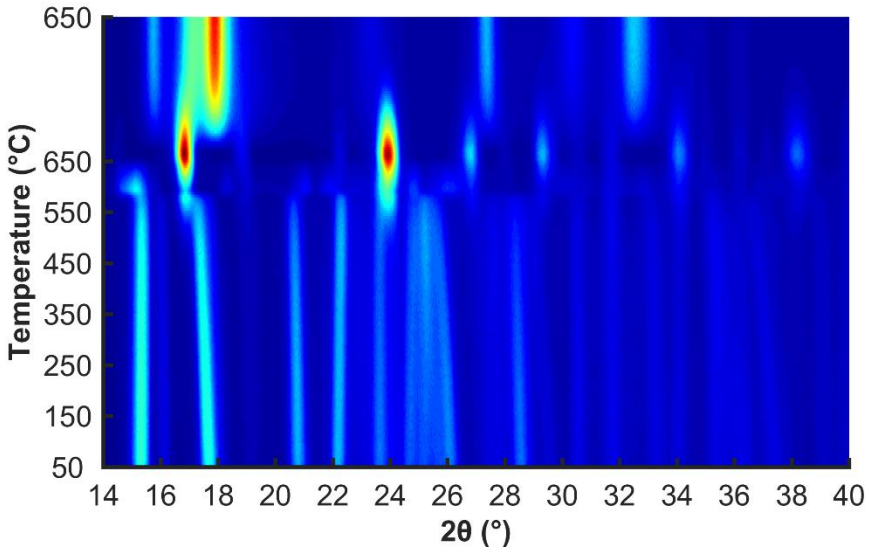

Figure 9-1: On top view of diffraction patterns collected during in situ carburization experiment of sample A2 displaying phase transformation from MoO_3 to MoO_2 and finally β-Mo_2C. Conditions: Tramp = 1 °C/min, Tfinal = 650 °C, SV = ±21 L/h/g_{cat}, carburization mixture: H_2/ CH_4/ N_2 = 9% / 2% / 89%, P = 1 atm, 1 scan per 5 minutes, total of 181 scans, step size 0.0287° and time per step is 0.2 seconds. X-ray source: molybdenum.

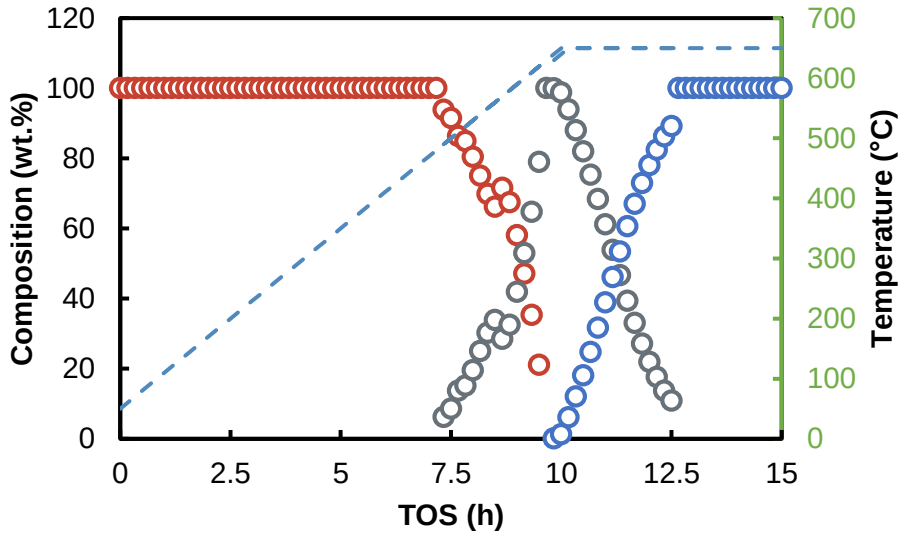

Figure 9-2: Composition of the catalyst calculated using Rietveld refinement of the in situ XRD carburization sample A2. Phases shown: MoO_3 (red), MoO_2 (grey) and β-Mo_2C (blue). Conditions: Tramp = 1 °C/min, Tfinal = 650 °C, SV = ±21 L/h/g_{cat}, carburization mixture: H_2/ CH_4/ N_2 = 9% / 2% / 89%, P = 1 atm, 1 scan per 5 minutes, total of 181 scans.

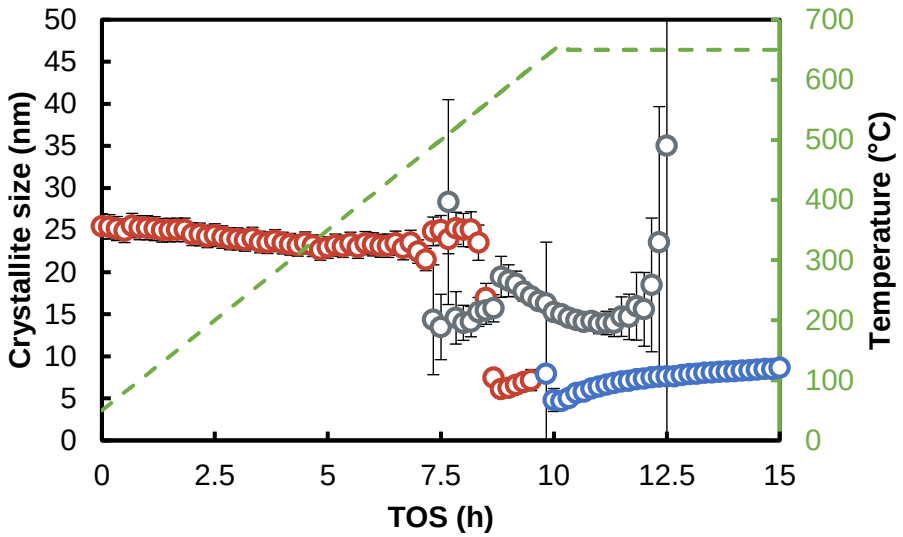

Figure 9-3: Crystallite sizes of the catalyst calculated using Rietveld refinement of the in situ XRD carburization sample A2. Phases shown: MoO_3 (red), MoO_2 (grey) and β-Mo_2C (blue). Conditions: Tramp = 1 °C/min, T_{final} = 650 °C, SV = ±21 L/h/g_{cat}, carburization mixture: H_2 / CH_4 / N_2 = 9% / 2% / 89%, P = 1 atm, 1 scan per 5 minutes, total of 181 scans.

9.7 Appendix G

Table 9-6: Carbon balance corrected CH4 and CO2 data for all FT runs.

Run		*Uncorrected data*						*Corrected data*	
		X_{CO}	CH_4	CO_2	HC	OX	Total	CH_4	CO_2
FT 1.1	A	85%	27%	25%	49%	0%	74%	37%	33%
	B	16%	21%	23%	52%	1%	76%	27%	31%
	C	4%	21%	20%	53%	14%	87%	24%	22%
	D	12%	19%	16%	50%	8%	74%	26%	22%
	E	72%	28%	25%	52%	0%	77%	37%	32%
	F	88%	29%	26%	47%	0%	73%	39%	35%
FT 1.2	A	46%	20%	43%	38%	0%	81%	24%	53%
	B	55%	24%	43%	51%	1%	95%	25%	45%
	C	15%	23%	46%	58%	11%	114%	20%	40%
FT 1.3	B	9%	22%	28%	51%	12%	91%	24%	31%
	C	12%	25%	36%	57%	24%	117%	21%	31%
	D	45%	30%	46%	60%	6%	112%	27%	41%
	E	20%	30%	38%	47%	8%	93%	32%	41%
FT 2.0	A	2%	10%	10%	27%	12%	49%	21%	20%
	B	1%	13%	9%	37%	18%	65%	21%	14%
	C	1%	15%	12%	42%	22%	76%	19%	16%
	D	2%	22%	29%	62%	23%	114%	20%	25%
	E	5%	18%	31%	48%	18%	98%	19%	32%
	F	14%	19%	35%	44%	10%	90%	21%	39%
	G	34%	20%	40%	43%	5%	88%	22%	45%
	H	15%	20%	33%	44%	13%	91%	22%	37%
	I	7%	20%	29%	46%	17%	91%	21%	32%
	J	6%	17%	26%	46%	15%	87%	20%	30%
	K	5%	20%	32%	58%	22%	111%	18%	29%
	L	4%	20%	31%	57%	24%	112%	18%	28%
FT 2.1	A	1%	8%	25%	19%	11%	55%	14%	46%
	B	4%	5%	22%	16%	8%	47%	11%	48%
	C	6%	7%	39%	24%	13%	76%	10%	52%
	D	10%	8%	41%	24%	11%	76%	10%	54%
	E	2%	10%	45%	32%	22%	99%	10%	45%
	F	17%	9%	41%	26%	11%	78%	12%	52%
	G	2%	9%	42%	30%	24%	96%	10%	44%
FT 2.2	A	2%	8%	43%	21%	9%	73%	11%	59%
	B	5%	9%	45%	29%	15%	89%	10%	51%
	C	8%	10%	46%	30%	14%	89%	11%	51%
	D	9%	12%	45%	31%	10%	86%	14%	52%
	E	16%	15%	46%	35%	10%	90%	17%	51%
	F	2%	13%	53%	40%	18%	110%	11%	48%
FT 2.3	A	4%	9%	33%	23%	16%	72%	12%	46%
	B	7%	10%	35%	25%	16%	76%	13%	46%

	C	10%	11%	39%	22%	17%	79%	14%	49%
	D	13%	12%	41%	24%	17%	81%	15%	50%
	E	16%	16%	43%	24%	13%	81%	19%	53%
	F	1%	50%	115%	n/a	n/a	n/a	n/a	n/a
FT 3.1	A	8%	11%	40%	25%	17%	81%	13%	49%
	B	8%	12%	41%	26%	21%	88%	14%	47%
	C	9%	13%	42%	27%	26%	95%	13%	44%
	D	6%	14%	42%	32%	27%	101%	14%	42%
FT 4.1	No NH_3	17%	6%	26%	16%	10%	53%	12%	50%
	NH_3	14%	6%	14%	10%	4%	40%	14%	34%
FT 4.2	No NH_3	22%	13%	41%	29%	16%	86%	15%	48%
	NH_3 - 1h	17%	18%	51%	40%	6%	97%	18%	52%
	NH_3 - 3h	23%	11%	29%	26%	11%	66%	16%	43%

9.8 Appendix H

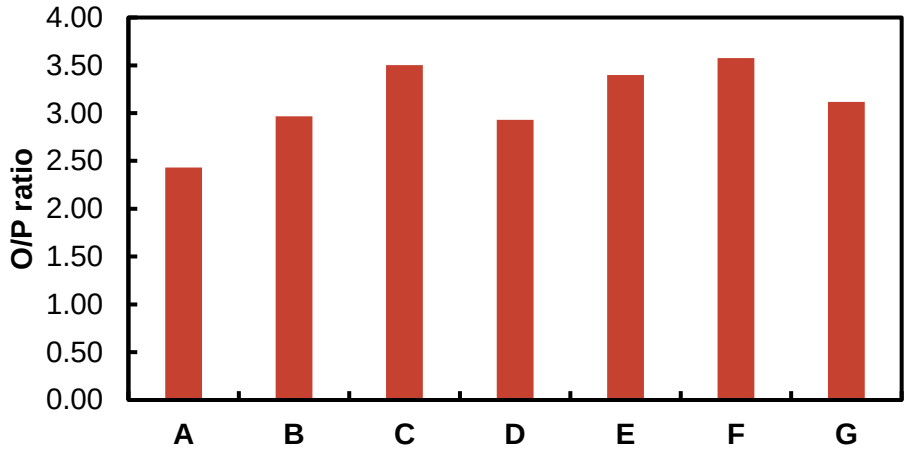

Figure 9-4: C_3-olefin to C_3-paraffin ratio of FT 2.1 with varying conditions: A) 260 °C, B) 280 °C, C) 300 °C, D) 320 °C, E) 280 °C, F) 350 °C and G) 280 °C. Process conditions: P = 45 bar, H_2 to CO ratio = 1 and GHSV = 8 L/h/g_{cat}.

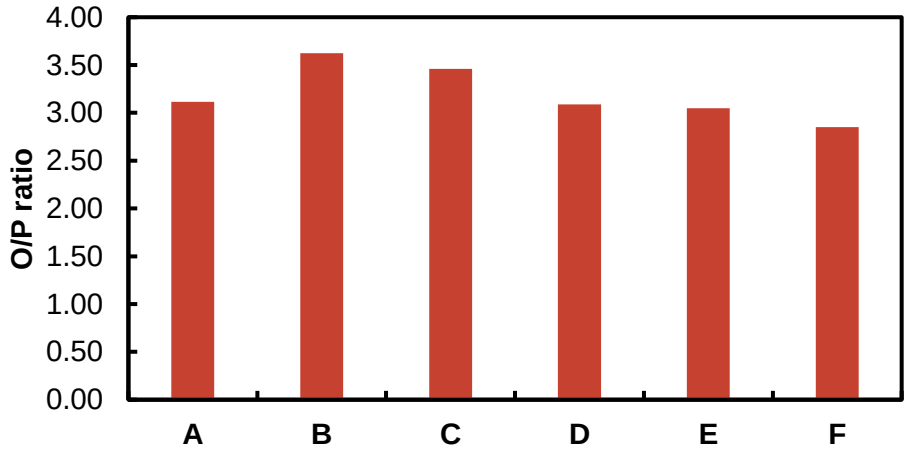

Figure 9-5: C_3-olefin to C_3-paraffin ratio of FT 2.2 with varying conditions: A) 260 °C, B) 280 °C, C) 300 °C, D) 320 °C, E) 350 °C and F) 280 °C. Process conditions: P = 45 bar, H_2 to CO ratio = 1 and GHSV = 8 L/h/g_{cat}.

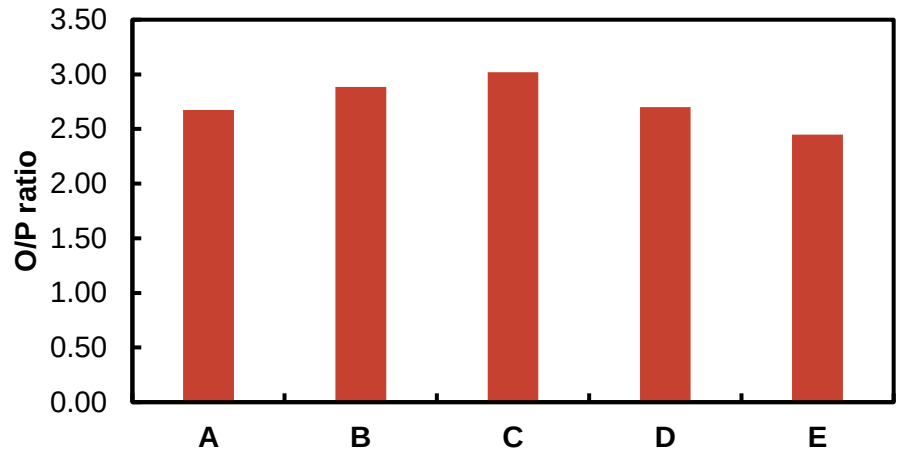

Figure 9-6: C_3-olefin to C_3-paraffin ratio of FT 2.3 with varying conditions: A) 260 °C, B) 280 °C, C) 300 °C, D) 320 °C and E) 350 °C. Process conditions: P = 45 bar, H_2 to CO ratio = 1 and GHSV = 8 L/h/g_{cat}.

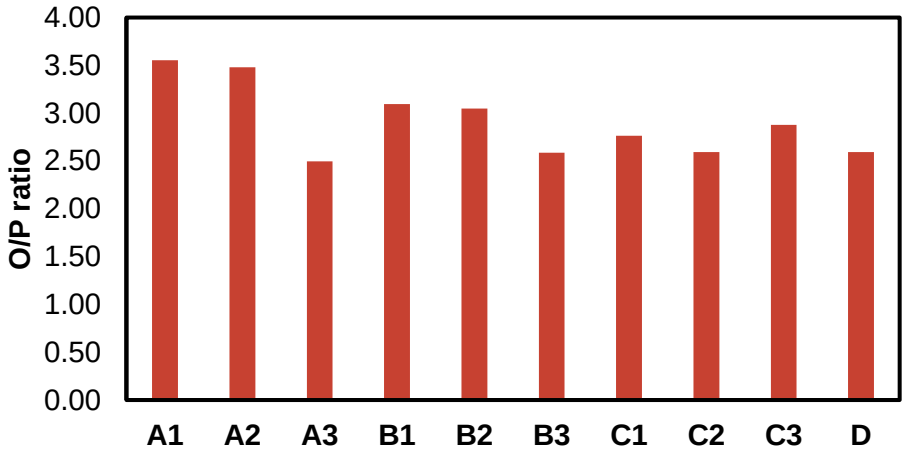

Figure 9-7: C_3-olefin to C_3-paraffin ratio of FT 3.1 with varying conditions: A) 45 bar, B) 55 bar, C) 65 bar and D) 45 bar at 1 hour (X1), 3 hours (X2) and 24 hours (X3) TOS, with X = A, B or C. Process conditions: T = 300 °C, H_2 to CO ratio = 1 and GHSV = 8 L/h/g_{cat}.

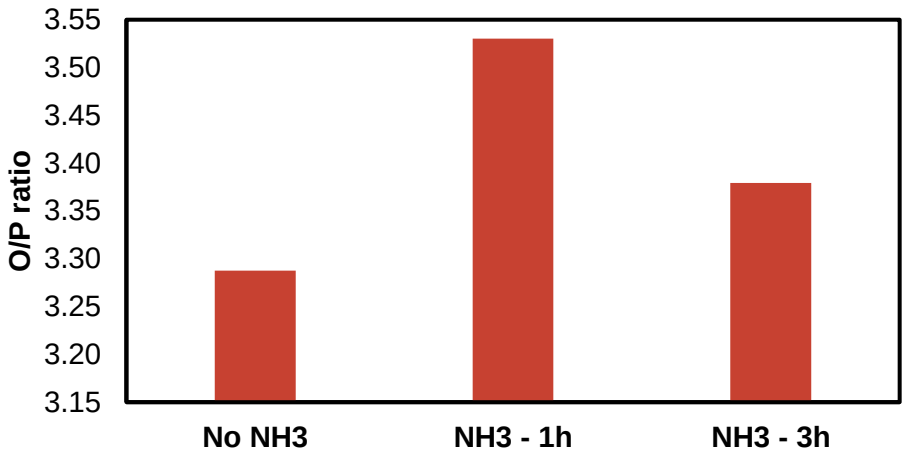

Figure 9-8: C_3-olefin to C_3-paraffin ratio of FT 4.2 in the absence and presence of ammonia.

9.9 Appendix I

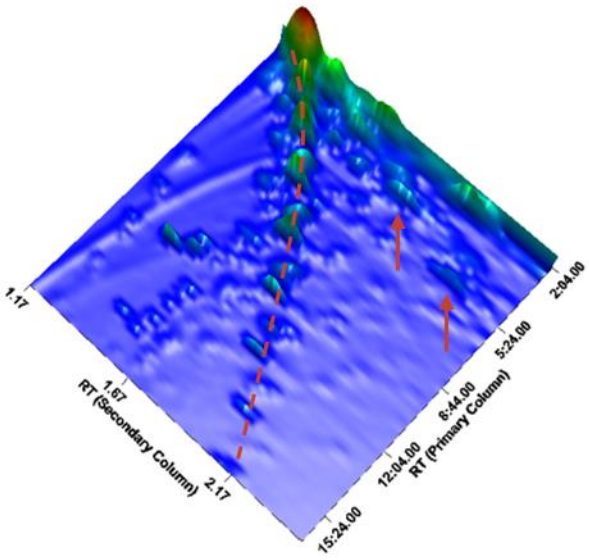

Figure 9-9: Image taken from the GCxGC analysis of FT 4.2 under normal FT conditions. Dashed lines indicate the linear and branched alcohols and the arrows indicate the aldehydes.

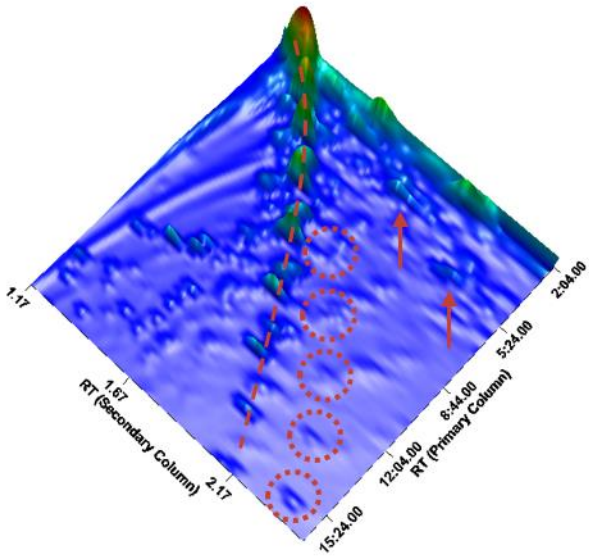

Figure 9-10: Image taken from the GCxGC analysis of FT 4.2 with co-feeding of 1.5 vol.% NH_3 for 1 hour. Dashed lines indicate the linear and branched alcohols, circles indicate the nitriles and the arrows indicate the aldehydes.

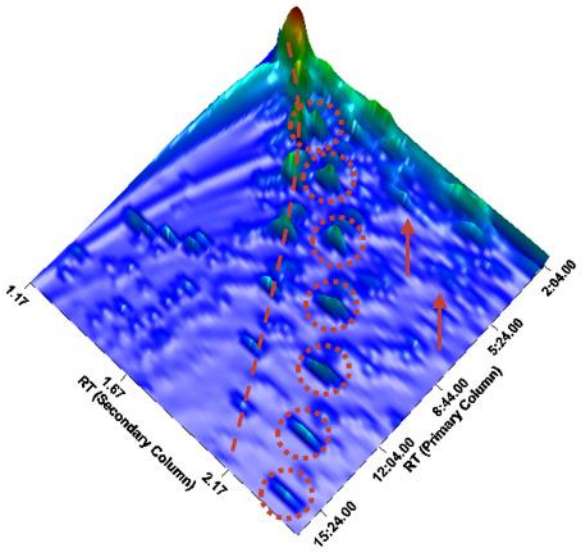

Figure 9-11: Image taken from the GCxGC analysis of FT 4.2 with co-feeding of 1.5 vol.% NH_3 for 3 hours Dashed lines indicate the linear and branched alcohols, circles indicate the nitriles and the arrows indicate the aldehydes.

9.10 Appendix J

Application for Approval of Ethics in Research (EiR) Projects
Faculty of Engineering and the Built Environment, University of Cape Town

APPLICATION FORM

Please Note:
Any person planning to undertake research in the Faculty of Engineering and the Built Environment (EBE) at the University of Cape Town is required to complete this form **before** collecting or analysing data.The objective of submitting this application *prior* to embarking on research is to ensure that the highest ethical standards in research, conducted under the auspices of the EBE Faculty, are met. Please ensure that you have read, and understood the **EBE Ethics in Research Handbook**(available from the UCT EBE, Research Ethics website) prior to completing this application form: http://www.ebe.uct.ac.za/usr/ebe/research/ethics.pdf

APPLICANT'S DETAILS		
Name of principal researcher, student or external applicant		Wijnand Marquart
Department		Chemical Engineering
Preferred email address of applicant:		Mrqwij001@myuct.ac.za
If a Student	Your Degree: e.g., MSc, PhD, etc.,	MSc
	Name of Supervisor (if supervised):	Dr. Nico Fischer
If this is a researchcontract, indicate the source of funding/sponsorship		Click here to enter text. c* change
Project Title		Molybdenum carbide as catalyst for Fischer-Tropsch synthesis with high oxygen selectivity/

I hereby undertake to carry out my research in such a way that:

- there is no apparent legal objection to the nature or the method of research; and
- the research will not compromise staff or students or the other responsibilities of the University;
- the stated objective will be achieved, and the findings will have a high degree of validity;
- limitations and alternative interpretations will be considered;
- the findings could be subject to peer review and publicly available; and
- I will comply with the conventions of copyright and avoid any practice that would constitute plagiarism.

SIGNED BY	Full name	Signature	Date
Principal Researcher/ Student/External applicant	Wijnand Marquart		**09 May 2017**

APPLICATION APPROVED BY	Full name	Signature	Date
Supervisor (where applicable)	Dr. Nico Fischer		**09 May 2017**
HOD (or delegated nominee) Final authority for all applicants who have answered NO to all questions in Section1; and for all Undergraduateresearch (Including Honours).	Click here to enter text. Hein Bohmann		10 May 2017
Chair : Faculty EIR Committee For applicants other than undergraduate students who have answered YES to any of the above questions.	Click here to enter text.		Click here to enter a date.

pp.

Page **1** of **1**